DISSERTATION

ISOLATION, INTERPRETATION, AND IMPLICATIONS OF PHYSICAL SOIL ORGANIC MATTER FRACTIONS IN SOIL SYSTEMS

Submitted by

Samuel J. Leuthold

Graduate Degree Program in Ecology

In partial fulfillment of the requirements

For the Degree of Doctor of Philosophy

Colorado State University

Fort Collins, Colorado

Summer 2024

Doctoral Committee:

Advisor: M. Francesca Cotrufo
Co-Advisor: Jocelyn M. Lavallee

Nathan Mueller
Meagan Schipanski

ABSTRACT

ISOLATION, INTERPRETATION, AND IMPLICATIONS OF PHYSICAL SOIL ORGANIC MATTER FRACTIONS IN SOIL SYSTEMS

Soil organic matter (SOM) is crucial to sustained ecosystem function, due to its role in regulating nutrient cycling, carbon (C) storage, and soil structure relevant to both food production and climate regulation. Since the early 1990s, physical fractionation methods have been used to separate bulk SOM into discrete components. The central aim of these methodologies is to simplify the complex heterogeneity of the bulk SOM pool by isolating fractions with more homogenous chemistries, formation pathways, and mechanisms of persistence. By understanding the relative distribution of C and nitrogen (N) among these various fractions, we gain appreciable insight into the mechanisms underlying fundamental soil biogeochemical processes. Despite their historic use, however, significant questions remain regarding the means of proper isolation and interpretation. This dissertation looks to these questions directly, reviewing and then interrogating the methods by which fractions separated before applying those fractionation schemes to answer key questions relating SOM to ecosystem function. The first section reviews the history and current state of physical fractionation methodologies, before using a triangulation of experimental evidence, including chemical, isotopic, and spectral indicators, to identify the best practices for laboratory use. These chapters advance our current understanding of SOM biogeochemistry by drawing an explicit link between the conceptual definitions of SOM fractions and the various procedural definitions that have been used historically. Across a range

of soils representative of agricultural land in the United States, we show that fractionation methods that separate particulate organic matter (POM) fraction by density isolate fractions more in line with the conceptual definition of POM than the more frequently used size separation. This work aims to unify understanding across the field of soil biogeochemistry and allows for more robust analyses and modeling efforts. The subsequent chapters use this approach to investigate fundamental questions around SOM stability and persistence. The mineral associated organic matter (MAOM) fraction has long been understood to be relatively stable, with slower turnover times and a more homogenous composition as compared to POM. Its accumulation has thus been discussed as a target for climate change mitigation. We leveraged a unique long-term experimental site with archived samples stretching back over 60 years to test this assumption, aiming to identify a dynamic fraction of MAOM by comparing the SOM composition of plots that had not received organic inputs over the course of the experiment against plots that had received regular inputs for six decades. Our spectral and isotopic analyses showed that a dynamic fraction of the MAOM existed and was primarily composed of plant derived compounds. As the exchangeable MAOM pool was exhausted due to a lack of fresh C inputs, we found that the composition of the MAOM pool became more strongly dominated by microbial byproducts. This work represents useful evidence towards a holistic understanding of the dynamic nature of SOM, and forces reimagining of long-held paradigmatic views.

One challenge in the current SOM biogeochemistry landscape is that often questions exist downstream of methodologies, such that the fractions that can be isolated drive the research that is conducted. By first identifying robust methodologies, in the second half of this dissertation we were able to ask specific questions about the link between SOM dynamics and ecosystem function. To this end, we pursued three different lines of inquiry: a field study in which the

objective was to link the fractional distribution of C and N to yield stability in agricultural systems, a field study that seeks to understand the persistence dynamics of SOM over a decadal scale in grassland systems, and a laboratory incubation that aims to discern the relative contributions of POM and MAOM in regard to plant available N. The first field study used samples from 9 working farms across the Central United States to better understand how SOM might moderate the spatiotemporal stability of crop yields at the field scale. Yield instability is a major cause of economic and environmental distress in row crop systems, and regional studies have suggested that increasing SOM may be able to mitigate variation in yield across time and space. The chapter presented here is the first study that attempts to identify a mechanistic link between SOM fractions and yield stability. In disagreement with regional and county scale studies, we found that SOM abundance was not linked to increased yield stability in cropping systems. Rather, unstable yield zones had significantly higher SOM content than stable zones, particularly in regard to the POM fraction. This work indicates that at the subfield scale, interactions between climate, topography, and management may be driving spatial patterns of both yield stability and SOM accumulation. This is a key insight, implying that some of the relationships between SOM and agronomic outcomes are scale dependent, and highlighting the need for field scale work to maintain relevance to growers. The second field study produced novel insights, tracing isotopically enriched litter and pyrogenic organic matter (PyOM) through various SOM fractions over the course of a decade, one of the longest tracer experiments that has occurred in grassland ecosystems. We found that after 10 years, the majority of the remaining litter derived C and N inputs were stored in the MAOM fraction, a result well aligned with our hypotheses. Interestingly though, the litter derived MAOM fraction formed rapidly (~ 1 year) and persisted at a relatively similar concentration for the duration of the study. This suggests the

potential for divergent persistence mechanisms of POM and MAOM, implying less inter-fraction transfer than previous frameworks have proposed and prompting re-evaluation of the mechanisms of MAOM formation and persistence. In contrast, the applied PyOM remained almost completely in the POM fraction over the 10-year period, reinforcing both the heterogeneity of the bulk SOM pool, and the myriad of persistence mechanisms that stabilize various SOM fractions. Given that PyOM is ubiquitous in soil regardless of burn history and can persist for hundreds of years, this result has critical importance for our understanding of turnover time of the POM fraction, and suggests that we may be underestimating the dynamic nature of POM when PyOM is not accounted for. Finally, in a lab incubation experiment, we took advantage of recent advances in isotopic measurement to prove recent theories around MAOM N accessibility. Whereas POM is often thought of as the fraction that provides nutrients in the short term, our two-week incubation showed that under certain conditions, the majority of plant available N may be derived from the MAOM fraction. This work validates proposed frameworks and is an important step towards understanding coupled C and N management in agroecosystems that could improve N use efficiency and increase producer sustainability. Overall, the work in this dissertation aims to provide a comprehensive overview of how fractions can and should be isolated, and the information gained via this fractionation.

By clarifying and advancing methodology to quantify SOM components and the understanding of their contribution to critical soil functions for the sustainability of food production and the mitigation of climate change this dissertation represents a major step forward for the study, modeling and managing of SOM in agricultural systems.

ACKNOWLEDGEMENTS

This dissertation represents the culmination of years of mentorship, kindness, and guidance by numerous individuals. I will endeavor to name as many as I can here but know that there are far more than I can fit on this page that I owe this product to. Proceeding chronologically, I am forever indebted to my parents for the support and kindness that they have provided since I was a just a little kid, splashing through puddles with a ruler and rubber boots. I had thought they would be apprehensive when I told them I was going to be a soil scientist, but they were nothing but encouraging at every step of the way. Thank you, Mom and Dad. I love you both. My grandparents are a source of both inspiration and support; it was my grandfathers' dedications to land stewardship and lives spent outside in the dirt that originally spurred this love of soil in me. I count myself lucky beyond limit to call Joanne Leuthold my grandmother—she likely knows as much about the work presented here as I do, thanks to her endless curiosity about what I was working on. Thanks for always picking up the phone, Nana, and thanks for truly listening when you did. Tony Hartshorn introduced me to soil and got me excited about it. My life would be quite different had I not met him. Fabian Menalled gave me my first shot at working in a lab, even after I bungled the interview. He and his lab taught me more about science in a year than I had learned throughout my entire education to that point. Erin Berryman and John Farley sent me out into the Colorado wilderness with a LI-8100 and their faith and allowed me to learn through trial and error how to lead a team. Stephanie Ewing and Rob Payn allowed me to explore what being a scientist really was and gave me outsized opportunities for my experience and age. The time I spent working with them prepared me for the rest of my career; I am extremely lucky to know them. Words on this page do not feel enough to thank Hunter Howe for her loving support,

her gracious understanding, and her constant backing. She is the foundation that underpins this whole operation— I would not be even half the man I am today without her. I love you, Hunter. Thank you, for everything. Hanna Poffenbarger took a gamble on me to be her first graduate student, and for that I'll be forever grateful. I learned so much from Hanna and my time in Lexington, not just about soil fertility and corn, but about navigating this world. My brother and roommate, Calvin, thank you for being who you are. Being able to come home and talk about something that is not POM and MAOM is more of a gift than you will ever realize. Nathan Mueller and Meagan Schipanski, thank you for being a part of my time here at Colorado State. You have both changed the way I think about agriculture in profound and meaningful ways, and I am so grateful for your insight and mentorship. To my friends and lab mates in the Soil Innovation Lab and beyond, thank you for your support, your mentorship, and most of all, your kindness. A PhD can be a lonely prospect at times, but thankfully I had you all. My time here was definitively better for it. None of this work would have been possible without the efforts of Michelle Haddix, Rebecca Even, Dan Ruess, Sam McNiel, Paige Lewis, and Brit Meis. Your assistance in the lab is unmatched; I would never have been able to do half the work detailed here without all of your help. To Michelle and Rebecca in particular, thank you for your kind patience, for never shying away from a question, and for never begrudging the interruption to your day that I inevitably darkened your door with. You are both fantastic scientists who deserve all of our admiration. I owe Jocelyn Lavallee a huge debt of gratitude, one I am not sure how I ever will repay. Jocelyn, thank you for all you have done— for meeting with me every week for three years, for encouraging me to follow my interests and passions, for supporting and advocating for me at every turn, and for engaging in single every interaction with a thoughtful kindness that never wavered. When I grow up, if I am lucky, I want to be Jocelyn Lavallee.

Finally, to Francesca, thank you. Thank you for believing in me, especially when I did not. Thank you for supporting me, advocating for me, teaching me. I have learned a lot about soil organic matter over the course of the last three years, but it pales in comparison to what I have learned about how to think critically, how to manage, how to mentor, how to show up with both passion and compassion. The last three years have been some of the most formative of my life, and while I owe that to everyone on this list in one way or another, you truly made it so.

Thank you, all. We are the sum of those we spend our time with; I count myself exceedingly lucky to have spent time with all of you. Happy reading.

DEDICATION

To Hunter Howe- whose mere existence makes the world brighter and who gives me purpose every single day. Thank you for your encouragement, your patience, and your unwavering love. Here's to the next adventure.

and

To Joanne Leuthold- the kindest, most curious person; the person we all wish was in the audience at our talks. A woman who understands that to be a great teacher, you have to be a great listener. May I grow up to be as interested and loving as you are.

TABLE OF CONTENTS

CHAPTER 1: INTRODUCTION

Soil organic matter (SOM) plays a crucial role in maintaining agroecosystem productivity, though the mechanisms of this effect are often loosely defined (Bauer and Black, 1994; King et al., 2020; Minasny and McBratney, 2018; Oldfield et al., 2022; Schjønning et al., 2018). Resolving these mechanisms is challenging, as SOM is composed of a heterogenous mixture of organic compounds of varying provenance (Chang et al., 2024; Lavallee et al., 2019; Whalen et al., 2022) and decomposition status (Cotrufo et al., 2015; Grandy and Neff, 2008; Lehmann and Kleber, 2015). Physical fractionation methods can separate this heterogenous mixture into fractions with more similar characteristics, which allows for increased insight into (agro)ecosystem function (Cotrufo et al., 2019; Cotrufo and Lavallee, 2022; Lavallee et al., 2020; Prairie et al., 2023) and SOM formation processes. In this dissertation, I attempt to gain a better understanding of the dynamics of physical SOM fractions through targeted inquiries around the methods for their separation, their biogeochemical dynamics within the soil system, and their formation, function, and stabilization in both managed and natural systems. Here, I present a brief overview of the chapters within the dissertation and their overarching linkages.

While physical fractionation methods have been employed widely by researchers since the early 1990s (Elliott and Cambardella, 1991), the number of publications that employ fractionation techniques has grown significantly in the past 10 years. This growth has been bolstered even further following publications that highlight the utility of fractions as a means for better understanding SOM dynamics outside of SOM formation and persistence specific contexts (Billings et al., 2021; Lavallee et al., 2020). The first two chapters of my dissertation examine the methods used to isolate these physical fractions directly and attempt to identify the best practices

for their application in ecosystem biogeochemical research. Chapter 2 provides a review of the rationale and history of physical fractionation methods and provides an overview of the major methodologies that are currently widely employed. Chapter 3 expands on this review and attempts to reconcile the conceptual definitions of various physical SOM fractions such as particulate and mineral associated organic matter (POM and MAOM, respectively) with procedural definitions that are assigned to them depending on a given methodology (e.g., size vs. density fractionation). Our primary goal here is to provide a common resource for researchers that lack an established fractionation procedure or tradition within their lab or institution, and to identify best practices for work that plans to investigate SOM fraction dynamics.

The methodological work in Chapters 2 and 3 provided useful insight into the methods most well-suited to isolate functional soil compartments (Curtin et al., 2019; Moni et al., 2012), that is to say those fractions of the SOM with more similar biogeochemical characteristics (e.g., C:N ratio, stable isotope composition, spectral absorbance patterns, etc.). However, they are not well suited to thoroughly investigate the composition and dynamics of SOM fractions across space and time. Chapters 4 and 7, in contrast, investigate directly the chemical and biological dynamics and behavior of these fractions in soil systems. The common conceptual definition of MAOM is that it is a relatively stable fraction, with slow turnover times and a longer mean residence time than POM (Kleber et al., 2015; Lavallee et al., 2020). However, recent work has highlighted that there is a portion of this fraction that can actively exchange with the soil solution (Daly et al., 2021; Jilling et al., 2018, 2021; Woolf and Lehmann, 2019), with implications for ecosystem biogeochemical cycling, and assumptions around SOM stability. In Chapter 4, we use diffuse reflectance infrared Fourier transformed (DRIFT) Mid-IR spectroscopy to characterize this dynamic portion of the MAOM fraction, leveraging a unique dataset of archived soils. We seek

to extend this line of inquiry in Chapter 7, where we intend to use a laboratory incubation to test how the distribution of carbon (C) and nitrogen (N) among physical fractions influences both the source of mineralized N, and the N mineralization rate. These chapters, building on the previous two, seek to improve our basic understanding of SOM fractions, with the goal of improving soil biogeochemical models and management recommendations around building SOM.

By establishing an understanding of SOM fraction characteristics and composition, we can apply our findings to better understand ecosystem function, as well as temporal patterns in SOM formation and stabilization. As I alluded to above, previous work has highlighted the role of SOM in determining agronomic outcomes such as yield stability (Kane et al., 2021; Williams et al., 2016). However, these studies have lacked mechanistic explanations, which we hypothesized was due to their consideration of SOM as a bulk entity. To address this, Chapter 5 examines the relationship between SOM fractions and subfield yield stability zones in production fields across the Midwestern US. We found surprising patterns which indicated divergent patterns of formation and stabilization between POM and MAOM fractions among the different stability zones. In Chapter 6, we look at these questions around formation and stabilization in a more targeted way, using isotopic tools in a long-term field incubation experiment. Specifically, we explored temporal patterns in SOM formation, transformation, and persistence among physical fractions under two inputs: plant litter, and pyrogenic organic matter. The results have important implications for our understanding of how SOM forms and persists on an understudied yet management relevant timescale (10 years).

Across chapters, the dissertation presented here is an attempt to use SOM fractionation in the most responsible way possible for advancing our understanding. Fractionation provides powerful insight into soil biogeochemistry; however, the results of fractionations must be examined within

the appropriate context. By first understanding what we're isolating (i.e., Chapters 2 – 4) when we do a fractionation, we can move forward confidently into understanding the implications of fractional distribution of C and N within the soil system (i.e., Chapters 5 – 7).

CHAPTER 2: PHYSICAL SOIL ORGANIC MATTER FRACTIONATIONS— A REVIEW[1]

Introduction

Soil organic matter (SOM) is a key renewable resource, providing several ecosystem services such as the regulation of nutrient cycling, soil water storage, and carbon sequestration. Soil organic matter is largely composed of diverse, relatively simple molecular compounds that are present in the soil solution, attached to mineral particles, or contained within fragmented organic residues (von Lützow et al., 2007). Over the last 40 years, continued advancements in SOM research have led to an increasing acceptance that to understand best the function, formation, and persistence of SOM, different components must be isolated and examined as critical parts of a greater whole (Cambardella and Elliott, 1992; Christensen, 2001; Lavallee et al., 2020; Lehmann and Kleber, 2015; Sollins et al., 1984). Several methods of separating SOM fractions have been developed, such as the now dismissed use of strong alkaline extractions to isolate organic molecules (Stevenson, 1994), or laboratory incubations that aim to determine turnover times of different SOM constituents (Paul et al., 1999). In this chapter, we focus our discussion on methods of isolating organic matter fractions by physical means.

Physical fractionation methods enable the isolation of SOM fractions that are less heterogenous in their turnover time, formation processes, and or chemical make-up than the bulk SOM. In

[1] The published version of this chapter can be cited as:

Leuthold, S.J., Haddix, M.L., Lavallee, J., Cotrufo, M.F., 2022. Physical fractionation techniques, in: Reference Module in Earth Systems and Environmental Sciences. Elsevier, p. B9780128229743000677. https://doi.org/10.1016/B978-0-12-822974-3.00067-7

contrast to other methods of SOM separation, physical fractionation methods reduce the potential for procedural artifacts or modification of the chemical composition of the final samples, and produce samples fit for further analysis (e.g., elemental and isotopic composition, hydrogen pyrolysis, etc.). Most importantly, these physical methods have been developed to separate SOM into fractions based on inherent physiochemical properties, which allows increased insight into the mechanisms of SOM formation, stabilization, and persistence of the different components.

A distinguishing feature of the current paradigm of SOM research has been an inquiry model that exists downstream from the methodology at the researcher's disposal. That is to say, the questions asked are often directly informed by the techniques for separating constituent fractions, rather than fractionation approaches dictated by the differences that exist in the function, formation, and persistence of the substances that comprise the organic component of the soil. The fractions we discuss in this chapter are by nature operationally defined, and the operational definitions will vary given the dogma of a given laboratory, institution, or researcher. While the wealth of high-quality research under this paradigm has brought about a deep understanding of SOM dynamics, the foundation is now strong enough such that we have the opportunity to craft questions using an inductive reasoning framework and to use methods that are informed by the scope of our inquiry, rather than inform it. Here we provide an overview of the different functional components of SOM, the relevance to research studies, and the ways in which researchers can go about separating these components. Our intention is to provide a resource for researchers to develop an understanding of the most typical products of physical fractionation schemes, the information they can provide, and the methods by which they can be isolated such that researchers can make informed decisions concerning the techniques they employ.

Conceptual Framework

The molecules within a given organic residue or exudate entering the soil have a variety of potential fates once they begin to decompose and become part of the SOM pool. The secretion of specialized extracellular enzymes by soil microbial communities transforms insoluble molecules such as cellulose, hemicellulose, lignin, suberin and pectin contained within the structural components of plant tissue into low molecular weight compounds by a repeated process of colonization and depolymerization. In contrast, exudates and soluble compounds within residue such as organic acids, amino acids, and sugars, are readily leached from the residue and enter the soil solution directly. Low molecular weight compounds can be assimilated into the microbial biomass or respired by soil microbes, but may also bypass microbial interactions altogether and associate with mineral surfaces, often creating strong and long lasting bonds (Liang et al., 2017). As microbial energy sources become exhausted and communities begin to turn over, the nitrogen-rich molecules contained in microbial byproducts and necromass have a similar range of fates as plant compounds, depending on their polymeric structure, solubility, and affinity for bonding to mineral surfaces.

The different structures, fates, and processing pathways of organic molecules after entering the soil leads to SOM that is diverse in its composition, functional properties, and accessibility to decomposers. Organic matter consisting of structural plant and microbial residues free from mineral association is defined as particulate organic matter (POM), the low molecular weight compounds in the soil solution are defined as dissolved organic matter (DOM), while the organic matter found in fine mineral associations is defined as mineral-associated organic matter (MAOM). While arguably there are no ‘uniform’ SOM fractions, it is useful to describe them as ‘primary’ when they are distinct from one another and ‘secondary’ when they are composite, i.e.,

formed from the aggregation of primary fractions (Christensen, 2001; Denef et al., 2010). Therefore, POM, MAOM, and DOM can be considered primary SOM fractions, as they occur as discrete conceptual units in the soil, and represent a fundamental level of structural complexity (Christensen, 2001). The secretion of extracellular enzymes or extracellular polymeric substances by microbes onto these primary fractions can facilitate further accumulation of soil particles and OM around them, leading to the formation of soil aggregate structures. As soil aggregates are composed of primary structures, they are considered secondary SOM fractions (Christensen, 2001; Denef et al., 2010). Aggregate formation typically occurs through persistent bonding facilitated by organic molecules, polyvalent cation complexes, and aluminosilicate minerals, often around an organic nucleus (Oades and Waters, 1991). Aggregated structures can protect POM by spatial isolation, and have also been shown to facilitate the formation of MAOM as intra-aggregate breakdown and microbial turnover occur (Witzgall et al., 2021). While all SOM will eventually be utilized by the soil microbial community, stoichiometric complexity and diversity, nutrient deficiencies, and oxygen or temperature limitations can moderate the rate and efficiency with which microbial degradation occurs (Lehmann et al., 2020). Thus, POM fractions are often separated between free and occluded in aggregates of different size fractions as a way to get more insight into their turnover time (Six and Paustian, 2014).

Just as the form and function of different SOM fractions vary, the physical characteristics associated with these different SOM fractions, including their size and density, and the size and density of the mineral particles or aggregates they may be associated with, varies among the different fractions (Figure 2.1). Taking advantage of these differences enables the separation of MAOM, POM, DOM, and additional fractions, free or as aggregates, by physical procedures. Despite physical SOM fractions being inherently operationally defined, the covariation in

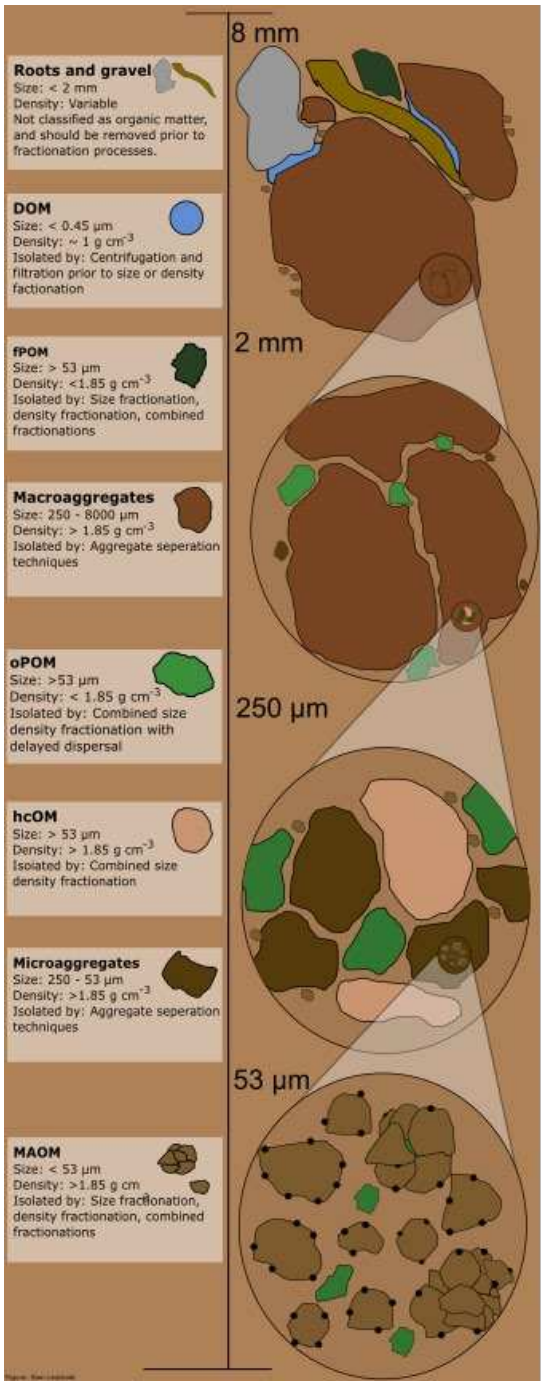

Figure 2.1 - Conceptual diagram of the fractions that can be isolated by various physical fractionation techniques. Macro- and micro-aggregates can be isolated using aggregate separation techniques, while mineral associated organic matter (MAOM), free and occluded particulate organic matter (fPOM and oPOM, respectively), coarse heavy associated organic matter (CHAOM) and dissolved organic matter (DOM) require size, density, or combined fractionation techniques.

physical characteristics of the fractions with the formation mechanisms, response to environmental changes, and chemical composition of the SOM fractions makes them a useful approach to study SOM dynamics.

Isolatable Soil Organic Matter Fractions

Particulate Organic Matter (POM)

Particulate organic matter is the term for the fraction of SOM primarily composed of structural materials of both plants and microbes (e.g., cell walls) that have undergone fragmentation and leaching losses but little to no depolymerization. The structural nature of POM makes it relatively light and coarse, leading to an operational definition of organic material with densities < 1.6–1.85 g cm-3, and or sizes > 53 μm. When separated by density fractionation, POM is often referred to as the light fraction, as its lower density allows separation with floatation. Depending on the type of fractionation scheme and the objectives of a given study, POM can be further fractionated into free and occluded POM. Free POM is uncomplexed POM that is suspended within the soil matrix and is recoverable prior to soil dispersal methods (Figure 2.1). In contrast, occluded POM refers to the fraction of POM that is protected within soil aggregates and is only recoverable following the dispersion of soil structures. Despite these differences in protection, both free and occluded POM fractions have similar sizes and densities (i.e., < 1.85 gm cm^{-3}).

Mineral Associated Organic Matter

Mineral-associated organic matter refers to the organic molecules that have sorbed to mineral surfaces or are occluded within highly stable fine microaggregate structures. The dominant molecular components of the MAOM fraction are low molecular weight compounds of plant and microbial origin such as amino sugars and microbial polysaccharides, as well as some more

diverse and complex molecules such as extra polymeric substrates, and microbial necromass. The bulk of organo–mineral associations occur with minerals of the silt and clay size, and as such the operational definition of MAOM is the organic material smaller than 50-60 μm and with a density > 1.6–1.85 g cm^{-3}. This fraction is often referred to in the literature as the heavy fraction when separated by density methods, or the silt and clay fraction when separated based on size. The organo–mineral bonds generally protect MAOM from microbial degradation, but recent work has shown that a fraction of MAOM can actively exchange with the soil solution. Previously, chemical methods such as acid hydrolysis have been used to quantify the amount of MAOM that is stable in its bonds and not actively exchanging with the soil solution (Ramnarine et al., 2018), but new methods for separating the exchangeable pool are actively being developed. Recent advances indicate that methods such as the application of oxalic acid or controlled incubations could provide another method of quantifying the ratio of exchangeable vs. stable MAOM (Jilling et al., 2018).

Other Primary Soil Organic Matter Fractions

Dissolved Organic Matter (DOM)

Dissolved organic matter (DOM) accounts only for about 1–2% of the total organic matter within a soil at a given time and is procedurally defined as the organic molecules that are water soluble and smaller than 0.45 μm. Some methodologies enable the direct measurement of DOM by extractions or centrifugation, though dissolved organic carbon (DOC) is often calculated as the difference between bulk soil carbon and the cumulative carbon recovered after fractionation (Zimmermann et al., 2007). It plays an important role as both a microbial energy and nutrient source, and as a precursor to MAOM formation.

Coarse Heavy Associated Organic Matter (CHAOM)

There is a fraction of the SOM that is associated with coarse (> 60–50 μm), heavy (> 1.6–1.85 g cm^3) particles (CHAOM), which can be isolated as another primary SOM component together with the POM and MAOM fractions when the fractionation scheme used includes both a size and a density separation (Mosier et al., 2021). This fraction has previously been termed both 'heavy POM' and 'coarse MAOM' and may consist of low molecular weight compounds sorbed to iron (Fe) or manganese (Mn) coatings on the outside of sand grains, microbial biofilms secreted on large primary particles, or POM encrusted with a mineral coating. The composition of this fraction varies depending on site characteristics, dispersion methods, and soil mineralogy. Although this fraction tends to account for a small percentage of the total soil organic carbon, it represents an important consideration when choosing a fractionation method. When size separations are used, it will become part of the POM fraction, but when density separations are used, it becomes part of the MAOM fraction. Ongoing research is attempting to better characterize this fraction and assign its functional role in the greater SOM pool, but currently it requires site-specific understanding to assess (Samson et al., 2020)

Soil Aggregates

Cohesion and fragmentation processes in the bulk soil lead to the formation of soil aggregates, groups of primary particles (i.e., POM, CHAOM, and MAOM) that are more strongly attached to each other than to other particles in the soil matrix. Aggregates vary in size and are often classified either as microaggregates (53–250 μm) or macroaggregates (250-8000 μm), depending on their diameter, or on the basis of their stability under applied stressors, such as repeated sieving or wetting and redrying. More stable aggregates retain their structure, and less stable ones disintegrate into the constituent primary fractions. Separating soils into different aggregate

size and stability fractions helps our understanding of SOM structure and can give important insight into SOM formation and cycling processes. However, because of the composite nature of aggregates, they cannot be quantified together with and compared to the fractions they are composed of. Therefore, aggregates must be dispersed during the fractionation procedure to account for and compare the SOM content of primary fractions. Combined methods have been developed that introduce dispersion at different stages to isolate primary fractions that occur within different aggregate size fractions, which can give insight into primary fraction protection and controls on heterogeneity in primary fraction turnover time.

Other SOM Fractions not Isolated by Physical Fractionation Methods

In contrast to the physically defined fractions described above, some SOM components have distinct chemical and functional properties, but lack distinct physical characteristics, and can be found distributed across physical fractions. Microbial biomass and pyrogenic organic matter are two such components. A small and ubiquitous SOM component, microbial biomass turns over quickly, and its methodological quantification is beyond the scope of this chapter (see Horwath and Paul, 1994 for further discussion). Pyrogenic organic matter (PyOM) is present in most soils and results from the transformation of plant material into highly condensed aromatic rings by combustion at high temperatures. These aromatic structures are resistant to decomposition, requiring large amounts of energy to sever the chemical bonds. Even in systems that do not burn regularly, PyOM can be relatively abundant across the primary soil fractions, with potential to influence the calculation of mean residence time. This ubiquity indicates that PyOM should often be considered more fully in SOM studies (Lavallee et al., 2019). Given the strong persistence of PyOM and its distinct properties from POM and MAOM it would be advisable to separate it from these fractions; the combined use of hydrogen pyrolysis or Mid-IR spectroscopy with

physical fractionation (Lavallee et al., 2019; Sanderman et al., 2021) hold promise for the feasibility of this approach at scale.

Aggregate Fractionation Methods

Various methods of aggregate fractionation have been proposed, primarily based on separation by size. Figure 2.2 provides an in-depth overview of the aggregate separation scheme developed by Six et al. (1999), which has been identified as reproducible and consistent during multi-laboratory comparison studies (Poeplau et al., 2018). A key consideration during aggregate fractionation is the method by which aggregates are separated during fractionation. One method of aggregate separation and isolation is 'slaking', the process of rapidly immersing air-dried soil in water before rapidly removing it. Air pressure within the aggregate is increased upon rapid submersion, and low stability aggregates are disrupted. In contrast, rewetting of aggregates prior to fractionation by gradual capillary saturation to a water content of 105% of the bulk soil does not readily disrupt low stability aggregates, as the disruptive force applied to the soil is much less than when slaked. In laboratory comparisons of slaking vs. rewetting methods, more microaggregates were recovered in slaked soils than in rewetted ones, and macroaggregate recovery was increased in the rewetted soils (Six et al., 2000).

The process of separating aggregates is performed by sieving for a set amount of time. Both dry sieving of undispersed soils and wet sieving of air-dried (slaking) or sieving of rewetted soils have been used to separate aggregate size fractions. However, dry sieving has been shown to overestimate enzyme activity, while wet-sieving has been shown to indicate more significant differences between isolated fractions (Nahidan and Nourbakhsh, 2018). Following separation of aggregate size classes, dispersions and further fractionation can be performed to isolate primary

Methodology

1) Weigh out approximately 50 g of air dried, bulk soil that has been sieved to pass through a 2-mm sieve and record weight to the 0.01 g.
2) Place weighed soil on top of a 250-µm sieve, and place the sieve into a large, clean container.
3) Fill the container with DI water until there is ~2 cm of liquid covering the sieve.
4) Allow sample to sit for 5 minutes in the water.
5) After 5 minutes, gently move the sieve up and down 50 times over the course of 2 minutes. Aggregates should just come out of the water on the upward stroke, and the sieve should not hit the bottom on the downward stroke.
6) Remove sieve from water and backwash aggregates that remain on top of the 250-µm mesh into a pre-weighed container.
7) Place a 53-µm sieve in a second, large, clean container, and then gently pour the effluent from the first container over the sieve.
8) Repeat step 5, and then backwash the aggregates that remain on the 53-µm sieve into a pre-weighed container.
9) Transfer effluent to 1-L centrifuge bottles, and centrifuge for 15 minutes at 3220 RCF.
10) Carefully pour off supernatant, and transfer silt and clay in bottles to pre-weighed container.
11) Place tins in oven to dry at 50 ℃ until all water has evaporated, and then weigh. The first sample collected is the macroaggregate fraction, the second the microaggregate fraction, and the third the silt and clay fraction.

Materials Required

- 40–50 g soil sieved < 2 mm
- 1 250-µm sieve
- 1 53-µm sieve
- DI water
- 2 clean large pans (e.g., plastic oil pans)
- 1-L centrifuge bottles
- 3 large, pre-weighed sample tins

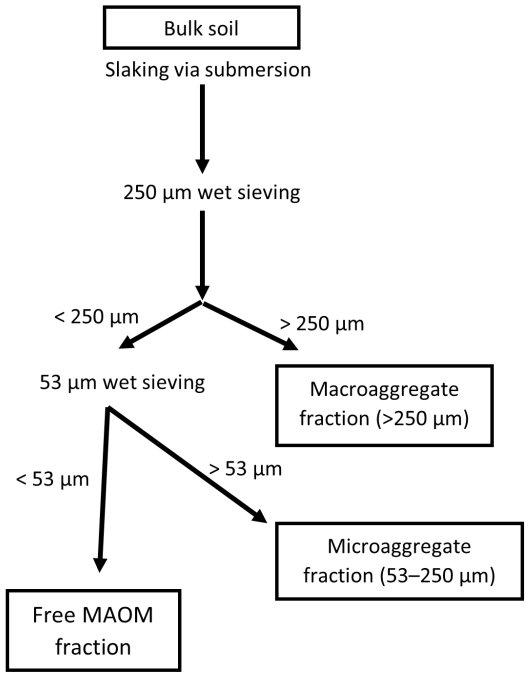

Figure 2.2 - Methods for physical fractionation of aggregates based on aggregate size.

fractions and separate the SOM fractions that are occluded within aggregates vs. suspended in the soil matrix (Six et al., 1998).

Primary Particle Fractionations

Dispersal Methods

A key step during all physical primary particle fractionations is aggregate dispersal, for which several methods have been developed. The objective of all soil dispersal techniques is to disrupt

the bonds between soil minerals such that the secondary aggregate structures are broken down into the constituent fractions. In practice, full dispersion is rarely if ever achieved; bonds in the microaggregate structures composed of silt and clay particles require tremendous energy to break, and as such some microaggregates will remain following the application of all dispersion methodologies. However, these fine aggregates (< 53 μm) function similarly to organic matter bonded to silt and clay-size particles, and the application of enough energy to disrupt these fine aggregates would probably damage the primary minerals, leading to transfer of carbon between fractions. Thus, after conventional aggregate dispersion they are considered procedurally as part of the MAOM fraction. A common side-effect of dispersal and liquid-mediated fractionation methods is the possibility of carbon transfer between fractions, which should be minimized at all steps of dispersal. Here we review the methodology for and the benefits and disadvantages of two of the most common types of soil dispersal methods: mechanical shaking and ultrasonic dispersion.

Mechanical shaking

Mechanical shaking methods of soil dispersal apply kinetic energy generated by sustained agitation to soils suspended in a liquid to fragment and disperse aggregates into smaller, primary particle fractions. Mechanical shaking can be performed in either a horizontal reciprocal shaker, which transfers energy to the soil solution by consistent movement back and forth along a single axis, or in an end-over-end shaker, which uses the falling of the soil solution to produce the energy necessary for dispersion. For reproducibility, shaking should be reported in terms of oscillations or rotations per minute, however, the shaking intensity is often reported qualitatively in the literature. Though to the authors' knowledge no studies have looked explicitly at shaking intensity, the consensus across studies indicates that shaking should be performed at a low-to-

moderate speed (e.g., 110 oscillations per minute). The addition of glass beads increases the energy transfer from the shaker to the soil suspension and better disperses soils. There is a risk of fragmenting POM when using glass beads, however, and of puncturing vacuoles in vegetative tissue causing it to become smaller and denser, possibly leading to a small transfer of POM to the MAOM during fractionation (Diochon et al., 2016).

Several liquids have been used as a medium for mechanical dispersal, including water (H_2O), sodium hexametaphosphate ($(NaPO_3)_6$; SHMP), and sodium polytungstate ($Na_6[H_2W_{12}O_{40}]$; SPT). Sodium hexametaphosphate is the most commonly used soil dispersant. Its molecular structure allows for the formation of unassociated complexes with cations and reduces the flocculation of clay minerals. However, the use of SHMP as a dispersant for SOM fractionation techniques can add a level of complexity and error to the results. Therefore, additions of SHMP to the soil must be either rinsed out of the soil by repeated washing with DI water or maintained in the sample throughout the analysis. Rinsing of the soils can lead to SOC leaching from fractions, compromising both total carbon recovery and the accuracy of results. Maintaining SHMP in the organic matter fractions can also lead to artificially inflated recoveries when examined on a mass basis, possibly obscuring loss during the fractionation process that could indicate poor recovery.

Shaking in water avoids the potential to change the chemical character of SOM fractions or add mass that may skew recoveries. A recent study indicated poor reproducibility with water extractions alone, however, as without a complementary dispersal additive water may not have the power to disrupt aggregates fully (Just et al., 2021). Mechanical shaking can also be performed in SPT, which can be convenient when SPT is used in further fractionation steps. However, similar to SHMP, SPT must be rinsed from samples prior to further analysis. Reviews

of rinsing procedures have demonstrated leaching of carbon from all fractions may occur, leading to underestimation of organic carbon across fractions (Plaza et al., 2019). In addition, a review of SPT has shown that it can contaminate samples with non-native nitrogen (N) and tungsten (W), especially in the mineral-associated fraction (Kramer et al., 2009). Mechanical shaking is a good method to use across a variety of soils since its dispersal power is less dependent on soil type than the alternative ultrasonic vibration presented below. For any method, the operator should use it with care and adjust shaking time and intensity, number of beads and rinsing of dispersal agent to minimize drawbacks.

Ultrasonic vibration

The second common method of soil dispersion is sonication, in which ultrasonic vibrations are applied to soil suspensions, disrupting bonds, and separating soil components. The general application of this method introduces ultrasonic waves into a solution containing non-dispersed soils. As the waves travel through the solution, alternating pressure conditions are created. Small bubbles are formed in low pressure areas, which then implode as the bubbles encounter high pressure areas. This implosion, and the force associated with it, disperses the secondary structures as the water jet that is created can have velocities that exceed 100 m sec $^{-1}$. One of the central benefits of this method is that it provides quantitative values of the amount of force used and is therefore theoretically reproducible. Soils with a high clay content create tightly bound microaggregates, which require a higher dispersion energy than more coarse soils. Therefore, the amount of force needed for proper dispersal varies between soil textures, minerologies, and structures, and must be calibrated prior to experimentation. The amount of sonication energy used to break aggregates from secondary into primary structures spans a broad range. In a review, Kaiser and Berhe (2014) report sonication energies used for dispersal ranging from 60–

10,000 J cm^{-3}. Researchers who work consistently with the same soils may benefit from using the calibrated values provided by sonication methods, large scale projects that encompass a variety of global soils with variable physiochemical characteristics will require approaches that are more consistent across samples.

Carbon transfer between fractions can occur when using sonication dispersal techniques as well. With POM, sonication can significantly fragment structural litter particles, leading to redistribution amongst all size fractions. Using energy levels between 280 and 420 J cm^{-3} Oorts et al. (2005) found that there was a transfer of 35–37% of the nitrogen and of 20–31% of the carbon from coarse POM into smaller size fractions following dispersal. However, this damage and subsequent carbon transfer has been found at energy levels as low as 90 J cm^{-3} (Amelung and Zech, 1999). This transfer can have important implications depending on ecosystem type and experimental goals. Even in systems where the coarse POM fraction is relatively small, the fragmentation and redistribution of this fraction has large implications for isotopic studies. Primary SOM fractions, because of differences in their formation, degree of microbial processing, and persistence, often have distinct isotopic values. As such, isotopic techniques such as ^{14}C that quantify age and turnover time, or ^{13}C and ^{15}N that quantify origin and degree of transformation can be considerably compromised by the transfer of even small amounts of organic matter among fractions (discussed further in Chapter 3).

For soil particles, excessive sonication energy can potentially damage the crystalline structure of minerals, resulting in bias in the recovery of different SOM fractions based on size. Several studies have documented fragmentation of sand separates into smaller fractions, especially as sonication energy exceeds 700 kJ cm^{-3}. Additional evidence of damage to silt particles has also been observed with scanning electron microscope techniques (Kaiser et al., 2012). Currently,

there is no evidence that sonication can fragment particles smaller than 20 μm (i.e., the clay fraction). However, the energy required to disperse small clay aggregates may exceed the energy that could fragment larger particles, such that these two extremes must be balanced. Calibration of the sonication energy is an important step in the dispersal process for optimizing aggregate dispersal while minimizing the amount of carbon transfer between particle-size classes and SOM fractions.

Size Fractionations

Several fractionation methods that use particle size as a differentiating factor between primary fractions have been established. These methods aim to separate primary SOM fractions after dispersal by sieving with different mesh sizes (Figure 2.3). Typically, sizes ranging between 53–60 μm are used to separate POM (>53 μm) from MAOM, but a cutoff at 20 μm to separate the fine MAOM is also used. In the review of fractionation methods by Poeplau et al. (2018), particle-size fractionation was found to be an effective way of isolating fractions that differed in their turnover times. The methodology of the size fractionation technique deployed by (Cotrufo et al., 2019) is shown in Figure 2.4.

Size fractionations are relatively simple and tend to have limited mass loss during the procedure. Furthermore, they require a low level of skill and laboratory infrastructure, are cost effective, and throughput can be relatively high (25–30 samples day^{-1}). Size fractionations have been used in several studies as an effective method of separating two functionally distinct SOM pools, i.e., POM and MAOM. They provide important insight into the formation and persistence of SOM in response to treatment. Those studies that have a large number of samples, or that expect a moderate to large effect size in response to treatment in either the MAOM or POM fraction are

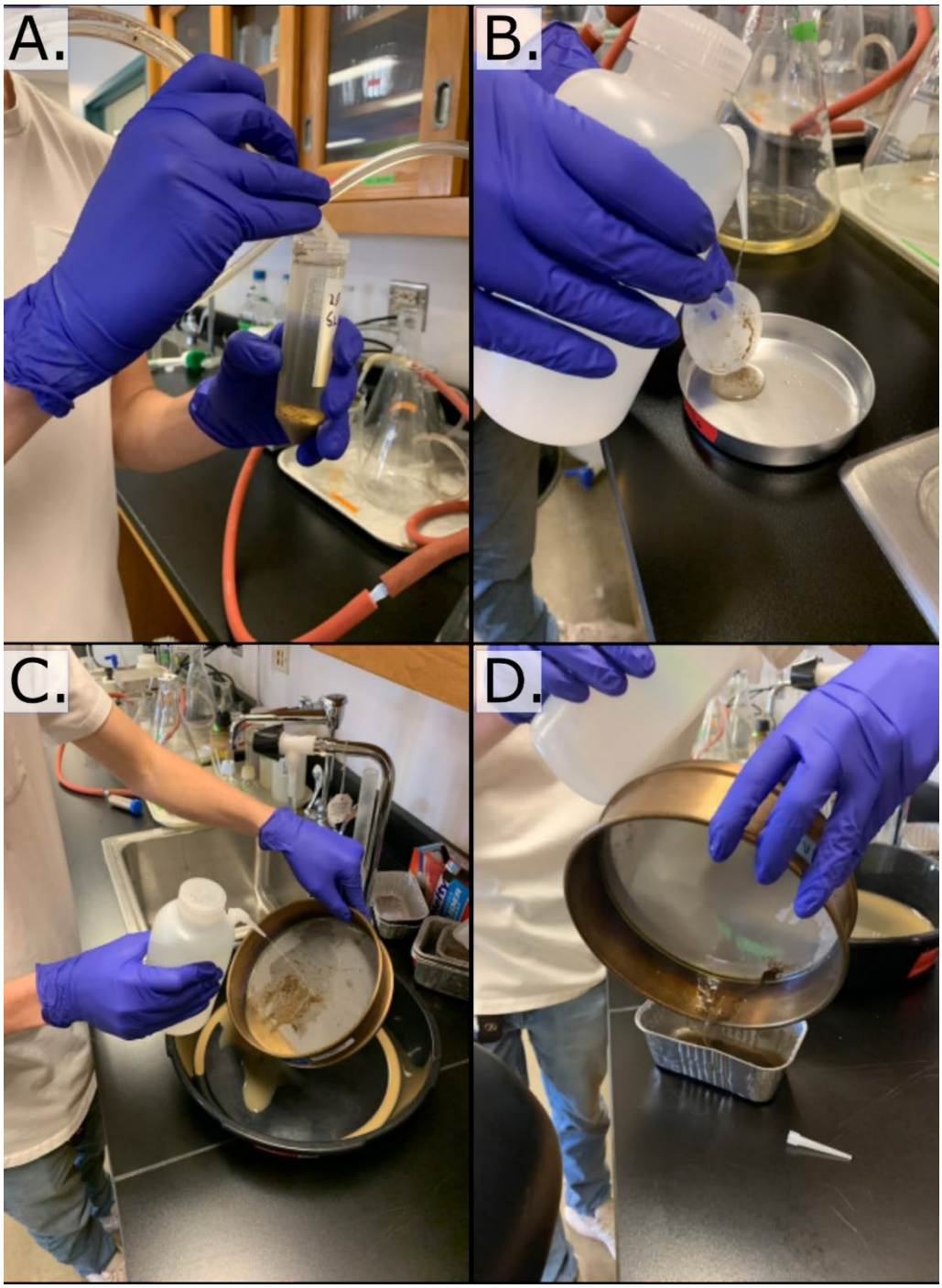

Figure 2.3 - Demonstrations of fractionation techniques and examples of equipment used. A.) Aspiration of the light fraction floated in SPT using vacuum filtration. B.) Transfer of light fraction from nylon filter to pre-weighed pan. C.) Wet sieving to separate MAOM from CHAOM (combined fractionation) or POM (size fractionation). D.) Back washing of CHAOM fraction into pre-weighed pans from after completion of sieving.

Methodology

1) Weigh out 5.25–5.75 g of air dried, bulk soil that has been sieved to pass through a 2-mm sieve into a pre-weighed centrifuge tube, and place in 60 ℃ oven overnight.
2) Take samples out of oven, cool in desiccator, and weigh samples + tubes to 0.01 g.
3) Add 12 small glass beads to the tube, then add 0.5% sodium hexametaphosphate to the 30 mL line and cap samples.
4) Shake the samples for 18 hours ± 15 minutes at ~112 oscillations per minute.
5) Place the 2000-µm sieve on top of the 53-µm sieve in a clean, large shallow pan. Shake sample to ensure all soil is in solution, then pour sample over the nested sieve.
6) Retrieve glass beads from 2000-µm sieve and wash any soil material onto the 53-µm sieve.
7) Rinse the 53-µm sieve with DI water until rinsing water runs clear, making sure also to rinse the sides of the sieve.
8) Back rinse the material remaining on top of the 53-µm sieve into a pre-weighed weighing pan and place in the oven at 60 ℃.
9) Transfer the effluent from the large shallow pan into a pre-weighed weighing pan and place in oven at ℃.
10) Once samples are completely dry, weigh and ensure that recoveries fall between 95 and 105% of sample mass. If recoveries are large, re-dry and reweigh samples.
11) If recoveries are acceptable, samples can be ground using a mortar and pestle and prepared for further analysis.

Materials Required

- 50 mL conical centrifuge tubes
- 0.5% sodium hexametaphosphate
- Pre-weighed weighing pans
- 2000 and 53-µm sieves.
- DI water
- Large, shallow pan

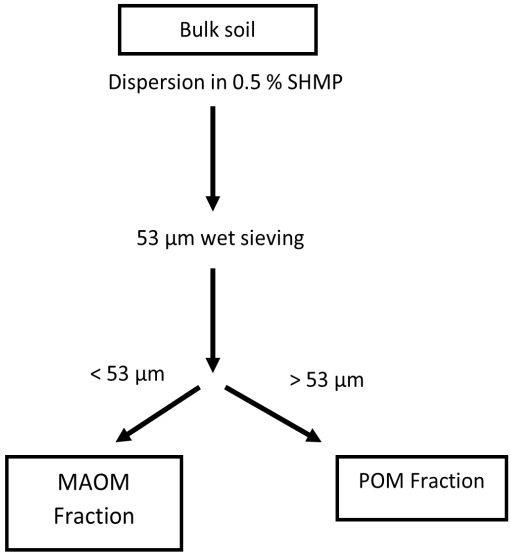

Figure 2.4 - Methods for physical fractionation of POM and MAOM based on primary particle size.

well suited for size fractionation methods. However, size fractionations can be limited in scope depending on the research objectives of a given study. Size fractionation methodologies are unable to separate occluded POM from free POM and cannot be used to isolate the CHAOM

fraction. Further, the DOM fraction will be grouped with the MAOM fraction if not isolated prior to the size fractionation.

Density Separations

An alternative method to size fractionations is to take advantage of the differences in density of mineral particles and partially decomposed litter fragments. Organic matter has a lower density than minerals, and when submerged and centrifuged in a liquid of a known density, it floats while the mineral-associated portion of the sample sinks. The lighter fraction can then be aspirated and analyzed separately from the heavier fraction (Figure 2.3). Sequential density fractionations combined with dispersion can also be used to separate the free POM from the aggregate-protected POM. In this case, the soil sample is initially subjected to little to no dispersion prior to density flotation and collection of the free POM. The sample is then more thoroughly dispersed, releasing low-density material that was occluded in aggregate structures, and the occluded POM can be separated by a second density flotation.

The most common solution used in density fractionations is SPT and, as mentioned above, some procedures also call for its use as a dispersing agent. Previous studies have also employed sodium iodide (NaI) as the heavy liquid for density fractionations, but found that the use of NaI may increase the pH of the soil solution, which has the potential to disrupt organo-mineral bonds and facilitate intra-fraction C transfer (Plaza et al., 2019). By changing the amount of water added to heavy liquid, the density can be manipulated to achieve different fractionation outcomes. Previous research by (Cerli et al., 2012) highlighted the differences in recovery of the light fraction across different densities. Their results suggest that a density of 1.6 g cm^{-3} is the optimal density for achieving maximum floatation of organic material and to minimize the presence of minerals in the light fraction. Most studies use densities of 1.8–1.85 g cm^{-3} to

maximize recovery of organic material not associated with minerals and to improve floatation. Even higher densities have been suggested but the risk of contamination by mineral particles increases as density increases. The ultimate density chosen for a given study should be as close to the maximum density of the organic materials present as possible, while minimizing potential mineral contamination of the light fraction. Calibration for individual sites may be necessary.

Sequential density fractionations, with progressively increasing densities, on dispersed soils have also been used to separate mineral-associated fractions with distinct mineralogical components after the removal of the light fraction, as demonstrated by Sollins et al., (2009). By increasing the density of the suspension liquid with each successive fractionation, it is possible to isolate a range of different MAOM fractions, including short-range order minerals such as allophanes (density: >2.0 g cm^{-3}), high activity phyllosilicates such as smectite (density: > 2.3 g cm^{-3}), framework silicates such as quartz and feldspars (density: > 2.7 g cm^{-3}), and oxides such as hematite and goethite (density: < 3.0 g cm^{-3}). This increased separation of the MAOM fraction can give further insight into the controlling factors on SOM persistence and formation across different soil environments. However, with each additional density flotation, the risk of decreasing recovery or carbon transfer between fractions becomes greater. Further, density fractionations are time intensive, as SPT must be rinsed from the samples several times during each step, expensive, and require greater laboratory skill to execute compared to size fractionations.

Overall, density fractionations are a useful tool for separating organic and mineral particles that may not differ in size but have other contrasting properties. Studies that are focused on the differences between formation pathways and cycling of POM will benefit from density

separations, as it enables explicit isolation of the most structural material derived fraction, in contrast with size separations.

Combined Separations

Aggregate, size, and density fractionations may be combined to separate the key functional organic matter pools and elucidate mechanisms of SOM formation and stabilization. These fractionation procedures allow for increased isolation of pools that may be grouped together in size or density fractions, such as CHAOM. In addition, when size and density are combined with aggregate fractionation, they enable a greater degree of differentiation of the organic carbon that is either occluded within aggregates in mineral and particulate forms, or free in the soil matrix (Six et al., 1999). These characteristics of the combined size–density fractionations provide a scheme that can approach the fractions identified more closely in the conceptual framework than size or density fractionations alone. In the comparison study by Poeplau et al. (2018), fractionation methods that combine a size with a density separation following complete dispersion were very effective in differentiating fractions with different turnover times, had average mass recoveries greater than 95%, and were reproducible across multiple fractionations. A typical scheme combining size and density fractionation schemes isolated four fractions: DOM, POM, CHAOM, and MAOM (Mosier et al., 2021; Figure 2.5). As with the density fractionation methods, further sequential density separations could be done to isolate particular mineralogical constituents. Similarly, further size fractionations could also be performed to isolate particular subclasses of particles (e.g., fine clay vs. silt, etc.). However, adding successive density or size cutoffs can decrease the overall efficacy of the fractionations; the risk of leaching carbon from the samples or transferring between fractions increases with the addition of further washing, shaking, or centrifugation steps (Poeplau et al., 2018).

Methodology

1) Weight out 5.5–6 g air dried, 2-mm sieved soils into a pre-weighed, acid washed centrifuge tube, and place tubes in 60 ^{o}C oven overnight.
2) The following day, weigh samples on a 4-place scale, and then add DI water to the 35 mL line and shake for 15 minutes on low (~112 oscillations per minute).
3) Rinse tubes and caps with DI water, and then balance tubes and centrifuge at 2325 RCF for 15 minutes.
4) Pour supernatant over a 20-µm nylon filter on a filtration unit, and transfer filtered liquid to a clean, new centrifuge tube.
5) With a squirt bottle, rinse any light fraction that accumulated on the filter into a small, pre-weighed pan.
6) Fill centrifuge tubes to 25 mL with 1.85 SPT and add 12 glass beads. Resuspend soil pellet and shake on low for 18 hours.
7) After shaking, rinse tube cap and side with SPT, and then balance tubes and centrifuge at 2325 RCF for 30 minutes.
8) Using a vacuum filter, aspirate the light fraction and SP T over a 20-µm nylon filter.
9) Transfer light fraction from filter to pre-weighed pans using a squirt bottle, and place pans in the 60 ^{o}C oven to dry.
10) Add DI water to the centrifuge tube up to the 30-mL line and resuspend the pellet. Rinse cap and sides, then balance and centrifuge for 20 minutes at 2325 RCF.
11) Pour supernatant off, and repeat the processes, adding water, suspending the pellet, and then centrifuging for 20 minutes at 2325 RCF. Repeat rinsing process one more time.
12) After rinsing, add water to 20 mL line, suspend pellet, and separate fractions by size, as described in steps 5–11 in **Box 2**.

Materials Required

- Pre-weighed 50-mL conical centrifuge tubes
- 0.5% sodium hexametaphosphate
- Pre-weighed weighing pans
- 2000-and 53-µm sieves
- DI water
- Large, shallow pan
- Centrifuge
- Oscillating shaker
- 4-mm beads
- Sodium polytungstate
- Filtration unit
- 20-µm nylon filter

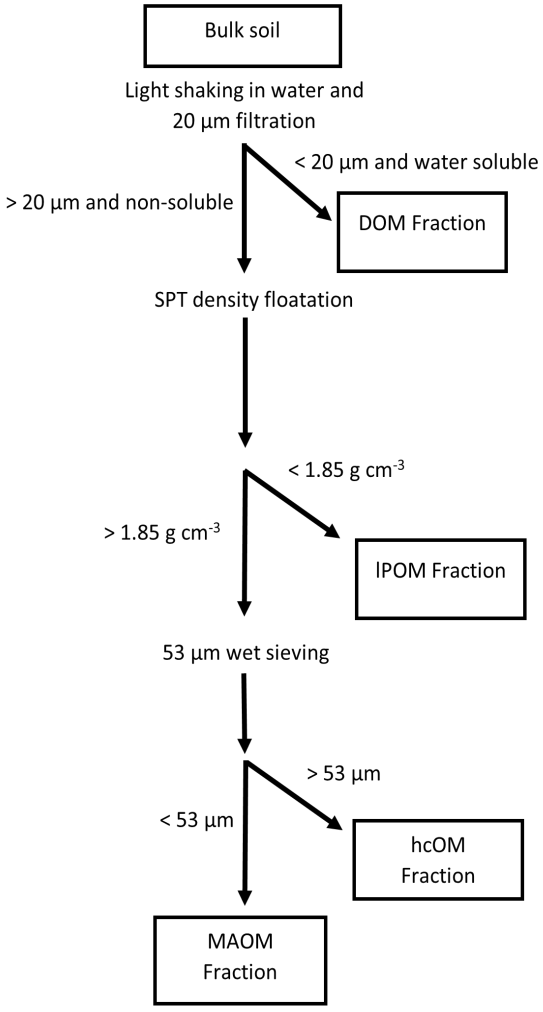

Figure 2.5- Methods for combined density and size fractionation of primary SOM fractions.

Chemical Free Physical Fractionations

There has been some recent research towards the development of chemical free physical fractionation methods because of the complications that can arise with chemical dispersants and density floatation media (Kaiser et al., 2010). As mentioned above, fractionation methods that immerse soils in any liquid can lead to redistribution of carbon between fractions, therefore, these methods present an alternative to the use of SHMP or SPT, possibly reducing the risk of carbon redistribution. This method uses a series of nested sieves, separating particles into six particle classes, ranging from 2 to < 0.315 mm. Soils are sieved prior to analysis, but not otherwise dispersed. A glass petri dish is then charged by rubbing it with cotton, and each particle class is placed separately on a clean stone plate. The charged petri dish is then place 2–5 cm above the stone plate and moved slowly over the sample. The distance between the charged surface and the size fractions must be calibrated manually for each sample to avoid the attraction of mineral particles. Following the attraction step, organic fractions must be examined visually for mineral contamination, and mineral particles removed. This procedure is then repeated five times for each fraction.

When tested across several arable and forest soils, this method resulted in considerable variation in the amount of organic matter separated from each of the sieved mineral fractions (Coefficient of Variation: 0.3–174%; Kaiser et al., 2009). However, when examined across mineral fractions, the variability accorded with the reproducibility reported for size and density fractions. Taken in tandem, these measures indicate a useful methodology for the separation of POM and MAOM but may be limited in their ability to separate different POM fractions (i.e., occluded vs. free POM). These methods are not as widely tested as those presented in previous sections but represent an interesting and important line of inquiry that should be further explored by research

groups. Given the potential drawbacks associated with sonication, shaking, and the use of SPT, non-aqueous non-dispersive methods may provide increased insight into SOM pools moving forward, as well as the role of SOM in facilitating N exchange. However, the time needed per sample, together with the requirement of manual calibration during each successive pass with the charged petri dish makes these methods cumbersome when dealing with large sample sizes.

Conclusions

Physical fractionation methods provide a means for researchers to isolate functionally distinct fractions of SOM. Unlike chemical and biological fractionation methods, physical fractionation methods take advantage of the inherent properties of both soil particles and organic material to separate SOM with different formation pathways, mechanisms of stabilization, and thus responsiveness to changes and overall persistence. Here we have reviewed several different possible methods for physical fractionations, including those based on particle size, particle density, and aggregate size. All have their pros and cons, and recovery of fraction mass and carbon (or nitrogen) need to be quantified at the end and reported. The methods examined provide a good foundation for functionally meaningful SOM fractionation, and we hope will continue to be improved and expanded upon by researchers moving forward. There are still important research questions that remain unanswered, such as the relationship between efficacy of the fractionation method and soil physiochemical properties, and if what we separate today as 'primary' fractions are indeed unique functional units (e.g., POM and MAOM), or are made of contrasting functional structures requiring further separation (e.g., exchangeable and stable MAOM). Continuation of this research will improve the tools at our collective disposal and advance this field further.

CHAPTER 3: CONTRASTING PROPERTIES OF SOIL ORGANIC MATTER FRACTIONS ISOLATED BY DIFFERENT PHYSICAL SEPERATION METHODOLOGIES[2]

Introduction

Physical soil organic matter (SOM) fractions present a useful means of simplifying the complex molecular composition of SOM into functionally distinct components (Cotrufo and Lavallee, 2022). While different studies often isolate fractions specific to their targeted inquiry, there is a growing interest in recognizing two physical SOM fractions as a basic framework under which questions related to SOM dynamics can be examined: particulate organic matter (POM), and mineral-associated organic matter (MAOM) (Billings et al., 2021; Lavallee et al., 2020). These fractions have conceptual definitions derived from their hypothesized formation pathways and stabilization mechanisms, as well as procedural definitions that arise from the methods used to isolate them (Leuthold et al., 2022a). The conceptual definition of POM can be understood as the portion of SOM composed of structural organic materials, such as the acid unhydrolyzable fraction of vegetative litter (Christensen, 2001b; Haddix et al., 2016) and, to a lesser extent, some types of microbial residue (Buckeridge et al., 2022; Witzgall et al., 2021). As a result of these primary constituents, POM is thought to have a higher carbon (C) to nitrogen (N) ratio than other physical SOM fractions (Cotrufo et al., 2019), and to possess a greater abundance of carboxylated aromatic and carbohydrate molecular groups (Calderón et al., 2011; Yu et al.,

[2] This published citation for this chapter is:
Leuthold, S., Lavallee, J.M., Haddix, M.L., Cotrufo, M.F., 2024. Contrasting properties of soil organic matter fractions isolated by different physical separation methodologies. Geoderma 445, 116870. https://doi.org/10.1016/j.geoderma.2024.116870

2022). Beyond occlusion in aggregate structures, the POM fraction lacks protection or stabilization mechanisms, and thus is considered to turn over relatively quickly. In contrast, MAOM is conceptually defined as low molecular weight organic compounds that have become associated with mineral surfaces or sequestered within highly stable microaggregate structures (Cotrufo and Lavallee, 2022; Kleber et al., 2015; von Lützow et al., 2008). These formation mechanisms stabilize organic matter in this fraction against microbial decomposition, such that MAOM is considered as a more stable and persistent fraction than POM (von Lützow et al., 2006). The molecular composition of MAOM is highly variable, consisting of a mixture of microbial necromass, extra polymeric substances, and polysaccharides, as well as soluble plant products such as root exudates and materials leached from litter. However, MAOM typically possesses a lower, more constrained C:N ratio than POM (Angst et al., 2021; Kleber et al., 2015; Sokol et al., 2019; Whalen et al., 2022). Divergence in the constituent chemistry, formation pathways, and microbial accessibility of these two SOM components supports their use as the foundation of a conceptual framework surrounding SOM dynamics (Lavallee et al., 2020).

Typically, fractionation methodologies take advantage of the covariation in physical properties of SOM (e.g., particle size, particle density) with the chemical composition and formation mechanisms of various conceptual fractions to isolate relatively distinct SOM pools (Leuthold et al., 2022a). Fractionations based on particle size divide soils based on a predetermined size cutoff, with the intention of isolating the fraction of SOM that is sorbed to reactive silt- and clay-sized particles (i.e., MAOM) from that which is not associated with those particles (i.e., POM). Size cutoffs vary (typically between 63-20 μm) across regions and institutional traditions, with some researchers isolating both silt and clay particles to represent the MAOM (e.g., Elliott and Cambardella, 1991; Leuthold et al., 2022), and some isolating only clay particles (e.g., Just et al.,

2021). Particle density fractionations take advantage of the relatively high density of mineral particles and anything sorbed to them (i.e., MAOM), in contrast to the low density of the free organic material (i.e., POM), separating them via floatation in a heavy liquid (liquid densities typically ranging from 1.6 – 1.9 g cm^{-3}; Cerli et al., 2012). These two methods can be combined, as well as repeated with sequential cutoffs to isolate additional fractions of interest (e.g., Moni et al., 2012; Sollins et al., 2009). Thus, in addition to the conceptual definitions of SOM fractions that rely on formation and function, POM and MAOM also have procedural definitions, such that POM is often > 53 μm or < 1.85 g cm^{-3} and MAOM is < 53 μm or > 1.85 g cm^{-3} (Lavallee et al., 2020a). To effectively use SOM fractions to advance understanding, fractionation procedures and the procedural definitions therein must be designed to isolate fractions that correspond well with the conceptual definitions.

For a procedural fraction to map well onto its associated conceptual definition, a level of uniqueness in chemical composition and biogeochemical function is required. Previous work has investigated the ability of a range of fractionation techniques to isolate discrete SOM fractions, using a variety of different metrics to determine how unique one fraction is from another (Elliott et al., 1996; Moni et al., 2012; Poeplau et al., 2018; Smith et al., 2002). For example, Curtin et al. (2019) assessed a procedural POM fraction as isolated by size (particle size > 50 μm), and found it to be neither unique or homogenous in formation mechanisms or molecular composition, concluding that it could not serve as a useful model pool. In contrast, Just et al. (2021) examined procedural POM and MAOM fractions isolated by size (POM > 20 μm), and found the two procedural fractions to be sufficiently unique based on estimates of turnover time. Assessments of fractionations that employ density separations have found different results still-- Sohi et al. (2001) examined SOM fractions isolated by both size and by density and found that while

particle size fractions often represented composites of both POM and MAOM, a fractionation that employed two density flotations isolated three fractions with distinct O-alkyl/alkyl-C ratios. Similarly, Demyan et al. (2012) found differences in the relative peak area of 4 density fractions analyzed by diffuse reflectance infrared Fourier transformed (DRIFT) spectroscopy, which the authors interpreted to indicate sufficiently unique levels of SOM stability. As evidenced by this range of contrasting results, the challenge of linking these conceptual definitions with a coherent procedural definition persists, despite the previous research on the matter.

As more researchers continue to adopt physical SOM fractionations as a means for understanding soil health, soil biogeochemical function, and soil C dynamics, there are some growing pains that operationalizing this relatively simple, dichotomous conceptualization must reckon with. The minimum necessary complexity for fractionation schemes to be effective is a key remaining question, especially as investigations of larger SOM fraction datasets become more commonplace (Begill et al., 2023; Cotrufo et al., 2019a). Given the number of samples required for accurate estimation of C stocks, especially in heterogeneous landscapes (Stanley et al., 2023), identifying SOM fractionation protocols which assign priority equally to both accuracy and throughput is a priority. If such fractionation protocols can be established, they further require assessment regarding their effectiveness across soils with different physicochemical properties. While several recent studies have assumed that SOM fractionation techniques are equally effective across variable soil types and characteristics without explicitly examining this assumption (Cotrufo et al., 2019; Georgiou et al., 2022; Heckman et al., 2022), soil properties may skew the results of analyses if not accounted for. A simple fractionation method that is robust to differences in soil characteristics therefore presents a powerful tool for researchers, however it has yet to be identified through testing.

Here we combine spectral, isotopic, and chemical characteristics of SOM fractions isolated by various SOM physical fractionation techniques in an attempt to identify the best procedure to isolate procedural POM and MAOM fractions consistent with their conceptual definition. Specifically, we have three objectives: 1) identify a single-step fractionation method isolates SOM fractions with the most distinct characteristics, 2) understand how soil properties such as texture, pH values, and Fe and Al oxide content influences the outcomes of various physical fractionation procedures, and 3) determine the similarities and differences in fractions that vary in their separation procedures but share the same conceptual definition in an attempt to improve understanding across methodologies. Using a variety of agricultural soils with variable textures, pH values, and parent materials, we compare four commonly used fractionation procedures: a separation of POM from MAOM by size or by density, and a separation by density and size, with full dispersal prior to fractionation, and a separation by size and density with dispersion delayed until after the removal of the free POM fraction. By combining disparate lines of evidence with a range of soils and methodologies, we provide an improved understanding of the common procedural fractions best representing current SOM biogeochemistry frameworks.

Materials and Methods

Soil Processing and Characterization

We obtained soils from agricultural experiment sites across the continental United States (Table 3.1). We chose to focus on agricultural soils for a number of reasons—while physical fractionation methods have been used for several decades to better understand SOM dynamics, their application in agronomic research is actively growing (Bowles et al., 2022; Jilling et al., 2020; Schipanski and Drinkwater, 2011), and agricultural soils are the target of most current large scale, high throughput fractionation projects. Further, regardless of fractionation technique,

Table 3.1: Site characteristics and measured soil properties for the samples used in this study.

Sample	USDA Soil Classification	MAP (mm)	MAT (°C)	Bulk soil organic C (%)	pH	Sand (%)	Clay (%)	OE Al Oxides (g kg^{-1} Soil)*	OE Fe Oxides (g kg^{-1} Soil)*
1	Udic Argiustoll	798	15.1	1.15	5.52	18.8	20.1	6.75	4.06
2	Aeric Epiqualf	1015	11.0	2.10	6.56	18.6	47.0	10.77	9.45
3	Typic Argiaquoll	1258	12.1	1.52	6.17	14.5	19.3	8.64	17.04
4	Fragic Glossaqualf	1005	10.2	2.11	6.07	25.7	38.2	9.91	20.95
5	Aquic Hapludelf	1048	10.5	1.35	5.51	20.6	43.0	7.48	27.43
6	Typic Paleudult	1336	14.4	2.24	6.81	25.9	49.6	11.31	7.95
7	Typic Ustipsamments	557	9.3	1.66	5.64	5.2	23.1	5.30	17.59
8	Typic Dystrudepts	1259	10.2	0.96	6.11	27.3	5.9	6.53	13.88
9	Typic Argiustoll	425	6.7	1.48	8.52	10.6	38.9	9.24	7.27
10	Humic Dystrudept	1406	15.6	1.84	5.53	30.4	35.9	8.85	7.60
11	Spodic Psammaquent	1428	22.4	0.41	5.56	95.9	2.0	1.88	2.38

*OE: Oxalate extractable

the POM fraction represents a relatively minor component of the agricultural SOM pool (Lugato et al., 2021; Vos et al., 2018), such that identifying methods of isolating a homogenous and scientifically useful POM fraction in systems where POM abundance is low is critical for understanding the linkages between this fraction and cropping system performance. While the soils we show here are not inclusive of all potential cropland soils, they do capture the central tendency of textures, pHs, and organic C for agricultural soils in the US (Table 3.1, Supplemental Figure 3.1).

Climate data for the sites were retrieved from local climate stations located at or near the soil sample location (Table 3.1). For samples retrieved from research farms, on-site meteorological data was retrieved. For samples retrieved from production fields, Mesonet data were used to calculate mean temperatures and precipitation. The mean annual temperature of the sites ranged from 6.7 to 15.6 ºC, and the mean annual precipitation ranged between 425 – 1428 mm. We characterized soil texture, which ranged between 5.2 - 95.9% sand, on air-dried, 2-mm sieved soils using the pipette method (Soil Survey Staff, 2022). Soil pH, measured using a Mettler Toledeo SevenDirect SD20 (Mettler Toledo, Columbus, OH) on a 1:1 soil water mixture, ranged between 5.5 - 8.5. We extracted the amorphous and poorly crystalline pools of Fe and Al oxides via acid ammonium oxalate extraction following Loeppert and Inskeep (1996). Oxalate-extractable Fe and Al oxide concentrations were quantified via inductively coupled plasma optical emission spectrometry (ICP-OES; PerkinElmer, Waltham, MA, USA), and ranged between 1.9-11.3 g Fe kg soil^{-1} and 2.4-27.4 g Al kg soil^{-1} (Table 3.1).

SOM Fractionation and Processing

While we acknowledge that none of the procedural fractions we discuss here map perfectly onto their conceptual definitions, we use the conceptual pool names to refer to the fractions we isolate throughout the rest of the manuscript for ease of communication, with subscripts to denote the fractionation technique that yielded the specific procedural fraction.

Size Fractionation

The size fractionation method employed in this study is similar to the methodology described in Leuthold et al. (2022a), adapted from Cotrufo et al. (2019). Soils were air dried and then sieved to 2 mm. Immediately prior to analysis, an 8 g subsample was oven-dried overnight at 60 °C to evacuate any residual ambient soil water. Thirty-five milliliters of dilute (0.5%) sodium hexametaphosphate (SHMP) was then added to the subsample, along with twelve ~4 mm glass beads. The samples were shaken at 112 rpm on a reciprocal shaker for 18 hours. The dispersed soil was then rinsed onto a 53 µm sieve, with all material that passed through the sieve considered MAOM (< 53 µm), and all material that remained on top of the sieve considered POM (> 53 µm), subsequently referred to as $MAOM_{Size}$ and POM_{Size}, respectively.

Density Fractionation

The density fractionation used in this study is adapted from the density fractionation procedure originally developed by Golchin et al. (1994). Air dried, 2 mm sieved soils were oven dried at 60 °C overnight to remove ambient moisture. Thirty-five mL of sodium polytungstate (SPT) was brought to a density of 1.85 g cm^{-3} and added to 8 g of the oven-dried soil, along with twelve ~4 mm glass beads. The samples were shaken for 18 hours on a reciprocal shaker at 112 rpm to disperse soil aggregate structures. Following dispersion, the soil solution was centrifuged at 2325

relative centrifugal force (RCF) for 20 minutes. After centrifugation, the supernatant containing the light fraction which had a density < 1.85 g cm^{-3} was aspirated via a vacuum filtration apparatus. The light fraction was then thoroughly rinsed with DI water and placed in the oven at 60 °C to dry to a constant weight. This fraction was designated as $POM_{Density}$. To remove any SPT that may have remained in the heavy fraction, the remaining soil was resuspended in DI water and then centrifuged again at 2325 RCF for 25 minutes. The supernatant was poured off, and this process was repeated two more times. The sample was then transferred to the oven and dried at 60 °C to a constant weight. Moving forward we refer to this fraction as $MAOM_{Density}$.

Combined Size Density 1 (Initial Dispersal)

The CSD1 fractionation method was adapted from Mosier et al. (2019) and is discussed in detail in Leuthold et al. (2022a). Eight grams of air dried, 2 mm sieved soils were oven dried overnight at 60 °C. Twenty-five mL of SPT (density = 1.85 g cm^{-3}) was then added to the oven-dried soils along with twelve ~4 mm glass beads, and the soils were shaken on a reciprocal shaker for 18 hours at 112 rpm to fully disperse secondary soil structures. The dispersed soil-SPT solution was then centrifuged at 2325 RCF for 20 minutes, after which the light fraction (< 1.85 g cm^{-3}) was aspirated off via vacuum filtration, rinsed with DI water and dried to a constant weight at 60 °C. This fraction is subsequently referred to as POM_{CSD1}. The remaining soil was resuspended and rinsed three times, as described above. After rinsing, the soil was resuspended in DI water once more, and separated via wet sieving on a 53 µm sieve into organic matter associated with a coarse, heavy soil fraction ($CHAOM_{CSD1}$; > 53 µm, > 1.85 g cm^{-3}), and a $MAOM_{CSD1}$ (< 53 µm, > 1.85 g cm^{-3}). The samples were then placed in the oven and dried to a constant weight at 60 °C.

Combined Size Density 2 (Delayed Dispersal)

The CSD2 fractionation method used to separate the non-occluded POM fraction (POM_{CSD2}, often referred to as the "free" POM), from the OM associated with the coarse heavy soil fraction and the occluded POM (we refer here as $CHAOM_{CSD2}$) and $MAOM_{CSD2}$ was adapted from the methods described by Haddix et al. (2020). Similar to the density fractionation methods described above, 25 mL of 1.85 g cm^{-3} SPT was added to 10 g of oven-dried, 2 mm sieved soil. The soil solution was then placed in a vacuum chamber (vacuum pressure = 20 psi) for 10 minutes to evacuate any air trapped with aggregate structures. Following air evacuation, samples were centrifuged at 2325 RCF for 30 minutes. The "free" POM fraction (POM_{CSD2}; < 1.85 g cm^{-3}, outside of aggregate structures) was then aspirated using a vacuum filtration system, rinsed with DI water, and placed in the oven at 60 °C till dried to a constant weight. The remaining soil was then resuspended in DI water and rinsed three times as described above. After rinsing, twelve ~4 mm glass beads were added to the soil samples, along with 30 mL of 0.5% SHMP. The samples were then shaken on a reciprocal shaker for 18 hours at 112 rpm. After dispersal, the samples were wet sieved to separate the occluded POM + coarse heavy fraction ($CHAOM_{CSD2}$; > 1.85 g cm^{-3} or originally trapped with aggregate structures, and > 53 μm) and the MAOM fraction ($MAOM_{CSD2}$; > 1.85 g cm^{-3}, < 53 μm), and placed in the oven at 60 °C.

Fraction Processing, C & N Concentrations, and Isotopic Analysis

After fractions were dried to a constant weight, the samples were weighed, and their mass recovery assessed. Mass recoveries between 95 and 105% were deemed acceptable, and samples falling outside of these bounds were fractionated again using the same methods until mass recovery was found to be acceptable. Fractions were then finely ground using a mortar and pestle. The sample C and N concentrations and their stable isotope compositions ($\delta^{13}C$ and $\delta^{15}N$)

were determined via an elemental analyzer coupled to an isotope ratio mass spectrometer (EA-IRMS, VarioIsotope Cube - Isoprime precision, Elementar, Langenselbold, Hesse, Germany). Samples were tested for inorganic carbonate presence by addition of 1 M HCl following the procedure for inorganic C quantification employed by the US Natural Resources Cooperative Services (Protocol 4E1a1a1a1-2; Soil Survey Staff, 2022). Samples that exhibited effervescence were acid fumigated for 6 hours prior to EA-IRMS analysis (Harris et al., 2001). Only one sample, sample 9, exhibited effervescence and was fumigated. Given that acid fumigation has been shown to alter the $\delta^{15}N$ signature (Harris et al., 2001), we analyzed both acid fumigated and non-fumigated samples, and present the $\delta^{15}N$ values derived from the non-fumigated, and organic C concentrations and $\delta^{13}C$ values from the fumigated samples.

Fourier Transformed Infrared Spectroscopy

Spectral characterization of SOM fractions

The spectral characteristics of bulk soils and physical SOM fractions were obtained via scanning in the mid-infrared spectral region. Roughly 40 mm^3 of finely ground sample was added to a 6 mm diameter well in a 96 well plate. Using a 6 mm dimeter rod, samples were then pressed to create an even surface, and excess sample removed using a micro-vacuum system. Each sample was then scanned 32 times at a spectral resolution of 4 cm^{-1} from 7500 to 600 cm^{-3} using a VERTEX 70/HTS-XT Fourier transform infrared spectrometer (Bruker Optics Inc., Billerica, MA, USA). Prior to scanning each sample, a reference spectrum was obtained by a gold-filled reference well. The spectrometer used to obtain absorbance data used a mercury cadmium telluride detector which was cooled using liquid N.

Samples were scanned in quadruplicate, except when sample mass fell below the amount necessary for replication which were scanned as duplicates. To assess the accuracy of each sample's scans, a reference spectrum for each sample was selected (typically the first of the 4 replicates scanned). The correlation between the absorbance of the reference spectrum and the remaining spectra was assessed, and if any correlation between the spectra of a given fell below 0.996, those samples were rejected and rescanned. If the correlations passed the 0.996 threshold, the four (or two) replicates were averaged together to determine final spectral values for the sample. Following sample assessment, spectra were trimmed to encompass only the region between 4000 and 600 cm^{-1}.

Spectral subtraction

To isolate the organic spectral signatures in samples composed of both mineral and organic substrates (i.e., CHAOM, MAOM, and POM_{Size}), we employed a spectral subtraction technique as reviewed by Margenot et al. (2016) to subtract the spectra of the mineral components from those of the corresponding full fractions. Briefly, an approximately 500 mg subsample of finely ground fraction was ashed at 550 ^{O}C for 20 minutes, and then allowed to cool to room temperature. These samples were then analyzed for spectral characteristics as described above and subjected to the same quality control procedure. Once the spectra of the ashed samples were aggregated, they were baseline corrected using the basline() function in the *prospectr* package (version 0.2.6) in R version 4.2.2 (Stevens and Ramirez-Lopez, 2022). The corresponding non-ashed spectra was similarly baseline corrected prior to subtraction. To minimize artifacts during the subtraction process, a subtraction factor was derived for each sample by minimizing the average absorbance in spectral bands representing mineral bonds after subtraction. Specifically, we aimed to minimize the absorbance in the bands between 1800 and 2000 cm^{-1}, which can

represent the quartz overtones present in mineral soils (Margenot et al., 2019). The derived subtraction factors ranged from 0.85 – 0.99. After derivation of the subtraction factor, the ashed spectra was subtracted from the original spectra as described in Eq. 3.1:

$$Organic\ Spectra = Spectra_{Ashed} - \left(Spectra_{Reference} \times SF\right) \quad \text{(Eq. 3.1)}$$

where $Spectra_{Ashed}$ is the baseline corrected spectral signature after organic removal, $Spectra_{Reference}$ is the spectra from the unaltered sample, and SF is the derived subtraction factor.

Data analysis

Fraction C, N, and C:N ratio

We used linear mixed models to test for differences in C and N concentrations and C:N ratios within a given fraction due to fractionation method. The mixed models were built using the *lme4* package in R (v.1.1-31; Bates et al., 2015), and evaluated using the anova() function in the *stats* package (v. 4.2.2; R Core Team, 2022). The linear models met the assumptions of the ANOVA; homogeneity of variance for the models was assessed using the leveneTest function in the *car* package (Fox and Weisberg, 2019), and that residuals were normally distributed was confirmed using the shapiro.test function in the *stats* package. Pairwise comparisons between the different fractionation methods were made via examinations of contrasts using the *emmeans* package (Lenth, 2022). Model structure was such that fractionation method was a fixed effect, and the sample ID was included as a random effect. We chose to include sample as a random effect as we wanted to account for the differences in soil properties such as texture and mineralogy among our various soils but were not interested in testing those variables as main effects in this set of analyses.

Within Fractionation Isotopic Differences

As the isotopic value of a given soil fraction is mediated by the isotopic composition of incoming litter (e.g., via differences in C_3 vs. C_4 photosynthetic pathways), rather than examining isotopic signatures of fractions across soils, we examined the difference between the isotopic signatures of the MAOM and POM fractions of a given sample isolated by a given methodology. We employ the term isotopic difference (ID) to describe this relationship. Importantly, we did not calculate an isotope discrimination factor between MAOM and POM since we do not want to imply a C direct transfer between these two fractions. We examined the $ID_{MAOM\text{-}POM}$, defined as the difference between the $\delta^{13}C$ values of the MAOM and the POM fractions for a given sample, across all 4 fractionation methodologies. In this context, positive ID values indicate that the MAOM fraction is ^{13}C enriched, whereas negative values indicate that it is ^{13}C depleted, relative to the POM fraction. ID values of 0 indicate no difference in the $\delta^{13}C$ of the two fractions.

Principal Component Analysis of Spectral Data

Principal component analysis (PCA) was used to assess the differences between spectral characteristics of the SOM fractions. The scanned wavenumbers were reduced into two dimensional PCA space, and the separation of the fractions assessed. Samples were scaled and mean centered prior to analysis. To understand the distribution of sample scores across the principal components, we investigated the component loadings for PCA axis 1 and PCA axis 2 across all wavenumbers in the trimmed spectral dataset, with deviation from 0 indicating the relative importance of those bands in determining a samples position in PCA space. We also used PCA to examine the separation of the fractions after the removal of mineral spectral bands via spectral subtraction of the ashed fractions, using a similar methodology to that described above.

The PC analyses for both the ashed and unashed soils was conducted in R v 4.2.2 using the PCA function in the *FactoMineR* 2.3 package (Lê et al., 2008).

Dissimilarity analysis of SOM fraction spectral data

To understand the influence of soil physicochemical properties on the characteristics of procedural fractions isolated by various physical fractionation methods, we used a permutational analysis of variance, with dissimilarity matrices built using the full range of spectral data obtained for each fraction (i.e., 4000 – 600 cm^{-1}). The dissimilarity matrix was constructed using the vegdist function in the *vegan* package in R v 4.2.2 (Oksanen et al., 2022; R Core Team, 2022), and the PERMANOVA analysis was performed using the adonis2 function, also contained within the *vegan* package. While the main effects of fractionation and soil physiochemical property (e.g., sand, clay, oxalate-extractable Al oxides, etc.) may have a significant impact on the spectral characteristics of the SOM found within a procedural fraction, we focused on the interaction between these main effect terms, such that a significant interaction would indicate that the dissimilarity between samples was a result of a given fractionation method under a set of soil conditions. Sets of fractions that represent a given fractionation representation of a conceptual fraction (e.g., POM_{Size}, $POM_{Density}$, POM_{CSD1} and POM_{CSD2}) were analyzed together. Significant interactions were interpreted as those with a p-value < 0.05.

Results

Carbon and Nitrogen in SOM Fractions

Carbon and Nitrogen Concentrations

Relative C concentrations varied amongst the fractions isolated by the different procedures (Figure 3.1A). Fraction %C values ranged from 0.1 – 38.5%, 0.0 – 2.1%, and 0.6 – 8.2%, for the

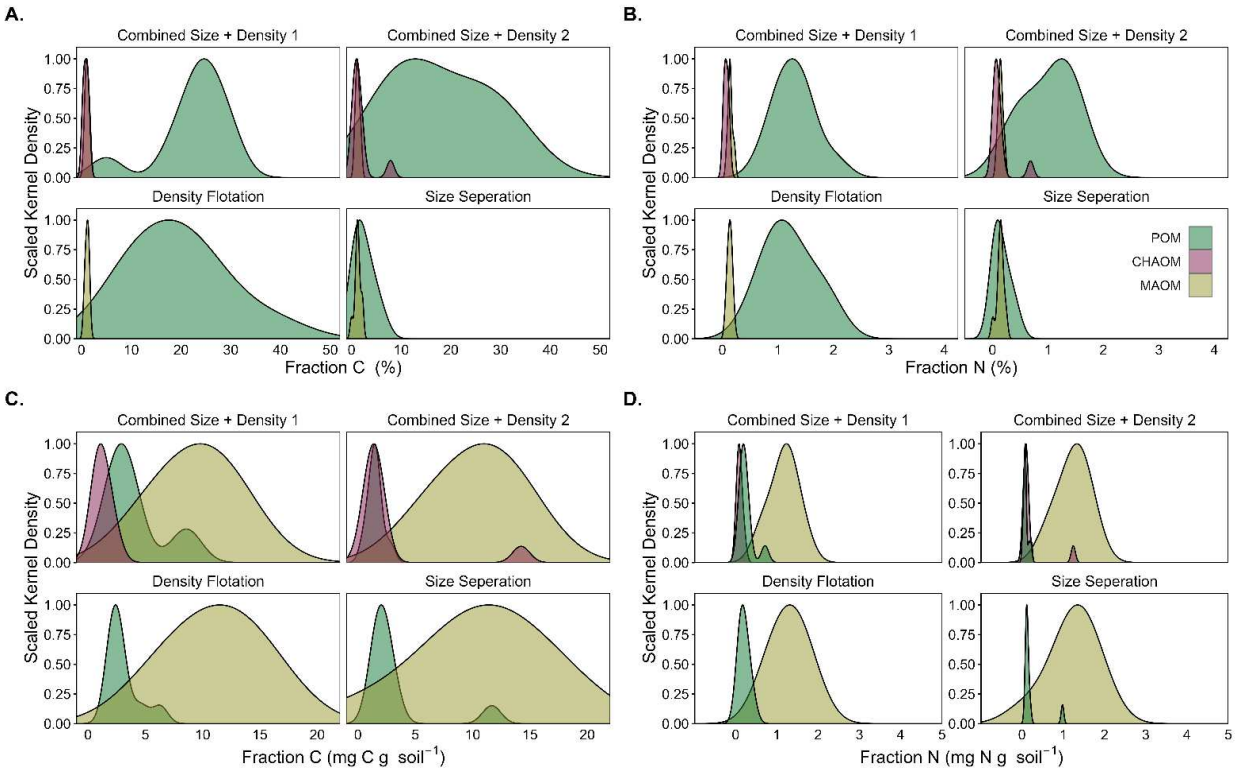

Figure 3.1 – Carbon and nitrogen concentrations on a relative basis (Panels A and B), and an absolute (Panels C and D) for all fractions isolated by various techniques. Within a panel, an individual graph shows the distribution of C and N values with a fraction for a given fractionation. The different isolated procedural fractions are indicated by different colors (POM: Green; CHAOM: Purple; MAOM: Khaki).

POM, CHAOM, and MAOM fractions, respectively. Of the fractionations we evaluated here, only the CSD1 and CSD2 isolated a CHAOM fraction. We observed some evidence that the presence of the occluded POM fraction within $CHAOM_{CSD2}$ fraction increased the %C value relative to the $CHAOM_{CSD1}$; the average $CHAOM_{CSD2}$ C concentration was 1.0 ± 0.2%, while the average $CHAOM_{CSD1}$ C concentration was only 0.8 ± 0.2%, a marginally significant difference ($p = 0.07$; Figure 3.1A). Despite a substantial range in values when examining relative %C values, normalization of the fraction C by fraction mass led to more constrained values within fractions across fractionation schemes (Figure 3.1C). When normalized by fraction mass (i.e., accounting for mass contribution of each fraction to the bulk soil), fraction C concentrations ranged from 0.5 – 11.7 mg POM C g soil^{-1}, 0.02 – 2.5 mg CHAOM C g soil^{-1}, and 0.1 – 17.7 mg

MAOM C g soil^{-1}. POM-C varied somewhat by fractionation method, ranging from an average of 1.3 ± 0.2 mg C g soil^{-1} for POM_{CSD2} to 3.9 ± 0.7 mg C g soil^{-1} for POM_{CSD1}. Pairwise comparisons indicated a significant difference between the absolute C concentrations of POM isolated by the CSD1 method compared to the other methods, but the effect size was relatively subdued ($p < 0.001$; Figure 3.1C). Average absolute MAOM C concentrations were generally consistent across fractionation methods, though tended to be higher in the one-step methods ($MAOM_{Density}$: 10.2 ± 1.3, $MAOM_{Size}$: 10.0 ± 1.8, $MAOM_{CSD1}$: 8.6 ± 1.1, $MAOM_{CSD2}$: 9.5 ± 1.3 mg MAOM C g soil^{-1}).

Relative fraction %N was more constrained than %C, but still showed marked variation among fractions. In the POM fraction, %N ranged from 0.01% to 2.0%. The CHAOM and MAOM fractions exhibited less variability, with %N ranging from 0.01% to 0.2%, and 0.0% to 0.5%, respectively (Figure 3.1B). In the POM_{Size} and $MAOM_{Size}$ fractions, the average fraction %N values were similar (0.1 ± 0.04 and 0.2 ± 0.04%, respectively). In contrast, methods that employed a density separation step isolated POM fractions with relative N concentrations an order of magnitude higher than those in the MAOM fraction ($POM_{Density}$: 1.1 ± 0.2%, POM_{CSD1}: 1.2 ± 0.1%, and POM_{CSD2}: 0.9 ± 0.2%). The $MAOM_{Density}$ had an average relative N concentration of 0.2 ± 0.02%, similar to the average relative N concentrations of the $MAOM_{CSD1}$ (0.2 ± 0.02%), $MAOM_{CSD2}$ (0.2 ± 0.02%), and $MAOM_{Size}$ (0.2 ± 0.04%). The $CHAOM_{CSD1}$ fraction had an average %N value of 0.1 ± 0.01%, which was not significantly different than the $CHAOM_{CSD2}$ fraction with a %N value of 0.1 ± 0.02% ($p = 0.22$). Similar to the patterns observed for C, normalizing the fraction N by fraction mass constrained the range of values across fractions, minimizing the differences due to the dilution effect of soil particles inclusion in some fractions (Figure 3.1D). The range of absolute N concentrations was between 0.02 and 1.0

mg N g soil^{-1} in the POM fractions, 0.02 to 0.2 mg N g soil^{-1} in the CHAOM fractions, and 0.04 to 1.9 mg N g soil^{-1} in the MAOM fractions. Similar to the observations across fractionation techniques for absolute C concentrations, the MAOM fraction was relatively homogenous across methods; the average absolute N concentrations for the $MAOM_{Size}$ was 1.1 ± 0.2 mg N g soil^{-1}, whereas the average absolute N concentration for the $MAOM_{CSD1}$, $MAOM_{CSD2,}$ and $MAOM_{Density}$ fractions were 1.1 ± 0.1, 1.1 ± 0.2, and 1.2 ± 0.2 mg N g soil^{-1}, respectively. The difference between the size fractionation and those that employed a density separation was significant only when comparing the $MAOM_{Size}$ and $MAOM_{CSD1}$, however (p = 0.01).

Fraction C:N Ratios

The C:N ratios of the fractions isolated were more consistent across fractionation schemes than the C or N concentrations (Figure 3.2). The MAOM fractions had the lowest average C:N ratios across fractionation schemes (8.8 ± 0.38), followed by the CHAOM (13.4 ± 0.37), and then the POM (17.3 ± 0.68). Within the MAOM fractions, the C:N ratio ranged from 7.0 – 10.2, with the one-step fractionations having more similar average C:N ratio ($MAOM_{Density}$: 8.9 ± 0.4, $MAOM_{Size}$: 8.8 ± 0.2) than the combined fractionations ($MAOM_{CSD1}$: 8.6 ± 0.7, $MAOM_{CSD2.}$: 9.1 ± 0.8). The CHAOM fraction C:N ratios ranged from 10.1 – 16.0 and exhibited a significant distinction between the $CHAOM_{CSD1}$ and the $CHAOM_{CSD2}$ methodologies (12.7 ± 0.5 and 14.3 ± 0.5, respectively; p-value = 0.014), further reinforcing the role of the occluded POM fraction in differentiating the CHAOM fractions. The POM fractions had the most variability in its C:N ratios both within and across fractionation schemes, partially reflecting the differences in characteristics of the plant inputs among the sites surveyed, as well the composite nature of the POM_{Size} fraction (Figure 3.2). Across fractionations, the observed POM C:N ratios ranged between 6.3 and 27.9. Similar to the MAOM, differences were observed between the single step

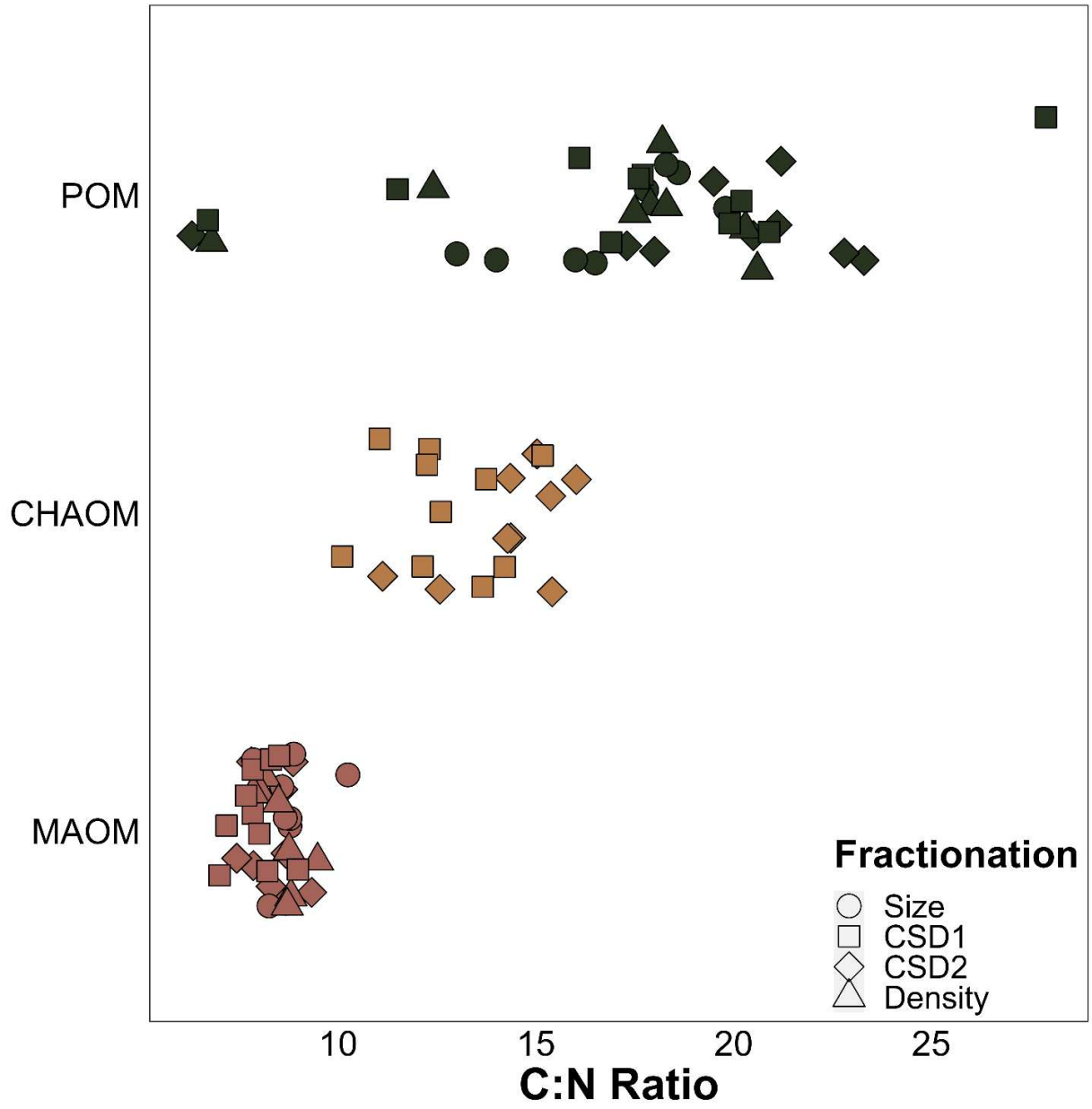

Figure 3.2 – Carbon to nitrogen ratios of the procedural fractions isolated by the various physical fractionation techniques. Different color-shape combination indicates different fractionation procedures. Note that the points have been jittered along the y-axis to increase readability.

and the combined methodologies—average C:N ratios for the POM_{Size} and $POM_{Density}$ samples were 16.6 ± 0.9 and 16.2 ± 1.3, respectively. In contrast, the combined fractionations yielded a

higher POM C:N ratio on average (POM_{CSD1}: 17.4 ± 1.6, POM_{CSD2}: 18.9 ± 1.5), though these differences among fractionation method were not significant (p -value = 0.495).

Carbon and Nitrogen Recovery

On average, the size fractionation had the highest C and N recovery, with 98.2 ± 6.0 % and 90.8 ± 6.1% of the initial sample C and N recovered, respectively (Supplemental Figure 3.2). This likely reflects the lack of a rinsing step in the size fractionation procedure; all potentially solubilized organic matter should be contained within the sample during this method. In contrast, the CSD2 fractionation, which has both an additional shaking step during dispersal and several rinsing steps to eliminate SPT contamination, had the lowest average C and N recovery, with only 88.0 ± 2.6% of initial C and 86.6 ± 2.8% of initial N recovered. Similar N recoveries were observed in the density and the CSD1 fractionation (82.0 ± 6.4 and 81.3 ± 5.4%, respectively), though carbon recovery following these fractionations was higher (90.0 ± 5.4 and 91.3 ± 5.3%, respectively) than for CSD2.

Despite average recoveries that are consistent with values often reported in the literature, there was some evidence that soil physiochemical properties had an effect on recovery level within a given fractionation, as we observed wide ranges in C and N recovery for individual samples across fractionation schemes. For instance, the C recovery for the single-step fractionation methods ranged from 70.3% - 126.2% for the density fractionation, and 73.0% - 134.0% for the size fractionation. Similar results were observed for N (72.4 – 126.0% for density, and 76.0 – 132.0% for size; Supplemental Figure 2). Combined fractionations generally had lower C and N recoveries, with the CSD1 fractionation ranging from 70.4 – 133.0% of C and 61.4 – 122.0% of N, and the CSD2 fractionation ranging from 71.9 – 97.4% of C, and 70.4 – 101.0% of N. Given that the bulk soil that is used as a reference for recoverable C and N, variation introduced during

the subsampling process could have resulted in aliquots for bulk soil that were more or less C and N rich than the aliquot used for fractionation, which may explain some of the range in recovery across methodologies.

SOM Fraction C & N Stable Isotopes Composition

Patterns in the isotopic composition of fractions

Across fractionation methodologies, the most negative $\delta^{13}C$ and $\delta^{15}N$ values were found in the POM fraction, and the least negative $\delta^{13}C$ and $\delta^{15}N$ values were found in the MAOM fraction (Figure 3.3). On average across fractionation schemes, POM $\delta^{13}C$ was -23.7 ± 0.4‰, CHAOM $\delta^{13}C$ was -23.6 ± 0.4‰, and MAOM $\delta^{13}C$ was -22.1 ± 0.3‰. Fractionation methodologies seemed to play a role in determining the resulting isotopic composition of some of the fractions, but not all three. Within the POM fractions, the POM_{Size} was more positive on average than fractionations that employed a density floatation, though this difference was not significant (p-value = 0.142). Average POM_{Size} $\delta^{13}C$ was -23.2 ± 1.0 ‰, whereas the $POM_{Density}$, $POM_{CSD1,}$ and POM_{CSD2} $\delta^{13}C$ values were -23.7 ± 0.7‰, -23.9 ± 0.9 ‰, and -24.2 ± 0.6‰ respectively. Within the MAOM, fractionation method did not lead to significant differences in the $\delta^{13}C$ values among the isolated fractions ($MAOM_{Density}$: -22.4 ± 0.6‰,, $MAOM_{CSD1:}$ -22.3 ± 0.6‰, $MAOM_{CSD2}$: -22.1 ± 0.5‰, and $MAOM_{Size}$: -21.6 ± 0.8‰; p-value = 0.766). The CHAOM $\delta^{13}C$ was also similar between fractionation methods; $CHAOM_{CSD1}$ had an average $\delta^{13}C$ value of -23.8 ± 0.8‰ and the $CHAOM_{CSD2}$ $\delta^{13}C$ value was -23.4 ± 1.0‰ (p-value = 0.674; Figure 3.3).

Nitrogen isotopic composition followed trends in C isotopes, with the MAOM fraction having the highest ^{15}N enrichment, with an average $\delta^{15}N$ of 5.0 ± 0.3 ‰. The average POM fraction

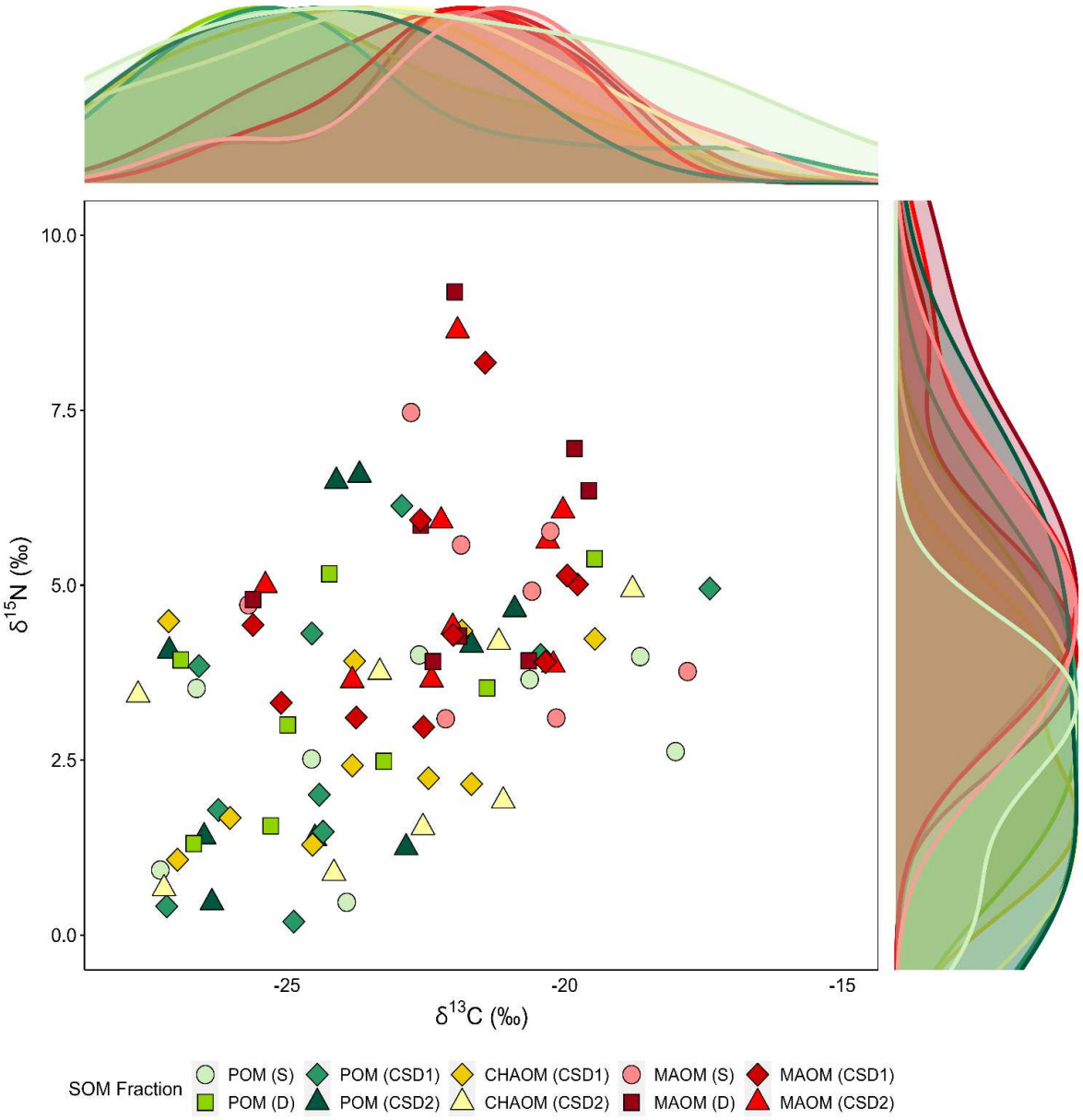

Figure 3.3 – Biplot of isotopic composition of SOM fractions isolated by various fractionation schemes. Different colors represent different fractions (POM: green; chaOM: yellow; MAOM: red), with different shading and shapes indicating the fractionation method. Distribution plots along the x and y axes show the scaled distribution of isotopic composition for ^{13}C and ^{15}N, respectively.

$\delta^{15}N$ was 3.0 ± 0.29 ‰ and was similar to the average CHAOM $\delta^{15}N$ of 2.6 ± 0.3 ‰. The one-step fractionation methods have divergent effects on POM and MAOM $\delta^{15}N$ composition – POM_{Size} had average $\delta^{15}N$ of 2.7 ± 0.5‰, and an average $MAOM_{Size}$ $\delta^{15}N$ of 4.8 ± 0.5‰. In contrast, $POM_{Density}$ had an average $\delta^{15}N$ of 3.0 ± 0.5‰, but $MAOM_{Density}$ had a $\delta^{15}N$ of 5.4 ± 0.5‰. The combined methodologies had similar average POM $\delta^{15}N$ values (POM_{CSD1}: 3.0 ± 0.6‰, POM_{CSD2}: 3.4 ± 0.8 ‰), and had MAOM $\delta^{15}N$ average more similar to size separated MAOM than density separated ($MAOM_{CSD1}$: 4.7 ± 0.5 ‰, $MAOM_{CSD2}$: 5.1 ± 0.5‰) (Figure 3.3). The average CHAOM $\delta^{15}N$ was similar between fractions; $CHAOM_{CSD1}$ had an average $\delta^{15}N$ value of 2.8 ± 0.4 ‰, and the $CHAOM_{CSD2}$ fraction had an average $\delta^{15}N$ of 2.3 ± 0.6‰.

Isotopic Differences

The isotopic difference between POM and MAOM $\delta^{13}C$ was relatively similar between all fractionations that employed a density separation step, with an average $ID_{MAOM\text{-}POM}$ of 1.98‰, and had a coefficient of variation (CV) of 0.86. In contrast the average isotopic difference between the POM_{Size} and $MAOM_{Size}$ was only 1.38‰, and had a CV value of 2.29, indicating both increased similarity in the isotopic values of the two fractions relative to the other methodologies and increased variability in the fractions isolated by size fractionation (Figure 3.4). We performed similar analyses to understand the isotopic difference between the CHAOM and POM fractions, as well as the CHAOM and MAOM fractions. The effect of the delayed dispersion in the CSD2 fractionation was evident in the both the $ID_{MAOM\text{-}CHAOM}$ and the $ID_{CHAOM\text{-}POM}$; the average IDs for the CSD1 fractionation were 1.46 ± 0.28 ‰ and 0.12 ± 0.25‰, respectively, whereas the CSD2 fractionation yielded average isotopic differences of 1.36 ± 0.38‰ and 0.79 ± 0.31‰.

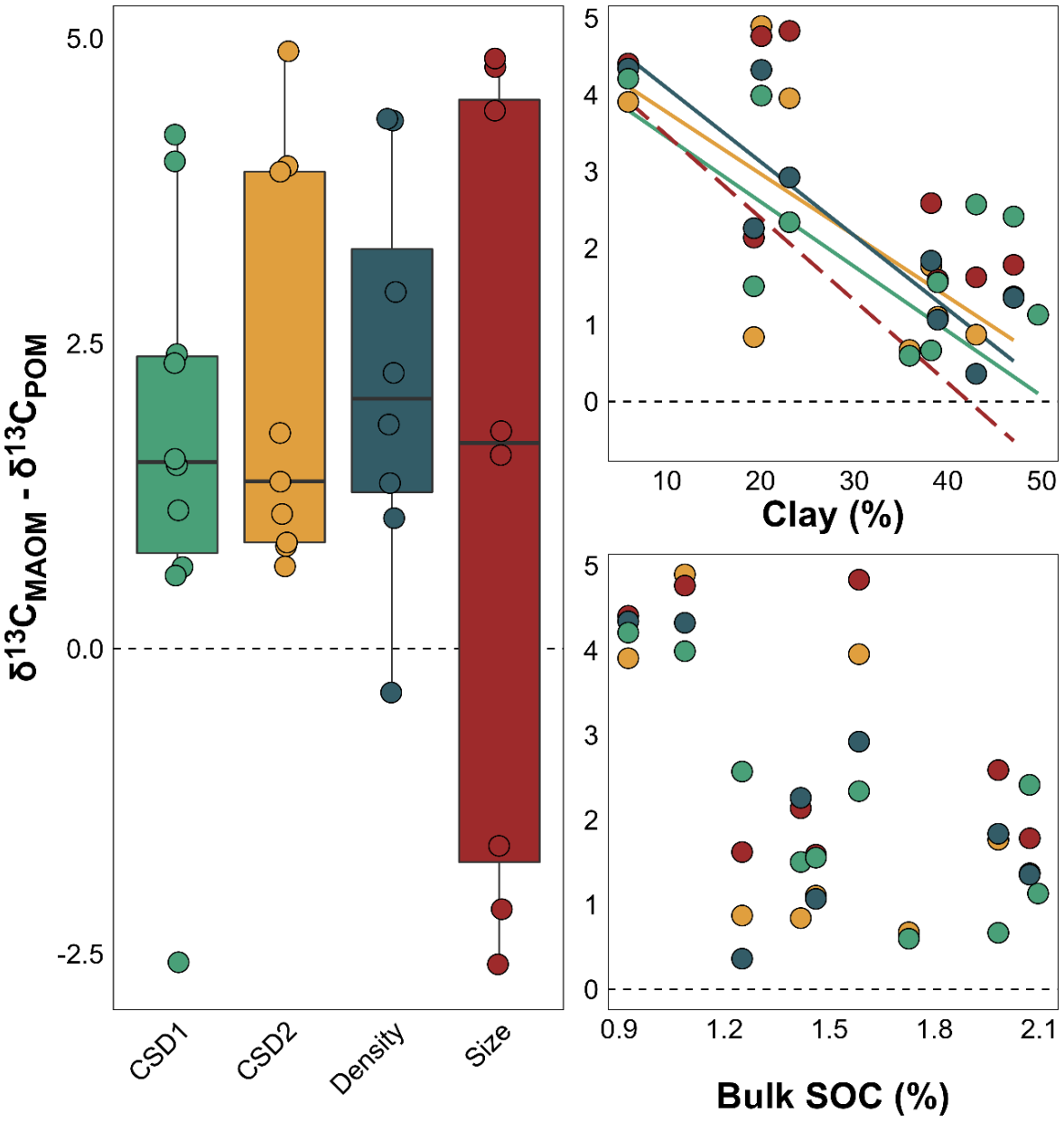

Figure 3.4 – Results of isotopic difference analysis for individual samples across fractionation methodologies (n = 11). In the left-most panel, boxplots show the distribution of the $ID_{MAOM-POM}$ for the different methods, where overlaps with zero indicate no difference in the isotopic composition of the POM and MAOM fractions. In the right panels, the results of the regression between $ID_{MAOM-POM}$ and clay content (top) and bulk SOC (bottom). Different colors correspond to the different methodologies.

To better understand the drivers of differences in ID among fractionation methodologies, we regressed the $ID_{MAOM\text{-}POM}$ against two soil physiochemical properties: clay percentage and bulk SOC. We found that the $ID_{MAOM\text{-}POM}$ tended to decrease as the clay content increased (Figure 3.4). The significance of this relationship was moderated by fractionation procedure—the fractionations that included a density floatation had a significant negative relationship with clay content (p-values - CSD1: 0.05; CSD2: 0.04; Density: <0.01) but was not significant for the size fractionation (p-value = 0.22). Similar patterns were also found for oxalate-extractable Al oxides (data not shown). Interestingly, none of the regressions against bulk SOC were significant (p-values > 0.05), indicating an independence of fractionation efficacy across SOC levels.

SOM Fraction Spectral Analysis

Patterns in the spectral signatures of SOM fractions

We used principal component analysis to understand the differences in spectral signatures among fractions isolated by different fractionation methodologies (Figure 3.5A). The starkest separation among fractions was along PCA axis 1, with the POM derived from density fractionations clustering in the positive PCA space, and the POM_{Size}, the CHAOM fractions, and the MAOM fractions clustering together in negative PCA space. To assess the specific wavelengths that drove the differentiation along PCA axis 1, we examined the axis loadings for each wavenumber along PCA axis 1 (Supplemental Figure 3.2A). Negative loadings along PCA axis 1 were associated with aromatic C groups, as well as carboxylic C groups. Additionally, the quartz overtone stretch (~2000 – 1800 cm^{-1}) had a significant negative loading throughout the width of the band, explaining why the mineral composite fractions were separated from the POM fractions isolated via density, which contains little if any mineral material (Supplemental Figure 3.3A). Positive loadings along axis 1 corresponded to polysaccharide content, as well as the

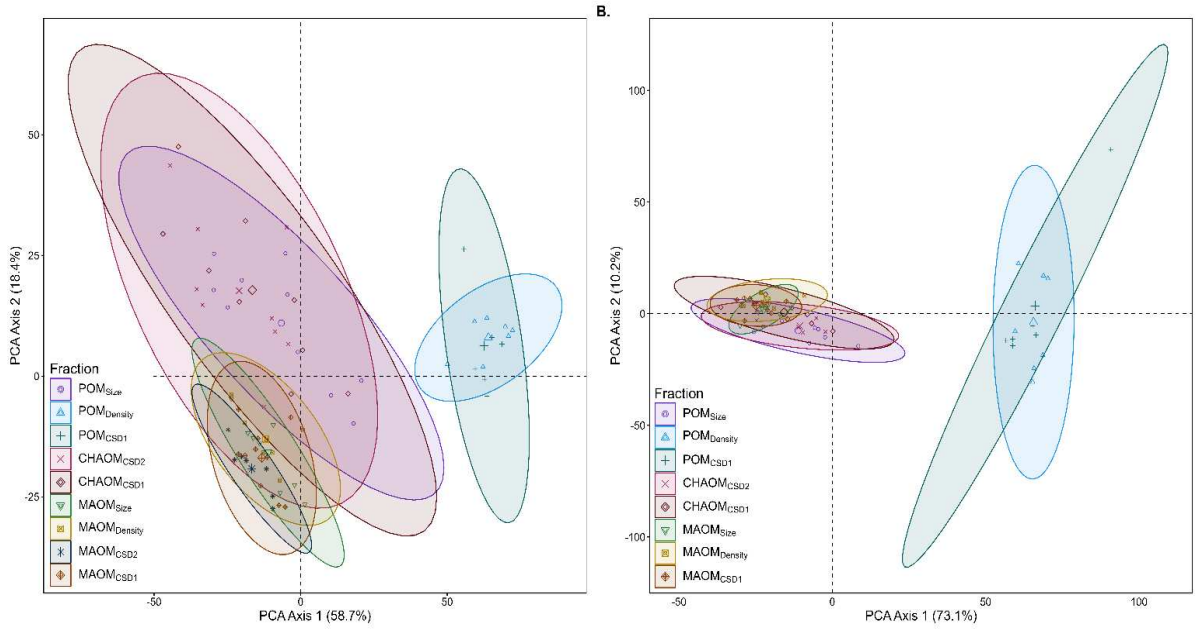

Figure 3.5 – Results of principal component analysis for spectral wavenumbers of the different procedural fractions for A.) unaltered samples, and B.) samples that underwent ash spectral subtractions prior to analysis. Different color/shape combinations indicate different procedural fractions, and separation along either axes indicates dissimilarity in the spectral signature of the fraction. Note that, due to sample size limitations, POM_{CSD2} was excluded from both analyses, and $MAOM_{CSD2}$ was not included in the spectral subtraction analysis.

cellulose C-O stretch (1000 – 1080 cm^{-1}). Separation along PCA axis 2 occurred primarily within sample group and did not explicitly differentiate any isolated fraction from another. However, we did observe that the CHAOM fractions, as well as the POM_{Size}, distinguished themselves from `the tightly clustered MAOM fractions along this axis (Figure 3.5A). In our analysis of the axis loadings, we found that the bending of aliphatic C bonds, as well as the presences of amide groups, and to a lesser extent, variation in carboxyl C groups, drove separation along PCA axis 2. The MAOM fraction was more tightly clustered than either the POM or the CHAOM fractions along both axes, while the CHAOM and POM fractions both showed variability in both axes, with dissimilarity in both axis 1 and axis 2 leading to the spread of values relative to MAOM (Figure 3.5A). Of note is the consistency in the clustering of the CHAOM between the

$CHAOM_{CSD1}$ and $CHAOM_{CSD2}$ fractionations, despite the presence of the occluded POM within the $CHAOM_{CSD2}$ fraction.

To capture the chemical features of the OM component of the different fractions, independent of the absorbance of the associated minerals, we employed the same PCA analyses on spectra that had mineral peaks subtracted out (see methods for details). Despite the removal of mineral bands, a similar pattern in the organization of the fractions occurred in PCA space, however we observed a much tighter clustering of the fractions that contained a mineral component along PCA axis 2 (Figure 3.5B). There is a similar pattern in the range of variability among the mineral fractions however, with CHAOM and POM_{Size} showing a larger spread across PCA axis 2 than MAOM in both the subtracted and unaltered spectral analyses. Examining the PCA loadings for either axis, we observed that the quartz overtones stretch had a positive loading effect generally, which leads to a lack of explanatory power for the arrangement of the $POM_{Density}$ and POM_{CSD1} relative to the other fractions. Instead, the bands that represent organic molecular groups such as carbonyl and carboxyl C, phenols, and aromatic groups had high positive loadings, possibly indicating that the abundance of these molecules in the density isolated POM fractions overwhelms differences in the molecular composition of the fractions when examined in PCA space (Supplemental Figure 3.3B). Additionally mineral bands that describe differences in the silt and clay particles vs. sand particles could add further explanation to the collapse of the spectral distributions of the mineral fractions following subtraction, but do not fully explain the spread across PCA axis 2 (Figure 3.5B).

PERMANOVA Results

We constructed dissimilarity matrices using the spectral data for the several procedural fractions that correspond with the same conceptual fraction (i.e., POM_{Size}, $POM_{Density}$, POM_{CSD1}, and

POM_{CSD2} for POM; $CHAOM_{CSD1}$ and $CHAOM_{CSD2}$ for CHAOM; $MAOM_{Size}$, $MAOM_{Density}$, $MAOM_{CSD1}$, and $MAOM_{CSD2}$ for MAOM), and then used a PERMANOVA analysis to understand drivers of differences between procedural fractions. We tested for an interactive effect of soil physicochemical properties and fractionation method on dissimilarity. We did not find any significant interactions between the fractionation methodologies and any of the physicochemical properties we investigated (Table 3.2), leading us to conclude that fractionation procedures perform similarly across most agricultural soils. Generally, soil properties had little ability to explain the arrangement of the dissimilarity matrices, though oxalate-extractable Al oxides had a significant explanatory role in the dissimilarity in MAOM and CHAOM fractions. Fractionation did not have a significant main effect in either the MAOM or CHAOM analyses but did consistently have a significant main effect in the POM fraction (Table 3.2). Fraction C content was only significant for the POM fractions, whereas in the MAOM and CHAOM fractions, the abundance of C did not have significant explanatory power.

Discussion

Our results indicate that, in the agricultural soils we examined, the MAOM fraction generally maintains consistent spectral, isotopic, and chemical characteristics independent of the physical fractionation method employed. In contrast, the POM fraction is sensitive to fractionation technique, and studies that aim to use natural abundance isotopic tools or spectral characteristics to investigate POM and MAOM pools are recommended to employ a density floatation to isolate the POM fraction. Interestingly, we did not find interactions between fractionation method and the range of soil properties surveyed, indicating that the fractionation methods we applied can be used effectively across a range of soil types.

Table 3.2 – Results of PERMANOVA analyses of interactions between soil physicochemical factors and fractionation methodologies. Analysis was repeated for each fraction, using the model specifications shown. Both r^2 and significance values are reported; bolded values indicate a significant results at $p < 0.05$.

Fraction	Model Specification	Variable Effect	Fractionation Effect	Interaction Effect
POM	Clay x Fractionation	**0.08, 0.015**	**0.81, 0.001**	0.01, 0.536
	Sand x Fractionation	0.00, 0.582	**0.90, 0.001**	0.02, 0.223
	OE Al Oxides x Fractionation	0.02, 0.310	**0.88, 0.001**	0.01, 0.487
	OE Fe Oxides x Fractionation	0.03, 0.109	**0.86, 0.001**	0.00, 0.838
	Total SOC x Fractionation	0.03, 0.088	**0.86, 0.001**	0.00, 0.705
	Fraction C x Fractionation	**0.39, 0.001**	**0.49, 0.001**	0.01, 0.440
CHAOM	Clay x Fractionation	0.12, 0.222	0.02, 0.805	0.13, 0.220
	Sand x Fractionation	0.09, 0.365	0.02, 0.786	0.03, 0.787
	OE Al Oxides x Fractionation	**0.29, 0.042**	0.02, 0.745	0.02, 0.783
	OE Fe Oxides x Fractionation	0.02, 0.826	0.02, 0.823	0.03, 0.746
	Total SOC x Fractionation	0.02, 0.883	0.02, 0.835	0.03, 0.739
	Fraction C x Fractionation	0.22, 0.087	0.05, 0.586	0.07, 0.388
MAOM	Clay x Fractionation	0.07, 0.282	0.17, 0.423	0.06, 0.952
	Sand x Fractionation	0.09, 0.104	0.17, 0.310	0.14, 0.447
	OE Al Oxides x Fractionation	**0.19, 0.016**	0.18, 0.226	0.05, 0.935
	OE Fe Oxides x Fractionation	0.05, 0.402	0.17, 0.476	0.02, 0.997
	Total SOC x Fractionation	0.05, 0.403	0.17, 0.461	0.04, 0.998
	Fraction C x Fractionation	0.15, 0.046	0.16, 0.390	0.05, 0.960

OE: Oxalate Extractable

Comparison of procedural fractions across fractionation techniques

Particulate organic matter

Consistent with the conceptual definition of POM, the procedural POM fractions isolated in our study tended to have higher, less constrained C:N ratios (Figure 3.2) as well as more depleted $\delta^{15}N$ and $\delta^{13}C$ values than the CHAOM and MAOM (Figure 3.3). While the C concentration of the POM fraction was only marginally affected by fractionation methods (mean SD = 1.7 g C kg $soil^{-1}$; Figure 3.1), based on our analyses we argue that a density separation is required to isolate a POM fraction most consistent with its conceptual definition.

To realize the potential of POM and MAOM as indicators of ecosystem function or as biogeochemical model pools, the isolated fractions must represent distinct functional units in the soil (Moni et al., 2012), possessing discrete characteristics indicative of their unique dynamics. Our analysis of the spectral characteristics of the POM fractions (Figures 3.5A and 3.5B), as well as the variability in the $ID_{MAOM\text{-}POM}$ for POM_{Size} (Figure 3.4), suggest that while $POM_{Density}$, POM_{CSD1}, and POM_{CSD2} meet this threshold for consideration of a distinct functional unit, POM_{Size} does not. It is possible that the isotopic and spectral characteristics of the POM_{Size} fraction is diluted by organic matter either associated with soil particles > 53 μm (i.e., CHAOM) or occluded within highly stable microaggregates with a diameter > 53 μm that were not dispersed via mechanical shaking. Previous work has demonstrated the presence of organo-mineral bonds in the sand sized fraction (Curtin et al., 2019; Li et al., 2013), specifically due to metal oxide coatings on sand grains that form strong associations with organic matter (Sollins et al., 2006; Steffens et al., 2017) or transient bonding sites linked to microbial byproducts or root exudates (Ridgeway et al., 2024). The results of our PERMANOVA analysis support this explanation – oxalate-extractable Al oxides played a significant role in explaining dissimilarity in

the CHAOM fraction spectra, suggesting they may play a role in stabilizing C in this sand sized fraction (Table 3.2). Despite having a similar C concentration to other POM fractions, the potential alteration of the POM fraction when isolated by size suggests that POM_{Size} is best characterized as composite fraction (i.e., POM and CHAOM) rather than a discrete functional soil component and does not map on as well onto the conceptual definition of POM as POM isolated by density fractionation (Bornemann et al., 2010; Calderón et al., 2011; Ramírez et al., 2020).

Mineral associated organic matter

The MAOM C concentrations were only slightly affected by fractionation choice, with $MAOM_{Size}$ having a significantly higher C concentration than MAOM isolated by protocols that employed a density separation step (i.e., CSD1, CSD2, and Density; Figure 3.1). This may be due to inter-fraction transfer of POM C with a particle size < 53 μm into the MAOM fraction during the size fractionation procedure. Inter-fraction transfer of C during wet sieving has been observed in previous studies (Curtin et al., 2019). The removal of POM material via aspiration prior to size separation (such as in the CSD1 or CSD2 fractionations) aims to avoid this potential transfer, as shown by the observed range of $ID_{MAOM\text{-}POM}$ values; MAOM isolated by size was less isotopically distinct from POM than MAOM isolated by any of the other methods, suggesting a partial incorporation of POM_{Size} into the $MAOM_{Size}$ fraction (Figure 4). Though we did not directly examine it here, we caution that this phenomenon may be further exacerbated when non-agricultural soils, in which a greater proportion of SOM may be found in POM, are fractionated by size alone.

Further assessment indicated little evidence of substantial stoichiometric (Figure 3.2), or spectral (Figure 3.5) alteration of the procedural MAOM fractions across fractionation schemes. In

contrast to POM_{Size}, this consistency in characteristics held true even when the CHAOM fraction was composited with the MAOM (i.e., in the single step density fractionation). This observation highlights the dominance of MAOM C in agricultural systems (Lugato et al., 2021), which is less readily diluted by the addition of the low C CHAOM fraction, as well as suggests the potential for characteristics of OM typically associated with MAOM to be present in the CHAOM. However, further work is needed to assess if this pattern holds in non-agricultural soils, where MAOM accounts for a smaller share of the total SOM (Hansen et al., 2024; Lugato et al., 2021).

Occluded particulate organic matter and coarse heavy associated organic matter

Several previous studies have indicated that the oPOM fraction is an important indicator for agroecosystem function (Cates and Ruark, 2017; Drinkwater and Snapp, 2022; Schipanski et al., 2010; Six et al., 2000) and SOM formation processes (Haddix et al., 2020; Witzgall et al., 2021). As a result of its physical occlusion, the oPOM fraction often exhibits evidence of having experienced a different level of microbial processing, leading to distinct $\delta^{13}C$ and $\delta^{15}N$ values and C:N ratios as compared to unoccluded or "free" POM (Gunina and Kuzyakov, 2014). As such, we included one of the most common fractionation schemes for the isolation of oPOM to assess whether this fraction represents a functionally discrete SOM pool that should be distinguished from free POM. The resulting $CHAOM_{CSD2}$ fraction is subject to the same shortcomings of the POM_{Size}; a dilution of the light fraction POM by sand sized particles, some of which may be associated with organic molecules via metal oxide coatings or microbially mediated bonding sites. While we did observe significant differences between the $CHAOM_{CSD1}$ and the $CHAOM_{CSD2}$ in terms of C content and C:N ratio (Figure 3.1, Figure 3.2), we observed no differentiation of spectral properties in our PCA (Figure 3.5) and the inclusion/exclusion of

the oPOM fraction within $CHAOM_{CSD2}$, did not explain any of the dissimilarity in spectral properties between the two CHAOM fractions (Table 3.2).

It is possible that our dispersion methods did not fully disrupt stable microaggregates, such that the true signal of the oPOM fraction is masked in our results (Kölbl et al., 2005), but given that these agricultural soils have low amounts of total POM, the occluded fraction is not large enough to distinguish a composite fraction (i.e., $CHAOM_{CSD2}$) from the other major constituents of that fraction (i.e., $CHAOM_{CSD1}$). While studies that seek to investigate the role of the occluded fraction directly should continue to develop and employ methods that isolate relevant and functionally distinct soil units (such as the methods described in Kölbl et al. (2005) that uses multiple density separations), our findings suggest that the additional labor of its separation in general SOM studies may not be proportional to the potential information gained, at least in agricultural soils. Overall, our findings show that the CHAOM fraction is more similar to the MAOM than the POM and should likely be grouped with it under the POM vs. MAOM conceptual framework following (Zhang et al., 2021). Under this dichotomous framework, the one-step density fractionation is therefore deemed most effective at matching procedural fractions with their conceptual definitions.

Influence of soil properties

Previous comparisons of different fractionation techniques (Moni et al., 2012; Poeplau et al., 2018) have focused on the reproducibility of results across fractionation protocols, choosing to work with 1 - 2 soils of similar physicochemical make-up. Other studies designed to understand the nature of SOM fractions across different soils tend to employ the same fractionation scheme for all samples (Calderón et al., 2011). Here we combine these two controls on SOM fraction characteristics, allowing for tests of interactive effects between physiochemical properties and

fractionation scheme. Generally, we found that fractionation methods tended to be robust across the range of soil properties we examined. We observed no evidence for significant interactions between soil physicochemical properties and the resulting spectral dissimilarity of a given fraction set (Table 3.2), indicating that the spectral characteristics of an isolated fraction depends more on the methodology than the soil properties. This observation holds for the other characteristics investigated here -- we also found no relationship between soil physiochemical properties and the recovery of SOM-C, SOM-N, or soil mass in our samples. While soil properties did influence the distribution of C and N among the fractions (e.g., higher proportions of CHAOM-C in sandy soils, more MAOM-C in Fe/Al oxide rich soils) there is no evidence that these soil properties influenced the efficacy of the fractionation schemes across our sample set.

Our mean C and N recoveries for this experiment were less than 100%, which can be expected as some loss of soluble C and N is known to occur during the fractionation procedure (Supplemental Figure 3.1; Crow et al., 2007). We expected that this would be more evident in the fractionations that employed a density separation because of the rinsing steps employed to remove SPT from the soil matrix in those protocols. However, while there was a trend towards decreased C and N recovery following the CSD2 fractionation, we did not observe a significant effect of fractionation on C and N recoveries. Further work characterizing the potentially solubilized C, such as was exhibited by Plaza et al. (2019) in which both the SPT and the water rinses are analyzed for C following fractionation, may provide more information as to the differences in the risk of C loss or transfer due to solubilization and exchange across the various fractionation methods. As SOM fractionation continues to become a more common analysis method across disciplines (Billings et al., 2021), our results imply that, generally, researchers can

focus their choice of fractionation procedure on the fractions that are most relevant to their specific question, rather than adapting to the soil conditions of their study sites.

We did observe that at the extremes of the soil physiochemical gradient, there are limits to the ability of fractionations to perform well and isolate discrete pools. One soil we solicited had a texture of 99% sand. Results from the fractionation of this soil were omitted from some of the analyses of spectral and stoichiometric fraction properties, as the physicochemical properties fall far outside the bounds of typical agricultural soils, and the resulting procedural fractions were challenging to assess and link to the associated conceptual fraction. While we expected fractionation mass to vary depending on fractionation scheme (e.g., POM_{Size} mass >> $POM_{Density}$), we observed that for this sandy soil, the color of the fractions was also altered during fractionation, clearly indicating a redistribution of C between fractions during the fractionation process. The original soil was a dark black color, yet the POM_{Size} and $CHAOM_{CSD1 \text{ and } CSD2}$ fractions which composed > 95% of the soil mass rapidly became a bright white upon wet sieving. In contrast, soil particles in the $MAOM_{Density}$ fraction retained their initial dark color. The lack of permanent binding sites in a sand dominated soil may have driven this phenomenon, as organic coatings that made up the bulk of the organic C in this soil were dissolved and transferred during the wet-sieving process, similar to observations by Xu et al. (2017). Further research at the texture extremes, be that Vertisols with high proportions of clay, or sandy soils such as the one presented above, is still necessary to understand the resulting fractions and accurately apply a POM vs. MAOM framework in these soils.

Recommendations and paths forward

The fractionation method chosen for a given project must be oriented to the objectives of the study and the questions being asked. Research that seeks to elucidate specific C accumulation

pathways may require specialized fractionation schemes that isolate very specific pools. However, researchers interested in separating total SOM into POM and MAOM fractions that reflect differences in mechanisms and drivers of formation and stabilization, potential for accrual and vulnerability to change (Cotrufo and Lavallee, 2022) can employ one-step fractionation methods that require less equipment and expertise to perform and have a higher throughput. Our experiment found that size fractionation was often an adequate method for estimating the C content of various physical fractions in agricultural soils, with comparable POM-C concentrations (g kg^{-1} soil) to density and combined methods, as well as similar mass, C, and N recoveries. However, we did observe significant differences between relative C concentrations of the POM fraction (i.e., %C) isolated by size, rather than density, and observed that the CSD1 fractionation isolated fractions with a higher absolute POM-C concentration (i.e., g C kg soil) than the other fractionations, including size. Further, we also found evidence that the composite nature of POM isolated via size fractionation led to a fraction with muddled isotopic and spectral qualities, indicating a mixture of formation pathways and biogeochemical function, as well as the potential for transfer of C from POM into MAOM during sieving. We did not observe the same issues when evaluating the single-step density fractionation, and therefore we recommend this methodology for researchers interested in specifically quantifying and characterizing a procedural POM fraction most in line with the current conceptual definition. Further, given the similarity in spectral qualities between the CHAOM fraction and the MAOM fraction, as well as the disparate contributions of C to the bulk C between these two fractions, we do not find using a one-step density fractionation will compromise the integrity of the MAOM fraction that is yielded. Indeed, our results suggest relatively similar formation pathways for these two fractions that allows for their combination under our current conceptual frameworks.

When scope of inquiry allows however, further research into the CHAOM fraction is needed. The stoichiometry and isotopic signature of this fraction distinguish it somewhat from the MAOM (Figure 3.2, Figure 3.4), such that its separation via a CSD1 fractionation may yield the most unique functional pools. Indeed, recent work has highlighted the fraction as an important precursor to stable MAOM formation, and it could represent a dynamic and important intermediary pool (Samson et al., 2020). Given the composite nature of the fraction, our results clearly show that the occluded POM fraction is not effectively isolated by the CSD2 fractionation. Similar to POM_{Size}, the $CHAOM_{CSD2}$ fraction contains sand-sized mineral particles which may include organo-mineral associations or highly stable microaggregates, leading to a composite fraction of occluded POM and CHAOM that is not unique nor homogenous in its makeup *(sensu* Curtin et al., 2019). Studies that focus on the occluded POM fraction should consider including a second density separation following dispersal of aggregate structures, such as the methodologies described by Kölbl et al. (2005).

Caveats and considerations

Our study investigated the ability of four of the most common physical fractionation techniques to isolate functionally distinct SOM fractions. However, a wide variety of other approaches exist in regard to fractionation methods, dispersion techniques, and the choice of heavy liquid (Leuthold et al., 2022a; Poeplau et al., 2018). For all the methods tested in our experiment, soils were dispersed via shaking with glass beads in a liquid solution (SHMP or SPT, depending on the methodology), rather than by ultrasonic vibration, a common alternative (Kaiser and Asefaw Berhe, 2014). While both methods have the potential to fragment soil and organic matter particles, leading to C transfer between fractions (Diochon et al., 2016; Oorts et al., 2005), mechanical shaking has the advantage of not needing soil specific calibration (Amelung and

Zech, 1999), allowing for consistent dispersal methodology across the range of soils we investigated. Additionally, while SPT has been shown to modify soil chemical composition (Morgun and Makarov, 2011), and its removal from resultant fractions via washing may mobilize C and lead to low C recovery (Plaza et al., 2019), we chose to use it as a heavy liquid for performing density separation in our study in an effort to replicate the most common techniques used across labs and traditions. While no physical fractionation method is perfect, we believe researchers need to be clear-eyed about the objectives of their experiment and choose the fractionation method that best aligns with their stated research goals.

Similarly, while we sought to capture a representative range of soil properties for agricultural lands (Supplemental Figure 3.1), our sample set does not capture the full range of soil physicochemical properties and formation factors that may be encountered in a given research project. For example, in alkaline soils, Ca and Mg ions can play a significant role in MAOM stabilization and persistence (King et al., 2023; Rasmussen et al., 2018), such that their presence may influence fractionation results. While we could not explore these processes in the present study given our soil set, we recommend further research on the efficacy of these methods in calcareous and cation-rich soils, and at other extremes of the soil physicochemical gradient.

Conclusions

Physical fractionation is a powerful tool for better understanding the form and function of SOM but requires a clear understanding of the fractions that are isolated. Our study demonstrates that when fractions are isolated using a one-step size fractionation, there is a risk of inter-fraction transfer of organic matter between fractions, and further, the composite POM_{Size} fraction is not well reconciled with the conceptual definition of POM. Thus, we recommend that a density separation is used to isolate the POM fraction, and that a combined size-density fractionation is

used whenever possible to continue advancing our understanding of CHAOM. We found that soil properties did not interact with fractionation performance and conclude that all the methods we tested are viable among most agricultural soils, however further research is needed for fractionation methodologies that are best suited to soils at the extremes of physicochemical gradients. Moving "beyond bulk" SOM (*sensu* Heckman et al., 2023) represents an important step towards improved biogeochemical understanding of the soil system but requires an understanding of the interoperability of the various methods to achieve, and further building on these findings and others (e.g., Poeplau et al., 2018, Just et al., 2021, Curtin et al., 2019) will allow for continued advances in the field.

CHAPTER 4: CHEMICAL AND SPECTRAL CHARACTERIZATION OF A DYNAMIC MINERAL ASSOCIATED ORGANIC MATTER FRACTION

Introduction

Physical fractions of soil organic matter (SOM) have differential formation pathways, stabilization mechanisms, and provide different ecosystems functions (Cotrufo and Lavallee, 2022). Mineral associated organic matter (MAOM) consists of low molecular weight compounds of plant and microbial origin bound to reactive mineral surfaces, and possess long mean residence times (Cotrufo and Lavallee, 2022). However, a fraction of the MAOM pool may exchange with dissolved organic matter in soil solution, with implications for ecosystem nitrogen (N) cycling (Daly et al., 2021) and soil carbon (C) persistence. Methods such as ramped pyrolysis have been used effectively to identify this sub-fraction of the MAOM (Cécillon et al., 2021), however, they remain difficult to scale.

Diffuse reflectance infrared Fourier transformed (DRIFT) spectroscopy is a powerful tool for quantifying and characterizing soil properties (Ng et al., 2022). As spectroscopic methods are highly sensitive to the detection of the functional groups of SOM, DRIFT spectroscopy has been employed to quantify bulk soil and SOM fraction organic C (Sanderman et al., 2021), C and N in MAOM (Ramírez et al., 2021), and to characterize the molecular composition of SOM fractions (e.g., Calderón et al., 2011). Previously work has employed DRIFT spectroscopy to identify stable components of bulk SOM (Barré et al., 2016), however, it remains an open question if this methodology can characterize the dynamic portion of the MAOM fraction.

In this experiment we examine the stoichiometric, isotopic, and spectral attributes of soils from two time-points, 1967 and 2019. One set of soils (n = 8) had been under continuous fallow for the duration of the experimental period, such that no new organic inputs had entered the system in over 50 years. The other set (n = 8) received biannual additions of green manure. We hypothesized that the lack of fresh organic inputs would lead to the disappearance of the dynamic MAOM pool, as it was steadily lost over time to maintain equilibrium with a shrinking DOM pool, a phenomenon which could be observed in the spectral signatures of the soils sampled at different periods. We further hypothesized that the remaining, stable MAOM would reflect increased microbial processing, evidenced by an increased C:N ratio, as well as a more enriched $\delta^{13}C$ composition compared to its original state, and the soil that had continued to receive inputs.

Materials and Methods

The soils used in this experiment were sampled in 1967 and 2019 from the Ultuna SOM experiment. The Ultuna soil organic matter experiment (FRAME-56) is located at the Swedish University of Agricultural Sciences, outside of Uppsala, Sweden (59.82 °N, 17.65 °E). The experiment began in 1956, though the field has likely been cultivated for centuries. Soils at the Ultuna site have been characterized as Typic Eutrochrepts or Eutric Cambisols according to the United States Department of Agriculture and the World Resource Base soils classification schemas, respectively. The soils in the top 20 cm are dominated by fine particles (36.5% clay and 41% silt), with 22.5% of the soil particle size distribution attributed to sand sized particles. The mean air temperature at the site is 5.8 °C, and the mean annual precipitation is 542 mm, classifying the climate at the site as warm-summer humid continental according to the Koppen-Gieger climate index. At the onset of the experiment in 1956, the soil pH was 6.6, soil C content was 15 g C kg $soil^{-1}$, and soil N content was 1.7 g N kg $soil^{-1}$ (Kirchmann et al., 1996). The full

experiment is made-up of 15 experimental treatments replicated across 4 blocks. Plots are 2 m x 2 m, and separated by 40 cm steel frames that extend about 30 cm into the soils and 10 cm above the soil surface to prevent transfer of soil between treatments (Kirchmann et al., 1996). The experimental treatments induced changes in surface elevation by up to 75 mm due to their effect on soil porosity (Kätterer et al., 2011). Crop rotations have varied over the course of the experiment. Between 1956 and 1999 it included mainly spring barley (*Hordeum vulgare* L.) and oats (*Avena fatua* L.), wheat (*Triticum aestivum* L.), fodder beet (*Beta vulgaris*), fodder rape (*Brassica napus*), mustard (*Brassica nigra)*, oilseed rape, and Swedish turnip (*Brassica napobrassica)* were occasionally grown, silage maize (*Zea mays* L.) has been growing continuously since the year 2000 (Kätterer et al., 2011).

We examined two treatments within the greater experiment: continuous bare fallow, or biannual additions of 4.23 Mg ha^{-1} grass derived green manure (46.2% C, 1.8% N; Gerzabek et al. (1997)). In both treatments, all aboveground residue is removed at harvest. We considered the MAOM that was lost over time in the fallow treatment representative of the dynamic MAOM pool and hypothesized that the difference in spectral signatures between MAOM sampled in 2019 and 1967 would reveal a loss of primarily plant-derived molecular compounds. In contrast, we expected the characteristics of the green manure treatment to be consistent between the two time points since its C stock is close to steady state (Kätterer et al., 2011).

Archived, air-dried, 2 mm sieved soil samples (n = 4 per treatment and year) were shipped to the USA and heat treated (110 ^{O}C for 18 hours) following USDA de-quarantining protocols. A combined-sized density fractionation was employed to isolate the MAOM fraction defined as >1.85 g cm^{-3} and < 53 μm. Briefly, six grams of air-dried, 2 mm sieved soils were dried overnight at 60 °C. Once oven-dry, 25 mL of sodium polytungstate (SPT; $H_2Na_6O_{40}W_{12}$),

adjusted to a density of 1.85 g cm^{-3} was added to the soils, along with 12 4-mm glass beads. The soil solution was shaken for 18 hours at 112 rpm to disperse aggregate structures, and then centrifuged at 2325 RCP for 20 minutes. Following centrifugation, the particulate organic matter (POM) fraction (defined as organic matter with a density < 1.85 g cm^{-3}) was aspirated via vacuum filtration, rinsed three times with deionized (DI) water, and dried to a constant weight at 60 °C. The remaining soil was resuspended in DI water, centrifuged at 2325 RCF for 25 minutes, and the supernatant poured off. This process was repeated two additional times to remove any residual SPT from the sample that could alter the mass of the fractions recovered. After these rinsing steps, the soil was resuspended in DI water once more, and separated via wet sieving on a 53 µm sieve into organic matter associated with a coarse, heavy soil fraction (CHAOM; > 53 µm, > 1.85 g cm^{-3}), and mineral associated organic matter (MAOM; < 53 µm, > 1.85 g cm^{-3}) (Leuthold et al., 2022). The samples were then placed in the oven and dried to a constant weight at 60 °C before being ground and analyzed. Oven dried, fine powdered MAOM samples from all soils were analyzed for %C, %N and $\delta^{13}C$ via elemental analysis-isotope ratio mass spectrometry (EA-IRMS, VarioIsotope Cube - Isoprime precision, Elementar, Langenselbold, Hesse, Germany). We used a 2-way ANOVA with an interactive effect of treatment and time to determine the differences in C, N, and $\delta^{13}C$ among the two time-points using the *lmerTest* (Kuznetsova et al., 2017) and *stats* packages in R (R Core Team, 2022).

Results and Discussion

We observed a significant effect of treatment, year, and their interaction on the composition of the MAOM fraction, as evidenced by changes in the C:N ratio, $\delta^{13}C$, and C concentrations (Table 4.1). In the bare fallow treatment, MAOM-C decreased by 41.2% (Figure 4.1A). The average C value (5.84 g C kg^{-1} soil) in the 2019 bare fallow samples was lower than the centennially stable

soil C pool (6.95 g C kg^{-1}) estimated by Cécillon et al. (2021) at this site, affirming that it represents a stable fraction of the MAOM-C pool. In the green manure treatment, MAOM-C

Table 4.1: Analysis of variance results for linear mixed models for mineral associated organic matter carbon (MAOM C) concentrations, C:N ratios, and $\delta^{13}C$ in response to treatment (continuous bare fallow vs. green manure application), year (1967 vs. 2019), and their interaction.

Response	Source	df	SS	F-ratio	P-value
MAOM C Concentration (g C kg $soil^{-1}$)	Treatment	1	34.928	146.976	< 0.0001
	Year	1	20.476	86.161	< 0.0001
	Treatment : Year	1	2.706	11.387	0.00820
MAOM C:N	Treatment	1	1.33403	8.9509	0.01124
	Year	1	1.27690	8.5676	0.01267
	Treatment : Year	1	0.02102	0.1411	0.71337
MAOM $\delta^{13}C$	Treatment	1	2.03535	88.4177	< 0.0001
	Year	1	0.27069	11.7591	0.01257
	Treatment : Year	1	0.00079	0.0342	0.85814

decreased by 20%, though bulk SOM C only changed by 7%, indicating that this loss may represent a redistribution of SOM among physical fractions (Supplemental Figure 4.1). In the bare fallow treatments, the MAOM C:N ratio decreased significantly (-8.8%, p = 0.04; Figure 4.1B) over the 52 years between samplings and by 2019 became much more constrained relative to that of the green manure treatment. We observed a significant increase in the $\delta^{13}C$ abundance (+3.0%, p = 0.03; Figure 4.1C) between the two time-points in the bare fallow treatment, indicating a transformation of the MAOM in these plots towards more microbially derived substrates (Barré et al., 2018). We did not observe a significant change in the MAOM C:N ratio in the green manure treatment between the sampling points (p = 0.09) but there was also an increase in $\delta^{13}C$ abundance (p = 0.0003) in this treatment.

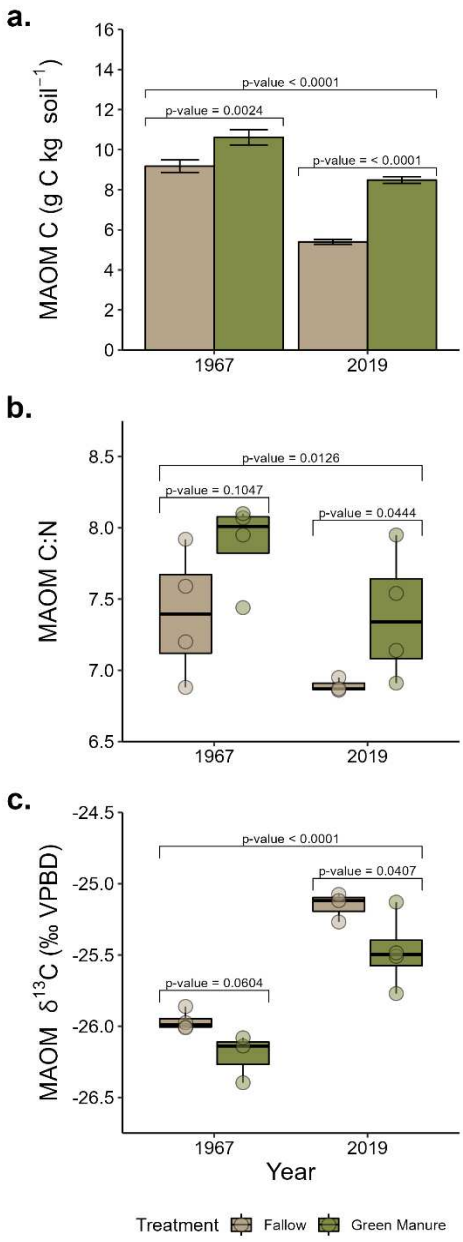

Figure 4.1 - a.) Mean mineral associated organic matter (MAOM) carbon content. Error bars indicate ± 1 standard error. b.) Boxplot of MAOM carbon to nitrogen ratios (C:N). Individual points are shown as measurements of each sample. c.) Boxplot of $\delta^{13}C$ composition. Individual points show sample $\delta^{13}C$ values. For all three measures, differences between the two time points within treatments are significant, whereas differences between treatments at each time point vary depending on comparison (n=4 per treatment and year; Table 4.1).

To characterize the dynamic MAOM fraction, we obtained spectral absorbance of the MAOM samples from 1967 and 2019. Each sample was scanned 32 times at a spectral resolution of 4 cm^{-1} from 7500 to 600 cm^{-3} using a VERTEX 70/HTS-XT spectrometer (Bruker Optics Inc., Billerica, MA, USA). Spectra were trimmed to 4000 to 600 cm^{-1}, smoothed using a Savitzky Golay filter and baseline corrected using the *prospectr* package in R (Stevens and Ramirez-Lopez, 2022). To isolate the organic band signals of the spectra, we ashed a subsample of the MAOM at 550 ^{O}C for 1 hour (Margenot et al., 2019). We subtracted the spectra of the ashed sample from the original sample after adjusting by a subtraction factor that was chosen to minimize the quartz overtones present between 2000 and 2400 cm^{-1} (Margenot et al., 2019). Subtraction factors ranged from 0.71-0.98. We then subtracted the average absorbance of the samples from 1967 from the samples from 2019 to arrive at a spectral difference over time.

Previous examinations at Ultuna indicated that differences in select MIR wavenumber absorbance could not fully identify persistent organic matter (Barré et al., 2016), and that the persistent fraction represented a mixture of plant and microbially derived compounds (Barré et al., 2018). However, by isolating the MAOM fraction, we were able to identify spectral regions that may be indicative of the molecular characteristics of dynamic MAOM (Figure 4.2). We observed similar patterns in the overall spectral function shape between the two treatments. However, as we hypothesized, the green manure treatment was much more similar between the two time points than the fallow treatment, showing limited decreases in absorbance across the surveyed bands. We observed a considerable increase in the amount of polysaccharidal and carboxyl molecules and in the MAOM fraction (1160 and 1280 cm^{-1}) for both treatments, indicating an increased signal of microbial processing (Kallenbach et al., 2016; Figure 4.2). We also observed a decrease in the absorbance of bands corresponding to aliphatic molecules (2850,

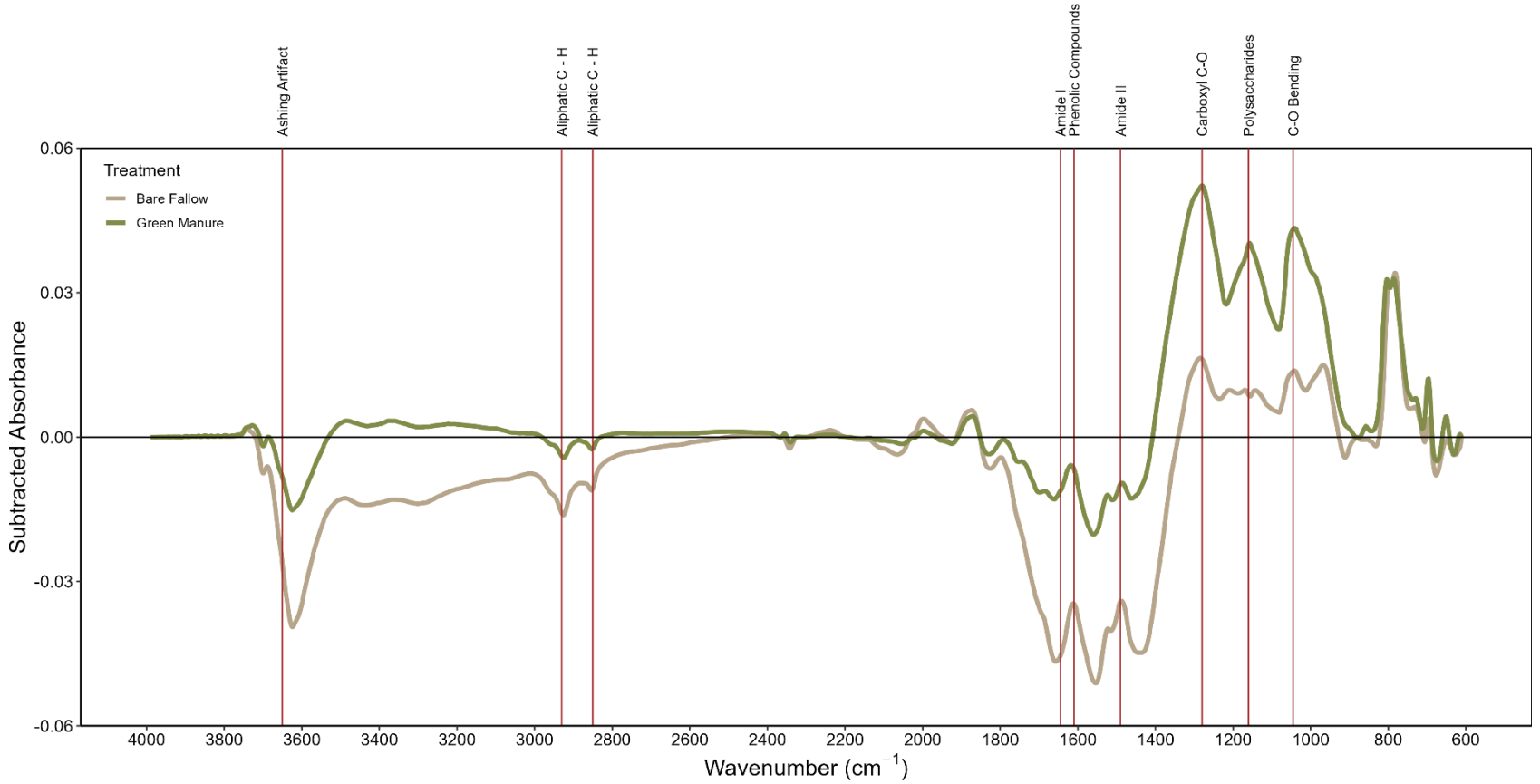

Figure 4.2 - Difference in the relative absorbance across wavenumbers for the ash-free MAOM samples from 2019 and 1967 (i.e., Absorbance of $MAOM_{2019}$ - Absorbance of $MAOM_{1967}$). Red vertical lines are used to indicate wavenumbers associated with specific organic functional groups. Positive values indicate an increased absorbance of corresponding organic matter functional groups over time, whereas negative values indicate a decrease in absorbance. Note that the peak at 3700 is related to an artifact of ashing the soils and is not to be interpreted as a difference in molecular character (Margenot et al., 2019).

2930) and amide molecules (1490 cm^{-1}), with the loss more drastic in the fallow treatment (Figure 4.2). The abatement of absorbance of H-rich aliphatics in the fallow treatment is in line with the observations of Cécillon et al. (2021) which showed that the dynamic fraction is more enriched in H containing molecules.

Conclusion

Overall, our results suggest that the dynamic MAOM in these soils was characterized by more plant-derived, aliphatic compounds, corroborating the transformation towards a higher proportion of microbial products in the persistent fraction as observed by Barré et al. (2018). This assertion is further evidenced by isotopic and stoichiometric indicators. Further work evaluating this pattern across additional soil minerologies and chemistries or combining with thermal analyses may allow for the development of methods for differentiating fractions of MAOM with different stabilities based on mid-IR absorbance.

CHAPTER 5: SHIFTS IN CONTROLS AND ABUNDANCE OF PARTICULATE AND MINERAL-ASSOCIATED ORGANIC MATTER FRACTIONS AMONG SUBFIELD YIELD STABILITY ZONES[3]

Introduction

A substantial amount of cropland area exhibits marked production variability from year to year (Basso et al., 2019; Driscoll et al., 2022). This phenomenon has been observed across scales, from global (Ray et al., 2015), to national (Renard and Tilman, 2019), down to the farm and subfield level (Maestrini and Basso, 2018). Previous work has demonstrated that interactions between climate (Leuthold et al., 2022b), geomorphology (Kravchenko et al., 2005), and edaphic characteristics (Al-Kaisi et al., 2016) are central drivers of this variability. These factors combine to create areas that are high-yielding under certain climatic conditions but low-yielding under others. The oscillating nature of these areas across time leads to their designation as "unstable," in contrast to "stable" areas, which maintain consistent yields regardless of a given growing seasons weather. While some level of year-to-year yield variability is inevitable, sustained yield instability represents an important source of environmental degradation, as well as increased economic uncertainty for farmers (Basso et al., 2019).

[3] The published version of this chapter can be cited as:

Leuthold, S.J., Lavallee, J.M., Basso, B., Brinton, W.F., Cotrufo, M.F., 2024. Shifts in controls and abundance of particulate and mineral-associated organic matter fractions among subfield yield stability zones. SOIL 10, 307–319. https://doi.org/10.5194/soil-10-307-2024

Increasing cropland soil organic matter (SOM) stocks has been associated with decreased yield instability (Qiao et al., 2022). A regional survey of cropping systems across China found a significant, negative relationship between crop yield variability and topsoil SOM concentrations (Pan et al., 2009). Other recent work has provided evidence that increasing SOM can reduce the effect of drought on crop production (Renwick et al., 2021), decreasing total crop losses and associated crop insurance indemnity payments by stabilizing yields over time (Kane et al., 2021). These results indicate that increasing SOM may be a viable management strategy for reducing crop yield variability, however the bulk of these studies take place at the regional scale (e.g., Pan et al., 2009, Kane et al., 2021), and it remains unclear if this association holds true at the subfield level.

One means by which the relationship between SOM and yield stability may be better understood is to separate the bulk SOM into discrete physical fractions. Physical SOM fractions allow for increased understanding into the function and formation of SOM. In particular, particulate organic matter (POM), and mineral associated organic matter (MAOM) have been shown to be well suited to act as indicators of SOM dynamics (Christensen, 2001; Cotrufo et al., 2019). Indeed, POM and MAOM have unique formation pathways (Cotrufo et al., 2015), different average turnover times (von Lützow et al., 2008), and tend to provision different ecosystem services in managed systems (Lavallee et al., 2020). In agricultural lands, the balance of these two fractions often skews heavily towards MAOM, with reported global to continental scale averages of 71.5 – 79% of C stored in the MAOM fraction (Lugato et al., 2021; Sokol et al., 2022), a distribution that can be attributed to a lack of consistent C inputs and frequent disturbances that can catalyze rapid POM decomposition (Lugato et al., 2021). Changes in POM C stocks therefore have the potential to act as an important indicator towards changes in

ecosystem processes—several researchers have previously identified it as a sensitive predictor of agronomic function (Schipanski et al., 2010), especially at the field scale.

Given the increased sensitivity of SOM fractions to environmental and management factors (Prairie et al., 2023) and the association between SOM and yield stability, SOM fractions may be able to act as robust indicators for subfield patterns of yield variability. Further combining SOM fractions with additional factors associated with yield stability such as topographic and soil physicochemical properties may prove even more useful. Tajik et al. (2012) explained 96-98% of the variability in soil enzyme activity using a combination of topographic and edaphic data, including SOM. Similar approaches have been applied to understand variability in soil microbial diversity and activity in row cropping systems (Kaleita et al., 2017). However, to the best of our knowledge, covariation in SOM fractions with state factors has not been explored as a means to understand spatiotemporal yield variability at the farm subfield scale.

Here we attempt to leverage the increased insight into ecosystem biogeochemistry that physical SOM fractions provide to better understand the relationship between yields, spatiotemporal yield stability and increasing SOM. Specifically, we asked: How do POM and MAOM distribute amongst areas of different yields and yield stabilities? As increasing POM is often associated with increased nutrient processing (Daly et al., 2021), aggregate formation (Witzgall et al., 2021), and improved soil structure, we hypothesized that POM-C would be highest in high-yielding, stable areas, and consequently that the ratio of POM:MAOM-C would be highest in these zones. Additionally, we expected these areas to have a higher amount of bulk SOM-C overall. Accordingly, we hypothesized the lowest POM:MAOM-C values would be observed in the unstable yield zones, indicating decreased SOM biogeochemical functioning, and that these unstable areas of the field would be relatively C poor as a result of inconsistent residue inputs. To

investigate these hypotheses, we performed a combined size-density fractionation on soils sampled from nine farms across the Central United States. At each farm, we sampled from areas of different yields (i.e., low, moderate, and high yielding), and different yield stabilities (i.e., stable and unstable). We used linear mixed effect models to examine the distribution of SOM among physical fractions as it related to the various stability zones and then supported our findings using a gradient boosting machine learning approach. Our goal was to understand if physical SOM fractions could be used as indicators of areas of various yield stability at the farm subfield scale, and consequently, if recommendations for improving yield stability could be gained via an understanding of fractional SOM distribution.

Materials and Methods

Site Descriptions and Soil Sampling

Nine farms across the upper Midwestern United States were sampled to assess the relationship between soil characteristics and crop yield stability (Figure 5.1, Table 5.1). The 30-year mean annual precipitation (MAP) ranged from 617 mm yr^{-1} – 702 mm yr^{-1}, and the average annual cumulative growing degree days (GDD) ranged from 1502 – 1989 (Table 5.1). Crop management information was obtained via communication with growers and land managers. Crop rotation varied amongst the farms however, wheat (*Triticum aestivum*), soybean (*Glycine max L.*), and maize (*Zea mays*) were the dominant crops in rotation at all sites (Table 5.1), and all sites were sampled during either the corn or soybean phase of the rotation. Nutrient management varied by farm as well, but as these were primarily working farms, we assumed that fertilizer management represents a mixture of economic and agronomic optimum rates for the region (see Fowler et al. (2024) for further discussion). Soils were sampled as described in Fowler et al. (2024). Briefly, at each farm, three 15 cm cores from three separate replicate areas of each

Table 5.1 – Major characteristics of farms from which soils were sampled for analysis. Growing season precipitation (GSP) and mean cumulative growing degree day (Cum. GDD) values represent 30-year means retrieved from the Gridmet data product.

Farm --	GSP (mm)	Mean Cum. GDD --	Soil organic (g C kg soil^{-1})	Soil pH --	Sand (%)	Silt + Clay (%)	Cropping system history --
210 Well	617	1522	11.0	6.49	64.2	35.8	C/S/C/S/W
F-71	701	1561	8.62	5.86	64.3	35.7	S/C/S/W
F-79-2	698	1559	9.66	5.68	64.5	35.5	W/S/C/S/W
Horn	637	1988	25.9	6.22	5.2	94.8	C/S/C/S/C
Micic	702	1753	16.5	6.00	52.2	74.8	S/C/S/C/S
South	643	1989	21.1	6.25	7.4	92.6	C/C/S/S/C
SR13	624	1513	13.6	6.21	39.5	60.5	W/S/C/S/W
Watt East	687	1741	20.1	6.51	25.2	74.8	C/S/C/C/S/C
F-79-2	644	1502	15.7	5.76	45.0	55.0	C/S/C/S/W

[+]: C- Corn (*Zea mays)*; Soybean (*Glycine max L.*); Wheat (*Triticum aestivum*). Reported for years available during study period which ended in 2020.

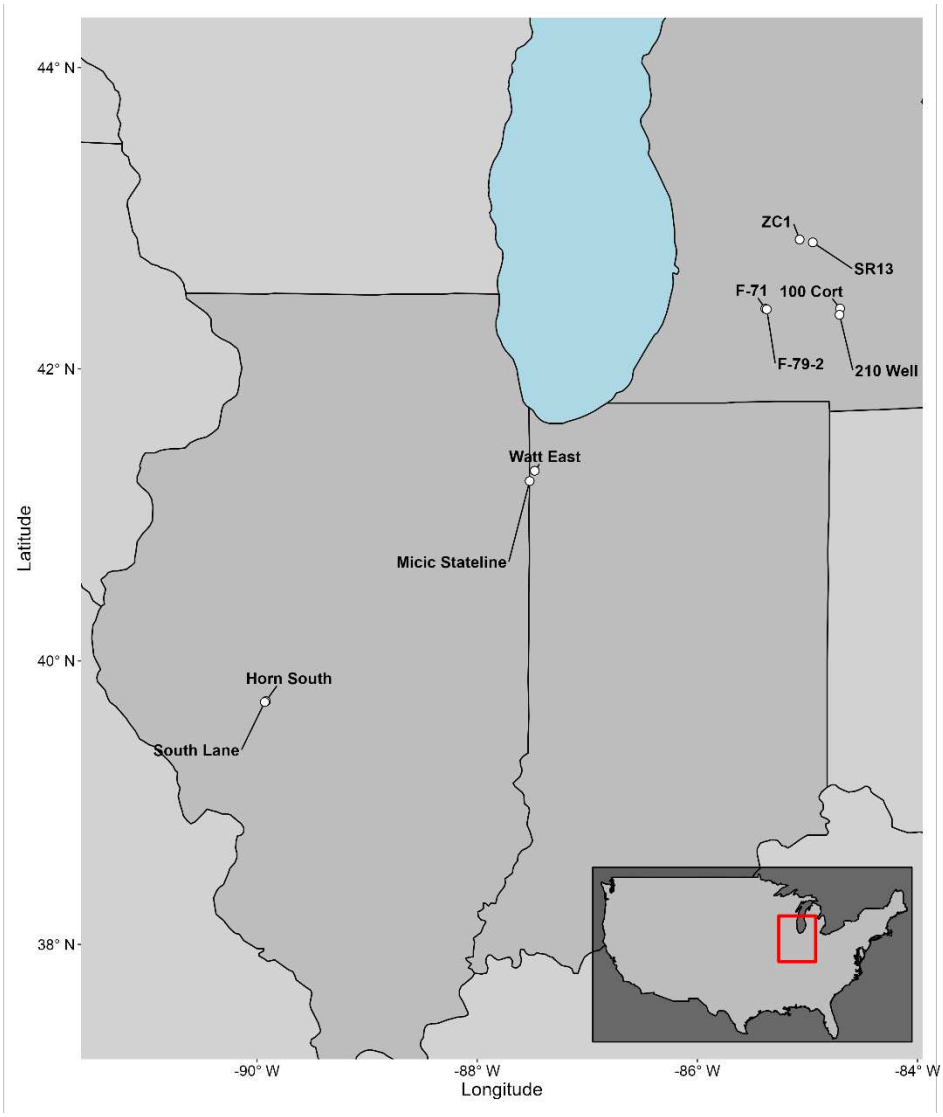

Figure 5.1 – Location of farms sampled for this analysis. Sampling took place in Indiana, Illinois, and Michigan, United States. Inset map shows the geographic location of the sampling region.

stability zones (i.e.., low-stable, medium-stable, high-stable, and unstable) were taken, such that 12 samples were collected from each farm (n = 108). Samples were then sent to Woods End Laboratory for characterization and analysis (Fowler et al., 2024).

Delineation of yield stability zones

Yield data was obtained using a real time kinematics global positioning system (RTK-GPS) enabled research combine with a yield monitor, which recorded crop yield at a 1-meter resolution. Following Maestrini and Basso (2018), raster yield data were scaled to the annual field average, and a yield level was calculated relative to the mean yield (i.e., high, medium, and low yields). Yield stability was then derived from the standard deviation (SD) of yield levels over time, with a SD value greater than +/- 15% designated as unstable. A full description of the delineation of yield stability zones is provided in Fowler et al. (2024). In the work presented here, in order to arrive at a unitless yield stability metric that accommodated differences in crop rotation, we also normalized the annual yield from the different zones by the yield in the high and stable zone for each year. We then used these normalized values to calculate zonal means and SD for the entire experimental period at each stability zone within each farm, and then calculated a coefficient of variation for yields by dividing the SD by the mean. The resulting metric (Yield CV) was well aligned with the stability zones derived from the SD as in Fowler et al. (2024), which we interpreted as a validation of this approach of quantifying stability numerically.

Soil processing and characterization

At Woods End Laboratory, the air-dried samples were sieved to 2 mm to remove root fragments and rocks, and ground prior to analyses. Soils were analyzed for a range of properties including soil pH using a 1:1 soil:water extract and pH electrode method, Mehlich I and Mehlich III extracted nutrients (NCERA-13, 2015), and cation exchange capacity (NCERA-13, 2015). Total soil organic C was measured via dry combustion at 900 °C using a Shimadzu TOC-L coupled to a Solid Sample Dry Combustion Module SSM-5000A (Shimadzu Corporation, Kyoto, Japan),

following manufacturer protocols (Shimdazu, 2017). Across sites, soil pH varied by almost an order of- magnitude, ranging from 5.68 – 6.51 (Table 5.1). Total soil organic C (SOC) varied amongst sites as well, ranging from 8.62 - 25.9 g C kg soil^{-1} (Table 5.1). Given our interest in the role of the fine fraction of soil particles in determining SOC dynamics, we did not measure texture directly. Instead, we inferred the proportion of silt and clay particles and the proportion of sand particles from results of our physical fractionation analysis (see below). In the soil we analyzed, the distribution of particle sizes ranged from relatively sandy soils (~ 64% sand) to soils dominated by fine particles (> 90% silt and clay particles; Table 5.1).

Physical fractionation and SOM analysis

A well homogenized subsample from all 108 samples was shipped to Colorado State University, where they were fractionated into physical SOM fractions using a combined size density fractionation as reviewed in (Leuthold et al., 2022a). Briefly, a 6-gram subsample of 2 mm sieved soils was dried overnight, then shaken in DI water for 15 minutes. The sample was then centrifuged, and the supernatant subjected to vacuum filtration of over a 20 μm nylon filter to isolate the dissolved organic matter fraction (DOM). Following the removal of the DOM, sodium polytungstate (SPT; $Na_6[H_2W_{12}O_{40}]$) adjusted to a density of 1.85 g cm^{-3} was added to each sample, and samples were shaken for 18 hours. After shaking, the samples were centrifuged, and the supernatant was aspirated via vacuum filtration using a 20 μm nylon filter. The material that remained on the filter was characterized as the POM fraction. The remaining mineral fraction was resuspended in DI water, centrifuged, and the resulting supernatant discarded. This rinsing procedure was repeated two more times to remove any residual SPT from the samples. Upon the fourth resuspension of the mineral fraction, the samples were separated via wet sieving into the

coarse heavy associated organic matter fraction (CHAOM; > 53 μm) and MAOM fractions (< 53 μm). These samples were then placed into the oven at 60 °C and dried to a constant weight.

Oven-dried samples were weighed, and mass recovery assessed. If the recovered mass was not between 95 and 105% of the initial sample mass, the fractionation was repeated until appropriate mass was reached. Two samples did not achieve acceptable recoveries despite repeated efforts such that we don't include them in the analysis presented here. After weighing, samples were ground to a fine powder using a mortar and pestle and analyzed for C and nitrogen (N) concentrations via a VELP CN802 Carbon Nitrogen Analyzer (VELP Scientific, Deer Park, NY). As the soils contained negligible content of inorganic C, total C values obtained through elemental analysis reflect fraction organic C. As the DOM fraction typically represents a minor fraction of the total SOM, especially in agricultural soils, we opted not to analyze it further after separation. However, we did find it necessary to separate the DOM and CHAOM fractions to isolate the POM and MAOM pools that are most homogenous in their composition and best map on to their conceptual definitions.

Topography and climate data acquisition

To create the dataset used in subsequent multivariate analyses, several databases were called upon using R version 4.2.2 (R Core Team, 2022). For each farm, 1-km gridded, daily climate data retrieved for the period between 2015 and 2020 from the Daymet Daily Surface Weather dataset (Thornton et al., 2022) using the R package *daymetr* (Hufkens et al., 2018). Climate data were trimmed to represent the average period of planting through harvest for major row crops in the Northern Corn Belt, starting on Julian Day 121 and ending on Julian Day 304. The Daymet dataset provides daily maximum and minimum temperatures, which we averaged to construct a daily mean temperature. We calculated growing degree days with a base temperature of 10 °C,

such that heat units only accumulated when mean air temperatures exceeded 10 °C. Elevation data were retrieved from the USGS 3D Elevation Program using the get_tiles function contained within the *terra* package in R (Hijmans, 2022). To better capture landscape-level trends, we resampled and aggregated the elevation data using a factor of 8, based on an iterative analysis of the scale at which geomorphic features in agricultural land were most pronounced. The we then used the terrain function in the *terra* package to calculate slope and topographic position indices (TPI), a measurement of the elevation of a given grid-cell relative to the grid-cells surrounding it (higher values indicate a relatively higher grid cell, and vice-versa).

Data analysis

Mixed linear model and regression analysis

We used mixed effect linear models to test for differences in soil texture, soil pH, SOM-C, POM-C, and MAOM-C among stability zones. Models were built using the *lme4* package in R (v.1.1-31; Bates et al., 2015), and evaluated using the anova() function in the *stats* package (v. 4.2.2; R Core Team, 2022). Pairwise comparisons were made using examinations of the estimated marginal means of each stability zone contrasts pair using the *emmeans* package (Lenth, 2022). In the models we examined, stability zone was a fixed effect, and farm was a random effect. The alpha level for significant differences was set to 0.05. We also examined relationships between soil texture and MAOM-C and POM-C, as well as average crop yield and yield CV and soil texture and topographic indices via linear regression, using the lm() function in the *stats* R package (R Core Team, 2022). To account for differences in cropping rotation, edaphoclimatic characteristics, and management history, we scaled the response variables to the farm level using z-scores, with the mean and standard deviation of the population calculated at the site level,

similar to the approach of (Aksoy et al., 2016). All results presented below have been scaled using this method unless explicitly noted.

Assessing feature importance via gradient boosting

We used a supervised classification machine learning approach, regularized gradient boosting, to identify and understand potential indicator variables for delineating yield stability zones. We reclassified the stability zones into binary categories, stable and unstable, and then randomly split the dataset into training and testing datasets such that 80% of the data were contained in the training dataset, and 20% in the testing dataset. We included all SOM fraction data in the model matrix, as well as soil physical property data, nutrient data, and topography data. After training the model, we tested the optimized model on the training set, and assessed its accuracy in classifying yield zones based on soil and topography characteristics. We repeated this process 1000 times to arrive at an average model accuracy. From this ensemble of gradient boosting results, we extracted the edaphic, biogeochemical, and topographic variables that had the largest and most consistent impact on zone delineation.

Results and Discussion

To better understand the relationship between increasing SOM and spatiotemporal yield heterogeneity, we fractionated soils from areas of different yields and yield stabilities across 9 farms in the Upper Midwestern US. Our experimental goals and hypotheses were informed by a growing body of literature that shows that increasing SOM correlates with increased yield stability (Kane et al., 2021; Pan et al., 2009; Williams et al., 2016). Given that different physical fractions of SOM are thought to have different functions, we predicted that examining the fractions would give increased insight into the mechanisms behind the SOM-yield stability relationship. Specifically, we hypothesized that total SOM would be highest in high-yielding,

stable areas, and that these areas would have a higher POM:MAOM-C value than areas of the field that were more unstable. Contrary to our hypotheses however, we found that, on average, unstable zones had higher SOM-C stocks than stable yielding zones (Fowler et al., 2024). Additionally, while we found significant differences in the amount of POM- and MAOM-C among different stability zones, we did not observe significant differences in POM:MAOM-C. These findings challenge the often-assumed direction of causality whereby higher SOM supports higher yielding (Bauer and Black, 1994; Ma et al., 2023; Oldfield et al., 2022) and more stable cropping systems (Williams et al., 2016). Instead, our results indicate that causal linkages between SOM and yield stability may be bi-directional, depending on the scale of the inquiry (e.g., field vs. county vs. region). Here we present the results of our study, discuss potential drivers of POM and MAOM storage at the subfield scale, and evaluate the implications of our findings in regard to soil health indicators and soil C storage goals.

Patterns of C storage in bulk SOM and fractions

When examined across the farms in our study, we observed significant differences in the total SOM-C, MAOM-C, and POM-C storage between our four different yield-stability zones. Post-hoc analyses of the differences between zones in SOM-C indicated that unstable zones had 25.7% more SOM-C on average than low-yielding stable zones ($p = 0.016$; Figure 5.2A). We also observed trends towards increased SOM-C in the unstable zones relative to the other two stable zones based on estimated marginal means, however these differences were not significant ($p = 0.475$ and 0.331, respectively; Figure 5.2A). These observations run in contrast to current paradigms that indicate increasing crop yield stability in response to increasing SOM content. For instance, Pan et al. (2009) showed that the average yield variability decreased by 5% for every 1% increase in SOM (i.e., SOM-C x 1.72) when examined at the regional scale across

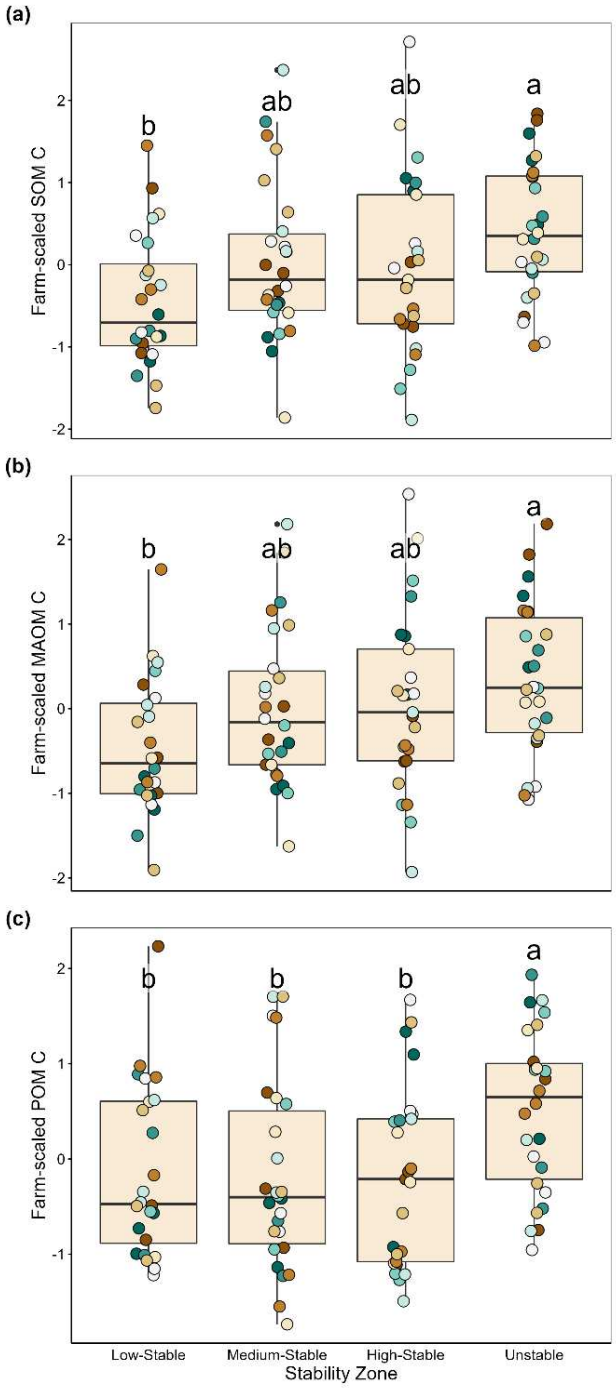

Figure 5.2 – Normalized concentrations of total soil organic carbon (SOM-C) (a.), mineral associated organic matter carbon (MAOM-C) (b.), and particulate organic matter carbon (POM-C) (c.) among the various stability zones. Different colored points represent different farms. To account for edaphoclimatic differences among farms, we scaled all data using z-scores prior to analysis, with the mean and standard deviation calculated at the farm level, yielding a unitless metric to compare by. Different lower-case letters indicate significant differences ($p < 0.05$). Points are offset horizontally to improve readability of the plot.

Chinese provinces. Although our data do not yield robust regressions between SOM-C and yield CV, the general trend of the data indicates increasing variability as standardized SOM increases (Supplemental Figure 5.1; $p = 0.077$, $r^2 = 0.02$). The MAOM-C results mirror the patterns we observed in SOM-C, with significant differences among stability zones ($p = 0.023$; Figure 5.2B), and post-hoc tests indicating that the low-yielding stable zone had significantly less MAOM-C than the unstable ($p = 0.013$), while the medium- and high-yielding zones were not significantly different than unstable zones ($p = 0.522$, 0.662; Figure 5.2B). The consistency of these two patterns is not suprising, as MAOM-C accounted for ~77% of the SOM-C in our data on average, consistent with previous examinations of agricultural soils (Sokol et al., 2022). Subfield variation in MAOM-C content has been observed in previous studies (Usowicz and Lipiec, 2017), but to the best of our knowledge, the covariation with yield stability such as this has not been examined thus far.

The POM-C content showed a different pattern across yields and stability zones from the patterns we observed for SOM-C and MAOM-C contents (Figure 5.2). While we still found a significant difference between stable and unstable zones, stable zones showed similar POM-C levels, regardless of average yield ($p = 0.019$, Figure 5.2C). This contrasts our original hypothesis, that POM-C would be highest in high-yielding, stable zones as a result of increased organic inputs in the form of both aboveground crop residue and crop roots (Gosling et al., 2013; Sokol et al., 2019). Our results indicate that POM-C abundance was not driven by yield or residue inputs, rather other characteristics of unstable yield zones may have led to increased POM-C stocks relative to stable areas.

Evaluation of POM:MAOM-C ratio as an indicator of biogeochemical function

The POM:MAOM-C ratio, has been suggested as a useful indicator for soil biogeochemical function (Cotrufo et al., 2019). Previous work has shown that the balance of POM-C to MAOM-C may help to explain the mineralization rate of organic N (Daly et al., 2021; Grandy et al., 2022), as well as help to identify soils that are approaching mineral C saturation *sensu* Stewart et al. (2007) (Castellano et al., 2015; Just et al., 2023). It has been also posited that a decreasing POM:MAOM-C ratio may indicate when residue inputs outpace residue decomposition, assuming fragmentation processes are not inhibited (Just et al., 2023). Despite similar POM-C levels across the various stable yield zones and covariation in yield with MAOM-C in our data, however, we observed no significant differences in the POM:MAOM-C ratio across the different yield stability zones ($p = 0.170$, Supplemental Figure 5.2). This similarity across zones, despite differences in POM- and MAOM-C among different stability zones, is likely the results of the reasonable expected effect size of changes in POM:MAOM-C ratio in agricultural soils that are inherently MAOM-C rich and POM-C poor (Prairie et al., 2023, Lugato et al., 2021). To exemplify this issue, across all of our samples, the average POM-C was 2.0 g C per kg soil, and the average total SOM-C was 15.9 g C per kg soil, with an average POM : MAOM-C ratio of 0.16. If POM-C was increased by 50%, to 3.0 g C per kg soil, SOM-C would increase by 5.9 %, but the POM : MAOM-C ratio would adjust only to 0.23, an ecologically insignificant shift well within the observed range of our data (0.02–0.42; Supplemental Figure 5.2). As such, we were unable to use it as a metric to understand differences in SOM formation and function among different stability zones. We suggest that for POM:MAOM-C ratio to be a useful indicator, further research is needed on how to best contextualize and understand this measure when applied to agricultural systems. For example, exploring the ratio of POM-C to exchangeable

MAOM-C may present a more actionable indicator, if robust methods of exchangeable MAOM-C can be identified (Daly et al., 2021; Jilling et al., 2018a).

Drivers of carbon accumulation in MAOM

To explore the possible mechanisms behind the variability in MAOM-C content among different yield-stability zones, we examined a set of edaphic characteristics known to be well correlated to MAOM storage (Hassink, 1992). As expected, MAOM-C had a significant, positive relationship with the proportion of fine particles within a sample ($p < 0.001$, $r^2 = 0.30$; Supplemental Figure 5.3). This relationship partially explained the patterns we observed in MAOM-C across stability zones (Figure 5.2B); when we examined the difference between MAOM-C in unstable and low-yielding, stable zones as a function of the difference in fine particles, the differences in MAOM-C became negligible when particle distributions were similar ($p = 0.002$, $r^2 = 0.297$; Supplemental Figure 5.4). On average across sites, however, we observed significant differences in the proportion of silt and clay particles across stability zones, with unstable and high-yielding, stable zones having significantly higher farm-scaled silt and clay values than medium- and low-yielding stable zones ($p < 0.001$; Figure 5.3). We posit that these differences are a result of the topographic settings of the unstable and high-yielding stable zones, corroborated by our observation of a significant relationship between the silt and clay content in soil and the TPI ($p < 0.001$, $r^2 = 0.10$). As observed by Maestrini and Basso (2018), both high-yielding, stable zones and unstable zones are often located in depositional areas that receive downslope contributions of fine soil particles on the decadal timescale. Our study finds a similar distribution of stability zones amongst low-lying areas, with both the high-yielding, stable zones and the unstable zones having a relatively high fine particle content (Figure 5.3) and being found primarily in lower areas of the field (Figure 5.4). Our findings thus corroborate previous observations of crop yield

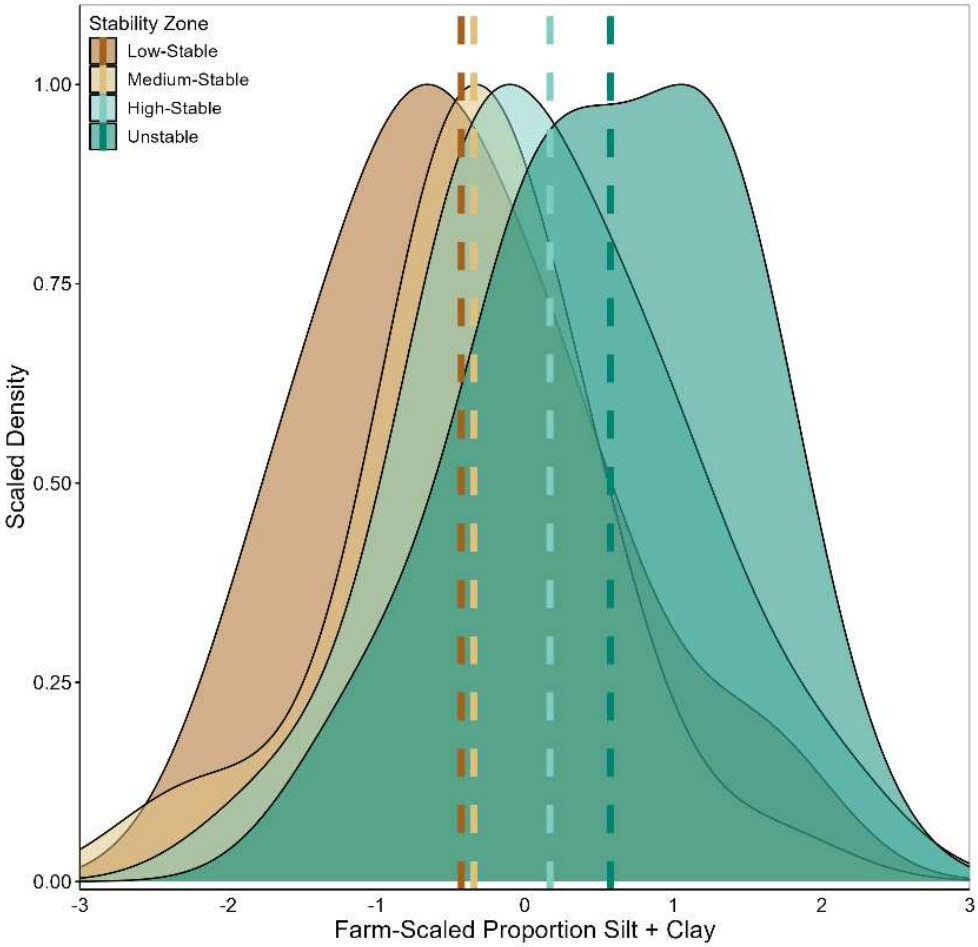

Figure 5.3 –Scaled density plot of z-scored silt and clay content of soils from various stability zones. Dashed lines indicate the mean z-score for the corresponding stability zone.

heterogeneity in areas of topographic complexity (Kravchenko and Bullock, 2000; Maestrini and Basso, 2018; Leuthold et al., 2021). The similarity in texture and topography between unstable and high-yielding, stable zones highlight an important point: unstable zones have a capacity to be especially high-yielding under the right environmental conditions (Fowler et al., 2024; Martinez-Feria and Basso, 2020). Further research into the properties of these unstable zones, such as impeded soil drainage or impediments to rooting ability may help to disentangle what makes

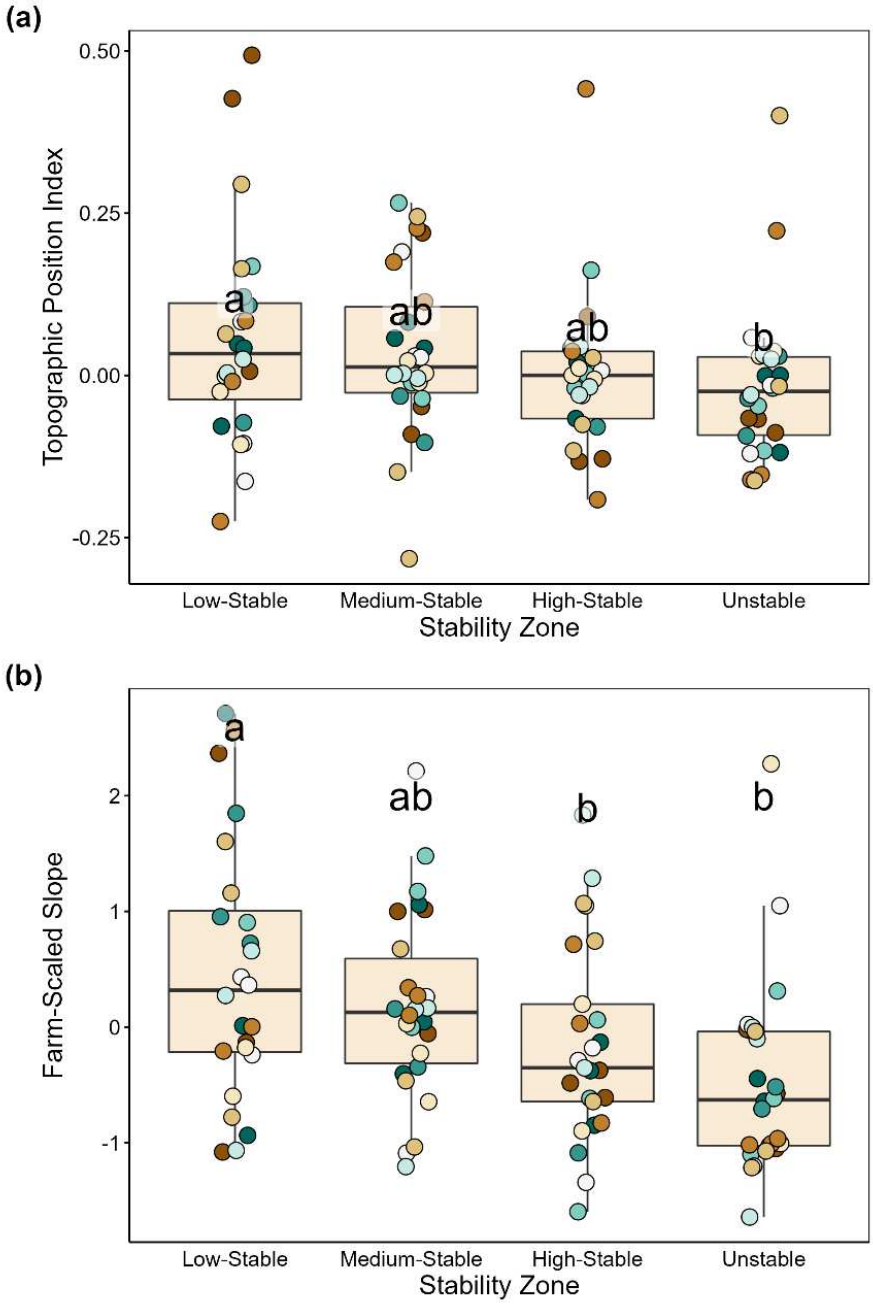

Figure 5.4 – a.) Topographic position index values across the various stability zones. Lower values indicate a point in space lower than its surroundings, while higher values indicate relatively elevated locations and b.) Slope values scaled using z-scores to the individual farm level. Different colored dots represent different farms. Different lower-case letters indicate significant differences ($p < 0.05$). Points are offset horizontally to improve readability of the plot.

some areas with similar texture and topography consistently high yielding, while others are especially sensitive to environmental stressors.

In addition to these edaphic controls, we also observed an association between increasing yields and increasing MAOM-C content. Linear regression analysis indicated that as mean yield within a stability zone increased, so did MAOM-C. This relationship was weak, likely reflecting the influence of cropping system, soil physicochemical properties, and climate on variability in MAOM-C and yield ($p = 0.048$, $r^2 = 0.08$; Supplemental Figure 5.5). However, this result does mirror recent studies that support causal linkages between increasing productivity and increased MAOM-C (Hansen et al., 2024; King et al., 2023; Prairie et al., 2023). Indeed, there are a number of pathways by which increasing yield (and the associated increase in crop residue) can increase the amount of MAOM-C, especially in areas of the field that are receiving inputs of eroded minerals that may have a high capacity for sorption of dissolved organics (Van Oost and Six, 2023). Understanding relationships between topography, productivity, and mineralogy is thus key for understanding how MAOM-C accumulates in croplands, and how sampling strategies must be designed to capture accurate estimates of cropland SOC stocks and their spatial variability.

Mechanisms for increased POM-C storage

In contrast to MAOM-C, POM-C did not closely follow the patterns of total SOM-C content variation observed across our yield stability zones, and POM-C content in unstable zones was significantly higher than in all stable zones ($p = 0.019$), which had the same POM-C content independent of yields (Figure 5.2C). Further diverging from patterns in MAOM-C, we could not identify any edaphic or cropping system properties that helped to explain patterns in POM-C—it was not correlated with average yield ($p = 0.337$, data not shown), even when accounting for

differences in cropping system (reported in Table 5.1). We did observe significant, positive relationships between POM-C and soil texture ($p < 0.001$; data not shown), and soil pH ($p < 0.001$ and $p = 0.009$, respectively; data not shown), both of which have been suggested as potential controls on POM-C accumulation (Hansen et al., 2024; Kögel-Knabner and Amelung, 2021). In our study however, our observation of parallel increasing of POM-C and texture may be indicative of covariation in these measurements across our stability zones rather than a signal of a causality, and pH did not vary systematically across the stability zones in a way that would help to explain the patterns of POM-C variation ($p = 0.224$).

Given that we did not observe evidence that POM-C conferred additional stability to cropping systems, as our original hypothesis, we propose an alternative hypothesis consistent with our findings (Figure 5.5) is that the accumulation of POM-C within areas of increased spatiotemporal yield heterogeneity is controlled by constrains on decomposition outpacing those on productivity during the unfavorable climate years. Unstable zones tend to have a higher incidence of water-logging (Leuthold et al., 2021; Maestrini and Basso, 2018), which can impact both soil microbial activity and crop productivity. While these hydrologic stressors most often are discussed in regard to their detrimental effect on crop yield – early season saturation can reduce crop root viability and emergence (Wenkert et al., 1981), limited oxygen availability under saturated conditions also reduces the capacity of the microbial community to depolymerize and break down POM and alters microbial community structure (Bowles et al., 2018; Cates et al., 2022). This reduced decomposition could contribute to multi-season feedback in these unstable zones; under optimal conditions, decomposition and nutrient mineralization may be increased relative to stable yield areas due to the increased amount of available POM-C. The ecosystem services provided by POM (e.g., increased aggregation and nutrient availability), combined with optimal

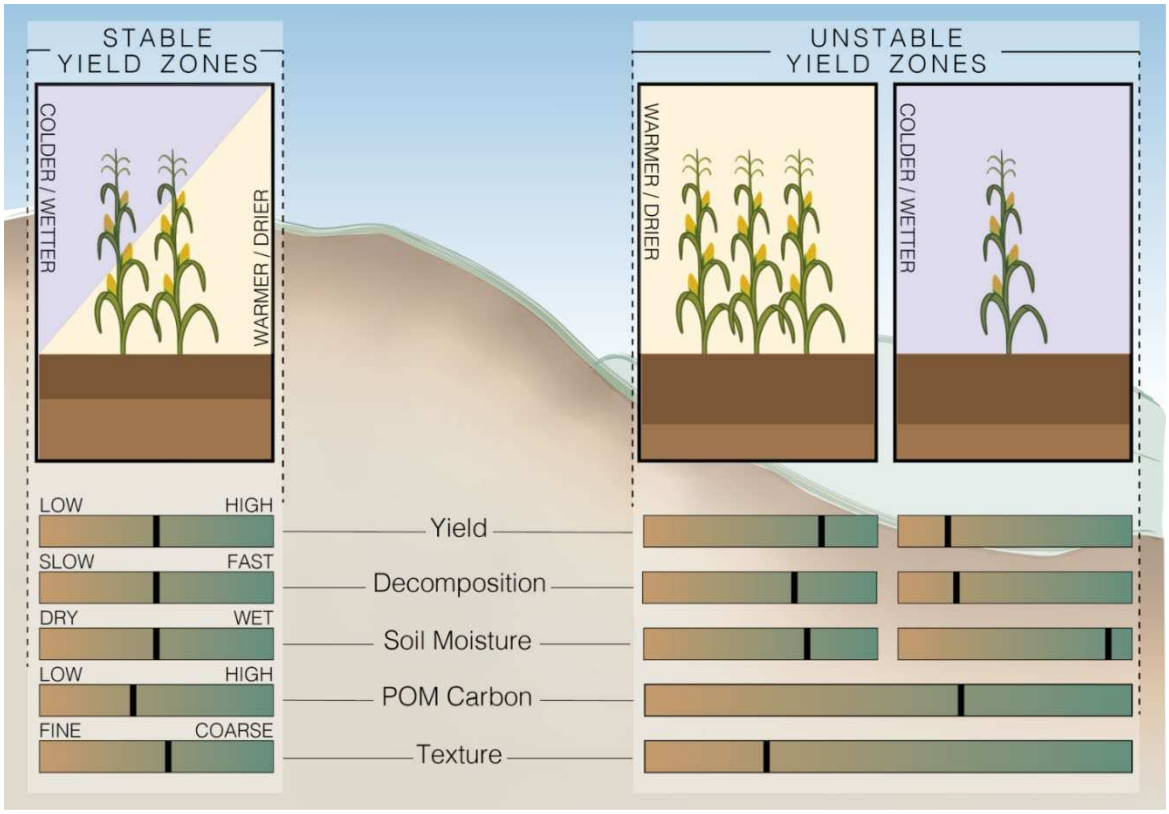

Figure 5.5 – Conceptual model of proposed biogeochemical differences between stable and unstable yield zones. Stable zones, often in upslope positions, are characterized by consistent yields across weather conditions, partially due to a decreased incidence of saturated conditions. The same conditions allow for a consistent rate of particulate organic matter (POM) decomposition and nutrient provisioning across growing seasons. In contrast, low-lying, unstable yield zones experience much more drastic shifts in their soil water status from year to year, altering the rate of POM decomposition. In wetter years, in which saturated soil conditions are more likely, decomposition rates are slowed, leading to an accumulation of POM. Under dry or optimal conditions, low-lying, deeper, more finely textured soils that are characteristic of the unstable yield areas may maintain increased water retention, leading to an advanced rate of nutrient cycling, increased productivity relative to the rest of the field, and subsequently, increased inputs to the POM pool.

soil-water conditions, could then encourage increased productivity and yields, potentially leading to replenishing POM stocks that may have been decreased over the course of the optimal season (Figure 5.5). This hypothesis is partially corroborated by the topographic characteristics of our various stability zones (Figure 5.4). We examined both the farm-scaled TPI and the average slope for each stability zone, and found that high-yielding, stable zones and unstable zones both had

significantly lower average slopes, and significantly lower TPI values than low- and medium-yielding stable areas ($p = 0.001$ and $p < 0.001$, respectively; Figure 5.4). Additionally, we observed a significant, negative relationship between the position index and POM-C; as TPI increased, the amount of POM-C decreased ($p = 0.004$; Supplemental Figure 5.6). We did not observe the same relationship with slope ($p = 0.903$), which could be due to different topographic positions having similar slopes (e.g., summit and footslope positions). Some evidence for this is offered by the results of including an interaction term between slope and stability zone, which yields a significant result ($p = 0.029$). Fowler et al. (2024) found similar relationships; they indicated that topographic variables such as slope and the log of flow accumulation (i.e., topographic wetness index) were adequate predictors of SOM-C and other soil health indicators in these fields, potentially highlighting how POM-C can act as an indicator of soil biogeochemical dynamics. These important trends lend some credence to our framework (Figure 5.5), though a considerable amount of variance in POM-C remains unexplained by these factors ($r^2 = 0.07$ for TPI and 0.09 for slope x stability zone respectively).

Our gradient boosting analysis also supports our alternative hypothesis for increased POM storage in unstable yield zones. We used a gradient-boosted random forest analysis to determine important predictors of stable vs. unstable yield zones. Our model was able to predict stable vs. unstable zones with ~72% accuracy, and over the course of 1000 iterations, identified POM-C and TPI as the most important variables in characterizing the zones (Figure 5.6). Thus, while our original hypothesis of POM acting to increase yield stability may not be supported by these data, our results do show that the POM-C content may serve as a useful and important indicator for areas prone to increased heterogeneity or variability in decomposition status when robust subfield sampling is employed. Future work that links soil microclimate data to decomposition

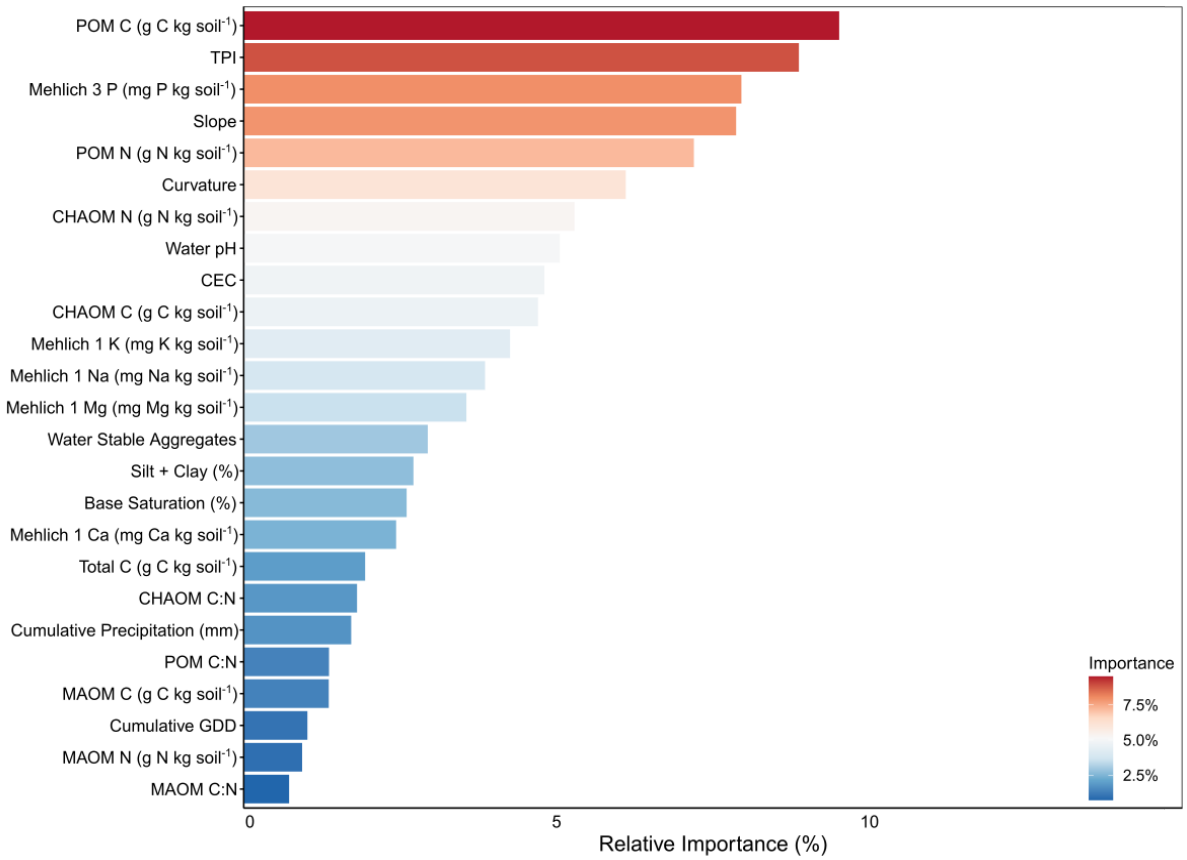

Figure 5.6 – Relative importance of variables in predicting yield stability zones as determined by the gradient boosted random forest model employed here. Relative importance represents the average of the feature importance over the course of 1000 model iterations. (POM: Particulate organic matter, CHAOM: Coarse, heavy organic matter, MAOM: Mineral associated organic matter, C: Carbon, TPI: Topographic Position Index, P: Phosphorus, N: Nitrogen, CEC: Cation exchange capacity, K: Potassium, Na: Sodium, Mg: Magnesium, GDD: Growing degree days).

rate across areas of complex topography will help to further elucidate the drivers of fractional SOM distribution among yield stability zones. Microbial community composition may also help provide insight into the means by which different fractions of organic matter accumulate and persist in heterogenous areas.

Conclusions

We examined the difference in C storage in bulk SOM and among SOM physical fractions in soils sampled from different yield stability zones from nine farms across the upper Central United States. Whereas previous analyses have found increased crop yield stability with increasing SOM, our results indicate that this relationship may not always hold true depending on the scale of inquiry. At the subfield scale, we found increased POM-C in unstable yield zones, which may be an indicator of reduced decomposition. We also found increased MAOM-C in unstable zones, which was well correlated with increased incidence of fine-particles and increased yield potential in these zones. Given the continued rise of precision agriculture technologies (Basso and Antle, 2020), increased understanding of the mechanisms that confer stability unto a given area within a crop field are of paramount importance. Our work does not stand in contrast to previous publications that show that cropping system heterogeneity may be reduced with increasing SOM concentrations, but instead offers an important insight that the controls on the relationship between SOM and stability depends on the scale of inquiry, and that at the subfield scale, unstable zones may be characterized by increased SOM-C, especially in the POM fraction. Our results provide step towards understanding how geomorphology, inter-annual weather variability, and cropping system productivity interact to determine the distribution of SOM among physical fractions across heterogenous crop fields, and can serve to improve nutrient management strategies, carbon sequestration objectives, and guide robust sampling for the quantification of farm-scale SOM stocks.

CHAPTER 6: DECADAL PERSISTENCE OF SOIL ORGANIC MATTER FORMED FROM LITTER AND PYROGENIC INPUTS

Introduction

Soil organic matter (SOM) is a critical component of ecosystem nutrient cycling and productivity, as well as the global carbon (C) sink. In most terrestrial systems, plant litter constitutes a primary source of SOM. Additionally, pyrogenic organic matter (PyOM) accounts for a significant proportion of inputs into SOM in fire prone systems (Lavallee et al., 2019), the implications of which are increasingly important to understand as fire frequency is expected to increase (Huang et al., 2015; Pellegrini et al., 2018). Understanding the mechanisms by which plant-derived C and nitrogen (N) that enter the soil system as either litter or PyOM persist as SOM is thus key to understanding land-atmosphere C exchange in current and future climate and management scenarios. Long-term persistence of SOM has been attributed to associations between organic molecules and soil minerals (Kleber et al., 2015), chemical recalcitrance of highly condensed aromatic compounds (Aber et al., 1990; Lavallee et al., 2019), and energetic or spatial constraints (Cotrufo and Lavallee, 2022) on microbial decomposers (Six et al., 2000). As a consequence of this variety in stabilization mechanisms, SOM represents a mosaic of plant and microbially derived compounds in various stages of decomposition (Whalen et al., 2022). The distribution of these compounds among physically or chemically defined SOM fractions characterized by different mechanisms of stabilization such as particulate organic matter (POM), organic matter associated with the coarse, heavy soil fraction (CHAOM), mineral associated organic matter (MAOM), and PyOM can help forecast the persistence of the SOM pool (von

Lützow et al., 2008), and better inform models of land-atmosphere-energy and greenhouse gas exchange (Zhang et al., 2021).

Despite its importance, the fate of C and N that enter the SOM pool through decomposition of organic inputs, such as plant litter or PyOM, often remains opaque on management relevant timescales. Coupling fractionation with isotope tracing is a powerful way to quantify the fate of SOM inputs (Cotrufo et al., 2015; Haddix et al., 2016; Hicks Pries et al., 2017); short-term incubations provide important insight around SOM formation dynamics (Cotrufo et al., 2015a), and radiocarbon tracing studies can provide valuable information on centennial and millennial timescales (Shi et al., 2020). However, studies that couple isotope labeling with SOM fractionation at the decadal time scale are limited, and have been primarily performed in forest ecosystems (Hatton et al., 2012; Hicks Pries et al., 2017). This has led to uncertainty surrounding how different fractions of SOM transform and persist on scales relevant to soil C sequestration goals (Dynarski et al., 2020) or in C rich ecosystems such as grasslands, presenting an important gap in our understanding of the current paradigms of SOM formation and storage. A full understanding of decadal scale C storage and cycling is further limited by a focus on litter derived SOM; despite evidence that PyOM is ubiquitous in soils and has an impact on C stocks and SOM mean residence time (Lavallee et al., 2019; Sanderman et al., 2021), it remains understudied (Bird et al., 2015).

To address this gap in understanding, we returned to 10-year in-field incubations of ^{13}C and ^{15}N enriched aboveground plant litter (Cotrufo et al., 2015) and PyOM (Soong and Cotrufo, 2015) to evaluate transformations and persistence of plant derived C and N in physical SOM fractions in the top soil of a temperate tallgrass prairie ecosystem (Kansas, USA; mean annual temperature = 12.8 ^{O}C, mean annual precipitation = 835 mm), constituting, to our knowledge, the first isotope

tracing study of its duration in a grassland system. We combined the isotopic labeling with physical fractionation and stoichiometric analyses to quantify the proportion and degree of microbial transformation of leaf litter and PyOM-derived C and N which remained as POM, CHAOM, and MAOM, roughly a decade after litter or PyOM addition to the soil surface. We hypothesized that despite the initial litter C loss during pyrolytic conversion of litter to PyOM, the distinct chemical recalcitrance and low-density nature of this fraction would lead to sustained preservation in the POM fraction over the course of the experiment. We also hypothesized that after ten years, little litter derived SOM would remain, and that which did remain would be in the MAOM fraction. We expected this decadally persistent litter derived MAOM to have a C:N ratio that reflected increased microbial processing compared to that of litter derived MAOM observed at earlier sampling dates.

Materials and Methods

Experimental Site

Both the litter and PyOM incubations were conducted at the Konza Prairie long-term ecological research station in Kansas, USA. The ecosystem is a temperate continental, tall-grass prairie with a mean annual precipitation of 835 mm, and a mean annual temperature of 12.8 ^{O}C. The dominant vegetation at the site is Big bluestem (*Andropogon gerardii*), which accounts for approximately 80% of the total ground cover. Soils are derived from limestone and shale parent material and are generally silty clay loam Mollisols. Prescribed burning is a common management practice at this experimental station, and the site of the experiment (Konza designation RB20) had been burned annually between 1972 and 2000. Other than a wildfire in 2008, it has not been burned since 2000. Across our studies, the mean soil organic C (SOC) stock to 5 cm was 3923 g C m^{-2} (± 52 g C), and the mean soil total N stock was 302 g N m^{-2} (± 5 g N).

There was no temporal trend to bulk C and N stocks in our observations, indicating that the system had reached steady state (Supplemental Figure 6.1), nor were there significant differences between the SOM stocks at the litter site and at the PyOM site. The C:N ratio of the bulk SOM was 12.7 (± 0.1), with no significant difference among harvest dates (Supplemental Figure 6.2).

Creation of isotopically derived litter and pyrogenic material

To create the litter applied in this initial incubation, *A. gerardii* was grown from seed for 22 weeks in a continuous ^{13}C and ^{15}N labeling chamber as described previously(Soong et al., 2014). The use of the chamber allowed for the production of litter enriched to 3.3804 atom % ^{13}C and 3.9917 atom % ^{15}N. After reaching maturity, litter was air-dried, trimmed to 20 cm lengths, and homogenized. Water content was measured on three oven-dried sub samples (65 ^{O}C), and masses were corrected to dry-weights. Oven dried samples were finely ground and analyzed via elemental analysis-isotope ratio mass spectrometry (EA-IRMS; Carlo Erba NA 1500 coupled to a VG Isochrom continuous flow IRMS, Isoprime inc.) for C and N concentration and ^{13}C and ^{15}N isotopic composition. For the production of PyOM, the ^{13}C and ^{15}N isotopically labeled *A. gerardii* above ground plant biomass was pyrolyzed for 4 hours at 450 ^{O}C, using a muffle furnace with ultra-high purity nitrogen flow. These pyrolysis conditions were chosen to produce an isotopically labelled PyOM that was structurally and chemically similar to natural PyOM that was recovered from the field site after a wildfire. Proximate and ultimate analysis indicated that the produced PyOM was similar in ash content and pH to natural PyOM collected at the field site(Soong and Cotrufo, 2015). Subsamples of the created PyOM were analyzed for C and N concentrations as well as ^{13}C and ^{15}N isotopic composition via EA-IRMS analysis as described above.

Incubation Experiments

Both the litter and the PyOM incubation experiments were designed as repeated measures randomized complete block designs with four replicates per sampling point. Two treatments were established in both experiments: the organic input (i.e., the labeled litter or PyOM) and a bare soil control (i.e., no input addition). Polyvinyl chloride (PVC) collars (20 cm diameter and 10 cm tall) were inserted 5 cm into the soil surface to designate experimental units. Plants were removed from the area within the collars via herbicide addition and manual removal. On September 29th, 2010, 18.4 g dry-weight equivalent of the homogenized labeled litter was added to each of the litter-treatment collars, in direct contact with the soil surface. The PyOM experiment was established in a similar manner on May 8th, 2012, however the PyOM was gently mixed into the top 2 cm of soils to prevent erosive loss. To account for the litter loss that would occur during burning, 5.9 grams of PyOM was added to the PyOM treatment collars, commensurate with our 30% recovery during pyrolysis. A coarse PVC mesh screen (mesh size: 6.35 mm) was used to cover each collar to prevent fresh litter inputs. For the litter treatments, harvests occurred on October 8, 2011 (12 months from incubation), September 29, 2012 (24 months), September 25, 2023 (36 months), and October 13, 2020 (120 months). For the PyOM treatments, harvests were less frequent, and occurred on September 8, 2012 (4 months), April 4, 2013 (11 months), and October 13, 2020 (101 months).

For each harvest, soils from the bare soil control and the treatment collars were excavated using a hand-shovel, carefully removing the entire collar area in incremental depths (0-2 cm, 2-5 cm). We chose to focus on the top soil depths as previous samplings found little recovery of the isotopic label below 5 cm(Soong et al., 2016). Soils were stored at 4 ^{O}C during transport and prior to processing. Upon arrival at Colorado State University, soil samples were carefully

picked clean of leaves and roots, and sieved to 2 mm. For the litter treatment, undecomposed litter was carefully removed, and a subsample was oven-dried at 105 ^{O}C. The soil samples were fractionated using a combined size and density fractionation to separate SOM into physical fractions (i.e., POM, CHAOM, and MAOM) (Leuthold et al., 2022a). Briefly, soils were first dispersed by shaking with glass beads in sodium polytungstate (SPT; $H_2Na_6O_{40}W_{12}$) adjusted to 1.85 g cm^{-3}. After centrifugation, the POM was vacuum aspirated and well rinsed with DI water. The remaining heavy mineral fraction was separated into CHAOM (> 53 μm) and MAOM (< 53 μm) via wet sieving. For all harvests except the final harvest, the MAOM fraction was further separated into silt and clay associated organic matter via centrifugation, but here we present all data for MAOM as a combination of the silt and clay associated OM. The fractions were oven-dried (60 ^{O}C). All oven dry bulk soil and SOM fraction samples were finely ground and analyzed for C and N concentrations as well as ^{13}C and ^{15}N isotopic composition via EA-IRMS, as described above.

Data Analysis

Data analysis was conducted in R, version 4.3.2(R Core Team, 2022). To calculate the contributions of the litter and PyOM additions to the SOM fractions, we used a two-pool isotopic mixing model (Equation 6.1).

$$f_{Litter} = \frac{\delta_{Amended} - \delta_{Bare}}{\delta_{Litter} - \delta_{Bare}} \quad \text{(Eq. 6.1)}$$

where f_{litter} is the fraction of litter or PyOM derived SOM in the whole sample, $\delta_{Amended}$ is the δ^{13}C or δ^{15}N of the SOM fractions that received the enriched amendment, δ_{Bare} is the δ^{13}C or δ^{15}N of the bare soils SOM fraction, and δ_{Litter} is the δ^{13}C or δ^{15}N of the PyOM or litter addition, following refs 19 and 21. We determined the pool size of the SOM C and N by multiplying the C

or N stock (calculated using the gravimetric bulk density at Harvest 1) by the $f_{litter.}$ We tested for difference between sampling date using a linear mixed effects model in R, using the *lme4* and *lmerTest* packages (Bates et al., 2015; Kuznetsova et al., 2017; R Core Team, 2022). We specified our model with harvest date as a fixed categorical effect and replicate as a random effect. A similar approach was used to test for differences in input derived C:N ratio. Post-hoc comparisons of contrast coefficients were used to test pair-wise comparisons between specific harvest dates, using the Tukey adjustment in the *emmeans* package in R(Lenth, 2022; R Core Team, 2022). We calculated the temporal coefficient of variation as the standard deviation of the input derived C or N stocks divided by the mean of the input derived C and N stocks across sampling dates for each replicate, and tested for differences among fractions using a linear mixed model (via *lme4*) with replicate as a random effect and fraction as a fixed categorical effect (Bates et al., 2015; Kuznetsova et al., 2017).

Results and Discussion

Retention of above-ground litter and PyOM derived C and N in the soil after 10 years

After ten years, 7.03% of the initial above-ground litter C input (Figure 6.1) and 24.17% of litter N input was retained in the bulk SOM. These retention estimates are lower than previous measurements of litter derived SOC persistence over ten years from a conifer forest ecosystem (22-28% for C) (Hicks Pries et al., 2017), likely due to slower decomposition of needle versus grass litter due to differences in original litter chemistry and the higher relative proportions of unhydrolyzable material (Prescott et al., 2000).

Due to its inherent chemical recalcitrance (Schmidt et al., 2011), far more of the applied PyOM remained in the soil than litter material; 60.82% of PyOM derived C, and 53.43% of PyOM derived N was present in the bulk SOM after 8 and a half years of incubation. When the C loss

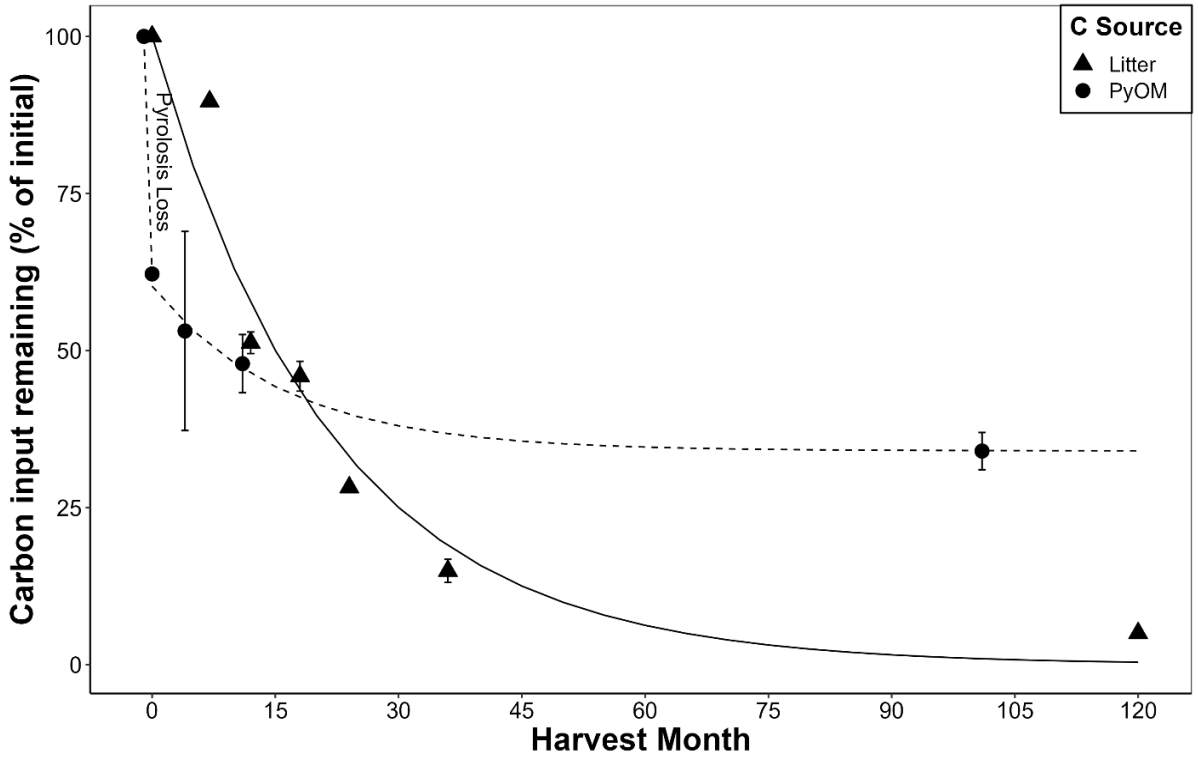

Figure 6.1 - Litter and pyrogenic organic matter (PyOM) derived C remaining in the top 5 cm of soil over the course of the decomposition experiment as percent of the initial. In September 2010 and October 2012, *Andropogon gerardii* litter and pyrolyzed material were applied to the soil surface of a tallgrass prairie, respectively. Subsequent harvests occurred at 7, 12, 18, 24, 36, and 120 months after installation for the litter (Triangles, solid line), and at 4, 11, and 101 months after installation for the PyOM (circles, dashed line). After accounting for the loss of C during the pyrolysis process (labeled), the PyOM retained significantly more carbon across the incubation period than the litter. Points represent mean values, and error bars represent standard errors (n = 4).

that occurs during the pyrolytic conversion of litter to PyOM is accounted for, the amount of PyOM derived C remaining at the end of the experiment decreases to 34.00%, a 38.8% loss during conversion (Figure 6.1). Regardless, the inherent metabolic challenge of mineralizing condensed aromatic and polyaromatic ring structures that compose PyOM (Aber et al., 1990; Bird et al., 2015) leads to a significant increase in decadal C storage compared to the litter treatment (Lavallee et al., 2019), consistent with previous hypotheses (Lehmann et al., 2021). While this suggests that introduction of PyOM material may be a robust method of increasing

ecosystem C storage, previous work in these sites also highlighted a tightening of the N cycle in response to PyOM additions, with decreased organic N availability in first 11 months following PyOM application (Soong and Cotrufo, 2015). The persistence of the PyOM on the decadal scale suggests that this decrease in SOM-N bioavailability may extend past the initial period and limit internal ecosystem N recycling in the years following above ground biomass burning and PyOM introduction into the system, subsequently limiting plant N uptake and ecosystem net primary productivity (Pellegrini et al., 2018; Soong and Cotrufo, 2015). Balancing C sequestration and N availability is thus an especially important management consideration in systems where PyOM is applied (i.e., via biochar application) or created via fire.

Decadal persistence of litter derived C and N in physical SOM fractions

As we hypothesized, in contrast to the 36 month harvest when the majority of litter derived SOM was found in the POM and CHAOM fractions (Figure 6.2) (Soong et al., 2016), after 10 years most of the remaining litter derived C and N was found in the MAOM fraction (65.83 ± 0.95 and 73.03 ± 0.98% of the remaining C and N, respectively; Figure 6.2). Some litter derived C and N persisted as POM (23.69 ± 1.09% remaining C and 23.69% ± 1.09% remaining N), and a portion was also present in the CHAOM fraction, though to a lesser degree (10.48 ± 0.95% remaining C, 7.48 ± 0.95% remaining N; Figure 6.2). This finding confirms the more rapid turnover of litter derived POM and CHAOM compared to MAOM at the decadal scale (Cotrufo and Lavallee, 2022), as these fractions lack protection mechanisms against mineralization beyond spatial occlusion.

Stoichiometry allows for some insight into the extent of microbial transformations of SOM, with SOM becoming more N rich as microbial processing occurs (Li et al., 2013). Similar to our original observations during early stages of litter decomposition (Soong et al., 2016), at the final

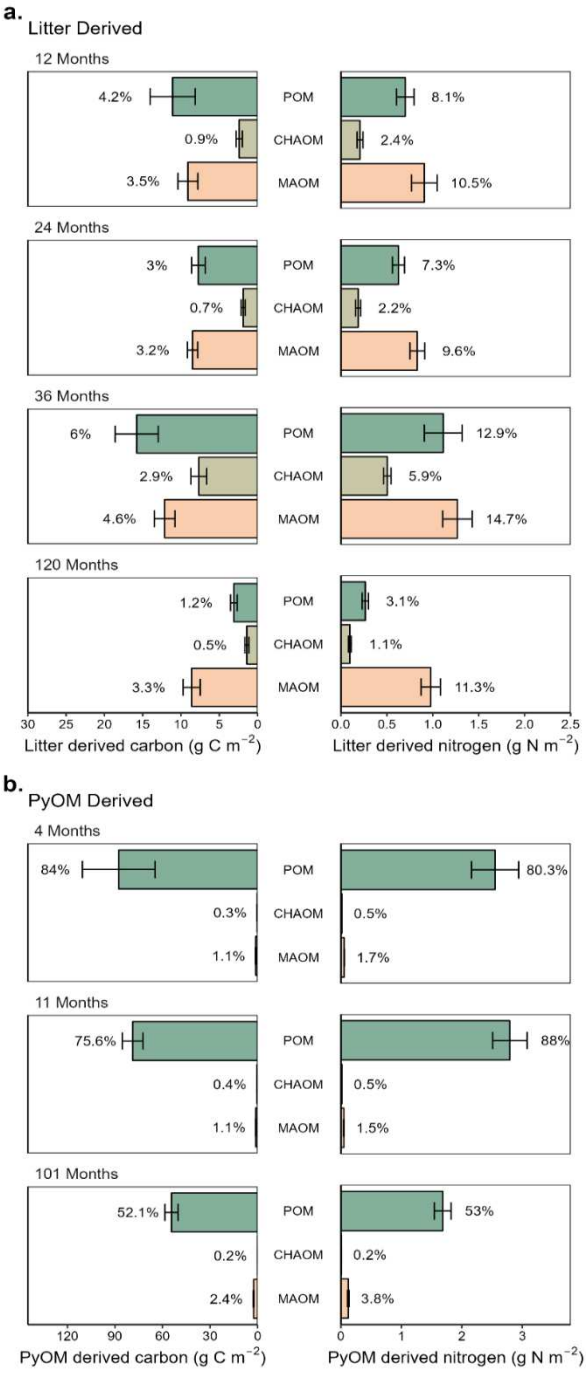

Figure 6.2- Distribution of (a) litter and (b) pyrogenic organic matter (PyOM) input-derived C (left) and N (right) among physical soil organic matter fractions at key harvest dates throughout the experiment. Bar length indicates mean C or N stocks to 5 cm, error bars represent standard error, and numbers next to the bars represent the percent of the initially added litter (261.2 g C m^{-2}; and 8.6 g N m^{-2}) and PyOM (104.2 g C m^{-2}; and 3.2 g N m^{-2}) C or N remaining in that fraction at harvest.

harvest date the litter derived C:N ratios varied significantly among fractions: the C:N ratio of the fractions were 11.57 ± 0.82, 14.10 ± 1.36, and 8.85 ± 1.00 for the POM, CHAOM, and MAOM fractions, respectively ($p < 0.001$; Figure 6.3). Pairwise comparisons of C:N ratio among our various harvest dates indicated no significant transformation of the C:N ratio of any of the three physical fractions over ten years of decomposition in the field. Initial harvests established that MAOM was formed within the first seven months of decomposition (Cotrufo et al., 2015), primarily through the mineral sorption of soluble plant components either directly (Sokol et al., 2019), or following microbial processing (Liang et al., 2017). However, given the duration of the initial experiment (Soong et al., 2016), it was unclear whether this MAOM would persist as a stable fraction of SOM, or would rapidly exchange with the soil solution as the POM and CHAOM fractions continued to be processed. After ten years, we observed little to no evidence that MAOM is actively exchanging with the litter pool or undergoing microbial transformations following the initial stabilization. Though we observed a slight decrease in the C:N ratio of the MAOM pool, pairwise comparisons indicate that it was not significantly altered between the 12-month and the 120-month sampling (C:N = 10.12 and 8.85, respectively; $p = 0.78$, Figure 6.3). Further, as the litter derived POM pool was decomposed over time, we did not observe a change in the size of the litter derived MAOM pool (Figure 6.2). Models of SOM formation that consider MAOM formation as the terminal stage of POM decomposition(Grandy and Neff, 2008) expect that as POM decomposes a fraction of that C should be transferred into the MAOM. While our isotopic methods cannot rule out exchange between decomposed POM and a dynamic MAOM pool (Woolf and Lehmann, 2019), the stability of the MAOM C:N ratio (Figure 6.3) and the apparent lack of new MAOM formation following POM decomposition (Figure 6.2)

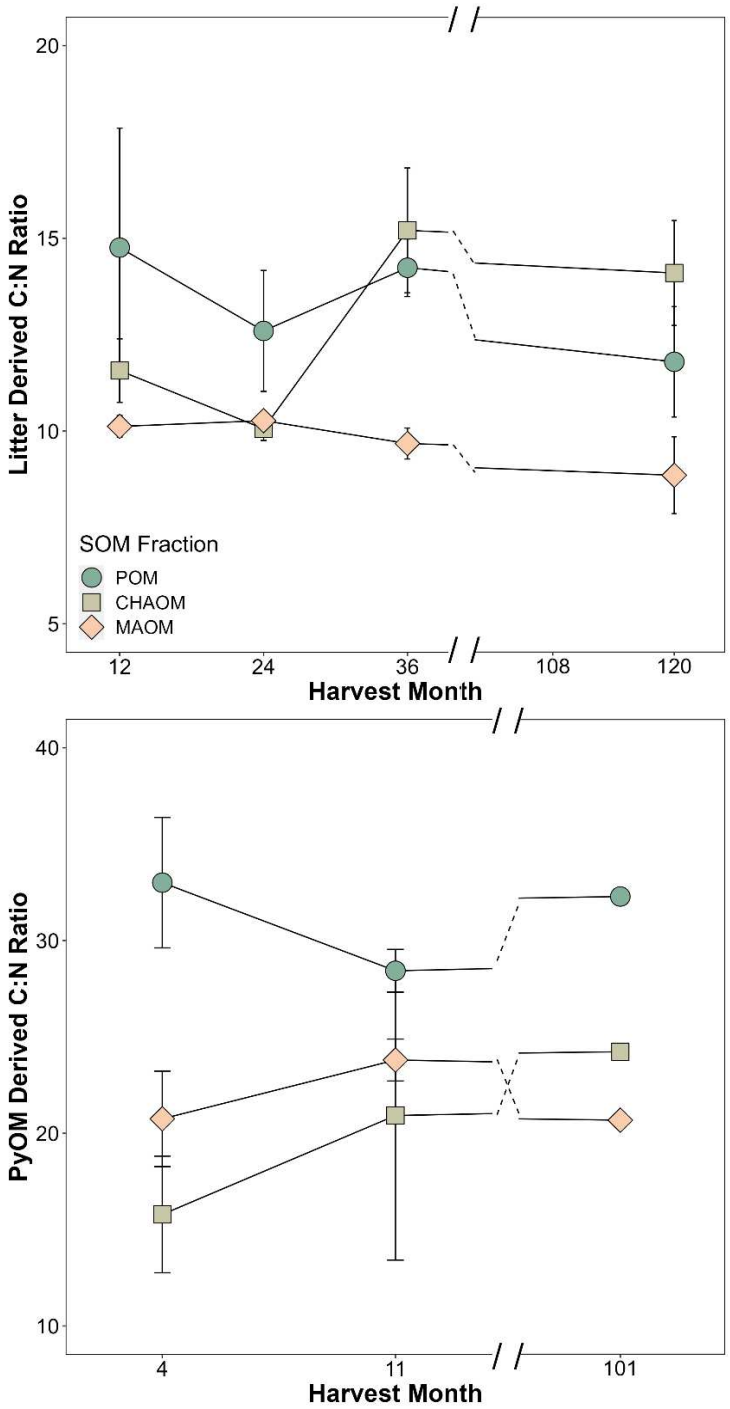

Figure 6.3 - Litter and PyOM derived carbon to nitrogen (C:N) ratios of physical soil organic matter fractions over the course of the incubation period Litter derived MAOM C:N was relatively stable over the course of the experiment, with no significant difference between the 12 month and the 120 month harvests ($p = 0.78$), indicating minimal microbial transformation. Similarly, the PyOM POM C:N ratio was relatively stable.

suggests that MAOM formation and persistence is in part independent of POM decomposition (Fulton-Smith and Cotrufo, 2019; Haddix et al., 2020).

In contrast to the MAOM dynamics, the CHAOM fraction showed a responsiveness to the decomposition of the POM fraction across the experimental period in terms of stoichiometry (Figure 6.3) and C and N retention (Figure 6.2, Figure 6.4). This fraction tends to be C and N poor, given the lack of reactive sorption sites and prevalence of sand sized particles, and is often combined with either the POM or MAOM during single-step physical fractionations (Leuthold et al., 2022a). However, CHAOM has been identified as a key intermediary in SOM formation pathways (Fulton-Smith and Cotrufo, 2019; Samson et al., 2020) and our results indicate that is an actively cycling fraction with rapid formation/loss dynamics across sampling periods (Samson et al., 2020). While sand particles do not have a surface charge that can sorb SOM, microbial communities and their turnover may be driving the development of transient binding sites via the excretion of extra-polymeric substances or other byproducts (See et al., 2022; Witzgall et al., 2021). Recent findings have partially substantiated this hypothesis, highlighting the role of root exudation in the formation of CHAOM (Ridgeway et al., 2023).

The temporal variability in the litter derived SOM fractions over the course of the experiment adds further credence to the decadal persistence of a rapidly stabilized MAOM fraction, and the transient nature of the POM and CHAOM fractions. The litter derived POM and CHAOM fractions exhibited high variability in their C stocks across sampling periods (82.48 ± 5.63% and 91.07 ± 9.73%, respectively), reflective of their formation and persistence behavior. Despite following a predictable pattern of peak formation (via fragmentation of litter material) occurring by full litter mass loss (Cotrufo et al., 2015a) and followed by sustained decay, the absolute amount of litter derived POM and CHAOM fluctuates significantly over the course of a decade.

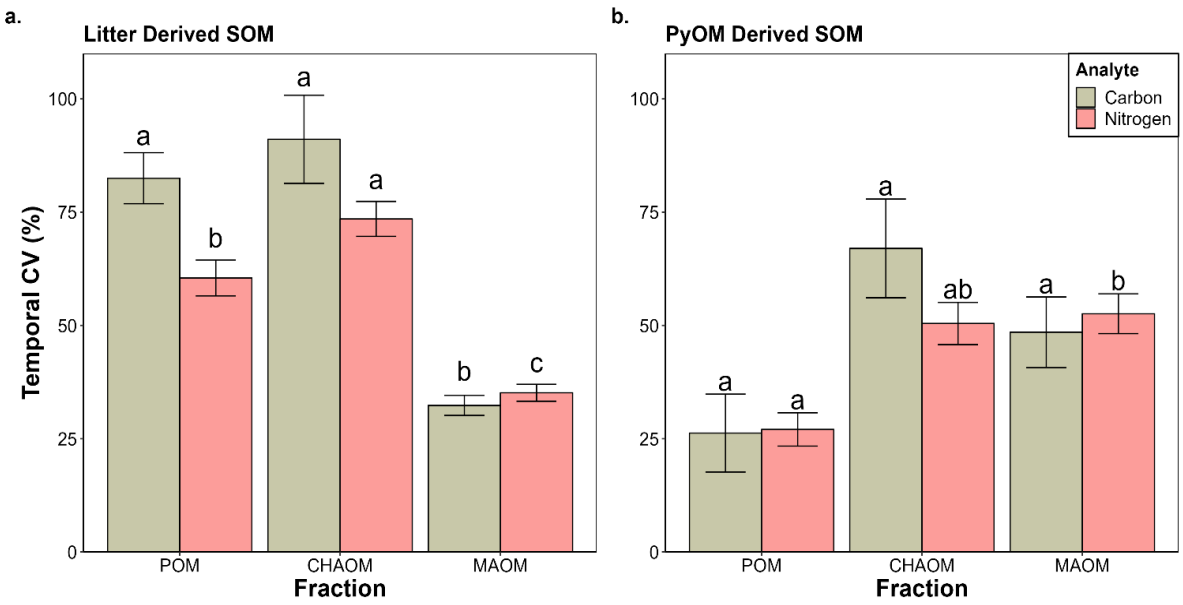

Figure 6.4 - Temporal coefficient of variation for the litter derived (a., left) and PyOM (b., right) derived C and N stocks throughout the experimental period. Litter-derived C and N in POM and CHAOM were significantly more variable over time than in MAOM, potentially indicating increased turnover and mineralization. For the PyOM, the low variability in the input-derived C and N fraction indicates the slow turnover of this material, attributed to the chemical recalcitrance of the condensed polyaromatic ring structure. Different letters above the bars indicate a significant difference in temporal CV for either analyte ($\alpha = 0.05$).

In contrast, the litter derived MAOM C remained relatively stable over the 10 years of the incubation (temporal CV = 32.35 ± 2.23%; Figure 6.4). Partially, this reflects the difference in turnover time and protection mechanisms between these fractions—POM and CHAOM are more accessible to microbial decomposers than MAOM (Cotrufo and Lavallee, 2022). However, the decreased variability in MAOM C and N stocks also corroborates the lack of new additions to the MAOM pool as POM and CHAOM are mineralized as observed with the litter-derived fraction stoichiometry (Figure 6.3). Indeed, the temporal CV of MAOM is similar to the temporal CV of other stable fractions, (e.g., PyOM-derived POM; Figure 6.4), further suggesting that it can be used as a proxy for stability of input-derived SOM fractions independent of mechanism of stabilization.

Pyrogenic organic matter as a distinctly persistent SOM fraction

In contrast to the litter treatment, the vast majority of the added PyOM was found in the POM fraction (i.e., particle density < 1.85 g cm^{-3}) at the final harvest (94.86 ± 0.52% and 92.32 ± 0.66% of the remaining C and N, respectively; Figure 6.2), with only minor amounts in the MAOM fraction (4.85 ± 0.54% C and 7.32 ± 0.72% N), and an insignificant amount in the CHAOM fraction (0.29 ± 0.05% C, 0.36 ± 0.07% N). The lack of transformation of the PyOM fraction from POM into CHAOM or MAOM fractions reinforces the inefficiencies in microbial processing of the complex molecular structures associated with PyOM (Bird et al., 2015) and is similar to observations from shorter incubations (Hilscher and Knicker, 2011). While we do observe a significant, 29.04% decrease in the total amount of PyOM material recovered between the 11 month and 101-month samplings (Figure 6.1), it is challenging to attribute this loss wholly to mineralization. Previous work at these sites showed that over the course of a year, only 3% of PyOM loss could be attributed to respiration losses, mainly occurring in the first two months following PyOM application (Soong and Cotrufo, 2015). One possibility is that some of the PyOM that was initially added moved vertically through the profile and accumulated below our sampling depth (i.e., 5 cm); rapid vertical translocation of PyOM associated with light fraction POM has been observed previously in column experiments (Schiedung et al., 2020).

Whereas the litter decomposition process we observed was well reconciled by the transfer of soluble material into the CHAOM (Samson et al., 2020) and MAOM fractions (Cotrufo et al., 2015a) and fragmentation and transfer of structural material into the POM fraction (Cotrufo et al., 2015a), we did not observe a similar temporal pattern with the applied PyOM (Figure 6.2). Instead, PyOM remained largely in the POM fraction for the duration of the 9-year experiment. The lack of significant differences in the temporal CV values further reinforce the non-reactivity,

or stability, of this fraction (Figure 6.4), with little transfer between SOM fractions or into the atmosphere during the time frame we examined. The persistence of the PyOM in the POM has important implications for our understanding of C storage (Pellegrini et al., 2018) and distribution of C among physical fractions in areas that undergo periodic burning (Lavallee et al., 2019) or receive biochar applications. If not directly characterized, PyOM has the potential to skew POM C stock calculations, and potentially misrepresent the residence time and dynamics of the POM fraction as it is conventionally conceptualized (Leuthold et al., 2022a). Techniques such as infrared spectroscopy (Sanderman et al., 2021) or ramped pyrolysis (Sanderman and Grandy, 2020) may help to differentiate PyOM from unburned plant and microbially-derived contributions to the POM fraction. in the future, better constraining the turnover time of these different components of physically separated POM.

Implications for understanding SOM persistence over decadal time scales

The persistence of SOM is a critical ecosystem service (Schmidt et al., 2011), however the forms and means by which SOM is maintained in ecosystems remain poorly constrained on the timescales relevant to management or the emergent soil C markets. Our results, novel in both duration and location, reinforce the notion that, in ecosystems which do not receive PyOM inputs, the fraction of SOM that is most stable on a decadal timeframe is the MAOM. The stoichiometric data suggest that the stabilization of this persistent fraction is largely independent of decomposition of other fractions (i.e., POM and CHAOM), and can occur quite rapidly. In ecosystems that do receive PyOM inputs, the persistence and apparent nonreactivity of the PyOM suggest that it is an exceedingly stable C sink. The original two-pathway model previously proposed based on work at this site provided information about SOM formation, but was limited in its ability to address stabilization (Cotrufo et al., 2015a). By returning to this site 7

years later, we show that MAOM formed via the association of soluble compounds represents a persistent fraction of SOM, adding further credence to the role of plant chemistry in determining SOM formation and persistence (Rocci et al., 2023). While we encourage additional studies investigating the decadal patterns in formation and persistence of litter derived SOM in other climates and ecotypes, these results provide an important advance in our ability to forecast the fate of organic C and N in the soil system and allow for management relevant estimates of the permanence of soil C.

CHAPTER 7: QUANTIFYING THE CONTRIBUTION OF MINERAL ASSOCIATED ORGANIC MATTER TO PLANT AVAILABLE NITROGEN POOLS UNDER VARIOUS SOIL ORGANIC MATTER CONDITIONS

Introduction

Despite the wide-spread adoption of mineral fertilizers, sustained agricultural production depends on continued mineralization of nutrients from cropland soil organic matter (SOM) (Lin et al., 2023; Tiessen et al., 1994). This reliance on SOM is evidenced by low nitrogen (N) use efficiency across cropping systems (Cassman et al., 2002), despite well-established crop N uptake requirements (Ciampitti and Vyn, 2012). Meta-analytical work has demonstrated that in some more severe cases, the majority of crop N is derived from sources other than applied fertilizers, highlighting SOM as a significant source of plant available N (Yan et al., 2020). The low efficiency of fertilizer N uptake by crops has significant deleterious effects on downstream ecosystems, leading to sustained environmental degradation (Howarth et al., 2011; Nolan et al., 1997), and impacting human health outcomes (Powlson et al., 2008). However, increasing synchrony between N application and uptake continues to remain challenging, partially due to the challenge and complexity of accurately predicting N mineralization rates at the time of N application (Archontoulis et al., 2020; Yin et al., 2020).

Physical SOM fractions such as particulate organic matter (POM) and mineral associated organic matter (MAOM) can increase our insight into the function of SOM in agricultural systems (Cotrufo and Lavallee, 2022), and may help to better parameterize N mineralization behavior at the farm scale. Historically, the POM fraction has been linked to short-term nutrient cycling

(Cotrufo and Lavallee, 2022; Wander, 2004), with previous lab incubation experiments having highlighted significant agreement between the size of the POM-N pool and N mineralization potential (Curtin et al., 2017; Thomas et al., 2016). The POM fraction is often conceptualized as a more microbially available fraction of the total SOM pool (Lehmann et al., 2020), lending a clear mechanism for the connection between availability of mineralized nutrients and the size of the POM pool. However, the MAOM fraction is considerably more abundant in cropland soils (Lugato et al., 2021; Hansen et al, 2023), as well as much more N rich than POM (average C:N ratios of 8 -13 vs. 10 – 40 for MAOM and POM, respectively; Lavallee et al., 2020), thus, it may play an important role in crop N availability and nutrition. Indeed, previous work has shown that in isolation and with all else held equal, the MAOM fraction mineralizes more N than the POM fraction (Villarino et al., 2023; Whalen et al., 2000), and that a reconsideration of MAOM stability is necessary (Kleber et al., 2021). This may be indicative of shifts in the microbial N use efficiency due to the divergent C:N ratios of POM and MAOM (Mooshammer et al., 2014). However, other work has detailed the means by which MAOM-N may be liberated from its bonds regardless of POM stoichiometry, including interactions with organic acids via plant root exudation or changes in redox state (Jilling et al., 2021; Keiluweit et al., 2015). However, recent work has also suggested that N rich molecules such as amino acids are likely to form more stable bonds in the MAOM fraction, due to a higher molecular charge density associated with these compounds. (Spohn, 2024). Thus, questions around mineral associated N remain open, with important implications for ecosystem nutrient cycling.

A recent framework put forth by Daly et al. (2022) incorporates the shifting microbial NUE associated with the relative amount of C and N present in both POM and MAOM, along with the concept of a dynamic exchange of N between the soil solution and soil minerals moderated by

sorption capacity and N supply. While it is established that MAOM-N can become available, previous studies that the Daly et al. (2022) framework builds upon are often conducted in the lack of other pools of N (such as POM), such that questions remain about the relative contribution of POM vs. MAOM to plant available N in soil. In particular, there has yet to be a robust assessment of how the balance between POM and MAOM (i.e., the POM:MAOM ratio) interacts with POM C:N stoichiometry to determine the source of plant available N among SOM fractions. A more thorough assessment of these dynamics will improve our understanding of N acquisition strategies across agricultural soils.

Here, we leverage new techniques in N isotope tracing to understand controls on SOM-N sourcing in agricultural soils in a controlled laboratory incubation. By fractionating and then reconstructing soils with an isotopically enriched MAOM fraction and natural abundance POM fraction, we were able to take advantage of simple two-pool mixing model to understand the contribution of each SOM fraction to the potentially plant available pool. We varied the total level of SOM-C, the ratio of POM to MAOM C, and the POM C:N ratio to understand the potential controls of microbial mineralization of POM and MAOM. We predicted that soils with a higher proportion of high C:N rich POM would source an increased proportion of mineralized N from the MAOM fraction, due to increased N limitation of the microbial decomposers. Further, we predicted that soils that possessed a higher amount of POM-N (i.e., a lower POM C:N) would mineralize less MAOM-N in the early stages of the incubation, but that MAOM-N mineralization would increase later as POM-N stocks became depleted. Our results provide an important step towards a more complete mechanistic understanding of soil N cycling, building on previous work such as that by Schimel and Bennet (2004), Jilling et al. (2018, 2020), and Daly et al. (2022).

Materials and Methods

Soil Sampling and Analysis

Particulate Organic Matter

We sampled two soils to isolate POM fractions with contrasting C:N ratios, one from a managed grassland ecosystem in Central KS, USA (high POM C:N: 33.3), and one from a long-term alfalfa field in Eastern NE, USA (low POM C:N: 17.8). Sampling for the high C:N POM soil was conducted on June 22, 2022 using shovels, excavating the top 10 cm from a number of microplots within a 100 m^2 area to minimize disturbance. The sampling of the low C:N POM soil was conducted using a front-end loader which removed the top 15 cm of soil from a 1 m x 3 m area from the center of the alfalfa field on November 10, 2022.

After sampling, soils were transported to Colorado State University and spread evenly across tables in the climate-controlled greenhouse space to air dry for several days. After the sample had reached an air-dried state, it was sieved at 8 mm, removing coarse aboveground and below ground biomass. Following the initial 8 mm sieving step, a subsample of the soil was sieved to 2 mm, again taking special care to remove any coarse plant debris that may be present in the soil, such as fine roots or fragments of biomass that was living at the time of sampling. The 2 mm sieved soils were fractionated using a one-step density fractionation adapted from the methods described in Leuthold et al. (2024). Briefly, 7 – 8 gram aliquots of 2 mm sieved soil were added to a 50 mL centrifuge tube, along with twelve 1-mm glass beads. To this centrifuge tube, 35 mL of deionized (DI) water was added, and the samples were shaken at a low intensity (121 rpm) for 18 hours to disperse aggregate structures. Following shaking the samples were centrifuged at 1165 RCF for 20 minutes to separate the light POM fraction from the mineral soil. The floating POM was then vacuum aspirated, transferred to clean storage containers, and dried to a constant

weight at 60 ^{O}C. Dried samples were left intact before being composited and homogenized prior to the microcosm preparation. We elected to use DI water rather than a heavy liquid for our density separations to avoid any potential alteration of the POM fraction that may have made it less microbially accessible. Subsamples of the composited, homogenized POM fractions were analyzed for C and N concentrations, as well as ^{15}N composition via EA-IRMS to confirm consistency within the POM end-member material for both treatments. The average δ^{15}N of the high and low C:N ratio POM was 2.6‰ and -0.5‰, respectively.

Mineral Associated Organic Matter

To isolate an isotopically enriched MAOM fraction that accurately represented SOM dynamics, we sought soils that had been exposed to ^{15}N enrichment over a period of time long enough to assure that the ^{15}N label was homogeneously distributed in the MAOM fraction, i.e., across the exchangeable and stable MAOM. We thus chose a soil that had been fertilized in April of 2015 with 3.6 atom% $^{15}NH_4{}^{15}NO_3$ at a rate of 202 kg N ha^{-1} as part of the experiment described by Poffenbarger et al. (2018), located near Ames, IA, USA. Soils were sampled to 10 cm depth from plots that had received the enriched fertilizer using a soil probe in November 2023, with samples focused on the general area of the banded N application. Samples were composited at the plot level and shipped fresh to Colorado State University after sampling. Once at CSU, soils were sieved to 8 mm fresh, allowed to air-dry, and then sieved to 2 mm. Soils were fractionated into MAOM using a one-step size fractionation, following Leuthold et al. (2024). Briefly, aliquots of 7-8 grams of the 2 mm sieved soil was added to a 50 mL centrifuge tube, along with twelve 1-mm glass beads. Similar to above, 35 mL of DI water was added to each tube before shaking the tubes for 18 hours at 121 rpm to disperse aggregate structures. Once shaking had been completed, soils were poured over a 53 μm sieve, and washed gently with DI water until the

water for the sample ran clear. Any material that passed through the sieve was designated as MAOM, placed in a clean container, and then dried to a constant weight at 60 ^{O}C. Once dry, samples were finely ground into a fine powder using a mortar and pestle and then composited and homogenized. Subsamples of the composited sample were analyzed for C and N composition and ^{15}N isotope composition via EA-IRMS. The average δ^{15}N of the composited MAOM was 22.4‰.

To maintain a constant texture within our experimental units while varying the amount of MAOM C, we performed the same procedure as above on soils from neighboring plots that had not retained a ^{15}N enrichment signal. Following the isolation of the MAOM sample, we ashed the MAOM in a muffle furnace set to 550 ^{O}C for 6 hours to remove all organic C and N from the sample. Full removal of organic C and N was confirmed via elemental analysis.

Incubation Experiment

Experimental Design

Our experiment was designed as a full factorial, randomized complete block design, with three treatments: SOC concentration (%), POM C:N, and POM:MAOM C ratio. Each treatment factor had two levels (typically high and low). For the SOC concentration treatment, our target SOC concentration for the low treatment was 0.50% C, and the target SOC concentration for the high treatment was 2.50%. As discussed above, we used two separate POM fractions from different ecosystems to achieve our POM C:N ratio treatment—the grassland soil POM had a C:N ratio of 33.2, and the POM isolated from the alfalfa field soil had a C:N ratio of 17.8. For our POM:MAOM ratio, our low treatment mimics the typical distribution of C in agricultural systems (20% POM – 80% MAOM), whereas the high treatment represents much more POM

than is typically present, even in regenerative management treatments (60% POM – 40% MAOM; Hansen et al., 2024; Sokol et al., 2022). Each treatment was replicated four times, unless noted otherwise. While mineralization is known to not significantly fractionate (Högberg, 1997), to account for any apparent isotopic fractionation due to possible selective mineralization of ON with different ^{15}N abundance, we also created experimental units for our endmembers, i.e., the two POM treatments and the MAOM. These were adjusted to an average SOC concentration of 1.50%, and contained either only the POM, or only the MAOM as a source of organic C and N, respectively. These endmember treatments were replicated two times.

Incubation Setup

Using the isolated fractions, we reconstructed soils with a specific texture, SOC concentration, and POM:MAOM C ratio in filtration units with 0.45 μm nylon filters (Thermo Scientific 09-740-24B, Thermo Fisher Scientific, Waltham, MA, USA). The amount of each constituent fraction added to the experimental units in order to achieve consistent textures and reach target SOC concentrations is presented in Table 7.1. For each experimental unit in a block, the constituent fractions were weighed separately, combined in an acid-washed glass beaker, and thoroughly mixed using a glass stir rod prior to transferring into the filtration units. All weighing equipment was thoroughly cleaned with 95% ethanol between samples to minimize the potential for ^{15}N contamination. The average dry soil weight of the experimental units was 28.8 g. The average texture of the reconstructed soil was 28.1% clay, 30.3% sand, and 41.6% silt, such that soil texture classification fell between loam and clay loam.

Table 7.1: Average amount of carbon (C), nitrogen (N), and total soil mass added to incubation units for the various soil organic carbon (SOC), particulate organic matter to mineral associated organic matter ratio (POM:MAOM), and POM C:N ratio treatments.

SOM Treatment	POM:MAOM C Ratio	POM C:N	POM (g)	POM C (mg)	POM N (mg)	MAOM (g)	MAOM C (mg)	MAOM N (mg)	Ashed Silt and Clay (g)	Ashed Sand (g)	Liquid weight at Field Capacity (g)
2.5	20:80	High	0.30	113.96	3.43	19.69	500.00	44.64	0.00	8.72	8.07
2.5	20:80	Low	0.33	137.16	7.71	19.69	500.00	44.64	0.00	8.72	8.07
2.5	60:40	High	0.90	341.98	10.29	9.84	250.00	22.32	9.84	8.72	6.35
2.5	60:40	Low	0.99	413.58	23.14	9.84	250.00	22.32	9.84	8.72	6.35
0.5	20:80	High	0.06	22.98	0.69	3.39	100.00	8.93	15.75	8.72	8.07
0.5	20:80	Low	0.07	27.48	1.55	3.39	100.00	8.93	15.75	8.72	8.07
0.5	60:40	High	0.16	61.67	1.85	1.97	50.00	4.46	17.72	8.72	6.35
0.5	60:40	Low	0.20	82.28	4.63	1.97	50.00	4.46	17.72	8.72	6.35

Nitrogen Mineralization Assay

To monitor the mineralization of N from the reconstructed soils, we adapted the method proposed by Curtin and Campbell (1992). Following construction of our experimental units, we leached native inorganic N out of the soils using 100 mL of 0.05 M KCl under vacuum at ~ -50 kPa. The extract was collected, transferred into acid-washed 50 mL centrifuge tubes, and frozen while awaiting analysis. We chose to use a lower molarity of KCl than the typical 2M KCl used for inorganic N extractions to avoid the accumulation of salts in the incubation units throughout the incubation periods, though our data suggests that this did not inhibit our ability to recover the full amount of inorganic N from the soils. Anoxic conditions and ponding that could lead to denitrification or rearrangement of the soil matrix within the incubation units were avoided by adding the KCl in stages, 5-10 mL at a time. The extraction was deemed to be finished after 100 mL of KCl had been added, and no further flow from the incubation unit into the reservoir was observed for at least 30 seconds. This process was repeated at 2 weeks (T1), 4 weeks (T2), and 6 weeks (T3) to understand the evolution of N mineralization over that period.

The differences in SOC concentration and POM:MAOM C ratios led to variable water holding capacities across our experimental units. In order to maintain a consistent level of moisture in the soils that accounted for these differences, we calculated a field capacity measurement following the pedo-transfer function developed by Bagnall et al. (2022), which accounts for differences in soil C, and maintained incubation units at this moisture throughout the experimental duration. For the high and low SOC treatments, the average volumetric water content at field capacity (θ_{VWC}) was 35.05% and 27.57%, respectively. To replace the nutrients that could be lost during the leaching process, we applied a N free nutrient mixture consisting of 0.002 M $CaSO_4$, 0.002 M $MgSO_4$, 0.005 M $Ca(H_2PO_4)_2$, and 0.0025 M K_2SO_4 following each leaching event, following

Curtin and Campbell (1992). To avoid spurious treatment differences due to unequal nutrient addition, the amount of nutrient solution added during moisture additions was equal to the smallest difference between the mass of soil water at field capacity (Table 7.1), and residual moisture remaining in the experimental units for each block. For the experimental units that required further additions of liquid to reach field capacity, DI water was used.

We conducted four vacuum filtration KCl extractions over the course of the experiment. During each extraction, 100 mL of 0.05 M KCl was added to each incubation unit and filtered through until 45 seconds passed between each drop. Across all extractions, our KCl recovery was 96.9%, such that very little KCl remained in the incubation unit following extraction. Samples were brought back up to calculated field capacity following extractions. Averaged across extractions and treatment combinations, we applied 4.6 mL of nutrient solution and 0.8 mL of DI H_2O to the incubation units per time step, ranging from 0.5 – 7.6 mL of nutrient solution and 0 – 3.7 mL of DI H_2O. Extraction efficiency improved as the incubation continued, such that the average nutrient solution addition increased as time went on.

We monitored moisture loss of the incubation units throughout the course of the experiment. As the incubation units were stored in a humid environment, moisture loss was generally minimal. On average, incubation units lost 12.2% of the initial moisture content between sampling periods, roughly equivalent to 0.9 ml. Given the total average amount of liquid that was present at field capacity (Table 7.1), this amount of moisture loss likely did not inhibit microbial activity or N mineralization activity.

Nitrogen analysis

Concentration analysis

The KCl extracts from the T0, T1, T2, and T3 samplings were analyzed for NO_3^- and NH_4^+ concentrations colorimetrically using an OI Analytical flow through analyzer (Xylem Inc., College Station, TX, USA) using the EPA 353.3 and EPA 350.1 methods, respectively. Samples were kept frozen until analysis, before being thawed overnight at 4 ^{O}C. The NH_4^+ concentrations were largely negligible throughout the course of the incubation and continued to decrease over time, presumably as the nitrifier population became more dominant. The mean NH_4^+ concentration across sampling periods was 0.28 ± 0.08 ppm. Given that we focused our isotopic analysis on the NO_3^- pool and considered NO_3^- the dominant N form in the incubations, we did not analyze the NH_4^+ results further.

^{15}N Isotope Analysis

We applied the methodology first described by Altabet et al. (2019) to determine the ^{15}N isotopic composition of the NO_3^- in the extracts from the T1 extraction. We chose to only apply the isotopic methods to the first timestep to avoid isotopic changes due to transfer of ON among fractions or recycling by the microbial community that may occur at later stages of the incubation. We believe this is a novel application of this methodology, which previously had been developed for the characterization of NO_3^- in seawater. In this procedure, frozen KCl extracts were thawed and allowed to come to room temperature. Meanwhile, 10 mL of Ti (III) chloride solution suspended in 15% HCl was added to a beaker containing 1.00 g of 99.9% pure Zn powder to remove any Ti(IV) impurities that may have been present. This reaction is allowed to occur until complete, determined by the subsidence of foaming. Once the Ti (III) reagent was

prepared, KCl extracts were diluted to ~0.2 mg L^{-1} NO_3^- using degassed, DI water at a target volume of 2 mL in reaction vials with butyl-grey septum caps. The Ti(III) reagent was added to the soil extracts at a 1:10 volume:volume ratio, and the reaction vials were immediately capped and swirled to begin the reaction. The reaction was allowed to take place over the course of 24 hours, during which the Ti(III) reacted with aqueous NO_3^- present in the samples to form N_2O gas. Following the results of Altabet et al. (2019), we assume that this process does not lead to significant isotopic fractionation, especially as sulfate concentrations in our soils were below the threshold (i.e., ~300 ppm) they observed matrix effects. As such, ^{15}N values derived from this methodology reflect the ^{15}N composition of NO_3^- in the soil solution at the time of extraction. However, we still attempted to account for any potential isotope effect by applying a mixing model where all end members had undergone this process, such that any potential fractionation would be accounted for in our mixing model.

Reacted samples were analyzed for ^{15}N-N_2O concentration using an IsoFLOW GHG gas analyzer (Elementar Langenselbold, Germany) coupled to an Isoprime PrecisION Isotope Ratio Mass Spectrometer (Elementar UK, Manchester, United Kingdom). We used the certified USGS34 KNO_3 standard as our calibration standard, which was blank corrected using KCl that had been passed through our experimental blanks. The intention of this blank correction was both to account for any N present in the DI water or KCl solution, as well as the N_2O present in the atmosphere of the reaction vials. Within each run, an in-house standard prepared from stock KNO_3 was analyzed every 10 samples.

Data Analysis

Isotopic Source Partitioning

To determine the relative proportions of POM and MAOM derived NO_3^- in the T1 samples, we used a two-pool isotopic mixing model, as shown in Equation 1, where $f_{POM\text{-}N}$ is the fraction of the NO_3^--N that was mineralized from the POM fraction,

$$_fPOM - N = \frac{\delta Soil\ Extract - \delta MAOM}{\delta POM - \delta MAOM} \qquad Eqn.\ 1$$

δSoil Extract is the ^{15}N composition of the NO_3^- present in the soil extracts, δMAOM is the average ^{15}N composition of the of the NO_3^- present in the extracts from the MAOM endmember treatments, and δPOM is the average ^{15}N composition of the NO_3^- present in the extracts from the POM endmember treatments. The fraction of NO_3^--N that was derived from the MAOM fraction ($f_{MAOM\text{-}N}$) was calculated as 1 – $f_{POM\text{-}N}$. We then applied the derived fraction to the mass of NO_3^- present in the samples at T1 to calculate a mass of POM-derived and MAOM-derived N.

Statistical Analysis

To test for the effect of treatment on the source of N, we constructed linear mixed models using the *lme4* and *lmerTest* packages in R v. 4.3.2 (Bates et al., 2015; Kuznetsova et al., 2017; R Core Team, 2022). We considered similar models with four different response variables: f_{MAOM} at T1, NO_3^- stock at T1, and POM and MAOM derived N stocks at T1. In these models, the main effects in the model were SOC concentration, POM:MAOM C ratio, and POM C:N ratio, as well as the interactions between these terms. Given the experimental design and sampling strategy, we also included a random effect of block. A second model comparing changes in cumulative NO_3^- mineralized over time had a similar structure, but also included a random effect of

sampling period nested within block to account for the repeated measures nature of our experimental design. Significant differences between treatments were assigned based on the results of a post-hoc comparison of contrasts based on estimated marginal means via the *emmeans* package (Lenth, 2022), using the Tukey adjustment and an alpha level of 0.05.

Results

Initial N Mineralization

We observed significant differences among all of our treatments in terms of NO_3^- mineralized over the course of the initial mineralization assay (Table 7.2). The total amount of NO_3^- mineralized over the initial two-week incubation ranged from 0.8 – 45.9 kg NO_3^- ha^{-1} and averaged 14.1 kg NO_3^- ha^{-1} across all treatments. Each of our main effects (i.e., SOM content, POM C:N ratio, and POM:MAOM C ratio) had significant effects on NO_3^- stocks (p-values <

Table 7.2: Results of analysis of variance of the linear mixed model assessing significant effects of soil NO_3^- mineralization during the initial two-week incubation. All effects were significant at $\alpha = 0.05$.

Effect	SS	Num DF	Den DF	F Value	P-Value
SOM Content	3882.9	1	19.5	544.5	< 0.0001
POM C:N Ratio	1011	1	19.5	141.8	< 0.0001
POM:MAOM C Ratio	855.9	1	19.1	120.0	< 0.0001
SOM Content x POM C:N Ratio	607.2	1	19.5	85.1	< 0.0001
SOM Content x POM:MAOM C Ratio	525.6	1	19.1	73.7	< 0.0001
POM C:N x POM:MAOM C Ratio	252.9	1	19.1	35.5	< 0.0001
SOM Content x POM C:N Ratio x	179	1	19.1	25.1	< 0.0001

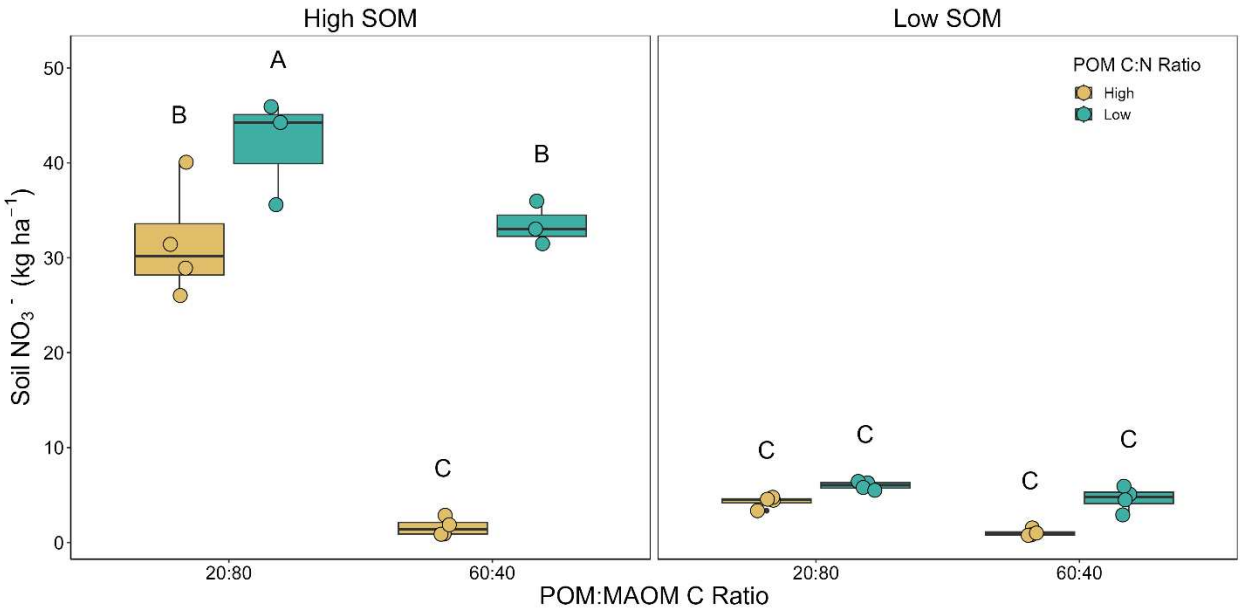

Figure 7.1 – Soil nitrate (NO_3^-) stocks after 2 weeks of incubation. Different colors represent treatments with different particulate organic matter (POM) carbon to nitrogen ratios (C:N). Different letters above the box plot indicate significant differences based on pairwise comparisons. Points have been jittered horizontally to improve readability.

0.001 for all; Figure 7.1). We also observed significant interactions between all of our main effects, including the three way interaction between SOM content, POM C:N, and POM:MAOM C (p-values < 0.001; Table 7.2).

Given the presence of significant interaction effects, to understand the difference between individual treatment combinations, we examined the contrasts of each treatment combination within our full linear mixed model (Supplemental Table 7.1). We observed significantly more N mineralized under the high SOM conditions than the low SOM conditions for three of the four treatments (Figure 7.1). Within these three high SOM treatment groups, the low POM:MAOM ratio, low POM C:N ratio mineralized significantly more NO_3^- than the low POM:MAOM ratio, high C:N ratio treatment (p-value = 0.002) and the high POM:MAOM, low POM C:N ratio treatment (p-value = 0.018), which were not significantly different from each other. The fourth

treatment combination under the high SOM content, the high POM:MAOM ratio, high POM C:N ratio, mineralized significantly less NO_3^- than any of the other treatments with high SOM. The amount of NO_3^- mineralized was not significantly different than any of the treatments under the low SOM treatment (p-value > 0.2 in all cases; Supplemental Table 7.1).

In contrast to the high SOM content treatment, under the low SOM content the differences in total NO_3^- mineralization amongst treatments were much more constrained. We observed no significant differences in full-model pairwise comparison among treatment combinations under the low SOM content treatment (Figure 7.1). The average NO_3^- stock among the low SOM treatments was 3.98 kg NO_3^- ha^{-1} and ranged from 0.76 – 6.43 kg NO_3^- ha^{-1}. Though significant interactions exist, the pairwise comparisons suggest little effect of POM C:N or POM:MAOM ratio at low SOM levels.

Isotopic tracing of NO_3^- sources

We measured the $\delta^{15}N$ isotopic composition of the NO_3^- present in the extracts taken after 2 weeks of incubation to understand the sources of potentially mineralizable N under various SOM conditions, before possible remixing occurred among fractions. We used a two-pool mixing model to determine the fraction of NO_3^- that was derived from organic N sorbed to the MAOM ($f_{MAOM\text{-}N}$) vs. the organic N mineralized from the POM fraction ($f_{POM\text{-}N}$). In the cases when the mixing model produced $f_{MAOM\text{-}N}$ values higher than 100% (i.e., the mixture $\delta^{15}N$ value was higher than the MAOM endmember $\delta^{15}N$ value), we used a 100% value. Across all treatments, we observed that 76.2% of the NO_3^- mineralized during the initial incubation period was derived from the MAOM fraction, with a range from 27.9% to 100.0% of total NO_3^- being MAOM derived (Figure 7.2). In contrast to the patterns we observed in the concentration data, we did not

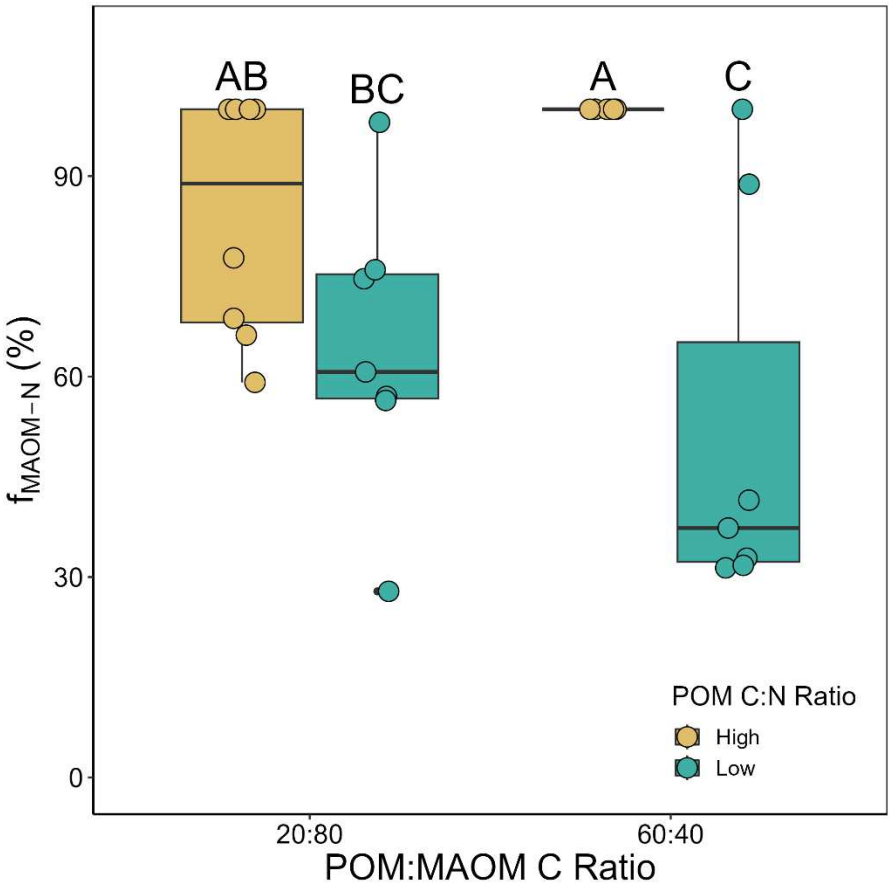

Figure 7.2- Proportion of nitrate sourced from the mineral associated organic matter (MAOM) fraction based on the two-pool mixing model. Results are averaged over the main effect of soil organic matter concentration. Different colors represent different particulate organic matter carbon to nitrogen ratios, and different capital letters represent significant differences among treatments based on pairwise comparisons. Points have been jittered horizontally to improve readability.

observe a significant effect of SOM content on the source of soil NO_3^- (p-value = 0.14). Our results indicate that the significant drivers of soil N source were the POM C:N ratio (p-value < 0.001), and the interaction between POM C:N and POM:MAOM (p-value = 0.05). Averaged across the SOM content treatments, we did not observe a significant difference between the different POM C:N ratios in the f_{MAOM-N} in the 20:80 POM:MAOM C ratio treatment (Figure 7.2). Soils with high C:N ratio POM had an average f_{MAOM-N} of 84.0 ± 6.3% and low C:N soils in the MAOM dominant treatment had an average f_{MAOM-N} of 64.4 ± 7.7% (p-value = 0.17; Figure 7.2). In the more POM rich treatment (60:40 POM MAOM C ratio), there was a significant effect

of POM C:N. The low C:N POM treatment $f_{MAOM\text{-}N}$ (51.9 ± 10.04%) was significantly lower than the high POM C:N treatment (100 ± 0%; p-value < 0.001).

We applied the $f_{MAOM\text{-}N}$ and $f_{POM\text{-}N}$ values to the calculated NO_3^- stocks mineralized by T1 to arrive at a relative contribution to soil mineral N stocks for all the treatments (Figure 7.3). Similar to the initial NO_3^- stocks, SOM content was a significant driver of POM-N and MAOM-N ($p < 0.001$ in both cases). In the high SOM treatment, MAOM derived NO_3^- accounted for 16.2 ± 3.2 kg ha^{-1}, while POM derived NO_3^- accounted for 9.4 ± 2.1 kg ha^{-1}, while in the low SOM treatment, MAOM derived NO_3^- accounted only for 3.0 ± 0.5 kg ha^{-1}, and POM derived NO_3^- was equal to 1.0 ± 0.3 kg ha^{-1}, on average. The amount of POM derived NO_3^- was affected by SOM content ($p < 0.001$), POM C:N ($p < 0.001$), but not POM:MAOM ratio ($p = 0.82$; Figure 7.3). In contrast, POM:MAOM ratio significantly altered the amount of MAOM derived NO_3^- ($p < 0.001$), especially in the high SOM soils (interaction effect $p < 0.001$). The POM C:N ratio and SOM content also impacted the MAOM derived N stock values ($p = 0.02$ and < 0.001, respectively). The amount of MAOM derived N was less sensitive to interactions between treatments than the amount of POM derived N; interactions between SOM content and POM C:N ratio ($p < 0.001$), POM C:N ratio and POM:MAOM ratio ($p < 0.001$), and the three-way interaction ($p < 0.001$) were all significant for POM derived N stocks, though these were not significant for MAOM derived N.

Evolution of NO_3^- over time

We measured NO_3^- concentrations at three timepoints to understand how the relative distribution of POM and MAOM would affect the cumulative N mineralization over time (Figure 7.4). We observed that generally, the patterns found in the initial extraction held over the course of the

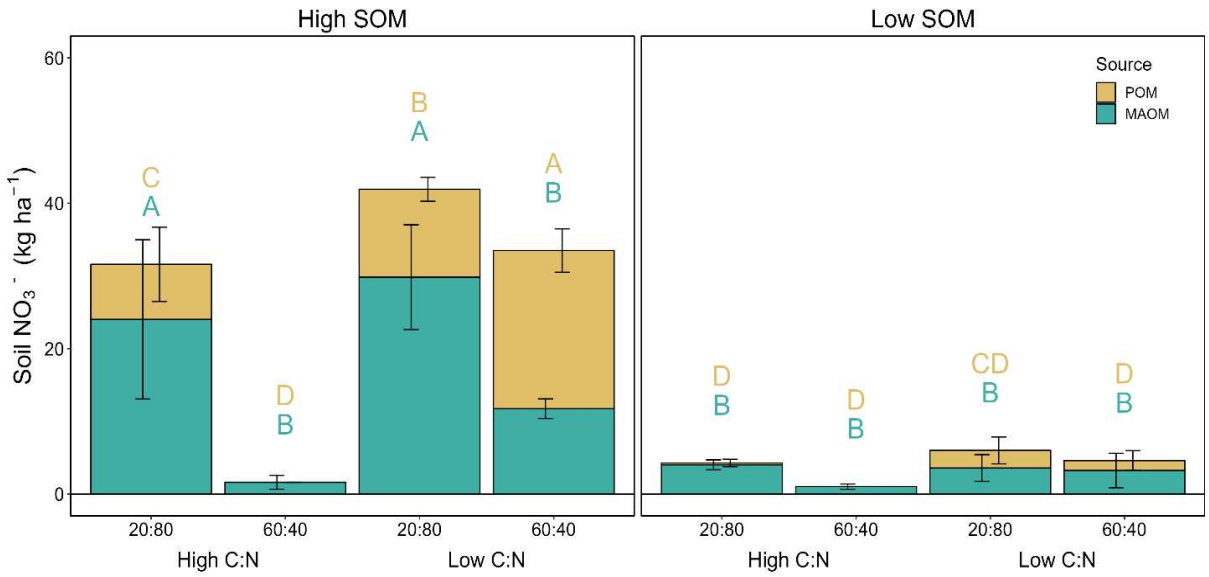

Figure 7.3 – Particulate and mineral associated organic matter (POM and MAOM, respectively) contributions to nitrate (NO_3^-) stocks after two weeks of incubation. Different colors in the bars correspond with sources, yellow for POM, teal for MAOM. Error bars indicate ± 1 SE. Different capital letters above the bars indicate significant differences between treatments based on pairwise comparisons, with the color of the letter corresponding to the fraction in question (i.e., yellow letters indicate significant differences in POM, teal letters for MAOM).

experiment, with the high SOM treatment mineralizing significantly more NO_3^- (p-value < 0.001). Similarly, POM C:N ratio and POM:MAOM C ratio both significantly affected cumulative N mineralization (p = 0.01 and 0.005, respectively). We did not observe the same significant interaction effects that we did in our examination of the initial concentration data, only the interactions between SOM content and POM C:N (p < 0.001) and between POM C:N and POM:MAOM C ratios (p = 0.002) were significant (Figure 7.4). Similar to the initial concentration data, the high POM C:N, high POM:MAOM C ratio treatment under the higher SOM content treatment was significantly lower than all other treatments that had high SOM conditions, and was more similar to the low SOM content treatments (Figure 7.4).

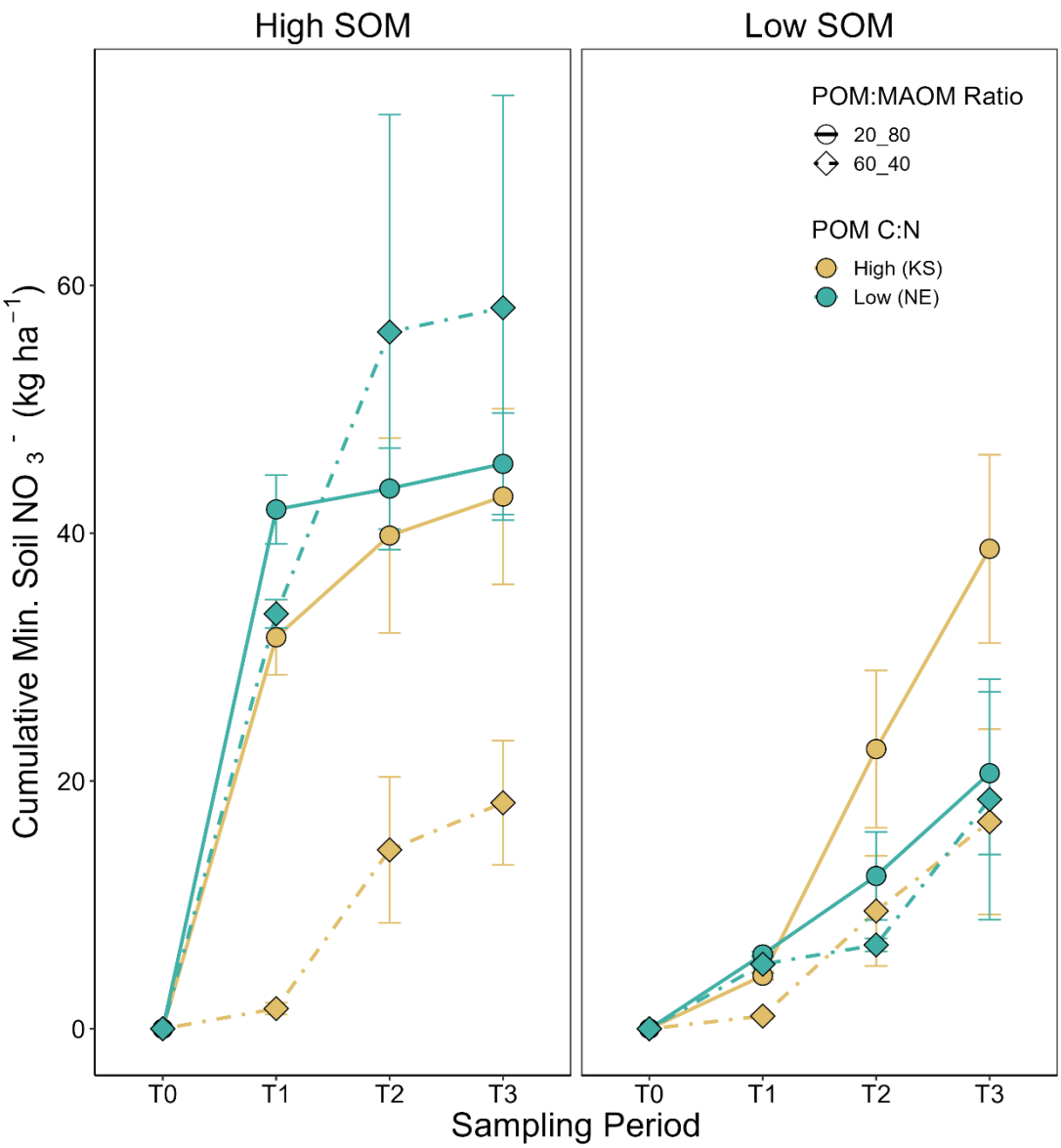

Figure 7.4- Cumulative mineralization of soil nitrate (NO_3^-) across the six-week sampling period. Samples were taken every 14 days. Different colored points and lines indicate different particulate organic matter (POM) carbon to nitrogen ratios (C:N), and different line types indicate different ratios of POM to mineral associated organic matter (MAOM) C. Error bars indicate ± 1 SE.

The shape of the accumulation curves differed between the high SOM content and low SOM content treatments (Figure 7.4). Whereas the majority of the high SOM content treatments experienced rapid mineralization in the first 2 weeks of incubation, the low SOM content soils did not. However, comparisons of the slopes between time points for each treatment combination

indicates more sustained mineralization in the low SOM soils, whereas some attenuation occurs in the high SOM treatment.

Discussion

In this experiment, we used isotopically distinct POM and MAOM combined in known ratios in an attempt to understand how the character of SOM, including POM C:N stoichiometry and the relative amounts of POM and MAOM C, would drive the SOM source of mineral N. We predicted that the presence of a C rich POM fraction (i.e., high POM C:N) would lead to increased MAOM-N mobilization across the course of the experiment. Further, we predicted that increasing the POM:MAOM ratio would lead to a higher amount of POM derived N, regardless of POM stoichiometry. Our results indicate that these predictions partially hold— high POM C:N treatments had a significantly higher proportion of N sourced from MAOM ($p < 0.001$). However, we observed that this effect interacted with the POM:MAOM ratio treatment, such that under higher POM:MAOM ratios, the effect of the high POM C:N was magnified. This work provides some insight into the biogeochemical drivers of MAOM-N mobilization, and offers evidence that MAOM-N is accessible to microbial decomposers even in the absence of external destabilizing forces such as root exudates (Jilling et al., 2021; Keiluweit et al., 2015).

C availability as a driver of N dynamics

We assumed that SOM content would drive the total amount of N mineralized proportional to the amount of total organic N that was available at the start of the incubation. This largely held true—we observed, on average, significantly lower total nitrate-N mineralized in the low SOM treatment after the initial incubation (Figure 7.1; $p < 0.001$). However, we also observed that the presence of high amounts of high C:N ratio POM (i.e., the high SOM, high POM C:N, high POM:MAOM ratio treatment combination) led to equally low inorganic N stocks, despite a 5

fold increase in the amount of organic matter present in that treatment (Figure 7.1). Previous work has argued that microbes are fundamentally C limited and that N limitation occurs only intermittently, primarily during the outset of decomposition of C rich substrate (Soong et al., 2020). Our results suggest that C limitation was alleviated during at least the initial two weeks of the incubation, and some of the treatments, especially those with increased POM-C, experienced significant N limitation. It has been well documented that residue composition can drive soil N transformation rates, especially immobilization (Zhao et al., 2018). Our findings suggest that abundant POM with low C:N drives patterns on N mineralization, possibly due to an increased NUE of the microbial community leading to N immobilization in response to N limitation (Mooshammer et al., 2014).

In addition to fate of net mineralized N, our results suggest that C availability was also a major driver of the source of N acquired by the microbial community. The conceptual model of SOM fractions argues that MAOM is a relatively stable pool protected from decomposition due to strong organo-mineral bonds, whereas POM lacks this protection and is readily available to decomposition (Lavallee et al., 2020). However, there is a growing body of evidence that demonstrates that portions of the MAOM pool are actively cycling in the soil system (Sokol et al., 2022; Woolf and Lehmann, 2019), leading to largely overlapping distribution of the turnover times of these two fractions (Cotrufo and Lavallee, 2022). Microbially mediated processes have been shown to be capable of liberating MAOM-N from mineral surfaces (Jilling et al., 2018; Li et al., 2021), often in response to the addition of exogenous C (Keiluweit et al., 2015). The mechanisms are in line with N mining hypotheses in which microbes shift extracellular enzyme production towards the breakdown of polymeric N containing substrates when N availability is limiting to their growth (Craine et al., 2007; Schimel and Bennett, 2004; Zhu et al., 2014). For

example, Wang et al. (2020) investigated the role of microbial decomposers in liberating N from the mineral associated fraction in N limited forest soils and found that the fungal community was capable of destabilizing MAOM-N via the exudation of hydrolytic enzymes. While our experiment was not designed to test specific mechanisms, our results further confirm the accessibility of MAOM-N to microbial decomposers (Figures 7.2 and 7.3) and suggest that MAOM-N may account for the dominant portion of plant available N under certain conditions, challenging the conception that POM is the primary source of nutrients in the soil system (Figure 7.3).

When examined as a whole, the isotope data (Figures 7.2 and 7.3), in combination with the temporal patterns in total NO_3^- stocks (Figure 7.4), suggest that POM stoichiometry and abundance are central drivers of MAOM-N mineralization. This is partially in line with the framework from Daly et al. (2022)—as POM C:N decreased (i.e., the amount of POM-N available to decomposers increased) and total POM N availability shifted, the $f_{MAOM\text{-}N}$ decreased (Figure 7.2). Additionally, as the ratio of POM:MAOM increased, this effect was magnified. While not significantly different in terms of $f_{MAOM\text{-}N}$, in treatments with a higher POM:MAOM ratio, we saw a trend both towards increased POM derived N when POM C:N was low and increased evidence of immobilization and MAOM-N mining in the high C:N soils relative to the 20:80 POM:MAOM treatments. Thus, N sourcing among physical SOM fractions may reflect pressure to mine N under certain soil conditions, exacerbated by high C:N inputs. This may represent a decoupling of C and N biogeochemistry in soils, leading to N limited systems having an increased C:N ratio in MAOM as microbial communities shift enzyme production to target N acquisition rather than C breakdown, potentially leaving C containing compounds on mineral surfaces largely intact (Chang et al., 2024; Rousk et al., 2016).

Implications for agroecosystem N management

Crop NUE continues to be low globally (Omara et al., 2019), largely due to overfertilization associated with poor SOM N supply predictions. In our study, we observed that strongest controls on N supply was SOM concentration, as well as the interaction between SOM and POM C:N. The higher SOM treatments mineralized significantly more N than the lower SOM treatments, except where immobilization outpaced mineralization (Figure 7.1). We observed that this exceeded a proportional increase—the proportion of total organic N that underwent mineralization was significantly higher in the high SOM treatment (0.8% vs. 0.6%, $p < 0.001$). At the broadest scope, this provides further evidence as to the effect of increasing SOM on soil fertility status (Bauer and Black, 1994; Ma et al., 2023). Indeed, our work affirms that a large pool of N in crops can be sourced from SOM mineralization (Yan et al., 2020), and that a substantial amount of that N is likely coming from the MAOM fraction (Daly et al., 2021; Jilling et al., 2021; Villarino et al., 2023). Globally, the average ratio of POM:MAOM in agricultural soils is ~24:76, similar to our 20:80 treatment (Hansen et al., 2024; Sokol et al., 2022). In those treatments, regardless of POM quality, more than half of the mineralized NO_3^- was sourced from the MAOM fraction during our initial incubation period (Figure 7.2). Although the POM fraction is often used as an indicator of soil health (Angst et al., 2023), these results suggest that to maximize crop use of mineralized soil N and reduce excess mineral fertilizer additions, increasing MAOM C and N stocks may be a more viable pathway. Previous work has shown that MAOM is more responsive to increased productivity than POM, (Hansen et al., 2024; Leuthold et al., 2024), such that conservation practices such as cover cropping can significantly increase MAOM-N in relatively short time periods (Jilling et al., 2020).

Given that organic N stocks in the MAOM fraction are order of magnitude higher than soil inorganic N stocks, regardless of mineral N application status, targeting management to increase mineralization and utilization of this pool is a robust means to improve agroecosystem sustainability. Increasing C inputs to the soil, via cover cropping or increased rotational complexity, may allow for increased MAOM utilization if properly constrained. Whereas previous work has suggested that high quality (i.e., low C:N) residue inputs may lead to increased efficiency of MAOM formation (Cotrufo et al., 2013), our findings suggest that the inverse of this phenomenon may also be true: increased C may lead to more MAOM utilization, especially in regards to N acquisition. However, this also leads to decreased plant available N via immobilization under an alleviation of C limitation for decomposers (Figures 7.1 and 7.4). As such, balancing C and N inputs into the soil such that microbial N acquisition can take advantage of the large N pool in MAOM without restricting crop N access is a priority when assessing management options. Cover crop mixtures, such as a grass and a legume species, may allow for this balance and better couple C and MAOM-N cycling, however further research on plant-soil interactions effect on N source is necessary.

Prior studies have shown that increasing mineral N stocks via fertilization can alter microbial N acquisition strategies and shift microbial communities towards higher bacteria:fungal ratios (Jia et al., 2020) which may decrease the MAOM destabilization ability of the community. Given that our incubation units did not receive any exogenous N inputs, it is unclear if the patterns in N sourcing and mineralization rate we observed would hold under conventional agricultural management. Given the evidence of immobilization under C rich environments (Figures 7.1 and 7.4), we hypothesize that an abundance of available mineral N may decrease bacterial NUE and lead to a greater proportion of POM decomposition (Daly et al., 2021), as microbes alter enzyme

production to seek out more easily accessible C sources (Grandy et al., 2008; Mooshammer et al., 2014). However, incorporating the observed dynamics into models of potential N mineralization that inform N application rate recommendations may allow for improved synchrony of MAOM-N acquisition by the crop during critical growth periods. Further research investigating sourcing over longer time periods such as the course of the growing season, or under field conditions with variable wetting and drying cycles will help to further elucidate the potential of MAOM-N to act as a substantial source of crop available N.

Considerations and Caveats

While our study provides useful and important insight into the source of organic matter derived N in the soil, there are some caveats that need to be considered. The first is the role of soil structure and aggregation in dictating soil function (King et al., 2020; Six and Paustian, 2014b). Microbial decomposers largely have access to the substrate in their immediate vicinity, or what can be transported via pore water (Dungait et al., 2012). This spatial accessibility to organic substrate is a key component of what C and N is mineralized in the soil system. Our soils in this experiment lacked structure, as a consequence of their recombined nature. The lack of aggregation led to a much smaller average pore space diameter than natural soils, altering water retention dynamics and possibly increasing access to POM and MAOM fractions that may have otherwise been protected from microbial attack. While we took pains to ensure that water content remained below the threshold of saturation, the presence of anoxic microsites and brief periods of denitrification cannot be ruled out. This becomes important, as for the high C:N POM treatments, we did observe $\delta^{15}N$ values in excess of our enriched MAOM endmember, indicating that there was likely some fractionation effect during N transformations in the soil, possibly due to ^{15}N-depleted N gaseous losses. Whereas fractionation effects due to mineralization or

nitrification process were accounted for by using extracted $\delta^{15}N$ as endmembers, it is possible that the high POM C:N treatments experienced an additional fractionation during the incubation process which led to these inflated $\delta^{15}N$ values. This may be indicative of some brief periods of denitrification, as immobilization tends to enrich the microbial biomass while depleting the isotopic ratio of the substrate (Dijkstra et al., 2009). However, given the trends in NO_3^- concentrations and the treatment specific effect, we believe that the risk of denitrification altering the $\delta^{15}N$ value is likely low in our study, and our bounding of the $f_{MAOM\text{-}N}$ value justified.

Of further consideration is the lack of N uptake or the presence of plant roots in our study. The majority of studies around MAOM-N mobilization have focused on the rhizosphere, given the role that root exudates can play in destabilizing the MAOM pool directly, or by priming the microbial community. Therefore, without roots, we may be underestimating the rate of MAOM-N production that is occurring in agricultural systems. Further examination of this effect, either by recombining SOM fractions and raising a plant in the known soil, or other methods, is paramount to understanding what the biogeochemical interactions that drive MAOM-N liberation and cycling are in the soil system.

Conclusions

We conducted an experiment to understand the source of mineralized N under various SOM conditions. Our findings suggest that MAOM-N is available to microbial communities as a N source, and the relative proportion of N sourced from this fraction is partially driven by the availability of C and N in other, more easily depolymerized fractions. These results add to a growing body of literature around MAOM-N access (Daly et al., 2021; Jilling et al., 2021, 2018a; Villarino et al., 2023), as well as lend further credence to hypotheses around dynamic sub pools of the MAOM fraction (Woolf and Lehmann, 2019; Zhang et al., 2021, Leuthold et al., in-

revision). A more robust understanding of MAOM-N dynamics, including improving management strategies to take advantage of MAOM-N availability, has the potential to improve crop NUE in agricultural systems. While this is a first step towards a more robust understanding of field-scale dynamics, our results demonstrate the MAOM-N is a considerable source of the N available to crops and should be considered as such.

CHAPTER 8: CONCLUSION

Soil organic matter (SOM) has been examined, conceptualized, and separated through a varied set of lenses and approaches. A non-exhaustive list includes the humic/fulvic acid model of secondary synthesis (see Lehmann and Kleber, 2015 as a review), thermal fractionation of specific organic compounds (Stoner et al., 2023), subdivision into the conceptual pools the underlie the bulk of our process-based ecosystem models (Parton, 1996), and of course, through physical fractionation methodologies (Rocci et al., 2023). These final sets of methods, which rely on the covariation of organic matter constituents with the physical properties of soil particles, continue to gain popularity due to the wealth of information they provide. The want for a means to subdivide SOM to better understand it stems from the fact that SOM exists at the heart of ecosystem function. The division of this heterogenous mixture of organic substrates into like pools allows for critical insight into the nuance around SOM formation, function, and persistence. Physical fractionation is a robust way of doing so, a point I have attempted to emphasize throughout the course of this dissertation. By separating SOM into physical fractions such as the particulate organic matter (POM), mineral associated organic matter (MAOM), and further into the coarse heavy associated organic matter (CHAOM), we gain valuable insight and mechanistic understanding that both improves our basic understanding of soil processes, as well as provides a roadmap for improved ecosystem management. While management goals are varied, here I have attempted to show that by using robust fractionation methods (Chapters 2 + 3), we gain a better understanding of management for soil organic carbon (SOC) persistence (Chapters 4 + 5), for agronomic outcomes such as yield and yield stability (Chapter 6), and for improved recommendations around soil fertility (Chapter 7). Above all else, the work presented

within this dissertation aims to validate the use of fractions as a tool for understanding both the basic and the applied in regard to SOM form and function.

Regardless of the advances in understanding detailed here, however, important questions around SOM and how we differentiate between its myriad of constituent parts remain. Much of the work I presented operates under a dichotomous POM-MAOM paradigm (Chapters 2, 4, 6, 7) though an emergent objective of this dissertation has been to highlight the tensions of the current conceptual model. Given how variable the composition of SOM can be, there is clearly a need for the simplification that the two-fraction model we describe and pursue in Chapters 2 and 3 allows for, especially as research moves out from the lab and into field days or shifts from conversations between researchers to discussions among practitioners with experiments such as the one discussed in Chapters 6 and 7. However, the next set of questions should aim to challenge and expand upon the definitions I rely on throughout this dissertation. To provide a set of examples to demonstrate why-- the POM fraction does, on average, have a shorter mean residence time than that of the MAOM. However, as we demonstrate in Chapter 5, POM of a certain provenance can persist for decades in the soil, largely unaltered. How this impacts our understanding of this fraction, how it shifts our reliance on POM as a rapid response indicator, is something that is worthy of continued investigation. In the same vein, the MAOM fraction is protected from decomposition by its formation mechanisms—we show this to some extent in Chapter 5 as well. Chapters 4 and 7 though demonstrate thoroughly how accessible the MAOM fraction is, and how both the C and N within it will be readily mineralized under certain conditions. Indeed, in some systems, especially agricultural ones, the MAOM appears be more similar to the mythical ship of Thesus, maintained via the dynamic replacement of constituents that retain the same properties than to a passive reservoir of organic C and N. Finally, what of the

CHAOM? Too often disregarded as a byproduct of the fractionation method, here we show the chameleonic dynamism of this fraction. The wide range of spectral characteristics this fraction possesses (Chapter 2), as well as the various potential mechanisms of formation that range from metal hydroxide coatings to microbially mediated exudates, hint at a critical piece of the puzzle towards a better understanding of SOM formation and turnover. Our observations of CHAOM dynamics in Chapter 5 highlight that this fraction could act as the temporary repository of the products of POM decomposition, a pathway not often explored in previous studies. How we reckon with these deviations in our models of understanding introduces the critical nuance necessary for continued advancement of the field and an improved understanding of soil systems.

The basic questions of understanding around formation, persistence and composition are exciting, but the work presented here also begs further investigation via an applied lens. Chapter 6 highlights the scale dependency of the SOM-yield stability relationship, the mechanism of which, at larger scales, is still unresolved. Future work that applies the fractionation-based approach we used in Chapter 6 to broader scales will reveal key soil-plant-environment interactions, which is work that I look eagerly forward to. The nutrient management implications of the work in Chapter 7 are clear—complex soil systems have capacity to provide significant amounts of N, and we can likely modify the source of this N through management. Moving forward with thoughtful field experiments that take advantage of this understanding is something that really could have an impact on improving nitrogen use efficiency, a boon for both improving farm economics and the quality of life downstream from major agricultural areas. Further, the burgeoning SOC markets that can provide a secondary stream of income for farmers demand an understanding of permanence, a requirement for a robust C credit. The work we detail throughout this dissertation helps to start answering this question, but also highlights how

challenging it may be to fully discern. The tensions between the MAOM dynamics in Chapters 4 and 7 and the dynamics we observed in Chapter 5 exemplify this— there is a clear and present need to identify the management that leads to stabilization and destabilization of the MAOM fraction and incorporate that into our recommendations for producers who have an interest in participating in these marketplaces. To that end, additional use of spectroscopic tools for characterization and quantification of SOM dynamics is an exciting use case, one that we show the promise of in Chapters 3 and 4. Given the nature of this rapidly growing field, a host of questions can still be examined—can we scale this technology such that we can take the number of samples necessary to really understand SOM distribution across areas of heterogeneous landscapes? Can we move beyond soil properties, and start leveraging the data obtained via spectral analysis to understand the properties of ecosystems like productivity or saturation potential? These are some of the questions I am excited that this dissertation begins to set up.

The work I have presented here has been aimed at understanding SOM fractions more wholly, and further connecting them with the ecosystems in which they exist. As detailed above, we came at these objectives through a variety of approaches and revealed important mechanistic and conceptual findings. In closing this dissertation though, I want to highlight how the ideas presented both here and throughout this dissertation did not spontaneously generate. Rather, the work here is the direct result of the outstanding science that my predecessors and contemporaries have and continue to produce, as is the incremental nature of scientific understanding. Across the chapters presented here, and especially in Chapters 2 and 3, I drew significant inspiration from the historic work on fractionation and the means by which we can conceptualize physical fractions. Indeed, a similar number of authors helped to provide the insight necessary to approach questions around spectral characterization of fractions and fraction sub pools. The

robust history to the understanding of SOM formation and persistence provided the grounding and jumping off points that were so necessary for the questions asked in Chapter 4 and 5. Without this history, we would fully lack the necessary context to further advance understanding (Bird et al., 2015; Cotrufo et al., 2015b; Hicks Pries et al., 2017; Kleber et al., 2015, 2007; Lavallee et al., 2019; Lehmann et al., 2020; Lehmann and Kleber, 2015; Sokol et al., 2019; von Lützow et al., 2008; Witzgall et al., 2021). Yield stability and the interactions between topography, soil organic matter, and cropping systems is a line of inquiry that has been fundamental to my work as a scientist, and has an equally rich history of advancement across scientists and institutions (Basso et al., 2019; Bowles et al., 2020; Fowler et al., 2024; Jiang and Thelen, 2004; Kane et al., 2021; Kravchenko and Bullock, 2000; Kravchenko et al., 2005; Loveland, 2003; Maestrini and Basso, 2018; Martinez-Feria and Basso, 2020; Oldfield et al., 2022, 2018, 2018; Pan et al., 2009; Schjønning et al., 2018; Williams et al., 2016). Finally, there have been a number of researchers on the cutting edge of understanding around MAOM destabilization and the implications for N, whom I have long admired and drawn inspiration from, especially in regards to Chapter 7. These scientists, along with a myriad of others, who have advanced the field of soil biogeochemistry for decades set the stage for the dissertation I present here. With luck, this work will continue to do the same for those to come.

REFERENCE LIST

Aber, J.D., Melillo, J.M., McClaugherty, C.A., 1990. Predicting long-term patterns of mass loss, nitrogen dynamics, and soil organic matter formation from initial fine litter chemistry in temperate forest ecosystems. Can. J. Bot. 68, 2201–2208. https://doi.org/10.1139/b90-287

Aksoy, E., Yigini, Y., Montanarella, L., 2016. Combining Soil Databases for Topsoil Organic Carbon Mapping in Europe. PLOS ONE 11, e0152098. https://doi.org/10.1371/journal.pone.0152098

Altabet, M.A., Wassenaar, L.I., Douence, C., Roy, R., 2019. A Ti(III) reduction method for one-step conversion of seawater and freshwater nitrate into N2O for stable isotopic analysis of 15N/14N, 18O/16O and 17O/16O. Rapid Communications in Mass Spectrometry 33, 1227–1239. https://doi.org/10.1002/rcm.8454

Amelung, W., Zech, W., 1999. Minimisation of organic matter disruption during particle-size fractionation of grassland epipedons. Geoderma 92, 73–85. https://doi.org/10.1016/S0016-7061(99)00023-3

Angst, G., Mueller, K.E., Castellano, M.J., Vogel, C., Wiesmeier, M., Mueller, C.W., 2023. Unlocking complex soil systems as carbon sinks: multi-pool management as the key. Nat Commun 14, 2967. https://doi.org/10.1038/s41467-023-38700-5

Angst, G., Mueller, K.E., Nierop, K.G.J., Simpson, M.J., 2021. Plant- or microbial-derived? A review on the molecular composition of stabilized soil organic matter. Soil Biology and Biochemistry 156, 108189. https://doi.org/10.1016/j.soilbio.2021.108189

Archontoulis, S.V., Castellano, M.J., Licht, M.A., Nichols, V., Baum, M., Huber, I., Martinez-Feria, R., Puntel, L., Ordóñez, R.A., Iqbal, J., Wright, E.E., Dietzel, R.N., Helmers, M., Vanloocke, A., Liebman, M., Hatfield, J.L., Herzmann, D., Córdova, S.C., Edmonds, P., Togliatti, K., Kessler, A., Danalatos, G., Pasley, H., Pederson, C., Lamkey, K.R., 2020. Predicting crop yields and soil-plant nitrogen dynamics in the US Corn Belt. Crop Science 60, 721–738. https://doi.org/10.1002/csc2.20039

Bagnall, D.K., Morgan, C.L.S., Cope, M., Bean, G.M., Cappellazzi, S., Greub, K., Liptzin, D., Norris, C.L., Rieke, E., Tracy, P., Aberle, E., Ashworth, A., Bañuelos Tavarez, O., Bary, A., Baumhardt, R.L., Borbón Gracia, A., Brainard, D., Brennan, J., Briones Reyes, D., Bruhjell, D., Carlyle, C., Crawford, J., Creech, C., Culman, S., Deen, W., Dell, C., Derner, J., Ducey, T., Duiker, S.W., Dyck, M., Ellert, B., Entz, M., Espinosa Solorio, A., Fonte, S.J., Fonteyne, S., Fortuna, A., Foster, J., Fultz, L., Gamble, A.V., Geddes, C., Griffin-LaHue, D., Grove, J., Hamilton, S.K., Hao, X., Hayden, Z.D., Howe, J., Ippolito, J., Johnson, G., Kautz, M., Kitchen, N., Kumar, S., Kurtz, K., Larney, F., Lewis, K., Liebman, M., Lopez Ramirez, A., Machado, S., Maharjan, B., Martinez Gamiño, M.A., May, W., McClaran, M., McDaniel, M., Millar, N., Mitchell, J.P., Moore, P.A., Moore, A., Mora Gutiérrez, M., Nelson, K.A., Omondi, E., Osborne, S., Alcalá, L.O., Owens, P., Pena-Yewtukhiw, E.M., Poffenbarger, H., Ponce Lira, B., Reeve, J., Reinbott, T., Reiter, M., Ritchey, E., Roozeboom, K.L., Rui, I., Sadeghpour, A., Sainju, U.M., Sanford, G., Schillinger, W., Schindelbeck, R.R., Schipanski, M., Schlegel, A., Scow, K., Sherrod, L., Sidhu, S., Solís Moya, E., St. Luce, M., Strock, J., Suyker, A., Sykes, V., Tao, H., Trujillo Campos, A., Van Eerd, L.L., Verhulst, N., Vyn, T.J., Wang, Y., Watts, D., Wright, D., Zhang, T., Honeycutt, C.W., 2022. Carbon-sensitive pedotransfer functions for plant available water. Soil Science Soc of Amer J 86, 612–629. https://doi.org/10.1002/saj2.20395

Barré, P., Plante, A.F., Cécillon, L., Lutfalla, S., Baudin, F., Bernard, S., Christensen, B.T., Eglin, T., Fernandez, J.M., Houot, S., Kätterer, T., Le Guillou, C., Macdonald, A., Van Oort, F., Chenu, C., 2016. The energetic and chemical signatures of persistent soil organic matter. Biogeochemistry 130, 1–12. https://doi.org/10.1007/s10533-016-0246-0

Barré, P., Quénéa, K., Vidal, A., Cécillon, L., Christensen, B.T., Kätterer, T., Macdonald, A., Petit, L., Plante, A.F., van Oort, F., Chenu, C., 2018. Microbial and plant-derived compounds both contribute to persistent soil organic carbon in temperate soils. Biogeochemistry 140, 81–92. https://doi.org/10.1007/s10533-018-0475-5

Basso, B., Antle, J., 2020. Digital agriculture to design sustainable agricultural systems. Nat Sustain 3, 254–256. https://doi.org/10.1038/s41893-020-0510-0

Basso, B., Shuai, G., Zhang, J., Robertson, G.P., 2019. Yield stability analysis reveals sources of large-scale nitrogen loss from the US Midwest. Sci Rep 9, 5774. https://doi.org/10.1038/s41598-019-42271-1

Bates, D., Mächler, M., Bolker, B., Walker, S., 2015. Fitting Linear Mixed-Effects Models Using lme4. J. Stat. Soft. 67. https://doi.org/10.18637/jss.v067.i01

Bauer, A., Black, A.L., 1994. Quantification of the Effect of Soil Organic Matter Content on Soil Productivity. Soil Science Society of America Journal 58, 185–193. https://doi.org/10.2136/sssaj1994.03615995005800010027x

Begill, N., Don, A., Poeplau, C., 2023. No detectable upper limit of mineral-associated organic carbon in temperate agricultural soils. Global Change Biology 29, 4662–4669. https://doi.org/10.1111/gcb.16804

Billings, S.A., Lajtha, K., Malhotra, A., Berhe, A.A., Graaff, M. -A., Earl, S., Fraterrigo, J., Georgiou, K., Grandy, S., Hobbie, S.E., Moore, J.A.M., Nadelhoffer, K., Pierson, D., Rasmussen, C., Silver, W.L., Sulman, B.N., Weintraub, S., Wieder, W., 2021. Soil organic carbon is not just for soil scientists: measurement recommendations for diverse practitioners. Ecol. Appl. 31. https://doi.org/10.1002/eap.2290

Bird, M.I., Wynn, J.G., Saiz, G., Wurster, C.M., McBeath, A., 2015. The Pyrogenic Carbon Cycle. Annual Review of Earth and Planetary Sciences 43, 273–298. https://doi.org/10.1146/annurev-earth-060614-105038

Bornemann, L., Welp, G., Amelung, W., 2010. Particulate Organic Matter at the Field Scale: Rapid Acquisition Using Mid-Infrared Spectroscopy. Soil Science Society of America Journal 74, 1147–1156. https://doi.org/10.2136/sssaj2009.0195

Bowles, T.M., Atallah, S.S., Campbell, E.E., Gaudin, A.C.M., Wieder, W.R., Grandy, A.S., 2018. Addressing agricultural nitrogen losses in a changing climate. Nat Sustain 1, 399–408. https://doi.org/10.1038/s41893-018-0106-0

Bowles, T.M., Jilling, A., Morán-Rivera, K., Schnecker, J., Grandy, A.S., 2022. Crop rotational complexity affects plant-soil nitrogen cycling during water deficit. Soil Biology and Biochemistry 166, 108552. https://doi.org/10.1016/j.soilbio.2022.108552

Bowles, T.M., Mooshammer, M., Socolar, Y., Calderón, F., Cavigelli, M.A., Culman, S.W., Deen, W., Drury, C.F., Garcia y Garcia, A., Gaudin, A.C.M., Harkcom, W.S., Lehman, R.M., Osborne, S.L., Robertson, G.P., Salerno, J., Schmer, M.R., Strock, J., Grandy, A.S., 2020. Long-Term Evidence Shows that Crop-Rotation Diversification Increases Agricultural Resilience to Adverse

Growing Conditions in North America. One Earth 2, 284–293. https://doi.org/10.1016/j.oneear.2020.02.007

Buckeridge, K.M., Creamer, C., Whitaker, J., 2022. Deconstructing the microbial necromass continuum to inform soil carbon sequestration. Functional Ecology 36, 1396–1410. https://doi.org/10.1111/1365-2435.14014

Calderón, F.J., Reeves, J.B., Collins, H.P., Paul, E.A., 2011. Chemical Differences in Soil Organic Matter Fractions Determined by Diffuse-Reflectance Mid-Infrared Spectroscopy. Soil Sci. Soc. Am. J. 75, 568–579. https://doi.org/10.2136/sssaj2009.0375

Cambardella, C.A., Elliott, E.T., 1992. Particulate Soil Organic-Matter Changes across a Grassland Cultivation Sequence. Soil Science Society of America Journal 56, 777–783. https://doi.org/10.2136/sssaj1992.03615995005600030017x

Cassman, K.G., Dobermann, A., Walters, D.T., 2002. Agroecosystems, Nitrogen-use Efficiency, and Nitrogen Management. AMBIO: A Journal of the Human Environment 31, 132–140. https://doi.org/10.1579/0044-7447-31.2.132

Castellano, M.J., Mueller, K.E., Olk, D.C., Sawyer, J.E., Six, J., 2015. Integrating plant litter quality, soil organic matter stabilization, and the carbon saturation concept. Glob Change Biol 21, 3200–3209. https://doi.org/10.1111/gcb.12982

Cates, A.M., Jilling, A., Tfaily, M.M., Jackson, R.D., 2022. Temperature and moisture alter organic matter composition across soil fractions. Geoderma 409, 115628. https://doi.org/10.1016/j.geoderma.2021.115628

Cates, A.M., Ruark, M.D., 2017. Soil aggregate and particulate C and N under corn rotations: responses to management and correlations with yield. Plant Soil 415, 521–533. https://doi.org/10.1007/s11104-016-3121-9

Cécillon, L., Baudin, F., Chenu, C., Christensen, B.T., Franko, U., Houot, S., Kanari, E., Kätterer, T., Merbach, I., van Oort, F., Poeplau, C., Quezada, J.C., Savignac, F., Soucémarianadin, L.N., Barré, P., 2021. Partitioning soil organic carbon into its centennially stable and active fractions with machine-learning models based on Rock-Eval® thermal analysis (PARTY$_{SOC}$v2.0 and PARTY$_{SOC}$v2.0$_{EU}$). Geoscientific Model Development 14, 3879–3898. https://doi.org/10.5194/gmd-14-3879-2021

Cerli, C., Celi, L., Kalbitz, K., Guggenberger, G., Kaiser, K., 2012a. Separation of light and heavy organic matter fractions in soil - Testing for proper density cut-off and dispersion level. Geoderma 170, 403–416. https://doi.org/10.1016/j.geoderma.2011.10.009

Cerli, C., Celi, L., Kalbitz, K., Guggenberger, G., Kaiser, K., 2012b. Separation of light and heavy organic matter fractions in soil — Testing for proper density cut-off and dispersion level. Geoderma 170, 403–416. https://doi.org/10.1016/j.geoderma.2011.10.009

Chang, Y., Sokol, N.W., van Groenigen, K.J., Bradford, M.A., Ji, D., Crowther, T.W., Liang, C., Luo, Y., Kuzyakov, Y., Wang, J., Ding, F., 2024. A stoichiometric approach to estimate sources of mineral-associated soil organic matter. Global Change Biology 30, e17092. https://doi.org/10.1111/gcb.17092

Christensen, B.T., 2001. Physical fractionation of soil and structural and functional complexity in organic matter turnover. European Journal of Soil Science 52, 345–353. https://doi.org/10.1046/j.1365-2389.2001.00417.x

Ciampitti, I.A., Vyn, T.J., 2012. Physiological perspectives of changes over time in maize yield dependency on nitrogen uptake and associated nitrogen efficiencies: A review. Field Crops Research 133, 48–67. https://doi.org/10.1016/j.fcr.2012.03.008

Cotrufo, M.F., Lavallee, J.M., 2022. Soil organic matter formation, persistence, and functioning: A synthesis of current understanding to inform its conservation and regeneration, in: Advances in Agronomy. Elsevier, pp. 1–66. https://doi.org/10.1016/bs.agron.2021.11.002

Cotrufo, M.F., Ranalli, M.G., Haddix, M.L., Six, J., Lugato, E., 2019. Soil carbon storage informed by particulate and mineral-associated organic matter. Nat. Geosci. 12, 989–994. https://doi.org/10.1038/s41561-019-0484-6

Cotrufo, M.F., Soong, J.L., Horton, A.J., Campbell, E.E., Haddix, M.L., Wall, D.H., Parton, W.J., 2015. Formation of soil organic matter via biochemical and physical pathways of litter mass loss. Nature Geosci 8, 776–779. https://doi.org/10.1038/ngeo2520

Cotrufo, M.F., Wallenstein, M.D., Boot, C.M., Denef, K., Paul, E., 2013. The Microbial Efficiency-Matrix Stabilization (MEMS) framework integrates plant litter decomposition with soil organic matter stabilization: do labile plant inputs form stable soil organic matter? Glob Change Biol 19, 988–995. https://doi.org/10.1111/gcb.12113

Craine, J.M., Morrow, C., Fierer, N., 2007. Microbial Nitrogen Limitation Increases Decomposition. Ecology 88, 2105–2113. https://doi.org/10.1890/06-1847.1

Crow, S.E., Swanston, C.W., Lajtha, K., Brooks, J.R., Keirstead, H., 2007. Density fractionation of forest soils: methodological questions and interpretation of incubation results and turnover time in an ecosystem context. Biogeochemistry 85, 69–90. https://doi.org/10.1007/s10533-007-9100-8

Curtin, D., Beare, M.H., Lehto, K., Tregurtha, C., Qiu, W., Tregurtha, R., Peterson, M., 2017. Rapid Assays to Predict Nitrogen Mineralization Capacity of Agricultural Soils. Soil Science Society of America Journal 81, 979–991. https://doi.org/10.2136/sssaj2016.08.0265

Curtin, D., Beare, M.H., Qiu, W., Sharp, J., 2019. Does Particulate Organic Matter Fraction Meet the Criteria for a Model Soil Organic Matter Pool? Pedosphere 29, 195–203. https://doi.org/10.1016/S1002-0160(18)60049-9

Daly, A.B., Jilling, A., Bowles, T.M., Buchkowski, R.W., Frey, S.D., Kallenbach, C.M., Keiluweit, M., Mooshammer, M., Schimel, J.P., Grandy, A.S., 2021. A holistic framework integrating plant-microbe-mineral regulation of soil bioavailable nitrogen. Biogeochemistry 154, 211–229. https://doi.org/10.1007/s10533-021-00793-9

Demyan, M.S., Rasche, F., Schulz, E., Breulmann, M., Müller, T., Cadisch, G., 2012. Use of specific peaks obtained by diffuse reflectance Fourier transform mid-infrared spectroscopy to study the composition of organic matter in a Haplic Chernozem. European Journal of Soil Science 63, 189–199. https://doi.org/10.1111/j.1365-2389.2011.01420.x

Denef, K., Plante, A.F., Six, J., 2010. Characterization of soil organic matter, in: Kutsch, W.L., Bahn, M., Heinemeyer, A. (Eds.), Soil Carbon Dynamics: An Integrated Methodology. Cambridge University Press, pp. 91–126. https://doi.org/10.1017/CBO9780511711794.007

Diochon, A., Gillespie, A.W., Ellert, B.H., Janzen, H.H., Gregorich, E.G., 2016. Recovery and dynamics of decomposing plant residue in soil: An evaluation of three fractionation methods. European Journal of Soil Science 67, 196–205. https://doi.org/10.1111/ejss.12316

Drinkwater, L.E., Snapp, S.S., 2022. Advancing the science and practice of ecological nutrient management for smallholder farmers. Front. Sustain. Food Syst. 6, 921216. https://doi.org/10.3389/fsufs.2022.921216

Dungait, J.A.J., Hopkins, D.W., Gregory, A.S., Whitmore, A.P., 2012. Soil organic matter turnover is governed by accessibility not recalcitrance. Glob Change Biol 18, 1781–1796. https://doi.org/10.1111/j.1365-2486.2012.02665.x

Dynarski, K.A., Bossio, D.A., Scow, K.M., 2020. Dynamic Stability of Soil Carbon: Reassessing the "Permanence" of Soil Carbon Sequestration. Front. Environ. Sci. 8, 514701. https://doi.org/10.3389/fenvs.2020.514701

Elliott, E.T., Cambardella, C.A., 1991. Physical separation of soil organic matter. Agriculture, Ecosystems & Environment 34, 407–419. https://doi.org/10.1016/0167-8809(91)90124-G

Elliott, E.T., Paustian, K., Frey, S.D., 1996. Modeling the Measurable or Measuring the Modelable: A Hierarchical Approach to Isolating Meaningful Soil Organic Matter Fractionations, in: Powlson, D.S., Smith, P., Smith, J.U. (Eds.), Evaluation of Soil Organic Matter Models, NATO ASI Series. Springer, Berlin, Heidelberg, pp. 161–179. https://doi.org/10.1007/978-3-642-61094-3_12

Fowler, A., Basso, B., Maureira, F., Millar, N., Ulbrich, R., Brinton, W.F., 2024. Spatial patterns of historical crop yields reveal soil health attributes in US Midwest fields. Sci Rep 14, 465. https://doi.org/10.1038/s41598-024-51155-y

Fox, J., Weisberg, S., 2019. An R Companion to Applied Regression, Third. ed. Sage, Thousand Oaks CA.

Fulton-Smith, S., Cotrufo, M.F., 2019. Pathways of soil organic matter formation from above and belowground inputs in a Sorghum bicolor bioenergy crop. GCB Bioenergy 11, 971–987. https://doi.org/10.1111/gcbb.12598

Georgiou, K., Jackson, R.B., Vindušková, O., Abramoff, R.Z., Ahlström, A., Feng, W., Harden, J.W., Pellegrini, A.F.A., Polley, H.W., Soong, J.L., Riley, W.J., Torn, M.S., 2022. Global stocks and capacity of mineral-associated soil organic carbon. Nat Commun 13, 3797. https://doi.org/10.1038/s41467-022-31540-9

Gerzabek, M. h., Pichlmayer, F., Kirchmann, H., Haberhauer, G., 1997. The response of soil organic matter to manure amendments in a long-term experiment at Ultuna, Sweden. European Journal of Soil Science 48, 273–282. https://doi.org/10.1111/j.1365-2389.1997.tb00547.x

Golchin, A., Oades, J., Skjemstad, J., Clarke, P., 1994. Study of free and occluded particulate organic matter in soils by solid state 13C Cp/MAS NMR spectroscopy and scanning electron microscopy. Soil Res. 32, 285. https://doi.org/10.1071/SR9940285

Gosling, P., Parsons, N., Bending, G.D., 2013. What are the primary factors controlling the light fraction and particulate soil organic matter content of agricultural soils? Biol Fertil Soils 49, 1001–1014. https://doi.org/10.1007/s00374-013-0791-9

Grandy, A.S., Daly, A.B., Bowles, T.M., Gaudin, A.C.M., Jilling, A., Leptin, A., McDaniel, M.D., Wade, J., Waterhouse, H., 2022. The nitrogen gap in soil health concepts and fertility measurements. Soil Biology and Biochemistry 175, 108856. https://doi.org/10.1016/j.soilbio.2022.108856

Grandy, A.S., Neff, J.C., 2008. Molecular C dynamics downstream: The biochemical decomposition sequence and its impact on soil organic matter structure and function. Science of The Total Environment 404, 297–307. https://doi.org/10.1016/j.scitotenv.2007.11.013

Grandy, A.S., Sinsabaugh, R.L., Neff, J.C., Stursova, M., Zak, D.R., 2008. Nitrogen deposition effects on soil organic matter chemistry are linked to variation in enzymes, ecosystems and size fractions. Biogeochemistry 91, 37–49. https://doi.org/10.1007/s10533-008-9257-9

Gunina, A., Kuzyakov, Y., 2014. Pathways of litter C by formation of aggregates and SOM density fractions: Implications from 13C natural abundance. Soil Biology and Biochemistry 71, 95–104. https://doi.org/10.1016/j.soilbio.2014.01.011

Haddix, M.L., Gregorich, E.G., Helgason, B.L., Janzen, H., Ellert, B.H., Francesca Cotrufo, M., 2020. Climate, carbon content, and soil texture control the independent formation and persistence of particulate and mineral-associated organic matter in soil. Geoderma 363, 114160. https://doi.org/10.1016/j.geoderma.2019.114160

Haddix, M.L., Paul, E.A., Cotrufo, M.F., 2016. Dual, differential isotope labeling shows the preferential movement of labile plant constituents into mineral-bonded soil organic matter. Glob Change Biol 22, 2301–2312. https://doi.org/10.1111/gcb.13237

Hansen, P.M., Even, R., King, A.E., Lavallee, J., Schipanski, M., Cotrufo, M.F., 2024. Distinct, direct and climate-mediated environmental controls on global particulate and mineral-associated organic carbon storage. Global Change Biology 30, e17080. https://doi.org/10.1111/gcb.17080

Harris, D., Horwáth, W.R., Van Kessel, C., 2001. Acid fumigation of soils to remove carbonates prior to total organic carbon or CARBON-13 isotopic analysis. Soil Science Soc of Amer J 65, 1853–1856. https://doi.org/10.2136/sssaj2001.1853

Hassink, J., 1992. Effects of soil texture and structure on carbon and nitrogen mineralization in grassland soils. Biol Fertil Soils 14, 126–134. https://doi.org/10.1007/BF00336262

Hatton, P.-J., Kleber, M., Zeller, B., Moni, C., Plante, A.F., Townsend, K., Gelhaye, L., Lajtha, K., Derrien, D., 2012. Transfer of litter-derived N to soil mineral–organic associations: Evidence from decadal 15N tracer experiments. Organic Geochemistry, Organic Isotopes in Soil 42, 1489–1501. https://doi.org/10.1016/j.orggeochem.2011.05.002

Heckman, K., Hicks Pries, C.E., Lawrence, C.R., Rasmussen, C., Crow, S.E., Hoyt, A.M., von Fromm, S.F., Shi, Z., Stoner, S., McGrath, C., 2022. Beyond bulk: Density fractions explain heterogeneity in global soil carbon abundance and persistence. Global change biology 28, 1178–1196.

Hicks Pries, C.E., Bird, J.A., Castanha, C., Hatton, P.-J., Torn, M.S., 2017. Long term decomposition: the influence of litter type and soil horizon on retention of plant carbon and nitrogen in soils. Biogeochemistry 134, 5–16. https://doi.org/10.1007/s10533-017-0345-6

Hijmans, R.J., 2022. terra: Spatial Data Analysis.

Hilscher, A., Knicker, H., 2011. Degradation of grass-derived pyrogenic organic material, transport of the residues within a soil column and distribution in soil organic matter fractions during a 28month microcosm experiment. Organic Geochemistry 42, 42–54. https://doi.org/10.1016/j.orggeochem.2010.10.005

Högberg, P., 1997. Tansley Review No. 95 15N natural abundance in soil-plant systems. New Phytologist 137, 179–203. https://doi.org/10.1046/j.1469-8137.1997.00808.x

Howarth, R., Chan, F., Conley, D.J., Garnier, J., Doney, S.C., Marino, R., Billen, G., 2011. Coupled biogeochemical cycles: eutrophication and hypoxia in temperate estuaries and coastal marine ecosystems. Frontiers in Ecology and the Environment 9, 18–26. https://doi.org/10.1890/100008

Huang, Y., Wu, S., Kaplan, J.O., 2015. Sensitivity of global wildfire occurrences to various factors in the context of global change. Atmospheric Environment 121, 86–92. https://doi.org/10.1016/j.atmosenv.2015.06.002

Hufkens, K., Basler, D., Milliman, T., Melaas, E.K., Richardson, A.D., 2018. An integrated phenology modelling framework in R: modelling vegetation phenology with phenor. Methods in Ecology & Evolution 9, 1–10. https://doi.org/10.1111/2041-210X.12970

Jia, X., Zhong, Y., Liu, J., Zhu, G., Shangguan, Z., Yan, W., 2020. Effects of nitrogen enrichment on soil microbial characteristics: From biomass to enzyme activities. Geoderma 366, 114256. https://doi.org/10.1016/j.geoderma.2020.114256

Jiang, P., Thelen, K.D., 2004. Effect of Soil and Topographic Properties on Crop Yield in a North-Central Corn–Soybean Cropping System. Agronomy Journal 96, 252–258. https://doi.org/10.2134/agronj2004.0252

Jilling, A., Kane, D., Williams, A., Yannarell, A.C., Davis, A., Jordan, N.R., Koide, R.T., Mortensen, D.A., Smith, R.G., Snapp, S.S., Spokas, K.A., Stuart Grandy, A., 2020. Rapid and distinct responses of particulate and mineral-associated organic nitrogen to conservation tillage and cover crops. Geoderma 359, 114001. https://doi.org/10.1016/j.geoderma.2019.114001

Jilling, A., Keiluweit, M., Contosta, A.R., Frey, S., Schimel, J., Schnecker, J., Smith, R.G., Tiemann, L., Grandy, A.S., 2018. Minerals in the rhizosphere: overlooked mediators of soil

nitrogen availability to plants and microbes. Biogeochemistry 139, 103–122. https://doi.org/10.1007/s10533-018-0459-5

Jilling, A., Keiluweit, M., Gutknecht, J.L.M., Grandy, A.S., 2021. Priming mechanisms providing plants and microbes access to mineral-associated organic matter. Soil Biology and Biochemistry 158, 108265. https://doi.org/10.1016/j.soilbio.2021.108265

Just, C., Armbruster, M., Barkusky, D., Baumecker, M., Diepolder, M., Döring, T.F., Heigl, L., Honermeier, B., Jate, M., Merbach, I., Rusch, C., Schubert, D., Schulz, F., Schweitzer, K., Seidel, S., Sommer, M., Spiegel, H., Thumm, U., Urbatzka, P., Zimmer, J., Kögel-Knabner, I., Wiesmeier, M., 2023. Soil organic carbon sequestration in agricultural long-term field experiments as derived from particulate and mineral-associated organic matter. Geoderma 434, 116472. https://doi.org/10.1016/j.geoderma.2023.116472

Just, C., Poeplau, C., Don, A., van Wesemael, B., Kögel-Knabner, I., Wiesmeier, M., 2021. A Simple Approach to Isolate Slow and Fast Cycling Organic Carbon Fractions in Central European Soils—Importance of Dispersion Method. Frontiers in Soil Science 1, 1–14. https://doi.org/10.3389/fsoil.2021.692583

Kaiser, M., Asefaw Berhe, A., 2014. How does sonication affect the mineral and organic constituents of soil aggregates?—A review. J. Plant Nutr. Soil Sci. 177, 479–495. https://doi.org/10.1002/jpln.201300339

Kaiser, M., Wirth, S., Ellerbrock, R.H., Sommer, M., 2010. Microbial respiration activities related to sequentially separated, particulate and water-soluble organic matter fractions from arable and forest topsoils. Soil Biology and Biochemistry 42, 418–428. https://doi.org/10.1016/j.soilbio.2009.11.018

Kallenbach, C.M., Frey, S.D., Grandy, A.S., 2016. Direct evidence for microbial-derived soil organic matter formation and its ecophysiological controls. Nat Commun 7, 13630. https://doi.org/10.1038/ncomms13630

Kane, D.A., Bradford, M.A., Fuller, E., Oldfield, E.E., Wood, S.A., 2021. Soil organic matter protects US maize yields and lowers crop insurance payouts under drought. Environ. Res. Lett. 16, 044018. https://doi.org/10.1088/1748-9326/abe492

Keiluweit, M., Bougoure, J.J., Nico, P.S., Pett-Ridge, J., Weber, P.K., Kleber, M., 2015. Mineral protection of soil carbon counteracted by root exudates. Nature Clim Change 5, 588–595. https://doi.org/10.1038/nclimate2580

King, A.E., Ali, G.A., Gillespie, A.W., Wagner-Riddle, C., 2020. Soil Organic Matter as Catalyst of Crop Resource Capture. Front. Environ. Sci. 8, 50. https://doi.org/10.3389/fenvs.2020.00050

King, A.E., Amsili, J.P., Córdova, S.C., Culman, S., Fonte, S.J., Kotcon, J., Liebig, M., Masters, M.D., McVay, K., Olk, D.C., Schipanski, M., Schneider, S.K., Stewart, C.E., Cotrufo, M.F., 2023. A soil matrix capacity index to predict mineral-associated but not particulate organic carbon across a range of climate and soil pH. Biogeochemistry. https://doi.org/10.1007/s10533-023-01066-3

Kirchmann, H., Pichlmayer, F., Gerzabek, M.H., 1996. Sulfur Balances and Sulfur-34 Abundance in a Long-Term Fertilizer Experiment. Soil Science Society of America Journal 60, 174–178. https://doi.org/10.2136/sssaj1996.03615995006000010028x

Kleber, M., Bourg, I.C., Coward, E.K., Hansel, C.M., Myneni, S.C.B., Nunan, N., 2021. Dynamic interactions at the mineral–organic matter interface. Nat Rev Earth Environ 2, 402–421. https://doi.org/10.1038/s43017-021-00162-y

Kleber, M., Eusterhues, K., Keiluweit, M., Mikutta, C., Mikutta, R., Nico, P.S., 2015. Mineral–Organic Associations: Formation, Properties, and Relevance in Soil Environments, in: Advances in Agronomy. Elsevier, pp. 1–140. https://doi.org/10.1016/bs.agron.2014.10.005

Kleber, M., Sollins, P., Sutton, R., 2007. A conceptual model of organo-mineral interactions in soils: self-assembly of organic molecular fragments into zonal structures on mineral surfaces. Biogeochemistry 85, 9–24. https://doi.org/10.1007/s10533-007-9103-5

Kögel-Knabner, I., Amelung, W., 2021. Soil organic matter in major pedogenic soil groups. Geoderma 384, 114785. https://doi.org/10.1016/j.geoderma.2020.114785

Kölbl, A., Leifeld, J., Kögel-Knabner, I., 2005. A comparison of two methods for the isolation of free and occluded particulate organic matter. Journal of Plant Nutrition and Soil Science 168, 660–667. https://doi.org/10.1002/jpln.200521805

Kramer, M.G., Lajtha, K., Thomas, G., Sollins, P., 2009. Contamination effects on soil density fractions from high N or C content sodium polytungstate. Biogeochemistry 92, 177–181. https://doi.org/10.1007/s10533-008-9268-6

Kravchenko, A., Bullock, D.G., 2000. Correlation of Corn and Soybean Grain Yield with Topography and Soil Properties. Agronomy Journal 92, 75–83. https://doi.org/10.2134/agronj2000.92175x

Kravchenko, A.N., Robertson, G.P., Thelen, K.D., Harwood, R.R., 2005. Management, Topographical, and Weather Effects on Spatial Variability of Crop Grain Yields. Agronomy Journal 97, 514–523. https://doi.org/10.2134/agronj2005.0514

Kuznetsova, A., Brockhoff, P.B., Christensen, R.H.B., 2017. lmerTest Package: Tests in Linear Mixed Effects Models. Journal of Statistical Software 82, 1–26. https://doi.org/10.18637/jss.v082.i13

Lavallee, J.M., Conant, R.T., Haddix, M.L., Follett, R.F., Bird, M.I., Paul, E.A., 2019. Selective preservation of pyrogenic carbon across soil organic matter fractions and its influence on calculations of carbon mean residence times. Geoderma 354, 113866. https://doi.org/10.1016/j.geoderma.2019.07.024

Lavallee, J.M., Soong, J.L., Cotrufo, M.F., 2020. Conceptualizing soil organic matter into particulate and mineral-associated forms to address global change in the 21st century. Global Change Biology 26, 261–273. https://doi.org/10.1111/gcb.14859

Lê, S., Josse, J., Husson, F., 2008. FactoMineR: A Package for Multivariate Analysis. Journal of Statistical Software 25, 1–18. https://doi.org/10.18637/jss.v025.i01

Lehmann, J., Cowie, A., Masiello, C.A., Kammann, C., Woolf, D., Amonette, J.E., Cayuela, M.L., Camps-Arbestain, M., Whitman, T., 2021. Biochar in climate change mitigation. Nat. Geosci. 14, 883–892. https://doi.org/10.1038/s41561-021-00852-8

Lehmann, J., Hansel, C.M., Kaiser, C., Kleber, M., Maher, K., Manzoni, S., Nunan, N., Reichstein, M., Schimel, J.P., Torn, M.S., Wieder, W.R., Kögel-Knabner, I., 2020. Persistence of soil organic carbon caused by functional complexity. Nat. Geosci. 13, 529–534. https://doi.org/10.1038/s41561-020-0612-3

Lehmann, J., Kleber, M., 2015. The contentious nature of soil organic matter. Nature 528, 60–68. https://doi.org/10.1038/nature16069

Lenth, R.V., 2022. emmeans: Estimated Marginal Means, aka Least-Squares Means.

Leuthold, S.J., Haddix, M.L., Lavallee, J., Cotrufo, M.F., 2022a. Physical fractionation techniques, in: Reference Module in Earth Systems and Environmental Sciences. Elsevier, p. B9780128229743000677. https://doi.org/10.1016/B978-0-12-822974-3.00067-7

Leuthold, S.J., Lavallee, J.M., Basso, B., Brinton, W.F., Cotrufo, M.F., 2024. Shifts in controls and abundance of particulate and mineral-associated organic matter fractions among subfield yield stability zones. SOIL 10, 307–319. https://doi.org/10.5194/soil-10-307-2024

Leuthold, S.J., Quinn, D., Miguez, F., Wendroth, O., Salmerón, M., Poffenbarger, H., 2021. Topographic effects on soil microclimate and surface cover crop residue decomposition in rolling cropland. Agriculture, Ecosystems & Environment 320, 107609. https://doi.org/10.1016/j.agee.2021.107609

Leuthold, S.J., Wendroth, O., Salmerón, M., Poffenbarger, H., 2022b. Weather-dependent relationships between topographic variables and yield of maize and soybean. Field Crops Research 276, 108368. https://doi.org/10.1016/j.fcr.2021.108368

Li, H., Bölscher, T., Winnick, M., Tfaily, M.M., Cardon, Z.G., Keiluweit, M., 2021. Simple Plant and Microbial Exudates Destabilize Mineral-Associated Organic Matter via Multiple Pathways. Environ. Sci. Technol. 55, 3389–3398. https://doi.org/10.1021/acs.est.0c04592

Li, X.G., Chen, Z.M., Hang Li, X., Ma, Q., Lin, Y., 2013. Chemical Characteristics of Physically Separated Soil Organic Matter Fractions in Contrasting Arable Soils. Soil Science 178, 128–137. https://doi.org/10.1097/SS.0b013e318295602f

Liang, C., Schimel, J.P., Jastrow, J.D., 2017. The importance of anabolism in microbial control over soil carbon storage. Nature Microbiology 2, 1–6. https://doi.org/10.1038/nmicrobiol.2017.105

Lin, B., Li, R., Liu, K., Pelumi Oladele, O., Xu, Z., Lal, R., Zhao, X., Zhang, H., 2023. Management-induced changes in soil organic carbon and related crop yield dynamics in China's cropland. Global Change Biology 29, 3575–3590. https://doi.org/10.1111/gcb.16703

Loeppert, Richard H., Inskeep, W.P., 2018. Iron, in: Sparks, D.L., Page, A.L., Helmke, P.A., Loeppert, R.H., Soltanpour, P.N., Tabatabai, M.A., Johnston, C.T., Sumner, M.E. (Eds.), SSSA Book Series. Soil Science Society of America, American Society of Agronomy, Madison, WI, USA, pp. 639–664. https://doi.org/10.2136/sssabookser5.3.c23

Loveland, P., 2003. Is there a critical level of organic matter in the agricultural soils of temperate regions: a review. Soil and Tillage Research 70, 1–18. https://doi.org/10.1016/S0167-1987(02)00139-3

Lugato, E., Lavallee, J.M., Haddix, M.L., Panagos, P., Cotrufo, M.F., 2021. Different climate sensitivity of particulate and mineral-associated soil organic matter. Nat. Geosci. 14, 295–300. https://doi.org/10.1038/s41561-021-00744-x

Lützow, M. v., Kögel-Knabner, I., Ekschmitt, K., Matzner, E., Guggenberger, G., Marschner, B., Flessa, H., 2006. Stabilization of organic matter in temperate soils: mechanisms and their relevance under different soil conditions – a review. European Journal of Soil Science 57, 426–445. https://doi.org/10.1111/j.1365-2389.2006.00809.x

Ma, Y., Woolf, D., Fan, M., Qiao, L., Li, R., Lehmann, J., 2023. Global crop production increase by soil organic carbon. Nat. Geosci. 1–7. https://doi.org/10.1038/s41561-023-01302-3

Maestrini, B., Basso, B., 2018. Drivers of within-field spatial and temporal variability of crop yield across the US Midwest. Sci Rep 8, 14833. https://doi.org/10.1038/s41598-018-32779-3

Margenot, A.J., Calderón, F.J., Parikh, S.J., 2016. Limitations and Potential of Spectral Subtractions in Fourier-Transform Infrared Spectroscopy of Soil Samples. Soil Science Society of America Journal 80, 10–26. https://doi.org/10.2136/sssaj2015.06.0228

Margenot, A.J., Parikh, S.J., Calderón, F.J., 2019. Improving Infrared Spectroscopy Characterization of Soil Organic Matter with Spectral Subtractions. JoVE 57464. https://doi.org/10.3791/57464

Martinez-Feria, R.A., Basso, B., 2020. Unstable crop yields reveal opportunities for site-specific adaptations to climate variability. Scientific Reports 10, 2885. https://doi.org/10.1038/s41598-020-59494-2

Minasny, B., McBratney, A.B., 2018. Limited effect of organic matter on soil available water capacity. Eur J Soil Sci 69, 39–47. https://doi.org/10.1111/ejss.12475

Moni, C., Derrien, D., Hatton, P.-J., Zeller, B., Kleber, M., 2012. Density fractions versus size separates: does physical fractionation isolate functional soil compartments? Biogeosciences 9, 5181–5197. https://doi.org/10.5194/bg-9-5181-2012

Mooshammer, M., Wanek, W., Hämmerle, I., Fuchslueger, L., Hofhansl, F., Knoltsch, A., Schnecker, J., Takriti, M., Watzka, M., Wild, B., Keiblinger, K.M., Zechmeister-Boltenstern, S., Richter, A., 2014. Adjustment of microbial nitrogen use efficiency to carbon:nitrogen imbalances regulates soil nitrogen cycling. Nat Commun 5, 3694. https://doi.org/10.1038/ncomms4694

Morgun, E.G., Makarov, M.I., 2011. Use of sodium polytungstate in the granulo-densimetric fractionation of soil material. EURASIAN SOIL SCIENCE 44, 394–398. https://doi.org/10.1134/S1064229311040077

Mosier, S., Apfelbaum, S., Byck, P., Calderton, F., Teague, R., Thompson, R., Cotrufo, F., 2021. Adaptive multi-paddock grazing increases soil carbon and nitrogen stocks and stabilisation through mineral association in southeastern U.S. grazing lands. Global Change Biology 288.

Mosier, S., Paustian, K., Davies, C., Kane, M., Cotrufo, M.F., 2019. Soil organic matter pools under management intensification of loblolly pine plantations. Forest Ecology and Management 447, 60–66. https://doi.org/10.1016/j.foreco.2019.05.056

NCERA-13, 2015. Recommended chemical soil test procedures for the North Central Region. (No. North Cetral Regional Research Publication No. 221). Missouri Agricultural Experiment Station.

Ng, W., Minasny, B., Jeon, S.H., McBratney, A., 2022. Mid-infrared spectroscopy for accurate measurement of an extensive set of soil properties for assessing soil functions. Soil Security 6, 100043. https://doi.org/10.1016/j.soisec.2022.100043

Nolan, B.T., Ruddy, B.C., Hitt, K.J., Helsel, D.R., 1997. Risk of Nitrate in Groundwaters of the United StatesA National Perspective. Environ. Sci. Technol. 31, 2229–2236. https://doi.org/10.1021/es960818d

Oades, J.M., Waters, A.G., 1991. Aggregate hierarchy in soils. Australian Journal of Soil Research 29, 815–825. https://doi.org/10.1071/SR9910815

Oksanen, J., Simpson, G.L., Blanchet, F.G., Kindt, R., Legendre, P., Minchin, P.R., O'Hara, R.B., Solymos, P., Stevens, M.H.H., Szoecs, E., Wagner, H., Barbour, M., Bedward, M., Bolker, B., Borcard, D., Carvalho, G., Chirico, M., Caceres, M.D., Durand, S., Evangelista, H.B.A., FitzJohn, R., Friendly, M., Furneaux, B., Hannigan, G., Hill, M.O., Lahti, L., McGlinn, D., Ouellette, M.-H., Cunha, E.R., Smith, T., Stier, A., Braak, C.J.F.T., Weedon, J., 2022. vegan: Community Ecology Package.

Oldfield, E.E., Bradford, M.A., Augarten, A.J., Cooley, E.T., Radatz, A.M., Radatz, T., Ruark, M.D., 2022. Positive associations of soil organic matter and crop yields across a regional network of working farms. Soil Science Soc of Amer J 86, 384–397. https://doi.org/10.1002/saj2.20349

Oldfield, E.E., Wood, S.A., Bradford, M.A., 2018. Direct effects of soil organic matter on productivity mirror those observed with organic amendments. Plant Soil 423, 363–373. https://doi.org/10.1007/s11104-017-3513-5

Omara, P., Aula, L., Oyebiyi, F., Raun, W.R., 2019. World Cereal Nitrogen Use Efficiency Trends: Review and Current Knowledge. Agrosystems Geosci & Env 2, 1–8. https://doi.org/10.2134/age2018.10.0045

Oorts, K., Vanlauwe, B., Recous, S., Merckx, R., 2005. Redistribution of particulate organic matter during ultrasonic dispersion of highly weathered soils. European Journal of Soil Science 56, 77–91. https://doi.org/10.1111/j.1351-0754.2004.00654.x

Pan, G., Smith, P., Pan, W., 2009. The role of soil organic matter in maintaining the productivity and yield stability of cereals in China. Agriculture, Ecosystems & Environment 129, 344–348. https://doi.org/10.1016/j.agee.2008.10.008

Parton, W., 1996. The CENTURY model, in: Evaluation of Soil Organic Matter Models. Springer, pp. 283–291.

Paul, E.A., Harris, D., Collins, H.P., Schulthess, U., Robertson, G.P., 1999. Evolution of CO2 and soil carbon dynamics in biologically managed, row-crop agroecosystems. Applied Soil Ecology 11, 53–65. https://doi.org/10.1016/S0929-1393(98)00130-9

Pellegrini, A.F.A., Ahlström, A., Hobbie, S.E., Reich, P.B., Nieradzik, L.P., Staver, A.C., Scharenbroch, B.C., Jumpponen, A., Anderegg, W.R.L., Randerson, J.T., Jackson, R.B., 2018. Fire frequency drives decadal changes in soil carbon and nitrogen and ecosystem productivity. Nature 553, 194–198. https://doi.org/10.1038/nature24668

Plaza, C., Giannetta, B., Benavente, I., Vischetti, C., Zaccone, C., 2019. Density-based fractionation of soil organic matter: effects of heavy liquid and heavy fraction washing. Scientific Reports 9, 1–7. https://doi.org/10.1038/s41598-019-46577-y

Poeplau, C., Don, A., Six, J., Kaiser, M., Benbi, D., Chenu, C., Cotrufo, M.F., Derrien, D., Gioacchini, P., Grand, S., Gregorich, E., Griepentrog, M., Gunina, A., Haddix, M., Kuzyakov, Y., Kühnel, A., Macdonald, L.M., Soong, J., Trigalet, S., Vermeire, M.L., Rovira, P., van Wesemael, B., Wiesmeier, M., Yeasmin, S., Yevdokimov, I., Nieder, R., 2018a. Isolating organic carbon fractions with varying turnover rates in temperate agricultural soils – A comprehensive method comparison. Soil Biology and Biochemistry 125, 10–26. https://doi.org/10.1016/j.soilbio.2018.06.025

Poeplau, C., Don, A., Six, J., Kaiser, M., Benbi, D., Chenu, C., Cotrufo, M.F., Derrien, D., Gioacchini, P., Grand, S., Gregorich, E., Griepentrog, M., Gunina, A., Haddix, M., Kuzyakov, Y., Kühnel, A., Macdonald, L.M., Soong, J., Trigalet, S., Vermeire, M.-L., Rovira, P., van Wesemael,

B., Wiesmeier, M., Yeasmin, S., Yevdokimov, I., Nieder, R., 2018b. Isolating organic carbon fractions with varying turnover rates in temperate agricultural soils – A comprehensive method comparison. Soil Biology and Biochemistry 125, 10–26. https://doi.org/10.1016/j.soilbio.2018.06.025

Poffenbarger, H.J., Sawyer, J.E., Barker, D.W., Olk, D.C., Six, J., Castellano, M.J., 2018. Legacy effects of long-term nitrogen fertilizer application on the fate of nitrogen fertilizer inputs in continuous maize. Agriculture, Ecosystems & Environment 265, 544–555. https://doi.org/10.1016/j.agee.2018.07.005

Powlson, D.S., Addiscott, T.M., Benjamin, N., Cassman, K.G., de Kok, T.M., van Grinsven, H., L'hirondel, J.-L., Avery, A.A., van Kessel, C., 2008. When Does Nitrate Become a Risk for Humans? Journal of Environmental Quality 37, 291–295. https://doi.org/10.2134/jeq2007.0177

Prairie, A.M., King, A.E., Cotrufo, M.F., 2023. Restoring particulate and mineral-associated organic carbon through regenerative agriculture. Proceedings of the National Academy of Sciences 120, e2217481120. https://doi.org/10.1073/pnas.2217481120

Prescott, C.E., Zabek, L.M., Staley, C.L., Kabzems, R., 2000. Decomposition of broadleaf and needle litter in forests of British Columbia: influences of litter type, forest type, and litter mixtures 30.

R Core Team, 2022. R: A Language and Environment for Statistical Computing.

Ramírez, P., Calderón, F., Haddix, M., Lugato, E., Cotrufo, M.F., 2021. Using Diffuse Reflectance Spectroscopy as a High Throughput Method for Quantifying Soil C and N and Their Distribution in Particulate and Mineral-Associated Organic Matter Fractions. Frontiers in Environmental Science 9. https://doi.org/10.3389/fenvs.2021.634472

Ramírez, P.B., Calderón, F.J., Fonte, S.J., Santibáñez, F., Bonilla, C.A., 2020. Spectral responses to labile organic carbon fractions as useful soil quality indicators across a climatic gradient. Ecological Indicators 111, 106042. https://doi.org/10.1016/j.ecolind.2019.106042

Ramnarine, R., Voroney, R.P., Dunfield, K.E., Wagner-Riddle, C., 2018. Characterization of the heavy, hydrolysable and non-hydrolysable fractions of soil organic carbon in conventional and no-tillage soils. Soil and Tillage Research 181, 144–151. https://doi.org/10.1016/j.still.2018.04.010

Rasmussen, C., Heckman, K., Wieder, W.R., Keiluweit, M., Lawrence, C.R., Berhe, A.A., Blankinship, J.C., Crow, S.E., Druhan, J.L., Hicks Pries, C.E., Marin-Spiotta, E., Plante, A.F., Schädel, C., Schimel, J.P., Sierra, C.A., Thompson, A., Wagai, R., 2018. Beyond clay: towards an improved set of variables for predicting soil organic matter content. Biogeochemistry 137, 297–306. https://doi.org/10.1007/s10533-018-0424-3

Ridgeway, J., Kane, J., Morrissey, E., Starcher, H., Brzostek, E., 2023. Roots selectively decompose litter to mine nitrogen and build new soil carbon. Ecology Letters n/a, 0–11. https://doi.org/10.1111/ele.14331

Rocci, K., Cotrufo, M.F., Ernakovitch, J., Foster, E., Frey, S., Georgiou, K., Grandy, S., Malhotra, A., Reich, P., Schlerman, E., Wieder, W.R., 2023. Bridging 20 years of soil organic matter frameworks: empirical support, model representation, and next steps (preprint). Preprints. https://doi.org/10.22541/essoar.170293436.63506237/v1

Rousk, K., Michelsen, A., Rousk, J., 2016. Microbial control of soil organic matter mineralization responses to labile carbon in subarctic climate change treatments. Global Change Biology 22, 4150–4161. https://doi.org/10.1111/gcb.13296

Samson, M.É., Chantigny, M.H., Vanasse, A., Menasseri-Aubry, S., Angers, D.A., 2020. Coarse mineral-associated organic matter is a pivotal fraction for SOM formation and is sensitive to the quality of organic inputs. Soil Biology and Biochemistry 149. https://doi.org/10.1016/j.soilbio.2020.107935

Samson, M.-É., Chantigny, M.H., Vanasse, A., Menasseri-Aubry, S., Angers, D.A., 2020. Coarse mineral-associated organic matter is a pivotal fraction for SOM formation and is sensitive to the quality of organic inputs. Soil Biology and Biochemistry 149, 107935. https://doi.org/10.1016/j.soilbio.2020.107935

Sanderman, J., Baldock, J.A., Dangal, S.R.S., Ludwig, S., Potter, S., Rivard, C., Savage, K., 2021. Soil organic carbon fractions in the Great Plains of the United States: an application of mid-infrared spectroscopy. Biogeochemistry 156, 97–114. https://doi.org/10.1007/s10533-021-00755-1

Sanderman, J., Grandy, A.S., 2020. Ramped thermal analysis for isolating biologically meaningful soil organic matter fractions with distinct residence times. SOIL 6, 131–144. https://doi.org/10.5194/soil-6-131-2020

Schiedung, M., Bellè, S.-L., Sigmund, G., Kalbitz, K., Abiven, S., 2020. Vertical mobility of pyrogenic organic matter in soils: a column experiment. Biogeosciences 17, 6457–6474. https://doi.org/10.5194/bg-17-6457-2020

Schimel, J.P., Bennett, J., 2004. Nitrogen Mineralization: Challenges of a changing paradigm. Ecology 85, 591–602. https://doi.org/10.1890/03-8002

Schipanski, M.E., Drinkwater, L.E., 2011. Nitrogen fixation of red clover interseeded with winter cereals across a management-induced fertility gradient. Nutr Cycl Agroecosyst 90, 105–119. https://doi.org/10.1007/s10705-010-9415-z

Schipanski, M.E., Drinkwater, L.E., Russelle, M.P., 2010. Understanding the variability in soybean nitrogen fixation across agroecosystems. Plant Soil 329, 379–397. https://doi.org/10.1007/s11104-009-0165-0

Schjønning, P., Jensen, J.L., Bruun, S., Jensen, L.S., Christensen, B.T., Munkholm, L.J., Oelofse, M., Baby, S., Knudsen, L., 2018. The Role of Soil Organic Matter for Maintaining Crop Yields: Evidence for a Renewed Conceptual Basis, in: Advances in Agronomy. Elsevier, pp. 35–79. https://doi.org/10.1016/bs.agron.2018.03.001

Schmidt, M.W.I., Torn, M.S., Abiven, S., Dittmar, T., Guggenberger, G., Janssens, I.A., Kleber, M., Kögel-Knabner, I., Lehmann, J., Manning, D.A.C., Nannipieri, P., Rasse, D.P., Weiner, S., Trumbore, S.E., 2011. Persistence of soil organic matter as an ecosystem property. Nature 478, 49–56. https://doi.org/10.1038/nature10386

See, C.R., Keller, A.B., Hobbie, S.E., Kennedy, P.G., Weber, P.K., Pett-Ridge, J., 2022. Hyphae move matter and microbes to mineral microsites: Integrating the hyphosphere into conceptual models of soil organic matter stabilization. Global Change Biology 28, 2527–2540. https://doi.org/10.1111/gcb.16073

Shi, Z., Allison, S.D., He, Y., Levine, P.A., Hoyt, A.M., Beem-Miller, J., Zhu, Q., Wieder, W.R., Trumbore, S., Randerson, J.T., 2020. The age distribution of global soil carbon inferred from radiocarbon measurements. Nat. Geosci. 13, 555–559. https://doi.org/10.1038/s41561-020-0596-z

Six, J., Elliott, E.T., Paustian, K., 2000. Soil macroaggregate turnover and microaggregate formation: a mechanism for C sequestration under no-tillage agriculture. Soil Biology and Biochemistry 32, 2099–2103. https://doi.org/10.1016/S0038-0717(00)00179-6

Six, J., Elliott, E.T., Paustian, K., 1999. Aggregate and Soil Organic Matter Dynamics under Conventional and No-Tillage Systems. Soil Science Society of America Journal 63, 1350–1358. https://doi.org/10.2136/sssaj1999.6351350x

Six, J., Paustian, K., 2014. Aggregate-associated soil organic matter as an ecosystem property and a measurement tool. Soil Biology and Biochemistry 68, A4. https://doi.org/10.1016/j.soilbio.2013.06.014

Smith, J.U., Smith, P., Monaghan, R., MacDonald, A.J., 2002. When is a measured soil organic matter fraction equivalent to a model pool? European Journal of Soil Science 53, 405–416. https://doi.org/10.1046/j.1365-2389.2002.00458.x

Sohi, S.P., Mahieu, N., Arah, J.R.M., Powlson, D.S., Madari, B., Gaunt, J.L., 2001. A Procedure for Isolating Soil Organic Matter Fractions Suitable for Modeling. Soil Sci. Soc. Am. J. 65, 1121–1128. https://doi.org/10.2136/sssaj2001.6541121x

Soil Survey Staff, 2022. Kellogg Soil Survey Laboratory methods manual. (Soil Survey Investigations No. 42), Kellogg Soil Survey Laboratory methods manual. U.S. Department of Agriculture, Natural Resources Conservation Service.

Sokol, N.W., Sanderman, J., Bradford, M.A., 2019. Pathways of mineral-associated soil organic matter formation: Integrating the role of plant carbon source, chemistry, and point of entry. Glob Change Biol 25, 12–24. https://doi.org/10.1111/gcb.14482

Sokol, N.W., Whalen, E.D., Jilling, A., Kallenbach, C., Pett-Ridge, J., Georgiou, K., 2022. Global distribution, formation and fate of mineral-associated soil organic matter under a changing climate: A trait-based perspective. Functional Ecology 36, 1411–1429. https://doi.org/10.1111/1365-2435.14040

Sollins, P., Kramer, M.G., Swanston, C., Lajtha, K., Filley, T., Aufdenkampe, A.K., Wagai, R., Bowden, R.D., 2009a. Sequential density fractionation across soils of contrasting mineralogy: Evidence for both microbial- and mineral-controlled soil organic matter stabilization. Biogeochemistry 96, 209–231. https://doi.org/10.1007/s10533-009-9359-z

Sollins, P., Kramer, M.G., Swanston, C., Lajtha, K., Filley, T., Aufdenkampe, A.K., Wagai, R., Bowden, R.D., 2009b. Sequential density fractionation across soils of contrasting mineralogy: evidence for both microbial- and mineral-controlled soil organic matter stabilization. Biogeochemistry 96, 209–231. https://doi.org/10.1007/s10533-009-9359-z

Sollins, P., Spycher, G., Glassman, C.A., 1984. Net nitrogen mineralization from light- and heavy-fraction forest soil organic matter. Soil Biology and Biochemistry 16, 31–37. https://doi.org/10.1016/0038-0717(84)90122-6

Sollins, P., Swanston, C., Kleber, M., Filley, T., Kramer, M., Crow, S., Caldwell, B.A., Lajtha, K., Bowden, R., 2006. Organic C and N stabilization in a forest soil: Evidence from sequential density fractionation. Soil Biology and Biochemistry, Ecosystems in Flux: Molecular and stable isotope Assessments of Soil Organic Matter Storage and Dynamics 38, 3313–3324. https://doi.org/10.1016/j.soilbio.2006.04.014

Soong, J.L., Cotrufo, M.F., 2015. Annual burning of a tallgrass prairie inhibits C and N cycling in soil, increasing recalcitrant pyrogenic organic matter storage while reducing N availability. Global Change Biology 21, 2321–2333. https://doi.org/10.1111/gcb.12832

Soong, J.L., Fuchslueger, L., Marañon-Jimenez, S., Torn, M.S., Janssens, I.A., Penuelas, J., Richter, A., 2020. Microbial carbon limitation: The need for integrating microorganisms into our understanding of ecosystem carbon cycling. Global Change Biology 26, 1953–1961. https://doi.org/10.1111/gcb.14962

Soong, J.L., Reuss, D., Pinney, C., Boyack, T., Haddix, M.L., Stewart, C.E., Cotrufo, M.F., 2014. Design and Operation of a Continuous 13C and 15N Labeling Chamber for Uniform or Differential, Metabolic and Structural, Plant Isotope Labeling. JoVE (Journal of Visualized Experiments) e51117. https://doi.org/10.3791/51117

Soong, J.L., Vandegehuchte, M.L., Horton, A.J., Nielsen, U.N., Denef, K., Shaw, E.A., de Tomasel, C.M., Parton, W., Wall, D.H., Cotrufo, M.F., 2016. Soil microarthropods support ecosystem productivity and soil C accrual: Evidence from a litter decomposition study in the tallgrass prairie. Soil Biology and Biochemistry 92, 230–238. https://doi.org/10.1016/j.soilbio.2015.10.014

Spohn, M., 2024. Preferential adsorption of nitrogen- and phosphorus-containing organic compounds to minerals in soils: A review. Soil Biology and Biochemistry 194, 109428. https://doi.org/10.1016/j.soilbio.2024.109428

Stanley, P., Spertus, J., Chiartas, J., Stark, P.B., Bowles, T., 2023. Valid inferences about soil carbon in heterogeneous landscapes. Geoderma 430, 116323. https://doi.org/10.1016/j.geoderma.2022.116323

Steffens, M., Rogge, D.M., Mueller, C.W., Höschen, C., Lugmeier, J., Kölbl, A., Kögel-Knabner, I., 2017. Identification of Distinct Functional Microstructural Domains Controlling C Storage in Soil. Environ. Sci. Technol. 51, 12182–12189. https://doi.org/10.1021/acs.est.7b03715

Stevens, A., Ramirez-Lopez, L., 2022. An introduction to the prospectr package.

Stevenson, F.J., 1994. Humus Chemistry: Genesis, Composition, Reactions, 2nd Editio. ed. John Wiley and Sons Ltd., New York, NY.

Stewart, C.E., Paustian, K., Conant, R.T., Plante, A.F., Six, J., 2007. Soil carbon saturation: concept, evidence and evaluation. Biogeochemistry 86, 19–31. https://doi.org/10.1007/s10533-007-9140-0

Stoner, S., Trumbore, S.E., González-Pérez, J.A., Schrumpf, M., Sierra, C.A., Hoyt, A.M., Chadwick, O., Doetterl, S., 2023. Relating mineral–organic matter stabilization mechanisms to carbon quality and age distributions using ramped thermal analysis. Philosophical Transactions of the Royal Society A: Mathematical, Physical and Engineering Sciences 381, 20230139. https://doi.org/10.1098/rsta.2023.0139

Thomas, B.W., Whalen, J.K., Sharifi, M., Chantigny, M., Zebarth, B.J., 2016. Labile organic matter fractions as early-season nitrogen supply indicators in manure-amended soils. Journal of Plant Nutrition and Soil Science 179, 94–103. https://doi.org/10.1002/jpln.201400532

Thornton, M.M., Shrestha, R., Wei, Y., Thornton, P.E., Kao, S.-C., Wilson, B.E., 2022. Daymet: Annual Climate Summaries on a 1-km Grid for North America, Version 4 R1. https://doi.org/10.3334/ORNLDAAC/2130

Tiessen, H., Cuevas, E., Chacon, P., 1994. The role of soil organic matter in sustaining soil fertility. Nature 371, 783–785. https://doi.org/10.1038/371783a0

Usowicz, B., Lipiec, J., 2017. Spatial variability of soil properties and cereal yield in a cultivated field on sandy soil. Soil and Tillage Research 174, 241–250. https://doi.org/10.1016/j.still.2017.07.015

Van Oost, K., Six, J., 2023. Reconciling the paradox of soil organic carbon erosion by water. Biogeosciences 20, 635–646. https://doi.org/10.5194/bg-20-635-2023

Villarino, S.H., Talab, E., Contisciani, L., Videla, C., Di Geronimo, P., Mastrángelo, M.E., Georgiou, K., Jackson, R.B., Piñeiro, G., 2023. A large nitrogen supply from the stable mineral-associated soil organic matter fraction. Biol Fertil Soils. https://doi.org/10.1007/s00374-023-01755-z

von Lützow, M., Kögel-Knabner, I., Ekschmitt, K., Flessa, H., Guggenberger, G., Matzner, E., Marschner, B., 2007. SOM fractionation methods: Relevance to functional pools and to stabilization mechanisms. Soil Biology and Biochemistry 39, 2183–2207. https://doi.org/10.1016/j.soilbio.2007.03.007

von Lützow, M., Kögel-Knabner, I., Ludwig, B., Matzner, E., Flessa, H., Ekschmitt, K., Guggenberger, G., Marschner, B., Kalbitz, K., 2008. Stabilization mechanisms of organic matter in four temperate soils: Development and application of a conceptual model. Z. Pflanzenernähr. Bodenk. 171, 111–124. https://doi.org/10.1002/jpln.200700047

Vos, C., Jaconi, A., Jacobs, A., Don, A., 2018. Hot regions of labile and stable soil organic carbon in Germany – Spatial variability and driving factors. SOIL 4, 153–167. https://doi.org/10.5194/soil-4-153-2018

Wander, M., 2004. Soil organic matter fractions and their relevance to soil function. Soil organic matter in sustainable agriculture. CRC Press, Boca Raton, FL 67–102.

Wang, T., Tian, Z., Tunlid, A., Persson, P., 2020. Nitrogen acquisition from mineral-associated proteins by an ectomycorrhizal fungus. New Phytologist 228, 697–711. https://doi.org/10.1111/nph.16596

Wenkert, W., Fausey, N.R., Watters, H.D., 1981. Flooding responses inZea mays L. Plant Soil 62, 351–366. https://doi.org/10.1007/BF02374133

Whalen, E.D., Grandy, A.S., Sokol, N.W., Keiluweit, M., Ernakovich, J., Smith, R.G., Frey, S.D., 2022. Clarifying the evidence for microbial- and plant-derived soil organic matter, and the path toward a more quantitative understanding. Global Change Biology 28, 7167–7185. https://doi.org/10.1111/gcb.16413

Whalen, J.K., Bottomley, P.J., Myrold, D.D., 2000. Carbon and nitrogen mineralization from light- and heavy-fraction additions to soil. Soil Biology and Biochemistry 32, 1345–1352. https://doi.org/10.1016/S0038-0717(00)00040-7

Williams, A., Hunter, M.C., Kammerer, M., Kane, D.A., Jordan, N.R., Mortensen, D.A., Smith, R.G., Snapp, S., Davis, A.S., 2016. Soil Water Holding Capacity Mitigates Downside Risk and Volatility in US Rainfed Maize: Time to Invest in Soil Organic Matter? PLoS ONE 11, e0160974. https://doi.org/10.1371/journal.pone.0160974

Witzgall, K., Vidal, A., Schubert, D.I., Höschen, C., Schweizer, S.A., Buegger, F., Pouteau, V., Chenu, C., Mueller, C.W., 2021. Particulate organic matter as a functional soil component for persistent soil organic carbon. Nature Communications 12, 4115. https://doi.org/10.1038/s41467-021-24192-8

Woolf, D., Lehmann, J., 2019. Microbial models with minimal mineral protection can explain long-term soil organic carbon persistence. Sci Rep 9, 6522. https://doi.org/10.1038/s41598-019-43026-8

Xu, S., Silveira, M.L., Ngatia, L.W., Normand, A.E., Sollenberger, L.E., Ramesh Reddy, K., 2017. Carbon and nitrogen pools in aggregate size fractions as affected by sieving method and land use intensification. Geoderma 305, 70–79. https://doi.org/10.1016/j.geoderma.2017.05.044

Yan, M., Pan, G., Lavallee, J.M., Conant, R.T., 2020. Rethinking sources of nitrogen to cereal crops. Global Change Biology 26, 191–199. https://doi.org/10.1111/gcb.14908

Yin, X., Kersebaum, K.-C., Beaudoin, N., Constantin, J., Chen, F., Louarn, G., Manevski, K., Hoffmann, M., Kollas, C., Armas-Herrera, C.M., Baby, S., Bindi, M., Dibari, C., Ferchaud, F., Ferrise, R., de Cortazar-Atauri, I.G., Launay, M., Mary, B., Moriondo, M., Öztürk, I., Ruget, F., Sharif, B., Wachter-Ripoche, D., Olesen, J.E., 2020. Uncertainties in simulating N uptake, net N mineralization, soil mineral N and N leaching in European crop rotations using process-based models. Field Crops Research 255, 107863. https://doi.org/10.1016/j.fcr.2020.107863

Yu, W., Huang, W., Weintraub-Leff, S.R., Hall, S.J., 2022. Where and why do particulate organic matter (POM) and mineral-associated organic matter (MAOM) differ among diverse soils? Soil Biology and Biochemistry 172, 108756. https://doi.org/10.1016/j.soilbio.2022.108756

Zhang, Y., Lavallee, J.M., Robertson, A.D., Even, R., Ogle, S.M., Paustian, K., Cotrufo, M.F., 2021. Simulating measurable ecosystem carbon and nitrogen dynamics with the mechanistically defined MEMS 2.0 model. Biogeosciences 18, 3147–3171. https://doi.org/10.5194/bg-18-3147-2021

Zhao, Y., Zhang, J., Müller, C., Cai, Z., 2018. Temporal variations of crop residue effects on soil N transformation depend on soil properties as well as residue qualities. Biol Fertil Soils 54, 659–669. https://doi.org/10.1007/s00374-018-1291-8

Zhu, B., Gutknecht, J.L.M., Herman, D.J., Keck, D.C., Firestone, M.K., Cheng, W., 2014. Rhizosphere priming effects on soil carbon and nitrogen mineralization. Soil Biology and Biochemistry 76, 183–192. https://doi.org/10.1016/j.soilbio.2014.04.033

APPENDIX

Chapter 3 Supplemental Material

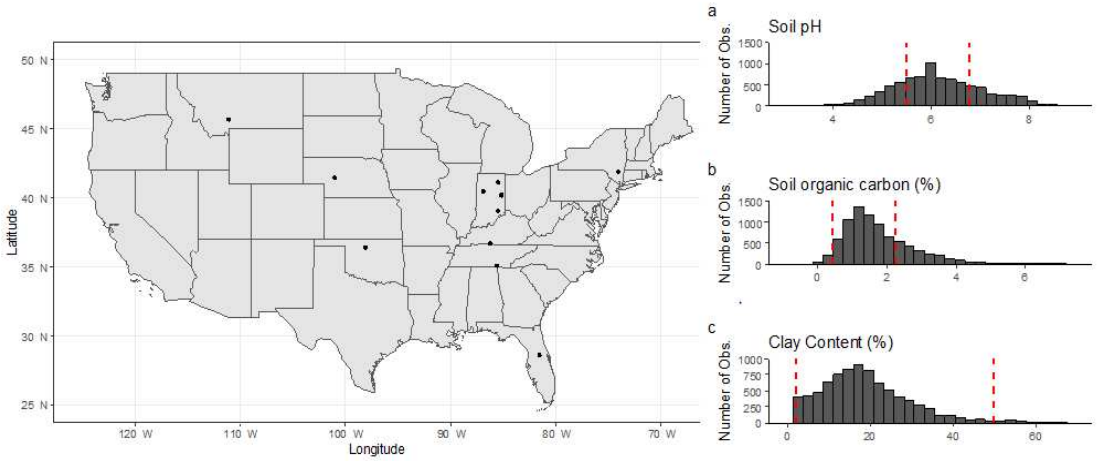

Supplemental Figure 3.1 – Distribution of sampling points across the continental United States (Left). Bounds of samples included in our study (dashed red lines) compared to the range of values present in US agricultural soils as derived from the Kellog Soil Survey Laboratory soil database.

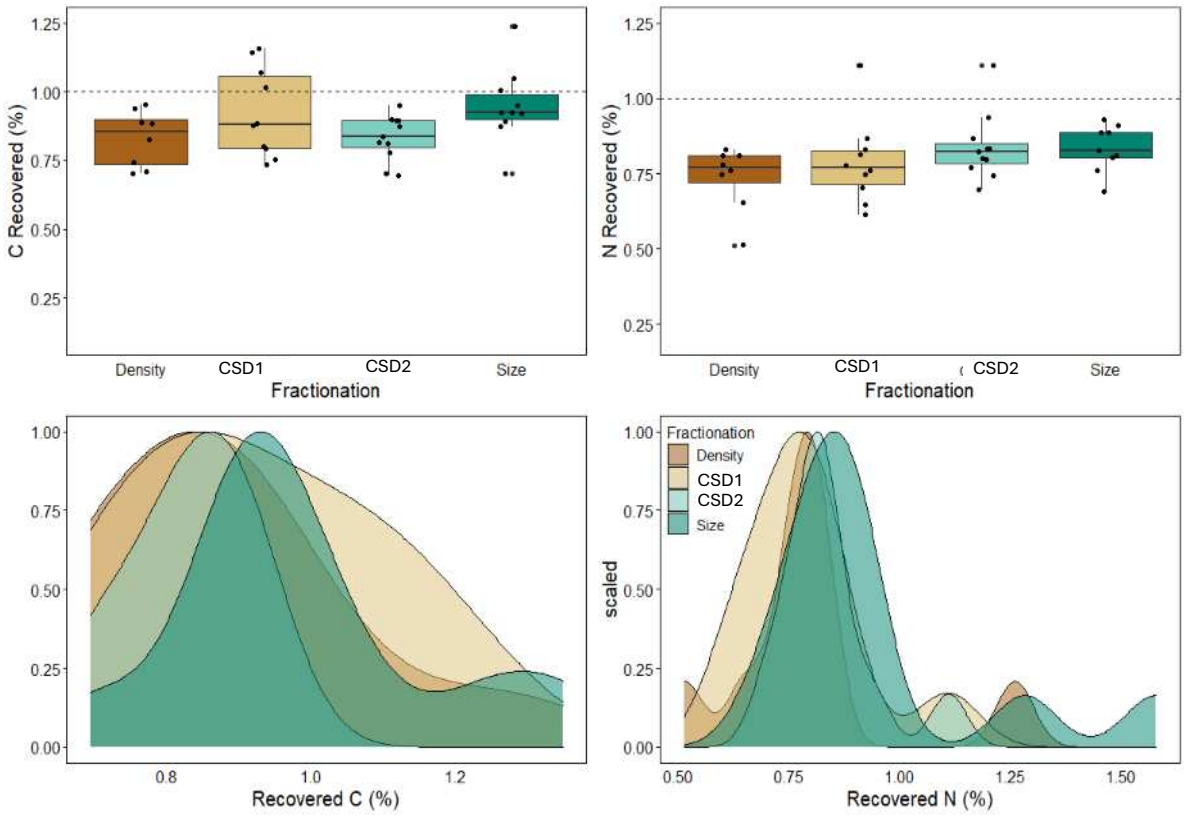

Supplemental Figure 3.2: Carbon (left) and nitrogen (right) recoveries for the various fractionation methods employed in the present study. Top boxplots indicate the range of values per fractionation method, with the solid line across the box in`dicating the median value. Bottom panels are density plots, showing the relative range of values among fractionation methods.

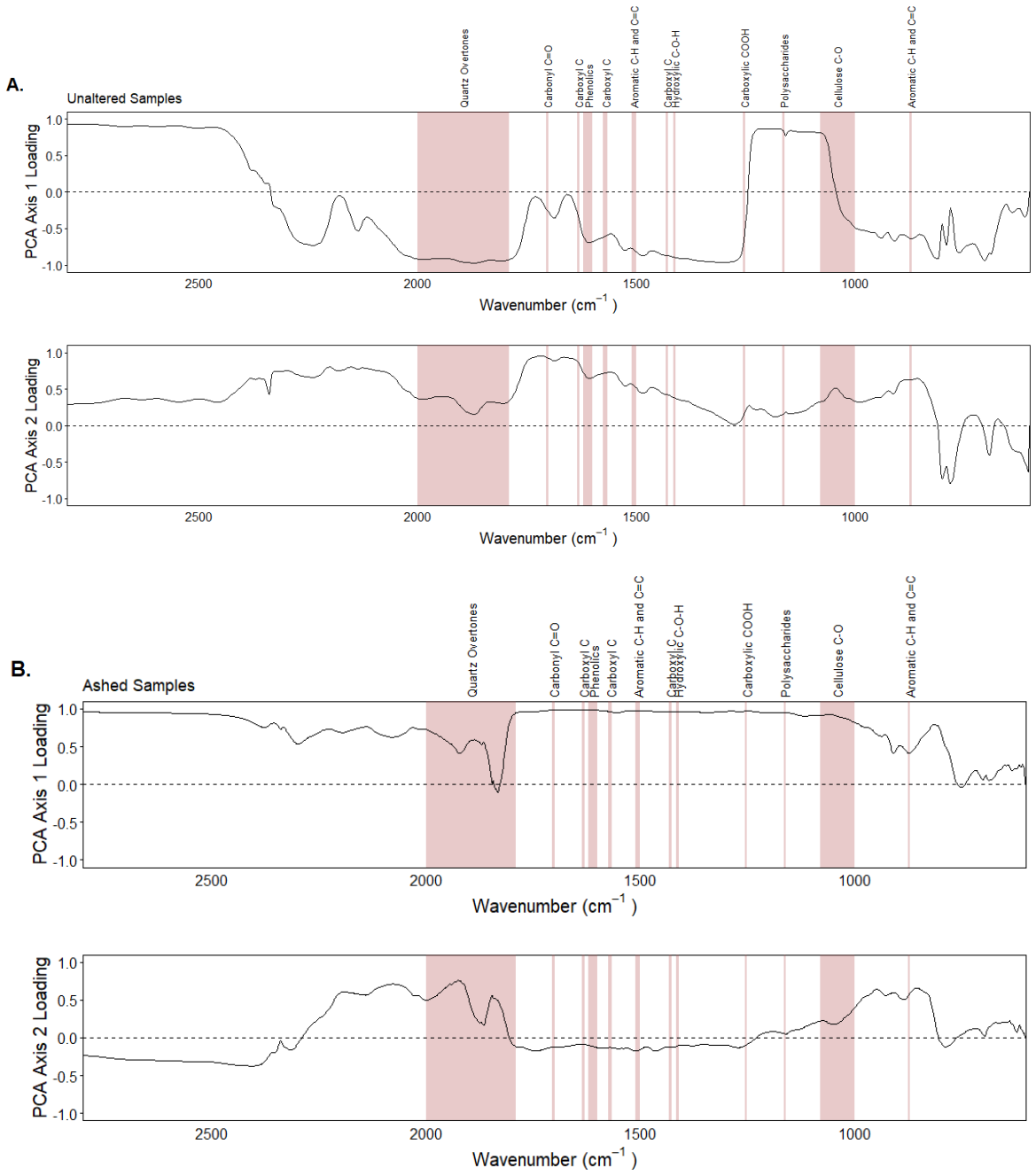

Supplemental Figure 3.3: Plots of wavelengths vs. PCA loadings corresponding to Figure 5A and 5B in the main text. Panel A shows the loading vs. wavelength relationship for unaltered samples, whereas panel B shows the relationship for the samples following spectral subtraction analysis. Red highlighted areas correspond to spectral bands associated with either mineral peaks, or molecular constituents of soil organic matter.

Chapter 4 Supplemental Material

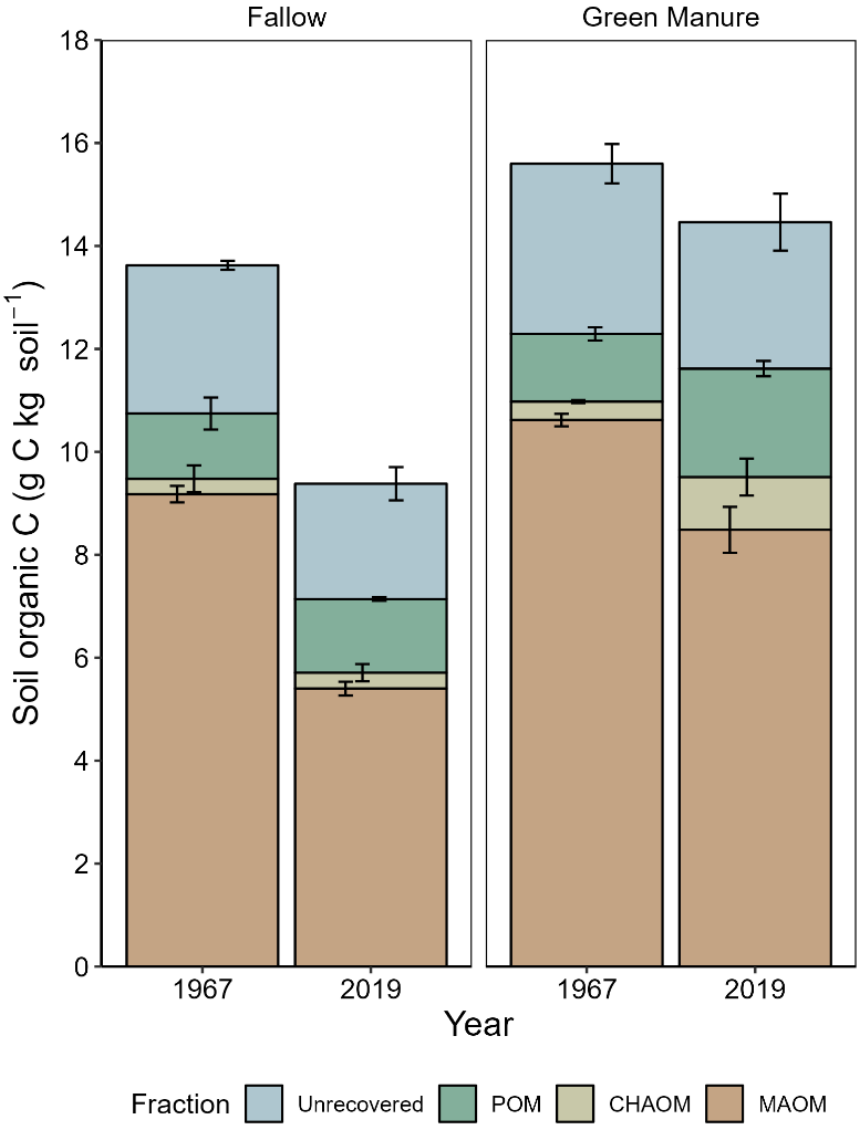

Supplemental Figure 4.1 – Distribution of organic carbon across particulate organic matter (POM), coarse heavy associated organic matter (CHAOM), and mineral associated organic matter (MAOM) in the bare fallow (left) and green manure (right) treatments, for either sample year. Error bars indicate ± 1 SE. Light blue bars represent the portion of carbon lost during fractionation as compared to bulk soil C analysis (mean C recovery = 78.3%). There were no significant differences in C loss among treatments or years.

Chapter 5 Supplemental Material

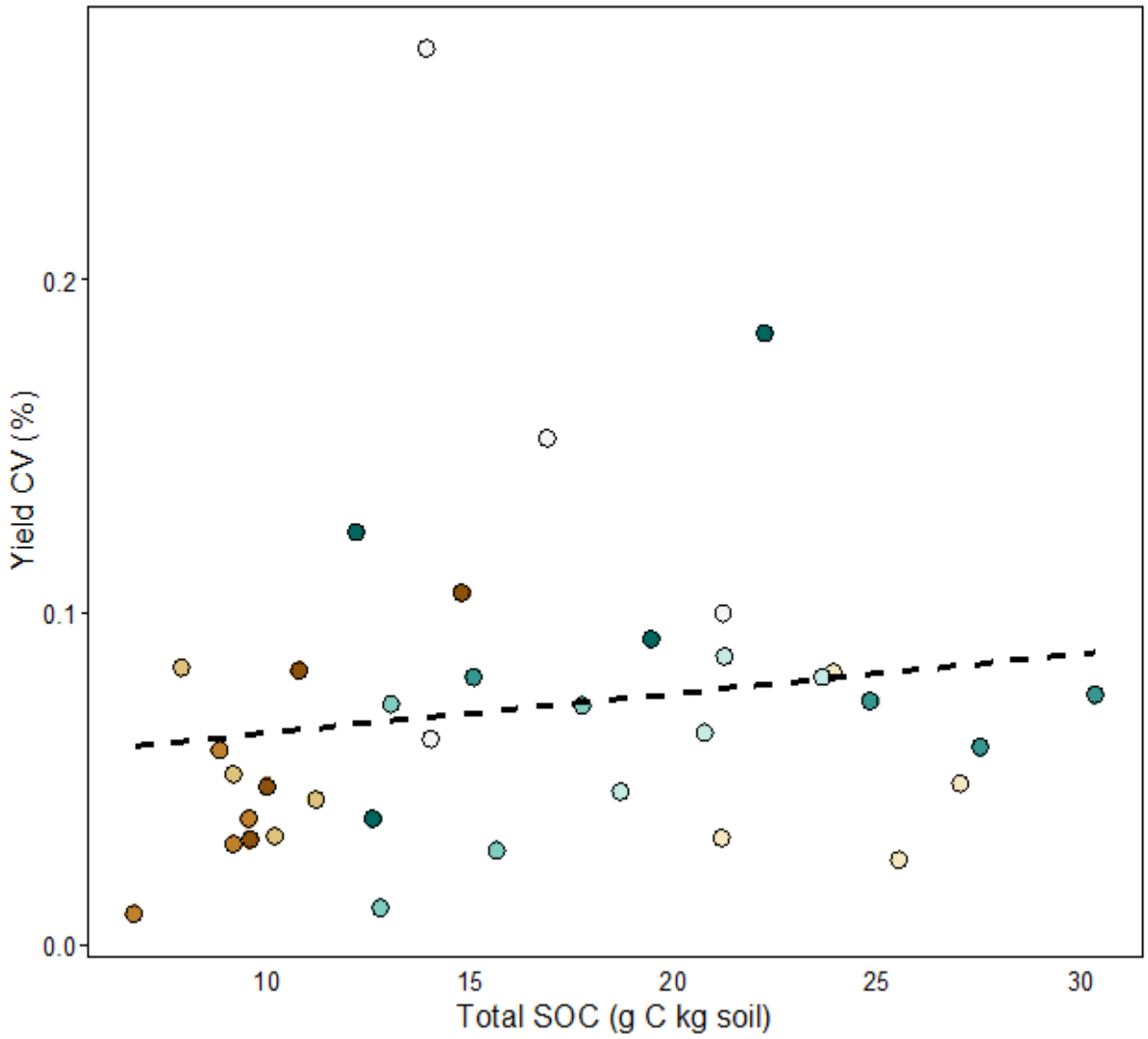

Supplemental Figure 5.1 – Linear regression of the coefficient of variation for crop yield at the stability zone level against total soil organic carbon (SOC) concentrations. Different colored points represent samples from different farms. Regression is marginally significant ($p = 0.096$, $r^2 = 0.02$).

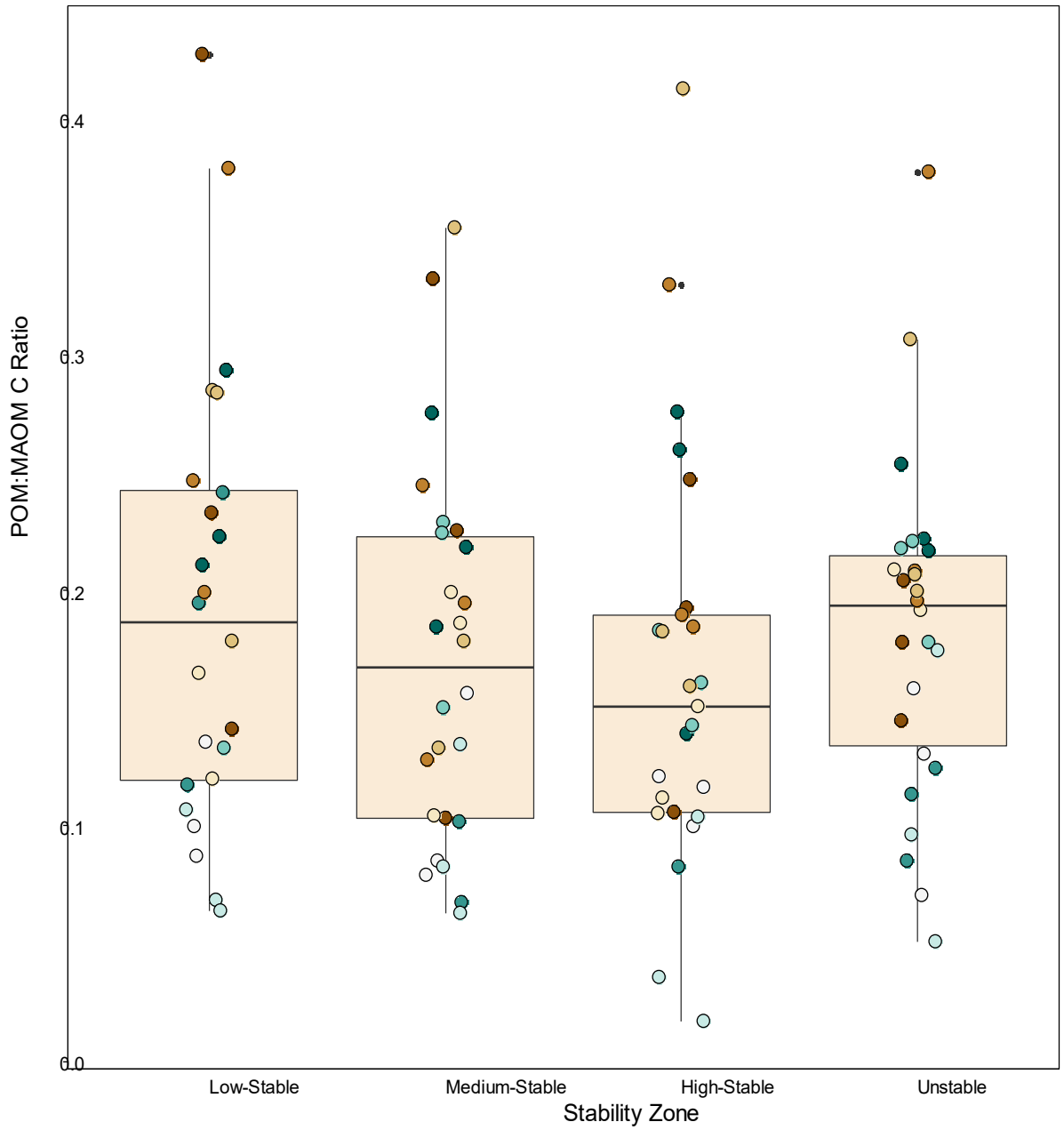

Supplemental Figure 5.2 – Ratio of POM-C to MAOM-C across the different stability zones. Different colored points represent different farms. Mixed linear models indicate no significant differences among stability zones ($p = 0.2778$).

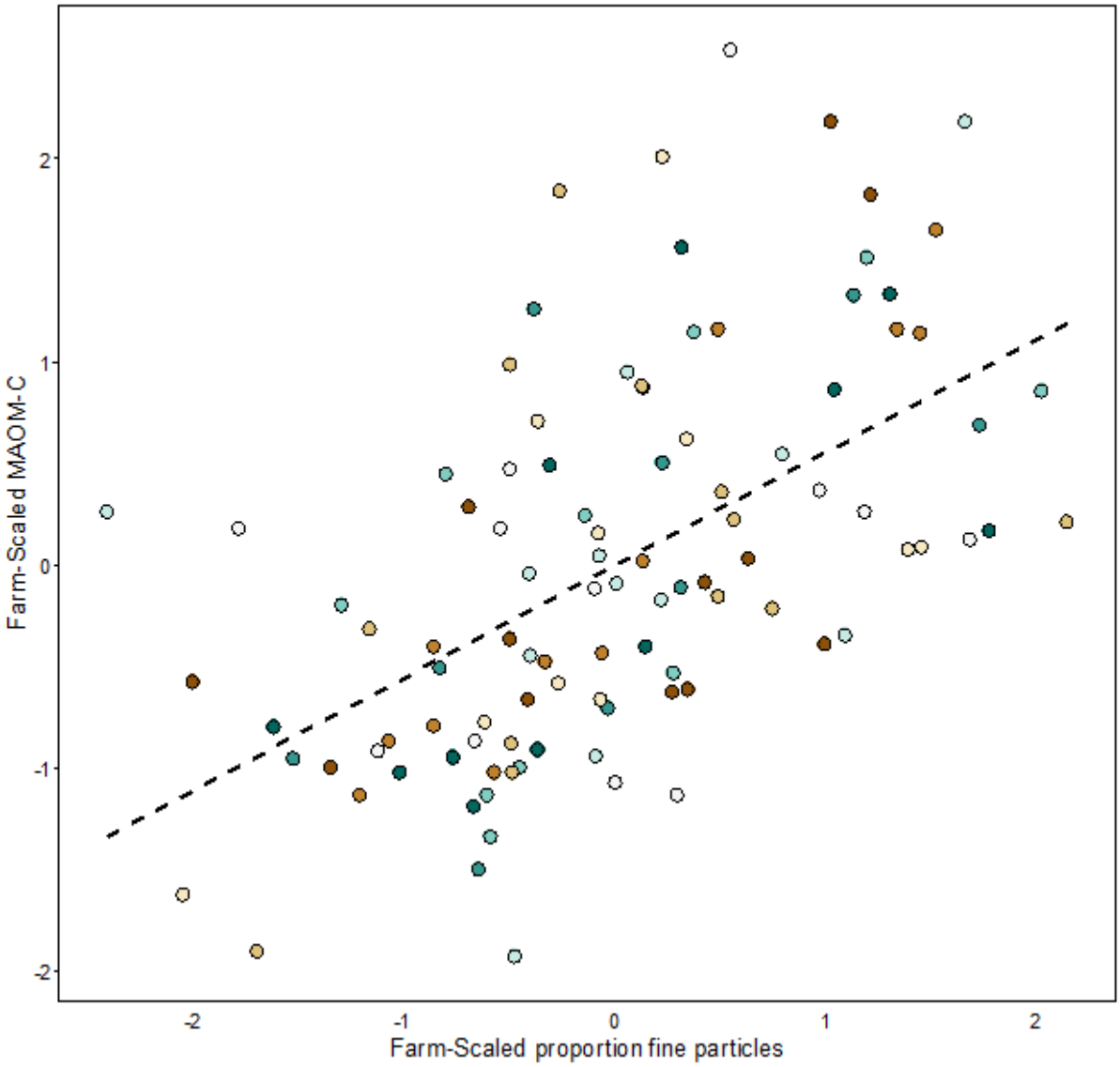

Supplemental Figure 5.3 – Regression between the farm-scaled (z-scored) mineral associated organic carbon (MAOM-C) content and the proportion silt and clay particles. Regression is significant ($p < 0.001$, $r^2 = 0.3086$).

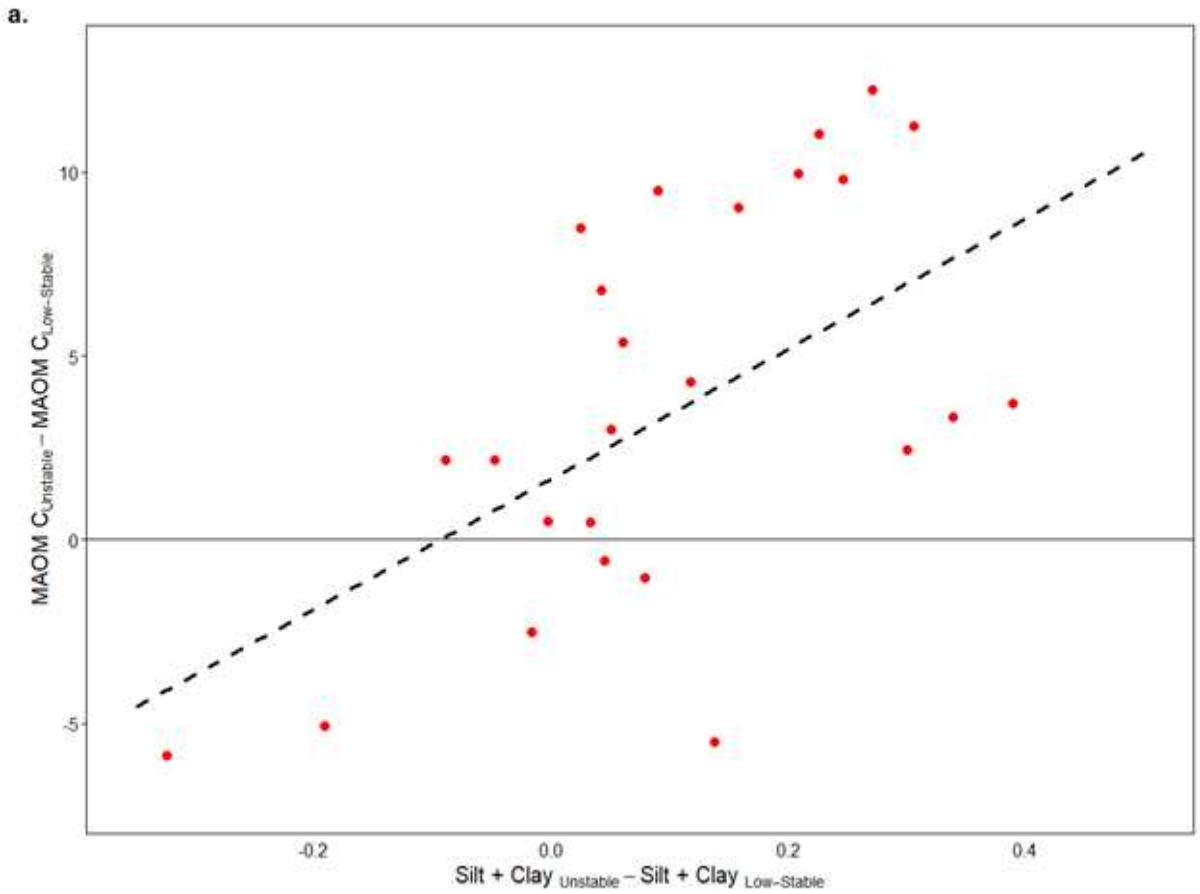

Supplemental Figure 5.4 – Regression between the difference between the unaltered (i.e., not scaled) proportion of silt and clay particles and the difference in unaltered mineral associated organic carbon (MAOM C) between unstable and low-yielding, stable zones. Regression is signficant ($p = 0.001$, $r^2 = 0.37$).

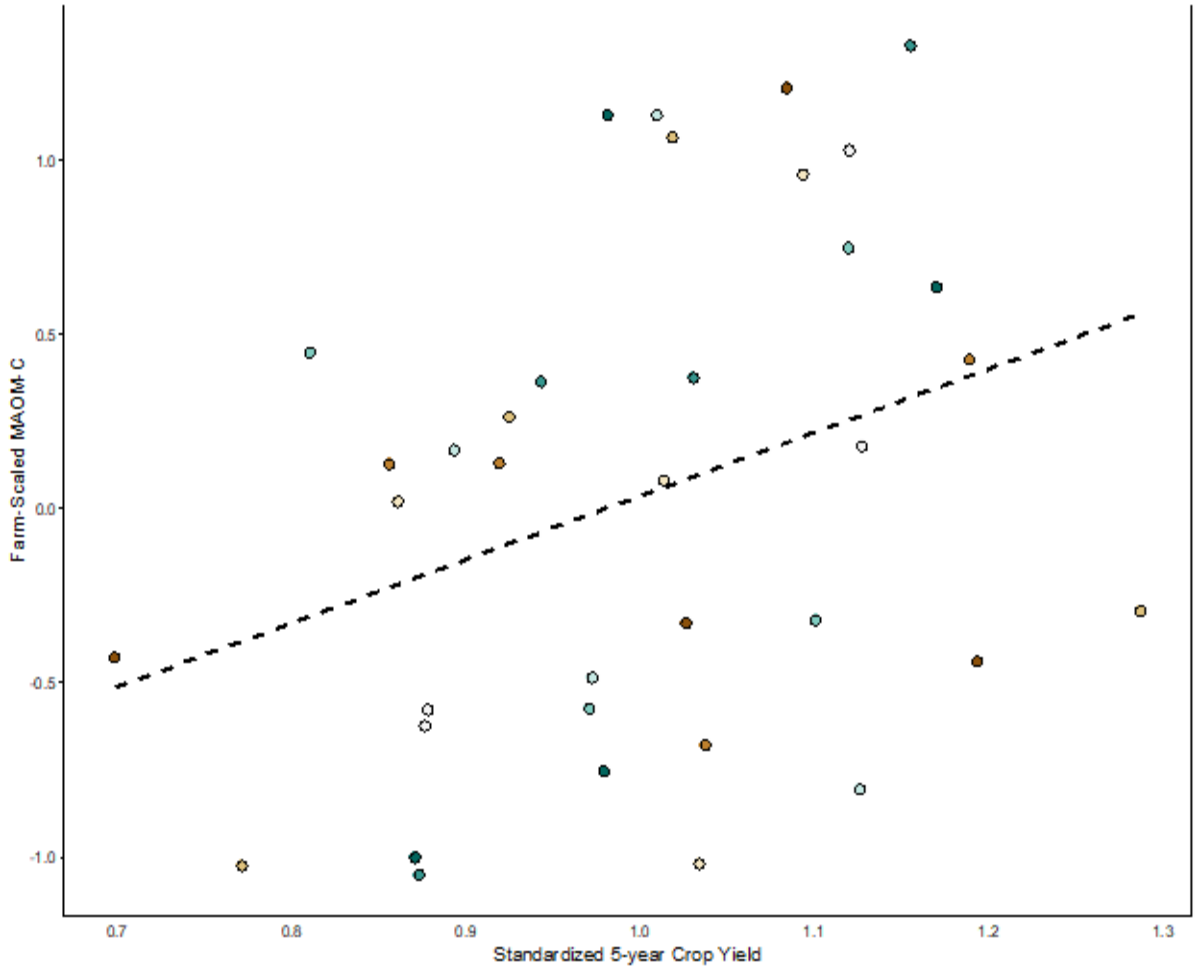

Supplemental Figure 5.5 – Results of linear regression between average, standardized crop yield in each stability zone at each farm over the study period and z-scored mineral associated organic matter carbon (MAOM-C). Regression is significant ($p = 0.048$, $r^2 = 0.110$). Different colored points represent different sampled farms.

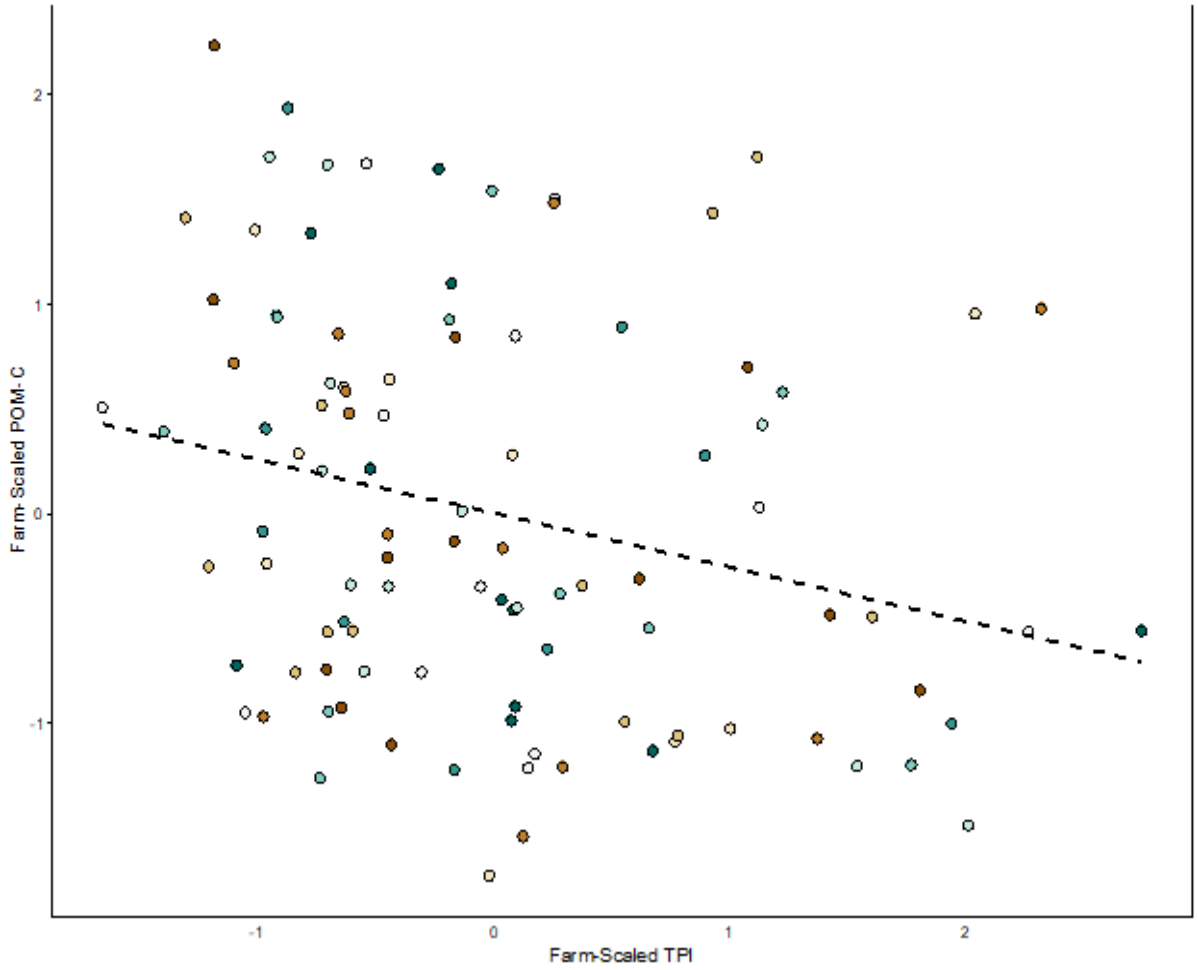

Supplemental Figure 5.6 – Results of linear regression the z-score of particulate organic matter carbon (POM-C) and the z-scored topographic position index (TPI). Regression is significant ($p = 0.020$, $r^2 = 0.053$). Different colored points represent samples from different farms.

Chapter 6 Supplemental Material

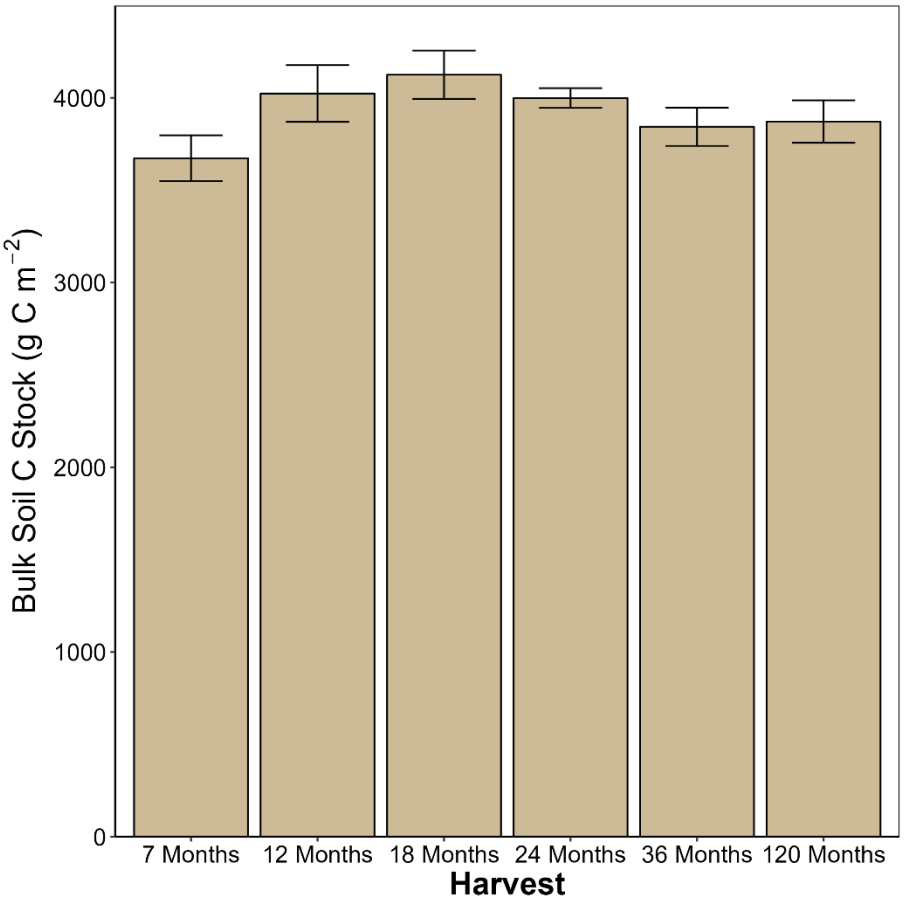

Supplemental Figure 6.1 - Bulk soil organic carbon (SOC) stocks to 5 cm depth in the experimental plots. The SOC stocks of the bulk soil did not significantly change over the course of the experiment, indicating that the system was at steady state throughout the incubation period. Column height represents mean SOC stock at time of sampling, error bars indicate ± 1 SE (n = 4).

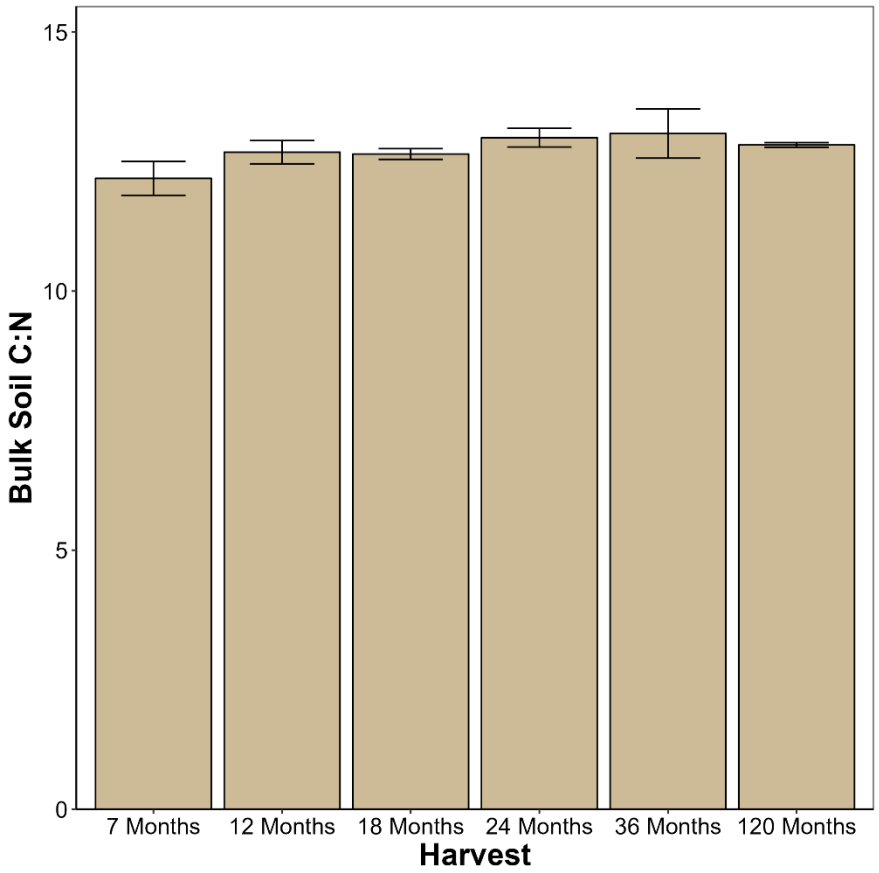

Supplemental Figure 6.2 - Bulk soil organic matter carbon to nitrogen ratio (SOM C:N) of the top 5 cm in the experimental plots. We observed no significant differences in bulk soil C:N ratio of the experimental plots throughout the course of the experiment. Bulk SOM C:N was higher than litter-derived SOM C:N, and lower than PyOM-derived SOM C:N. Column height represents mean SOM C:N at time of sampling, error bars indicate ± 1 SE (n = 4).

Chapter 7 Supplemental Material

Supplemental Table 7.1- Pairwise comparisons of treatments for soil nitrate (NO_3^-) stocks after 2 weeks of incubation.

Comparison	Estimate	SE	df	t.ratio	p-value
High SOM | Low POM:MAOM | High POM C:N - Low SOM | Low POM:MAOM | High POM	27.32	1.89	19.0	14.47	<.0001
High SOM | Low POM:MAOM | High POM C:N - High SOM |High POM:MAOM | High POM	29.98	1.89	19.0	15.88	<.0001
High SOM | Low POM:MAOM | High POM C:N - Low SOM |High POM:MAOM | High POM C:N	30.58	1.89	19.0	16.20	<.0001
High SOM | Low POM:MAOM | High POM C:N - High SOM |Low POM:MAOM | Low POM C:N	-10.14	2.07	19.4	-4.91	0.00
High SOM | Low POM:MAOM | High POM C:N - Low SOM |Low POM:MAOM | Low POM C:N	25.60	1.89	19.0	13.56	<.0001
High SOM | Low POM:MAOM | High POM C:N - High SOM |High POM:MAOM | Low POM C:N	-1.72	2.07	19.4	-0.83	0.99
High SOM | Low POM:MAOM | High POM C:N - Low SOM |High POM:MAOM | Low POM C:N	27.00	1.89	19.0	14.30	<.0001
Low SOM |Low POM:MAOM | High POM C:N - High SOM |High POM:MAOM | High POM C:N	2.66	1.89	19.0	1.41	0.84
Low SOM |Low POM:MAOM | High POM C:N - Low SOM |High POM:MAOM | High POM C:N	3.26	1.89	19.0	1.73	0.67
Low SOM |Low POM:MAOM | High POM C:N - High SOM |Low POM:MAOM | Low POM C:N	-37.47	2.07	19.4	-18.13	<.0001
Low SOM |Low POM:MAOM | High POM C:N - Low SOM |Low POM:MAOM | Low POM C:N	-1.72	1.89	19.0	-0.91	0.98
Low SOM |Low POM:MAOM | High POM C:N - High SOM |High POM:MAOM | Low POM C:N	-29.04	2.07	19.4	-14.05	<.0001
Low SOM |Low POM:MAOM | High POM C:N - Low SOM |High POM:MAOM | Low POM C:N	-0.32	1.89	19.0	-0.17	1
High SOM |High POM:MAOM | High POM C:N - Low SOM |High POM:MAOM | High POM C:N	0.60	1.89	19.0	0.32	1
High SOM |High POM:MAOM | High POM C:N - High SOM |Low POM:MAOM | Low POM C:N	-40.12	2.07	19.4	-19.41	<.0001
High SOM |High POM:MAOM | High POM C:N - Low SOM |Low POM:MAOM | Low POM C:N	-4.38	1.89	19.0	-2.32	0.33
High SOM |High POM:MAOM | High POM C:N - High SOM |High POM:MAOM | Low POM C:N	-31.69	2.07	19.4	-15.33	<.0001
High SOM |High POM:MAOM | High POM C:N - Low SOM |High POM:MAOM | Low POM C:N	-2.98	1.89	19.0	-1.58	0.76
Low SOM |High POM:MAOM | High POM C:N - High SOM |Low POM:MAOM | Low POM C:N	-40.72	2.07	19.4	-19.70	<.0001
Low SOM |High POM:MAOM | High POM C:N - Low SOM |Low POM:MAOM | Low POM C:N	-4.98	1.89	19.0	-2.64	0.20
Low SOM |High POM:MAOM | High POM C:N - High SOM |High POM:MAOM | Low POM C:N	-32.30	2.07	19.4	-15.63	<.0001
Low SOM |High POM:MAOM | High POM C:N - Low SOM |High POM:MAOM | Low POM C:N	-3.58	1.89	19.0	-1.90	0.57
High SOM |Low POM:MAOM | Low POM C:N - Low SOM |Low POM:MAOM | Low POM C:N	35.74	2.07	19.4	17.29	<.0001
High SOM |Low POM:MAOM | Low POM C:N - High SOM |High POM:MAOM | Low POM C:N	8.43	2.18	19.0	3.87	0.02
High SOM |Low POM:MAOM | Low POM C:N - Low SOM |High POM:MAOM | Low POM C:N	37.14	2.07	19.4	17.97	<.0001
Low SOM |Low POM:MAOM | Low POM C:N - High SOM |High POM:MAOM | Low POM C:N	-27.32	2.07	19.4	-13.22	<.0001
Low SOM |Low POM:MAOM | Low POM C:N - Low SOM |High POM:MAOM | Low POM C:N	1.40	1.89	19.0	0.74	0.99
High SOM |High POM:MAOM | Low POM C:N - Low SOM |High POM:MAOM | Low POM C:N	28.72	2.07	19.4	13.89	<.0001